DISSERTATION

FUNCTION OF cGMP-DEPENDENT PROTEIN KINASES THAT REGULATE MOLTING IN TWO DECAPOD CRUSTACEANS, *GECARCINUS LATERALIS* AND *CARCINUS MAENAS*

Submitted by

Talia Head

Department of Biology

In partial fulfillment of the requirements

For the Degree of Doctor of Philosophy

Colorado State University

Fort Collins, Colorado

Spring 2025

Doctoral Committee:

Advisor: Donald L. Mykles

Dan Sloan
Graham Peers
Ron Tjalkens

ABSTRACT

FUNCTION OF cGMP-DEPENDENT PROTEIN KINASES THAT REGULATE MOLTING IN TWO DECAPOD CRUSTACEANS, *GECARCINUS LATERALIS* AND *CARCINUS MAENAS*

Physiological regulation of molting in decapods is predominantly coordinated by two hormones, the neuropeptide molt-inhibiting hormone (MIH), and steroid molting hormones termed ecdysteroids. MIH is produced and secreted by the X-organ/sinus gland complex located in the eyestalk ganglia and negatively regulates the production of ecdysteroids in the molting gland (Y-organ, YO). MIH signaling begins with a cAMP-dependent triggering phase followed by a cGMP-dependent summation phase which ultimately leads to inhibition of mTORC1-dependent ecdysteroid synthesis. The involvement of cGMP in MIH signaling implicates the activity of cGMP-dependent protein kinase (PKG), although the downstream effects of PKG remain unknown. The goal of this work was to phylogenetically characterize PKGs in crustaceans, characterize the physiological effects of PKG-inhibition on YO ecdysteroid synthesis, and identify potential substrates and downstream effects of MIH-dependent PKG activity in the YO.

Two genes encoding PKG, *pkg1* and *pkg2*, were identified in crustaceans and are conserved across metazoans. Alternative splicing of the PKG1 N-terminal region yields three PKG1α and one PKG1β isoform in crustaceans. PKG1 sequences with a 14- to 17- amino acid insertion within the kinase domain were identified in ten decapods and one stomatopod, and may indicate that alternative splicing occurs outside of the N-terminal region. *In vitro* assays of paired

YOs incubated with MIH and PKG inhibitors were used to assess the effects of PKG activity on YO ecdysteroidogenesis in the European green shore crab, *Carcinus maenas*, and the blackback land crab, *Gecarcinus lateralis*. In the presence of MIH, inhibition of both PKG1 and PKG2 increased ecdysteroid synthesis relative to MIH alone, whereas PKG2 inhibition enhanced the effects of MIH. These data indicate that the two PKG isoforms have opposing roles in modulating ecdysteroidogenesis via MIH signaling in YOs. Specifically, PKG1 plays a dominant role in MIH signaling by inhibiting ecdysteroid synthesis, while PKG2 counters that inhibition and maintains basal ecdysteroidogenesis in the intermolt YO.

Transcriptomic analysis of the PKG isoforms expressed in the YO in both *G. lateralis* and *C. maenas* suggest that PKG1α2 may be the dominant isoform expressed in the YO. Transcriptomic expression of PKG2 is dramatically reduced at each point in the molt cycle relative to PKG1 expression. Differential expression of the two kinases may explain how MIH signaling balances ecdysteroid inhibition while maintaining the basal secretion needed for peripheral metabolism during intermolt.

Liquid chromatography/tandem mass spectrometry analysis of phosphopeptides enriched from PKG-inhibited YOs from *C. maenas* and *G. lateralis* revealed several novel potential substrates of PKG in the YO. Phosphopeptides were identified from proteins that regulate cytoskeletal organization, regulators of transcription and translation, and signaling pathways associated with growth factors and inhibition of the mechanistic target of rapamycin complex 1 (mTORC1). Together, these data indicate that PKG signaling in the YO is isoform-dependent, and may regulate ecdysteroidogenesis by interacting with multiple signaling pathways.

ACKNOWLEDGEMENTS

I sincerely thank my advisor Dr. Donald Mykles for his time, encouragement, advice, patience, and for not giving up on me when I left academia for 3 years to work in a kombucha brewery. Thank you for your continued mentorship over the last 15 years and shaping me into the scientist I am. You believed in me as an undergraduate aspiring marine biologist in Colorado, and did all you could to set me up for a successful research career. I really cannot thank you enough.

Thank you to my committee members, Dr. Dan Sloan, Dr. Graham Peers, and Dr. Ron Tjalkens for their support, feedback, and advice. And to all the Crab Lab members, human and brachyuran, who have come before me thank you for your foundational work and creating an inclusive and collaborative lab environment.

My deepest gratitude to all my friends in San Luis Obispo who let me couch surf for several months, my doors are always open. Thank you to Dr. Lars Tomanek for support and guidance with the proteomic work and hosting me at Cal Poly. And massive thanks to Frank Fabela for all his guidance and advice with proteomic workflows from sample prep to data analysis.

This work was supported by the National Science Foundation, the Society for Integrative and Comparative Biology, The Crustacean Society, and the 529 account my parents made when I was born before they knew I would go to 24th grade- thank you mom and dad.

DEDICATION

To my sister Cassandra and her friend Will

for enthusiastically listening to me talk about crabs while making pies in a gas station.

And to Diego, Mr. Binx, NightMan, Astro, Stella, Hank, Willie, Dolly, Ramen, Dill Pickle,

Sesame, Sprout, Smudge, Otter, Pepper, Shiva, and Loki

for enthusiastically listening to me talk about crabs while being cats.

TABLE OF CONTENTS

CHAPTER ONE

INTRODUCTION

Crustaceans are ecologically and economically important species. They comprise key components of trophic webs in an array of ecosystems, they are a vital food source both directly and indirectly for our growing human population, and several invasive decapod species are contributing to the destruction of vital habitats for other ecologically and economically important species. Decapod crustacean growth is restricted by the presence of an exoskeleton, making the regulation of molting vital to survival and fitness. Not only is growth modulated by the molting process, but reproduction is dependent on molting of female crustaceans. Further, the process of molting itself is dependent on environmental cues, such as seasonality, temperature, and the presence or absence of potential mates, competitors, or predators.

The work encompassed within this dissertation focuses on the regulation of molting in decapod crustaceans through molecular, physiological, and phylogenetic lenses. Molting in crustaceans is regulated by the signaling junction between two paired endocrine glands, the X-organ/eyestalk ganglia (XO/ESG) located in the eyestalks and the Y-organ (YO) located in the cephalothorax. Molt-inhibiting hormone (MIH), a neuropeptide hormone synthesized and secreted by the XO/ESG negatively regulates the production of the molting hormones, ecdysteroids, by the YO. Ecdysteroids secreted into the hemolymph by the YO mediate changes in peripheral tissues associated with molting. Levels of circulating ecdysteroids are kept to low titers by the action of MIH signaling within the YO until the animal is ready to progress towards molting. MIH signaling within the YO acts through the second messengers cAMP and cGMP

and ultimately inhibits mTORC1-dependent ecdysteroid synthesis. While we know the pathway through which MIH binding to the YO membrane results in an increase in cGMP, and we know that mTORC1 activity is required for ecdysteroid synthesis, the connection between the two signaling pathways is unknown. The work herein examines the role of cGMP-dependent protein kinase (PKG) as a key enzyme connecting MIH signaling to mTORC1 and ultimately ecdysteroid synthesis.

DECAPODA

Evolutionary history of Decapoda

Decapoda is a speciose order of pancrustaceans consisting of over ~17,500 extant species (WoRMS) that are morphologically and ecologically diverse (Wolfe et al., 2019; Davis et al., 2022). Decapods (crabs, shrimps, lobsters, and crayfish) have diversified over the course of roughly 455 million years to include marine, freshwater, and terrestrial lineages (De Grave et al., 2009; Bracken et al., 2010; Wolfe et al., 2019; Davis et al., 2022).

Decapod crustaceans occupy a breadth of global habitats, including coasts, estuaries, open ocean, hydrothermal seafloor vents, freshwater streams and lakes, mangrove forests, and semiterrestrial areas ranging from high-tide sand dunes to nearby forests (Wolfe et al., 2019; Watson-Zink, 2021). This habitat heterogeneity of decapods is a result of multiple ecological transitions from marine ancestors, many of which followed the Triassic-Jurassic extinction event (Wolfe et al., 2019).

Monophyly of the eleven decapod infraorders is supported by phylogenomic sequencing of 352 nuclear genes (Wolfe et al., 2019). The infraorder Brachyura represents true crabs, made up of 109 families and over 7,600 species, making it the most speciose of the decapod infraorders (Wolfe et al., 2024). Ecological transition from marine to terrestrial habitats is

observed as a gradient, including species occupying a range of habitats from low intertidal zones and estuaries (least terrestrial) to coastal forests and jungles (most terrestrial; Watson-Zink, 2021; Wolfe et al., 2024). Terrestriality has repeatedly evolved among the brachyuran families (Tsang et al., 2014; Watson-Zink, 2021; Wolfe et al., 2024). The ecological transition purportedly occurred through two transitional pathways- "direct" via intertidal zones, mangroves, and beaches, and "indirect" by means of estuaries and rivers (Tsang et al., 2014; Watson-Zink, 2021; Wolfe et al., 2024). Interestingly, reversal to marine from terrestrial ecology is estimated to have occurred 2 to 3 times within Brachyurans (Wolfe et al., 2024).

Ecological importance of Decapoda

Decapods serve as vital components of the ecosystems in which they are found. A wide range of high-order consumers prey upon decapods, while the decapod diet is largely dependent on the ecosystem in which they are found, and includes herbivores, detritivores, carnivores, and omnivores (Briones-Fourzán and Hendrickx, 2022). Many benthic decapods consume mollusks and other crustaceans and therefore play a substantial role in the trophic structure of benthic habitats by quelling herbivorous populations that deplete kelp, seagrass, and other algal growth (Boudreau and Worm, 2012). The population density of large benthic decapods has been observed to have an inverse relationship with the fishing of marine predators- that is, the loss of predatory fish due to overfishing results in ecosystems dominated by large benthic decapods (Boudreau and Worm, 2010; Steneck et al. 2011). Additionally, nearly all decapods have pelagic larvae thereby influencing composition and trophic structure of planktonic ecosystems (Briones-Fourzán and Hendrickx, 2022). Ultimately, decapods are a central link among trophic webs for a varied range of habitats.

In addition to their trophic roles in native habitats, decapods also constitute a growing number of invasive alien species worldwide. Invasive species are a threat to biodiversity in marine habitats as they compete for resources, including space and food, and frequently displace native species (Grosholz, 2002; Bax et al., 2003; Ricciardi et al., 2020; Cordone et al., 2023; Saborowski et al., 2023). Decapod, and particularly brachyuran, invaders have historically been introduced across the globe by means of ballast water, and to a lesser degree ship fouling, both of which are exceedingly difficult to detect and prevent (Carlton and Geller, 1993; Roman, 2006; Molnar et al., 2008). Among the most efficacious marine invaders are two brachyurans- the European green shore crab, *Carcinus maenas*, and the Asian shore crab, *Hemigrapsus sanguineus*. Phenotypic plasticity is a major mediator of an organism's ability to successfully invade non-native habitats, and these brachyuran invaders display plasticity in thermal response (Tepolt and Somero, 2014; Tepolt and Palumbi, 2020; Rato et al., 2024), reproductive strategy (Reese et al., 2024), and food preference (Fisher et al., 2023; Saborowski et al., 2023) among several other characteristics. This plasticity enables species to survive not only during periods of seasonal habitat decline, but it also allows these species to become successful invaders of regions experiencing shifts in climate to which native species cannot adapt quickly enough.

H. sanguineus shows a range of reproductive strategies spanning the latitude of its invasive range. At low latitudes, *H. sanguineus* uses an income breeding strategy, in which the energy used during reproduction is acquired concomitantly during the reproductive period (Reese et al., 2024). As latitude increases, the animals gradually switch to a capital breeding strategy, in which energy stores acquired outside of the breeding and reproductive period(s) are used to source offspring production (Reese et al., 2024). This switch in reproductive strategy also results in an increased reproductive capacity of the Asian shore crabs at the edge of the species'

invasive range, suggesting that this species has yet to reach the limits of its range expansion (Reese et al., 2024). In decapods, ecdysteroids are involved in reproduction and embryogenesis (Subramoniam, 2000), and the timing of molting and reproduction are interlinked (Subramoniam, 2000; Styrishave et al., 2004; Shyamal et al., 2014; Ventura et al., 2020; Tang et al., 2024), which indicate that plasticity in strategies for either or both molting and reproduction may facilitate the ability of decapods to become invasive.

C. maenas is consistently ranked among the "top worst invasive species" lists. It has spread to and maintains self-sustaining populations in coastal regions of every continent except Antarctica (Frederich and Lancaster, 2024). The effects of the green shore crab on its invaded range are well characterized, as the first documented invasion of this species occurred as early as 1817 (Blakeslee et al., 2010). Their invasions have led to the destruction of eelgrass beds (Neckles, 2015), soft-shell clam populations (Garbary et al., 2014), oyster beds (Pimentel et al., 2005), and coastal erosion (Orth et al., 2006; Neckles, 2015; Frederich and Lancaster, 2024). Interestingly, not all accounts of *C. maenas* invasion indicate negative ecological effects. In Cape Cod, Massachusetts, USA, the green shore crab plays a role in recovery of salt marshes as it outcompetes and displaces the native mud crab *Sesarma reticulatum*, which has been degrading marshes through the overconsumption of cordgrass in response to overfishing natural mud crab predators (Bertness and Coverdale, 2013; Frederich and Lancaster, 2024). Other accounts of predation on *C. maenas* by native gulls in New York City (Washburn et al., 2013) and Patagonia (Yorio et al., 2020) indicate that predation on the invasive species is not only beneficial to the gulls but may also relieve predation pressure on other native prey species.

Economic importance of Decapoda

Decapods contribute largely to regional economic stability as a fishery, both by capture and aquaculture production. As a group, 99.7% of crustacean species used in aquaculture production, and at least 47% of crustacean capture fisheries, are decapods (FAO, 2024). The decapod fishery is dominated primarily by the Pacific whiteleg shrimp (*Litopenaeus vannamei*), red swamp crawfish (*Procambarus clarkii*), Chinese mitten crab (*Eriocheir sinensis*), giant tiger prawn (*Penaeus monodon*), Oriental river prawn (*Macrobrachium nipponense*) and giant river prawn (*Machrobrachium rosenbergii*) (Till et al., 2023). Of all crustacean fishery production in 2022, 68% of the total production came from aquaculture, while the remaining 32% was from capture fisheries (FAO, 2024).

The aquaculture industry is growing at a rapid rate to meet the demands of a growing global population. Of the aquatic food available for human consumption, 57% is produced from aquaculture and of that 24.6% of the production is of crustaceans (FAO, 2024). Understanding molt regulation is vital to ensuring aquaculture practices are sustainable for long-term production. The number one aquatic species produced by both aquaculture and capture fisheries globally is *L. vannamei*. Of the 6.8 million tons produced in 2022, at least 99% was from aquaculture production (FAO, 2024). In 2019 the value of farmed marine shrimp was nearly 40 billion U.S. dollars and has certainly grown dramatically in the half a decade since (Emerenciano et al., 2022)

The shrimp aquaculture industry relies heavily on unilateral eyestalk ablation (ESA), or the removal of a single eyestalk, in female broodstock to stimulate gonadal development and reduce the timing of reproduction (Feijó et al., 2016; Insights, 2019; Kang et al., 2019; Zacarias et al., 2019; Emerenciano et al., 2022). ESA is a time-intensive process that can lead to an

increase in death or susceptibility to disease (Zacarias et al., 2019), and there is a growing concern among consumers about the welfare of animals subjected to ESA in the farms growing their food (Benchmark Insights, 2019; Emerenciano et al., 2022). The use of RNA interference (RNAi) provides a potential approach to stimulate breeding given the right genes are selected and the delivery method is effective and efficient, however it has yet to be applied commercially (Feijó et al., 2016; Insights, 2019; Kang et al., 2019; Emerenciano et al., 2022). Understanding the genetic and physiological basis of molting in decapods, and its interconnection with regulating reproduction, is a fertile (pun intended!) area of research that promises economical and food security to those who discover a viable molecular switch.

While shrimp aquaculture production can be a lucrative endeavor, it comes with great costs. Expansion of the shrimp aquaculture industry is a leading cause of mangrove forest destruction worldwide, with at least 1.4 million hectares of forest have been cleared for shrimp production (Taher et al., 2023). Mangrove forests are biodiversity hotspots and serve as nurseries for numerous marine species. Additionally, mangroves protect coastal regions from erosion and shelter coastlines from tropical storm events, providing at least some protection from the economic damages of large tropical storms and cyclones (Hochard et al., 2019). The intensification of shrimp farming requires higher energy and feed inputs, and results in an increase in effluent that can lead to downstream eutrophication and spread of pathogens and pests (Till et al., 2023). Ultimately, the sustainability is shrimp farming is a factor of the energy inputs (both electrical and stock feed), water consumption, greenhouse gas emissions, and land usage (Till et al., 2023).

In addition, molting will be affected by changing seawater temperature, salinity, pH, and increases in hormone-disrupting chemicals from agricultural runoff, which, in-turn, will affect

capture fisheries production (FAO, 2024). These ecological and climate disasters have the potential to disrupt economies directly, by impacting decapod aquaculture and capture fisheries, and indirectly by contributing to ecological collapse in areas that have tourism-based economies or rely on fragile shoreline ecosystems for protection from coastal erosion and storms.

Outside of the economics of decapod fisheries, they also provide revenue and innovation potential in terms of biopolymer production. Crustacean exoskeletons are composed of chitin, a biodegradable, non-toxic, antimicrobial polysaccharide that is the second most abundant polysaccharide in nature (Harish Prashanth and Tharanathan, 2007; Abdullah Al Balushi et al., 2021). Between 50-70% of the raw weight of crustacean exoskeletons contains chitin (Bulut et al., 2017), providing a wealth of material for bio-innovation. Biomedically, chitin is being studied for potential mechanisms of drug delivery and tissue engineering, such as artificial skin for wound dressings (Kashyap et al., 2005; Aranaz et al., 2021; Yee Kuen and Masarudin, 2022). Chitin harvested from seafood waste containing crustacean exoskeletons is processed into chitosan, which has adsorptive properties (Aranaz et al., 2021). Chitosan is used for batch treatment of wastewater where it reduces total dissolved solids, total suspended solids, turbidity, and both chemical and biochemical oxygen demand of wastewater (Abdullah Al Balushi et al., 2021).

SPECIES OF STUDY

Gecarcinus lateralis, the blackback land crab

The blackback land crab, *Gecarcinus lateralis* (Fréminville 1835) is a semi-terrestrial land crab found in the Florida Keys and Caribbean islands and along the Gulf of Mexico from South Padre Island, Texas, USA, along Central America on the side of the Caribbean Sea, to western Venezuela (Bright and Hogue, 1972). Reproduction of *G. lateralis* is tied to the ocean,

as adult females of this species release their eggs directly into the breaking waves along the shore (Bliss, 1979). The species undergoes planktonic larval development through five to six zoea stages and one megalopa stage and return to land upon molting into juveniles (Bliss, 1979; Willems, 1982). The crabs reside in burrows made along sandy dunes and vegetation just above the high tide line. They primarily eat plant matter, although they have been observed to be omnivorous and carnivorous at times (Bliss et al., 1978; Bliss, 1979; Willems, 1982; Wolcott and Wolcott, 1984). The blackback land crab has made an ideal laboratory species for studying brachyuran molting, as they are relatively easy to house and respond well to molt induction techniques, which will be described later.

Carcinus maenas, the European green crab

In its native range, *Carcinus maenas* (Linnaeus 1758) is referred to as the "shore crab", however broad spread invasions of this species globally have led to adoption of the "European green crab" or even just "green crab" as a primary identifier common name (Young and Elliott, 2020). The native range of *C. maenas* spreads along the northeast Atlantic coastline as far north as Norway and as far south as Mauritania (Young and Elliott, 2020). Invasion of *C. maenas* globally is believed to have spread by means of ballast water, and the species now has established populations along the Atlantic coast in northeastern North America, the Pacific coast in northwestern North America, and the coasts of South Africa, southern Australia, central Japan, and Argentina (Young and Elliott, 2020; Frederich and Lancaster, 2024).

C. maenas is a littoral crab that can be identified by the presence of five spines on either side of their eyes and three spines in between their eyes (Crothers, 1967). Despite the common name of green crab, *C. maenas* individuals can range in color from bright green to deep red depending on whether they are energetically investing growth (green) or reproduction (red;

Styrishave et al., 2004; Abuhagr et al., 2014a). *C. maenas* have planktonic larval development including four zoea stages and one megalopa stage before settling to the benthos as juveniles (Crothers, 1967; Young and Elliott, 2020). Juveniles molt frequently and can reach sexual maturity in six months, typically in 10-12 molts (Crothers, 1967; Monteiro et al., 2025).

The population of green crabs used in this dissertation are from Bodega Bay, California, USA where the invasive population was established around 1993 (Sheenan and Henry, 2001). This population of crabs typically molts twice per year, once in the spring and again in the late fall. This population is typically refractory to molt induction techniques (Abuhagr et al., 2014a), and may produce MIH in extra-eyestalk locations (Pitts and Mykles, 2017).

MOLTING IN CRUSTACEANS

Early studies

Records of scientific interest in crustacean molting date back to the early 18th century in two publications by French naturalist and entomologist René-Antoine Ferchault de Réaumur (Réaumur, 1712; 1718). Réaumur first described regeneration of lost limbs upon molting in crayfish during a time when preformation, or the idea that all parts of an organism were present in the egg or embryo, predominated developmental theories (Réaumur, 1712; Ashworth, 2024). In the early 19th century Jonathan Couch and his oldest son Richard Q. Couch described observations on molting in lobsters, crayfish, shrimp, and crabs (Couch, 1837a; 1837b; 1843a; 1858; Couch, 1843b; 1856). At the time they believed that the exoskeleton of the claws and legs separated longitudinally to allow the large appendages to exit confinement of the exoskeleton (Couch, 1837a; 1837b), but were later observed to pull themselves out “as if from boots” (Couch, 1858).

The Y-organ (YO) was first described in 1953 by French scientist M. Gabe in the European green crab, *C. maenas* (Gabe, 1953a; 1953b; Arvy et al., 1956; Gabe, 1956). His coworker G. Echalier concurrently showed that the YO exerts control over molting in decapods through a series of experiments involving the removal and/or implantation of the YO among individuals (Echalier, 1954; 1955; Arvy et al., 1956; Echalier, 1959; Koolman, 1982). At the same time, Gabe, Echalier, and Arvy found that the YO also influences the gonads, implying a role for the YO in the regulation of reproduction in decapods (Arvy et al., 1956).

Subsequently, a steroid hormone was isolated from the prothoracic gland of the silk moth *Bombyx mori* in 1954 by German scientists Peter Karlson and Adolf Butenandt (Arvy et al., 1956; Karlson and Sekeris, 1966a; Koolman, 1982). The name of this hormone was proposed at a symposium on advances in invertebrate endocrinology in Paris, France in July of 1955- ecdysone, from the Greek word ékdysis, to molt (Arvy et al., 1956). Further characterization of ecdysone revealed that there are several types of ecdysteroids based on the functional groups present or absent in the hormone (Karlson and Sekeris, 1966a; Adiyodi and Adiyodi, 1970; Willig, 1974; Chang and O'connor, 1977; Koolman, 1982; Soumoff and Skinner, 1983). Ecdysteroids were also isolated from plants in 1974 (Hikino and Takemoto, 1974).

Before the discovery of the YO, the sinus gland (SG), located in the eyestalks, was described in 1939, and identified to have regulatory effects on crustacean molting by implantation experiments (Brown and Cunningham, 1939). However, eyestalk ablation (ESA) was described as early as 1912 and found to accelerate molting in crustaceans (Rao, 1965). Between 1959 and 1964 the SG and YO were identified as opposing regulators of molting in crustaceans (Echalier, 1959; Passano and Jyssum, 1963; Josefsson and Kleinholz, 1964; Rao, 1965). Scientists understood that a molt-inhibiting hormone (MIH) was being synthesized and

secreted by the eyestalks, and in 1965 MIH was finally isolated and identified to be a peptide hormone (Rao, 1965).

While the characterization and identification of ecdysteroids and MIH continued through the 1980's (Carlisle, 1957; Karlson and Skinner, 1960; Passano and Jyssum, 1963; Josefsson and Kleinholz, 1964; Sekeris and Karlson, 1964; Carlisle, 1965; Rao, 1965; Karlson and Sekeris, 1966a; Adiyodi and Adiyodi, 1970; Willig, 1974; Chang and O'Connor, 1977; Koolman, 1982; Quackenbush and Herrnkind, 1983; Soumoff and Skinner, 1983; Webster, 1986), the study of molting in decapods also began to diversify beyond the identification of regulatory hormones. In 1962, Dorothy Skinner first described structural and metabolic changes to the decapod integument over the course of the molt cycle in the blackback land crab, *G. lateralis* (Skinner, 1962). Skinner characterized cellular level changes associated with the five major stages (A through E) of molting previously described by French scientist Pierre Drach (see Skinner, 1962; 1985a). The molt cycle for adult *G. lateralis* lasts between four to six months, with the intermolt stage (C_1) comprising the majority of the molt cycle (Skinner, 1962). The premolt period (D_0 through D_4) lasts approximately 30 days and is when the animals regenerate autotomized limbs, absorb the current exoskeleton and synthesize and new exoskeleton (Skinner, 1962). Premolt is followed by ecdysis (E), or the actual process of molting. Exuviation from the exoskeleton occurs through peristaltic movements and an increased intake of water in aquatic species or air in terrestrial species that allows for the animal to separate the carapace (Bliss and Boyer, 1964). After ecdysis, the animals recover in a postmolt period (A through B), during which the soft exoskeleton is stretched by an increased uptake of air or water and subsequently hardened (Skinner, 1962; Bliss and Boyer, 1964; Skinner, 1985b).

Limb regeneration associated with molting was examined, and the loss of multiple limbs was identified as a stimulus to ecdysis (Passano and Jyssum, 1963; Skinner and Graham, 1972; Skinner, 1985a; Mykles, 2001). The loss of partially regenerated limbs was then identified as a suppressor of ecdysis (Holland and Skinner, 1976; McCarthy and Skinner, 1977b). Later, a factor termed limb autotomy factor-proecdysis (LAF_{pro}) was determined to be secreted by secondary (2º) limb bud regenerates that formed after the loss of primary limb buds. LAF_{pro} inhibits molt cycle progression until the 2º limb regenerate starts growing and catches up to remaining 1º regenerates (Yu et al., 2002). Additional studies during this time period examined the interactions between molting and protein synthesis (Skinner, 1965; 1966; Mykles and Skinner, 1981; 1982; O'Brien et al., 1991; Mykles, 1992), molting and behavior (Tamm and Cobb, 1978; Bauer, 1981; Lipcius and Herrnkind, 1982; Wolcott and Wolcott, 1982; Harpaz et al., 1987); as well as molting and the environment (Bliss and Boyer, 1964; Aiken, 1969; Fowler et al., 1971; Weis, 1976; Skinner, 1985b).

In the mid 1980's molecular characterization of molting in crustaceans began through the use of pharmacological compounds to stimulate or inhibit molting *in vivo* and/or ecdysteroid production by the YO *in vitro*. Mark Mattson and Eugene Spaziani were the first to identify the role of cAMP and adenylate cyclase in mimicking MIH inhibition in the YO of the Pacific rock crab *Romaleon antennarium* (formerly *Cancer antennarius;* Mattson and Spaziani, 1985a). They continued this work to show that lysine vasopressin and arginine vasopressin both increase the intracellular accumulation of cAMP and mimicked the effects of MIH (Mattson and Spaziani, 1985a). This work marked the beginning of an investigation into molecular pathways that regulate molting that continues today.

The process and physiology of molting in crustaceans

Crustacean growth is restricted by the presence of a chitin-based exoskeleton that provides structure and support to the animals (Skinner, 1962). Growth in crustaceans is intermittent, as the exoskeleton cannot stretch in its fully sclerotized and calcified form. Instead, crustacean growth occurs through a process called molting, in which a new exoskeleton is synthesized beneath the existing, hardened exoskeleton, which is then actively shed in a process called ecdysis, or molting. Once the animal has molted the newly synthesized exoskeleton, which is "soft" and flexible, is expanded through the intake of water or air before becoming fully synthesized and sclerotized (Skinner, 1985a; 1985b; O'Halloran and O'Dor, 1988; Mykles, 2024).

Molting in crustaceans is a cyclical and unidirectional process that is divided into four major stages, named anecdysis (intermolt/IM), proecdysis (premolt; which can further be broken into early/EP, mid/MP, and late/LP), ecdysis, and metecdysis (postmolt/PM; Drach, 1939; Bliss and Boyer, 1964; Mykles, 2024). Progression through the molt cycle occurs through the action of ecdysteroids, a class of polyhydroxylated C27 steroid hormones that universally regulate molting in crustaceans (Karlson and Sekeris, 1966a; Mykles, 2011; Lafont et al., 2021). Ecdysteroids are synthesized from dietary cholesterol and while they serve the primary purpose of regulating molting, they also can affect metabolism and reproduction (Subramoniam, 2000; Mykles, 2011; Truman, 2019; Lafont et al., 2021). Ecdysteroid action in peripheral tissues stimulates preparatory processes such as absorption of calcium from the old exoskeleton and depositing that calcium into gastroliths, the secretion of epicuticle and exocuticle of the new exoskeleton, and atrophy of claw muscle (Skinner, 1962; 1965; 1966; Mykles and Skinner, 1981). In decapods, 20-hydroxyecdysone (20E) is the major bioactive form of ecdysteroid, although several other

bioactive forms are present and have various roles in systemic molt regulation (Lafont et al., 2021).

In crustaceans, ecdysteroid synthesis occurs in the Y-organs (YOs), located in the anterior cephalothorax; ecdysteroids are secreted into the hemolymph and distributed to peripheral tissues. Synthesis and secretion of 20E (and other ecdysteroids) by the YO is negatively regulated by a neuropeptide hormone aptly named molt-inhibiting hormone (MIH). MIH is synthesized in the paired X-organs (XO) and secreted by the sinus gland (SG) within the eyestalk ganglia (ESG). In non-insect crustaceans, circulating levels of ecdysteroid are low during intermolt and increase during progression into premolt (Mykles, 2011; Mykles and Chang, 2020).

Comparatively, metamorphic molts in insects are first stimulated by prothoracicotropic hormone (PTTH), produced by the *corpus cardiacum*. PTTH, in turn, stimulates the production of ecdysone by the prothoracic gland (PG), the insect equivalent of the YO (Mykles et al., 2010; Covi et al., 2012; Sin et al., 2015; Truman, 2019). In insects, ecdysone is hydroxylated into 20E in peripheral tissues, although unaltered ecdysone can also be active in specific circumstances of insect metamorphosis (Truman, 2019). In insects, circulating levels of ecdysteroids are low during intermolt and increase during metamorphic molts (Truman, 2019).

The stage of an animal in the molting process can be determined by a combination of circulating ecdysteroid titers; the R-index, which is the ratio of the size of limb regenerates to the carapace width (calculated as the length of the limb regenerate x 100 / carapace width); and the condition of the membranous layer, which is the inner-most layer of the intermolt exoskeleton (Table 1.1; reviewed in Mykles, 2024). During intermolt, the exoskeleton is composed of four layers: the epicuticle, exocuticle, endocuticle, and membranous layer (Fig. 1.1; Skinner, 1962;

Mykles, 2024). Intermolt, also called stage C_4, is characterized by low hemolymph ecdysteroid titers, a fully formed and calcified exoskeleton, including the presence of the membranous layer, and basal limb regenerates with an R-index between 8-10. In early premolt (D_0) hemolymph ecdysteroid titers begin to increase, claw muscles begin to atrophy, calcium is resorbed from the exoskeleton begins to be deposited in gastroliths, and limb regenerates grow to an R-index of 12-16. During early premolt, molting can be delayed by the loss of additional limbs or limb buds. If the animal progresses to mid-premolt (D_1), the animal becomes 'committed' and will proceed towards molting despite any additional losses of limbs. In mid-premolt, hemolymph ecdysteroid titers continue to increase, the membranous layer begins to degrade, claw muscle atrophy continues, and limb bud growth increases dramatically to an R-index of 16-24. In late premolt (D_{2-3}) circulating ecdysteroids rise rapidly and reach a peak, the new epicuticle and exocuticle are synthesized and the membranous layer is absent, large gastroliths are present, and the limb regenerates are fully grown ($R \geq 24$). Stage D_4 immediately precedes ecdysis (E) and is characterized by a sharp drop in circulating ecdysteroids and the animal begins to swallow water or air (Bliss and Boyer, 1964; Skinner, 1985a; Mykles, 2024).

The swallowing of water or air, dependent on whether the species is aquatic or terrestrial, splits the exoskeleton along the epimeral suture, located between the carapace and abdominal segment (Skinner, 1985a). During ecdysis, peristaltic contractions assist in the actively shedding the exoskeleton and the soft exoskeleton is stretched by the continued intake of water or air (Bliss and Boyer, 1964; Skinner, 1985a; Mykles, 2024). Postmolt extends over several stages (A, B, and C_{1-3}) as the animal recovers from molting before returning to intermolt. During postmolt, circulating ecdysteroid titers remain low, claw muscles grow, and the endocuticle is synthesized and calcified (Bliss and Boyer, 1964; Skinner, 1985a; Mykles, 2024).

Characteristics of the Y-organ throughout the molt cycle

The physiological state of the YO is distinctly characterized at each molt cycle stage (Fig. 1.2; Das et al., 2018; Head et al., 2019; Mykles and Chang, 2020). During intermolt, the YO is maintained in a basal state through MIH signaling. The YO synthesizes low levels of ecdysteroids which support basic physiological processes without tipping the scales into initiating entry into premolt (Subramoniam, 2000). MIH signaling genes and ecdysteroid synthetic genes (also called Halloween genes) are highly expressed in the intermolt YO transcriptome (Das et al., 2018; Benrabaa et al., 2023). High expression of Halloween genes transcripts indicates that the intermolt YO is primed for activation and increased ecdysteroid synthesis when the timing is right. Protein expression in the intermolt YO is dominated by metabolic proteins and reactive oxygen species (ROS) scavenging proteins (Head et al., 2019).

In early premolt the YO increases ecdysteroid synthesis. Differential expression of 16,142 contigs between intermolt and early premolt occurs (Das et al., 2018). Despite this large change in transcript expression, many of the Halloween genes do not change significantly in expression between IM/EP (Benrabaa et al., 2023). Protein expression of metabolic proteins increases in the early premolt YO relative to intermolt (Head et al., 2019). Hypertrophy of the YO is evidenced through increased expression of cytoskeletal proteins (Head et al., 2019). In this stage, ecdysteroid synthesis can be blocked *in vivo* and *in vitro* by rapamycin, an inhibitor of the mechanistic Target of Rapamycin (mTOR; Abuhagr et al., 2014b; Abuhagr et al., 2016; Mykles, 2024).

The mid premolt YO expresses the highest levels of cellular metabolism proteins (Head et al., 2019). Cytoskeletal proteins, as well as those involved in vesicular secretion are also evident during mid premolt, and an increased expression of proteins associated with protein

homeostasis and turnover are also expressed at this stage (Head et al., 2019). At this stage, the YO is insensitive to MIH, crustacean hyperglycemic hormone (CHH), and the loss of additional limbs or limb buds (Mykles, 2024). Transition of the YO into the mid-premolt stage from early premolt requires transforming growth factor-β (TGF-β)/myostatin/activin signaling and can be inhibited by the activin inhibitor SB431542 *in vivo* (Abuhagr et al., 2016; Mykles, 2024).

In late premolt, the proteome of the YO appears to show preparation for ecdysis and YO repression. While metabolic, ROS scavenging, and homeostasis proteins are still observed, the expression patterns more closely resemble those of intermolt than mid premolt (Head et al., 2019). Just before ecdysis, the YO abruptly halts ecdysteroid synthesis, leading to a sharp drop in circulating ecdysteroid titers which initiates the beginning of ecdysis (Mykles, 2024).

In postmolt, the YO is transcriptionally repressed and the secretion of ecdysteroids is extremely low or absent (Mykles, 2011; Das et al., 2018; Mykles, 2024). Some species of crabs undergo a terminal molt, after which the YO degenerates and prevents further growth (Chassard-Bouchaud and Hubert, 1976; Skinner, 1985a; Tamone et al., 2005).

Techniques to stimulate molting in laboratory or aquaculture settings

Multiple leg autotomy (MLA) is the loss or removal of limbs to stimulate molting. Molt cycle progression can be tracked by measuring the regeneration index (R-index) of regenerating limbs (length of limb bud x 100 / carapace width; Skinner and Graham, 1972). The number of autotomized limbs required to induce a molt is species-dependent, in *G. lateralis* the loss of five or more walking legs is required to stimulate precocious molting, and adults typically molt within 6-8 weeks (Skinner and Graham, 1972; Skinner, 1985a).

Regenerating limbs begin as basal regenerates, in which all of the tissue is differentiated, but the growth is limited, and the limbs remain small. Limb bud growth starts in early premolt,

and at this stage the loss of a limb bud can halt progression towards molting. New limb regenerate(s), called 2º limb buds, begin to form and progression towards molting is halted until the size of 2º limb buds reaches approximately that of the initial 1º limb buds (Skinner and Graham, 1972; Skinner, 1985a; Yu et al., 2002). This pause caused by the loss of a limb bud can only occur when the animal has not yet reached the mid-premolt, committed state (Skinner and Graham, 1972). A peptide factor produced by 2º limb buds called limb autotomy factor proecdysis (LAF_{pro}) is believed to cause the delay in molt cycle progression, although the mechanism through which it acts either on the YO, on peripheral tissues, or both, is not understood (Mykles, 2001; Yu et al., 2002). The identity of LAF_{pro} remains unknown but is believed to be an insulin-like peptide (ILP), as *Drosophila* ILP8 (Dilp8) is synthesized by damaged imaginal discs and inhibits ecdysteroid synthesis in the prothoracic gland (Garelli et al., 2012; Mykles, 2024).

MLA is typically used in the laboratory to induce precocious molting, through which we can study the YO at each molt stage. This method of molt induction is believed to most closely resemble a “natural” molt, although the influence of limb autotomy factors may activate YO signaling pathways that are not activated in a molting intact animal. Yet, animals in their native habitat lose limbs to predators or conspecific competitors, and so MLA remains a valid and meaningful method to induce molting in the laboratory.

Eyestalk ablation (ESA) is the removal of one or both eyestalks, as was previously mentioned in regard to the shrimp aquaculture industry. ESA induces precocious molting due to the acute withdrawal of MIH. ESA shortens the time to molting compared to MLA. However, crabs that have undergone ESA rarely survive ecdysis (Skinner and Graham, 1972; Skinner, 1985a; 1985b). Further, the loss of eyestalks causes widespread endocrine disruption, as the

eyestalk is the source of several neuropeptides in addition to MIH, including the crustacean hyperglycemic hormone (CHH), and gonad/vitellogenesis inhibiting hormone (GIH/VIH), ion transport peptide (ITP), and mandibular organ-inhibiting hormone (MOIH; Webster et al., 2012; Webster, 2015; Mykles, 2024). ESA does not resemble a natural molt because the complete loss of MIH and the other eyestalk-synthesized neuropeptides does not occur in nature. Despite this, ESA is a useful laboratory method. For example, upon dissection the YOs of *C. maenas* become immediately activated and can begin to synthesize and secrete ecdysteroids at an increased rate. By contrast, in *G. lateralis* dissected YOs do not immediately increase ecdysteroid production. For *in vitro* assays of *G. lateralis*, it is useful to use ESA 2-3 days prior to dissection to activate the YOs capacity for ecdysteroid synthesis.

SIGNALING PATHWAYS THAT REGULATE MOLTING

Regulation of ecdysteroid synthesis in the crustacean molting gland

The MIH is a neuropeptide that ranges from 74 to 79 amino acids in decapod species (Nakatsuji et al., 2009). Six cysteine residues are strongly conserved and form three stabilizing disulfide bonds (Cys^{7}-Cys^{44}, Cys^{24}-Cys^{40}, and Cys^{27}-Cys^{53}; Katayama et al., 2001; Nakatsuji et al., 2009; Webster et al., 2012). The MIH precursor contains a signal peptide 35 amino acids in length, in addition to the mature MIH peptide (Nakatsuji et al., 2009; Webster et al., 2012). MIH release from the eyestalk is pulsatile in nature, and its half-life in the hemolymph is between 5 to 10 minutes (Chung and Webster, 2005). The MIH receptor is hypothesized to be a G-protein coupled receptor (Kozma et al., 2024; Mykles, 2024). A subclade of Class A GPCRs identified in brachyurans, A34β, possesses an additional two-stranded β-sheet in the second extracellular loop, which may play a role in high-affinity binding to MIH (Kozma et al., 2024).

Binding of MIH to its receptor initiates a second messenger-mediated signaling cascade within the YO beginning with a brief increase in cAMP, followed by a prolonged increase in cGMP (Fig. 1.3; Mattson and Spaziani, 1985a; 1986a; 1986b; Saidi et al., 1994; Spaziani et al., 1999; Spiessberger et al., 2009; Mykles, 2021). MIH signaling through the action of cAMP and cGMP is well established, although the effects and relative importance of cGMP appears to be greater than that of cAMP in the majority of species, likely because of the sustained increase in cGMP relative to cAMP (reviewed in Covi et al., 2012). The involvement of cAMP and cGMP in the YO was determined by measuring intracellular cAMP and cGMP levels, using cyclic nucleotide analogs to activate respective protein kinases, and using various inhibitors of phosphodiesterases (PDEs; Mattson and Spaziani, 1985a; 1985a; 1986a; 1986b; Sedlmeier and Fenrich, 1993; Saidi et al., 1994; Nakatsuji et al., 2006; Covi et al., 2009; Nakatsuji et al., 2009). The activity of cyclic nucleotide monophosphates is generally mediated through the binding and activation of cyclic nucleotide-dependent kinases (Lorenz et al., 2017). Kinase activity assays to measure the activation of cAMP-dependent protein kinase (PKA) and cGMP-dependent protein kinase (PKG) in the YO upon incubation with MIH confirmed the involvement of cyclic nucleotide dependent protein kinases in MIH signaling (Vongliscynski and Sedlmeier, 1993; Böcking and Sedlmeier, 1994; Baghdassarian et al., 1996).

PKA activation triggers an influx of Ca^{2+}, activating calmodulin (CaM), which then activates nitric oxide synthase (NOS) directly by allosteric activation and indirectly by activating Ca^{2+}/CaM-dependent calcineurin (CaN), a phosphatase which dephosphorylates NOS (Covi et al., 2008; Mykles et al., 2010; Covi et al., 2012). Crustaceans only express one isoform of NOS, which contains a CaM-binding domain, indicating that crustacean NOS is most similar to mammalian eNOS and nNOS (Kim et al., 2004; McDonald et al., 2011). In the activated YO,

NOS is phosphorylated, suggesting that inactivation of NOS is a prerequisite for increased ecdysteroid synthesis (Lee and Mykles, 2006).

Incubation of the YO with NO donors or GC-I agonists inhibits ecdysteroid secretion *in vitro*, indicating a functional NO/cGMP signaling pathway (Covi et al., 2008). NO-dependent soluble guanylyl cyclase (GC-I) activation by NOS activity produces cGMP. cGMP is well established as a second messenger of MIH, and PKG activity is stimulated in the YO *in vitro* when incubated with cGMP and cGMP analogs (see Covi et al., 2009; Mykles et al., 2010; Chang and Mykles, 2011; Covi et al., 2012; Mykles, 2021). However, the downstream targets of PKG that result in inhibition of ecdysteroidogenesis remain unidentified.

In addition to the inhibitory regulation of MIH in the YO, other factors may stimulate ecdysteroid synthesis. Mattson and Spaziani demonstrated that incubation of YOs with Ca^{2+} ionophore, phosphatidylserine, and phorbol 12-myristate 13-acetate (PMA) *in vitro* stimulates ecdysteroid synthesis in *R. antennarium* (Mattson and Spaziani, 1987). This activation also overcame the inhibitory effects of incubation with sinus gland extract (MIH equivalents) and cAMP and was unaffected by a Ca^{2+} channel blocker. Taken together, these results indicate that protein kinase C (PKC) may play a stimulatory role in ecdysteroid synthesis in a pathway independent from MIH signaling (Mattson and Spaziani, 1987). Further, 99 GPCRs are transcriptionally expressed in the *G. lateralis* YO, indicating a highly complex network of signals aiming to regulate the production of ecdysteroids (Tran et al., 2019).

Conversion of cholesterol to ecdysteroid occurs through a series of reactions beginning with a Rieske oxygenase encoded by the gene *Neverland* (*Nvd*), resulting in 7-dehydrocholesterol (7DC). Subsequent conversion of 7DC to 5β-diketol is referred to as the "Black Box", as the enzymatic reactions that take place have yet to be fully characterized. A

series of hydroxylations by a group of cytochrome p450 monooxygenases encoded by Halloween genes (*Phantom/Phm*, *Disembodied/Dib*, *Spook/Spo*, and *Shadow/Sad*) results in ecdysone. Finally, a 20-hydroxylase *Shed* in decapods and *Shade* in insects converts ecdysone to the active form 20-hydroxyecdysone (20E; reviewed in Mykles, 2011; Lafont et al., 2021).

Regulation of ecdysteroid synthesis in insects

Ecdysteroids in insects stimulate metamorphic molts between larval, pupal, and adult stages. Ecdysteroid synthesis takes place in the insect prothoracic gland (PG) and is under stimulatory control, as opposed to the inhibitory regulation of MIH seen in decapods. Prothoracicotropic hormone (PTTH) is a neuropeptide secreted by the neurosecretory *corpus cardiacum*. PTTH is the primary stimulatory factor the regulates ecdysteroid production in the PG. The mature PTTH peptide is 109 amino acids in length and contains six cysteine residues which form three cysteine bonds, and a seventh conserved cysteine which forms an intermolecular bond to produce a homodimer (reviewed in Belles, 2020). The production of PTTH is highly coordinated by environmental cues including photoperiod and physiological cues, such as nutrient availability that is dependent on developmental stage (Gontijo and Garelli, 2018; Belles, 2020; Kannangara et al., 2021).

PTTH binds to a receptor tyrosine kinase (RTK; Rewitz et al., 2009) and activates a signaling cascade mediated by Ca^{2+} and cAMP (Fig. 1.4; reviewed in Mykles et al., 2010; Covi et al., 2012; Belles, 2020). Several protein kinases are activated by PTTH signaling, including PKA, protein kinase C (PKC), mitogen activated protein kinase (MAPK), phosphatidylinositol 3-linase (PI3K), and p70S6 kinase (S6K; Belles, 2020). Another neuropeptide, pigment dispersing hormone (PDF), has also been shown to stimulate ecdysteroid synthesis through binding to a GPCR (Iga et al., 2014; Belles, 2020). Insulin-like peptides (ILPs), also regulate ecdysteroid

synthesis in the PG. The ILP superfamily consists of insulin, insulin-like growth factors (IGF), and relaxins (Gontijo and Garelli, 2018). In insects, ILPs 2, 3, and 5 stimulate ecdysteroid synthesis in the PG, and are regulated primarily by critical weight of larvae (Kannangara et al., 2021). Conversely, the relaxin ILP8 (Dilp8), is secreted by damaged imaginal discs and attenuates ecdysteroid production, allowing time for regeneration of imaginal discs before metamorphic molts (Kannangara et al., 2021). Dilp8 directly inhibits ecdysteroid production in the PG by binding to a leucine-rich-repeat containing GPCR, Lgr3, and activating NOS (Jaszczak et al., 2016). Dilp8 indirectly inhibits ecdysteroid production by binding to Lgr3 in the *corpus cardiaca* and inhibiting the release of PTTH (Gontijo and Garelli, 2018; Kannangara et al., 2021). The regulation of ecdysteroid synthesis by PTTH, PDF, and ILPs converge on mTOR, which regulates the translation of ecdysteroid-synthesis genes (Belles, 2020). Similarities between YO and PG signaling pathways, yet differences in the respectively inhibitory or stimulatory mechanisms that regulate ecdysteroid synthesis, provide an evolutionary question about the divergence of these pathways between insects and (non-insect) crustaceans.

Mechanistic target of rapamycin (mTOR)

mTOR integrates a range of cellular inputs including nutrients and metabolic state, environmental cues, stress responses, and growth signals and coordinates the subsequent metabolic response of a cell to maintain metabolic homeostasis (Szwed et al., 2021; Panwar et al., 2023). mTOR is a serine/threonine protein kinase in the phosphoinositide kinase-related kinase (PIKK) family and is evolutionarily conserved from yeast to humans to crustaceans (Abuhagr et al., 2014b; Shi and Collins, 2023). Two large protein complexes, mTOR complex 1 (mTORC1) and mTOR complex 2 (mTORC2) contain mTOR as the catalytic subunit and are distinguished by differences in accessory proteins and substrates (Shi and Collins, 2023).

mTORC1 promotes protein synthesis, lipid metabolism, nucleotide synthesis, glycolysis, and mitochondrial biogenesis and suppresses autophagy and lysosomal biogenesis. mTORC2 primarily mediates cellular functions involved in cell survival and the organization of the cytoskeleton (reviewed in Liu and Sabatini, 2020; Szwed et al., 2021; Panwar et al., 2023; Shi and Collins, 2023).

Both complexes contain mTOR and mammalian lethal with SEC13 protein 8 (mLST8); while mTORC1 contains the regulatory-associated protein of mTOR (RAPTOR) and mTORC2 contains the rapamycin-insensitive companion of mTOR (RICTOR; Liu and Sabatini, 2020; Shi and Collins, 2023). DEP-domain-containing mTOR-interacting protein (DEPTOR) acts as an endogenous inhibitor of both mTOR complexes (Liu and Sabatini, 2020). mTORC1 is inhibited by rapamycin, as rapamycin-bound FKBP12 (FK506-binding protein of 12 kDa) blocks the active site of mTOR (Panwar et al., 2023). As suggested by the name of the mTORC2 companion RICTOR, mTORC2 is insensitive to rapamycin.

As ecdysteroid synthesis in the molting gland is dependent upon activation of mTORC1 (Abuhagr et al., 2014b; Abuhagr et al., 2016; Shyamal et al., 2018; Mykles, 2021), the remainder of this section will focus only on mTORC1. Canonical mTORC1 activation relies on a number of highly conserved proteins (Fig. 1.5; Shi and Collins, 2023). Direct activation of mTORC1 begins with amino-acid sensing Ras-related GTPases (RAGs) which translocate mTORC1 to the lysosomal surface (Liu and Sabatini, 2020; Shi and Collins, 2023). Here, mTORC1 interacts with another GTPase, Rheb (Ras homolog enriched in brain), which resides on the lysosomal membrane. In its GTP-bound form, Rheb allosterically activates mTOR (Liu and Sabatini, 2020; Shi and Collins, 2023). Upstream of this process, the tuberous sclerosis complex (TSC; a complex of hamartin-tuberin also known as TSC1-TSC2) induces the GTPase activity of Rheb

and inhibits the subsequent activation of mTORC1. TSC is highly regulated by phosphorylation and contains thirteen characterized phosphorylation sites, which can either activate or inhibit TSC (Ranek et al., 2019). Phosphorylation of TSC2 by protein kinase B (AKT), extracellular signal-regulated kinase (ERK), ribosomal S6 kinase 1 (RSK-1), and inhibitor of nuclear factor kappa-B kinase subunit β (IKKβ) inhibits TSC, thus activating mTORC1. Phosphorylation of TSC2 by AMP-activated protein kinase (AMPK) and glycogen synthase kinase 3β (GSK-3β) activate TSC, thus inhibiting mTORC1 (Fig. 1.5; reviewed in Liu and Sabatini, 2020; Szwed et al., 2021; Panwar et al., 2023; Shi and Collins, 2023).

The second messenger cyclic nucleotides cAMP and cGMP both play important regulatory roles in mTORC1 activation. Of course, these roles are not straightforward and whether they activate or inhibit mTORC1 depends on the cell type, signaling context, and physiological state of the cell (Shi and Collins, 2023). The cGMP/PKG pathway inhibits mTORC1 in human and mouse cardiomyocytes. This inhibition occurs through natriuretic peptide-stimulated cGMP synthesis, and subsequent PKG1 phosphorylation of TSC2 at Ser1365 and Ser1366 (Ranek et al., 2019; Oeing et al., 2020; Oeing et al., 2020). Conversely, in mouse brown adipose tissue, PKG activation by natriuretic peptides results in the direct phosphorylation of Raptor at Ser791 and consequent activation of mTORC1 (Liu et al., 2018). Whether this phosphorylation was a result of PKG1 or PKG2 was not examined.

To emphasize the point, ecdysteroid synthesis in the molting gland is dependent upon activation of mTORC1 (Abuhagr et al., 2014b; Abuhagr et al., 2016; Shyamal et al., 2018; Mykles, 2021). *In vitro* incubation of YOs with rapamycin as well as ESA followed by injection of rapamycin both inhibit ecdysteroid synthesis (Abuhagr et al., 2014b; Abuhagr et al., 2016; Shyamal et al., 2018). *mTOR*, *Rheb, AKT,* and *S6K* transcripts are upregulated in the YO of land

crabs stimulated to molt by either MLA or ESA (Abuhagr et al., 2014b; Abuhagr et al., 2016; Das et al., 2016; Shyamal et al., 2018). Additionally, YO transcript expression of ecdysteroid synthetic genes *Nvd, Phm, Spo, and Dib* were high not only in premolt but also during intermolt, indicating that the YO is primed for activation but decreased translation of these genes keeps ecdysteroid synthesis low (Benrabaa et al., 2023; Mykles, 2024).

cGMP-DEPENDENT PROTEIN KINASE

Post-translational modification (PTM) of proteins allow cells to respond rapidly to changes in their biological environment more quickly and efficiently than the time and energy required to synthesize completely new proteins (Zhong et al., 2023). Among PTMs, phosphorylation is both the most common and arguably the most important in terms of cell signaling (Tarrant and Cole, 2009; Ardito et al., 2017; Zhong et al., 2023). In humans, 586 different protein kinases and 186 phosphatases have been identified (Ardito et al., 2017). Kinases can be organized into seven major groups, of which the AGC kinases are one (Fig. 1.6A; Leroux et al., 2018). AGC kinases are serine/threonine kinases that include cAMP-dependent protein kinase (PKA), cGMP-dependent protein kinase (PKG), and protein kinase C (PKC), among several other closely related kinases (Fig. 1.6B; Ardito et al., 2017; Leroux et al., 2018).

Structure of PKG

PKG is encoded by two genes, *pkg1* and *pkg2*, and alternative splicing of the N-terminal of *pkg1* yields two isoforms- PKG1α and PKG1β (Gamm et al., 1995; Ørstavik et al., 1997). PKG is a homodimer of two identical polypeptides (i.e., either PKG1α, PKG1β, or PKG2) that contain both regulatory and catalytic subunits (Hofmann, 2020). The regulatory (R) domain of PKG is located in the N-terminal region and includes a leucine-zipper (LZ) motif, an

autoinhibitory (AI) site, and two cGMP-binding domains. The kinase domain is located in the C-terminal region (Fig. 1.7; Alverdi et al., 2008; Francis and Corbin, 2013; Hofmann, 2020).

The LZ mediates the formation of the PKG homodimer, and alternative spicing of *pkg1* yields two unique LZ domains that determine the subcellular location and activation of PKG1α and PKG1β (Hofmann, 2005; Francis and Corbin, 2013; Hofmann, 2020). The AI site is a pseudosubstrate that interacts with the kinase catalytic cleft in the kinase domain of the other monomer of the PKG homodimer (Kim and Sharma, 2021). Binding of cGMP induces a conformational change that allows binding of ATP by the catalytic domain, and subsequent autophosphorylation of the AI site releases it from the catalytic cleft, resulting in PKG activation (Wall et al., 2003; Alverdi et al., 2008).

Roles of PKG in model organisms

While PKGs are present in eukaryotic organisms ranging from ciliates to mammals, the characterization of PKGs has occurred primarily in mammalian and *Drosophila* systems for their respective roles in cardiovascular homeostasis and foraging behavior (Kalderon and Rubin, 1989; Allen et al., 2017; Anreiter et al., 2017; Allen et al., 2018; Hofmann, 2018; Leroux et al., 2018; Ranek et al., 2019; Oeing et al., 2020). In mammals, a longer dimerization domain found in PKG1β results in a decreased sensitivity to cGMP, requiring about a 10-fold higher cGMP concentration for activation than PKG1α (Ruth et al., 1997; Casteel et al., 2005; Casteel et al., 2010; Francis and Corbin, 2013); reviewed in (Hofmann, 2020).

In addition to the previously discussed role of PKG1 in mTORC1 regulation, PKG1 also mediates the tone of smooth muscle cells by inducing relaxation (Schröder, 2022). PKG1 phosphorylates and inactivates Rho-kinase, which maintains myosin light chain (MLC) phosphatase in an active state and induces dephosphorylation of MLCs and subsequent

relaxation of smooth muscle cells (Kato et al., 2012). PKG1α also binds to Rho-A, thereby inhibiting activation of Rho-kinase, allowing for dephosphorylation of MLCs by MLC-phosphatase (Schröder, 2022).

Another fascinating role of mammalian PKG1 involves nuclear compartmentalization and regulation of gene expression. PKG1 contains a nuclear localization signal (NLS) near the ATP-binding region of the kinase domain (Gudi et al., 1997). Proteolytic cleavage of PKG1 is required for nuclear translocation of the enzyme (Gudi et al., 1996; Gudi et al., 1997; Gudi et al., 2000; Kato et al., 2013; Chen and Roberts, 2014). Cleavage of PKG1 removes the LZ and AI, resulting in a constitutively activated C-terminal fragment called PKG1γ (Kato et al., 2013). The proteolytic enzyme that cleaves PKG1 has not been identified, but is hypothesized to be a proprotein convertase named furin (Kato et al., 2013). PKG1γ has been shown to activate cAMP-responsive binding protein (CREB) and general transcription factor 2 (TFII-I), and increase the expression of transcription regulators *c-fos* and *JunB* (Gudi et al., 1996; Gudi et al., 1997; Gudi et al., 2000; Kato et al., 2013; Chen and Roberts, 2014). Inositol 1,4,5-triphosphate receptor-associated cGMP-kinase substrate (IRAG) translocates PKG1β to the membrane of the endoplasmic reticulum where the complex mediates Ca^{2+} release (Casteel et al., 2008). IRAG binding prevents proteolysis and nuclear translocation of PKG1β, but not PKG1α, indicating that IRAG binds to a region of the N-terminus that differs between the two isoforms (Casteel et al., 2008).

In *Drosophila*, the two genes which encode for PKGs are conserved, although the naming convention is opposite to that of the nomenclature for mammalian PKGs (MacPherson et al., 2004; Anreiter et al., 2017; Allen et al., 2018). *dg1* encodes a protein most similar to mammalian PKG2, while *dg2* encodes several proteins most similar to mammalian PKG1 (Morton and

Hudson, 2002; MacPherson et al., 2004; Vasquez et al., 2023). *Dg2*, is also known as *foraging* (*for*), and consists of twelve exons and encodes twenty-two splice variants (Vasquez et al., 2023). Eight putative protein isoforms, P1, P1α, and P2-7, are encoded by the 22 *for* transcripts. The majority of differences in these transcripts occurs through alternative splicing of exons encoding the LZ domain, although two transcripts encode proteins that lack LZ and AI domains, and one of those also has a truncated cGMP-binding domain (Vasquez et al., 2023).

Discussion of the role of PKG2 is notably absent. In mammals, PKG1 has been the main focus of study for decades, primarily because of its identified role in smooth muscle relaxation and cardiac health. PKG2 has been primarily characterized for its role in mediating ion balance in epithelial cells of the intestine (Wang et al., 2014,Vaandrager, 2005 #126). PKG2 is also highly expressed in neurons (De Vente et al., 2001). Many studies completely fail to mention PKG2, or fail to distinguish which PKG isoform was examined, although further study usually reveals that PKG1 is involved.

Roles of PKG in decapods

In decapods, PKGs are involved in several processes in a tissue-dependent manner. The role of PKG in MIH signaling in the YO has been previously discussed in this chapter. Of note, in *G. lateralis*, a PKG-encoding transcript was highly expressed in YOs of intact, intermolt males, and expression decreased with progression towards molting in response to MLA and ESA (Das et al., 2018; Shyamal et al., 2018).

In the Pacific white shrimp *L. vannamei*, vitellogenesis is stimulated by the accumulation of vitellin in the oocytes. Vitellogenin, a precursor of vitellin, is synthesized in the hepatopancreas, and its synthesis is under inhibitor control by type-II vitellogenin-inhibiting hormone (VIH-2). VIH-2 signaling in the hepatopancreas initiates NO-independent

GC/cGMP/PKG signaling, and PKG is presumed to activate MAPK signaling, which leads to the inhibition of vitellogenin transcript expression (Chen et al., 2018). Also, CHH binding to gill tissue activates PKG, PKA, and PKC pathways to regulate ammonia secretion and ion balance (Zhang et al., 2020).

SUMMARY AND RESEARCH OBJECTIVES

Understanding crustacean molting is key to developing sustainable aquaculture practices, ecosystem and fisheries management, and identifying and mitigating the effects of endocrine disruptors in agricultural runoff and climate change. Although the stimulatory or inhibitory mechanisms that govern ecdysteroid synthesis differ in insects and crustaceans respectively, the role of mTOR in the YO and PG is conserved. The study of mechanisms regulating crustacean molting can broadly inform research regarding molting in arthropods. For example, endocrine disruptors used in agriculture to mitigate nuisance insects also have endocrine disrupting effects on crustaceans encountering the chemicals through runoff (Knigge et al., 2021).

The crustacean YO is an ideal model for the integration of physiological, transcriptomic, and proteomic data into a "phenomic" model. The YO has only one identified function, to produce ecdysteroids, yet is regulated at transcriptional, translational, and post-translational levels from multiple inputs. Thus, the effect of numerous conditions, from environmental to physiological, can be quantified through measurements of ecdysteroid synthesis, transcript and protein expression, and post-translational modifications.

The goal of this dissertation is to identify a link between the MIH signaling pathway and mTORC1-dependent ecdysteroid synthesis in the YO, by examining the role of PKG. Several lines of evidence indicate that MIH-activated PKG in the YO inhibits ecdysteroid synthesis through both direct and indirect inhibition of mTORC1: 1) the role of cGMP in MIH signaling,

2) the convergence of pathways on mTOR in both the YO of decapods and the PG of insects, and 3) evidence of direct and indirect regulation of mTORC1 activity by PKG in mammals (Fig. 1.8). Examination of this hypothesis is addressed in the four chapters that follow. Chapter 2 presents a phylogenetic characterization of PKG-encoding transcripts across pancrustaceans and presents the effects of inhibition of both PKG1 and PKG2 on ecdysteroid synthesis. Chapter 3 reports changes in transcript expression of PKG isoforms in the decapod YO in each molt stage, as well as tissue-specific expression of PKGs. Chapter 4 examines the global and phospho-proteome of the YO in response to both MIH signaling and concurrent PKG inhibition. Finally, Chapter 5 summarizes these findings and presents an updated hypothesis regarding the role of PKGs in the YO.

Table 1.1. Relationship between YO state and traits, circulating ecdysteroid titers, condition of the exoskeleton, and limb regenerates at each stage of the molting cycle.

Molt Stage	**C_4 Intermolt**	**D_0 Early Premolt**	**D_1 Mid Premolt**	**$D_{2,3}$ Late Premolt**	**D_4 Late Premolt**	**E Ecdysis**	**A Early Postmolt**	**B Postmolt**	**C_{1-3} Late Postmolt**
Description	Anecdysis	Proecdysis				Ecdysis	Metecdysis		
YO State	Basal	Activated	Committed	Committed	Repressed	Repressed	Repressed	Repressed	Repressed
YO Synthetic Capacity	Basal	Increasing	High	High	High	Low	Low	Low	Low
Ecdysteroid Titers	Basal	Medium	High	High	Low	Low	Low	Low	Low
YO Sensitivity to MIH	High	High	Low	Low	Low	-	High	High	High
Exoskeleton	Complete & sclerotized	Complete, beginning to dissolve membranous layer	Enlargement of epidermal cells, apolysis of membranous layer continues; Synthesis of new epicuticle and exocuticle; Ca^{2+} absorbed and deposited into gastroliths	Membranous layer completely dissolved; Synthesis of new exoskeleton continues	New epicuticle and exocuticle completely synthesized	-	Epicuticle and exocuticle are soft	Formation of the endocuticle begins	Synthesis of endocuticle continues, membranous layer formed in stage C_3
Limb Regeneration	Formation of basal regenerates, tissue is differentiated	Majority of growth into "limb bud", segments observable	Limb bud continues to grow	Limb buds at maximal size	Limb buds at maximal size	-	-	-	-
R-Index	0 - 10	10.1 - 15	15.1 - 23	≥ 23	-	-	-	-	-

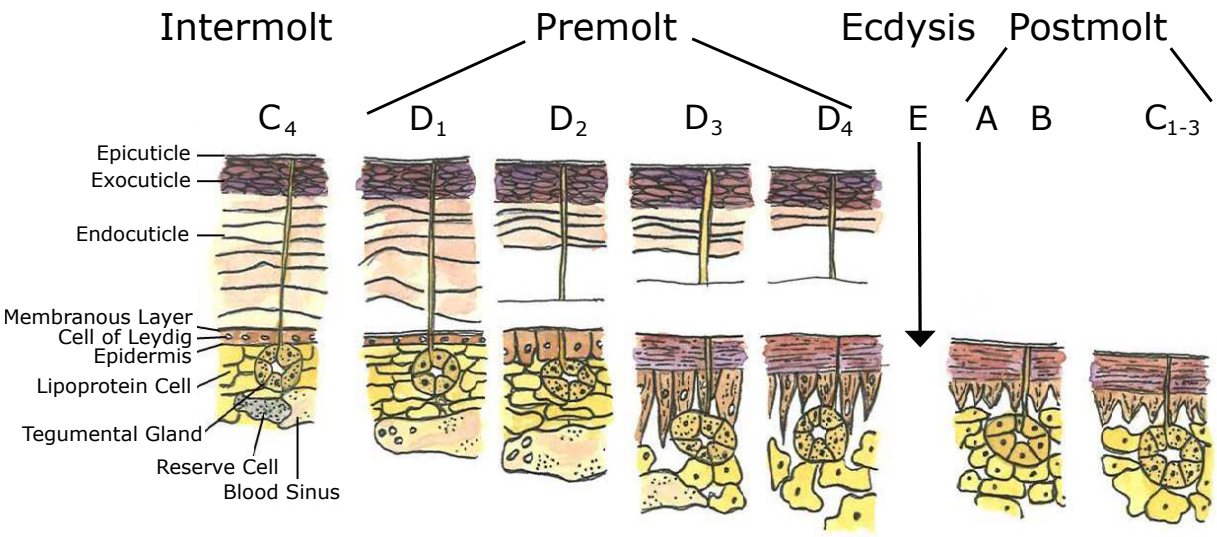

Figure 1.1. Integumentary changes in the crustacean exoskeleton with progression through the molt cycle. Figure from (Head, 2017), based on (Skinner, 1962).

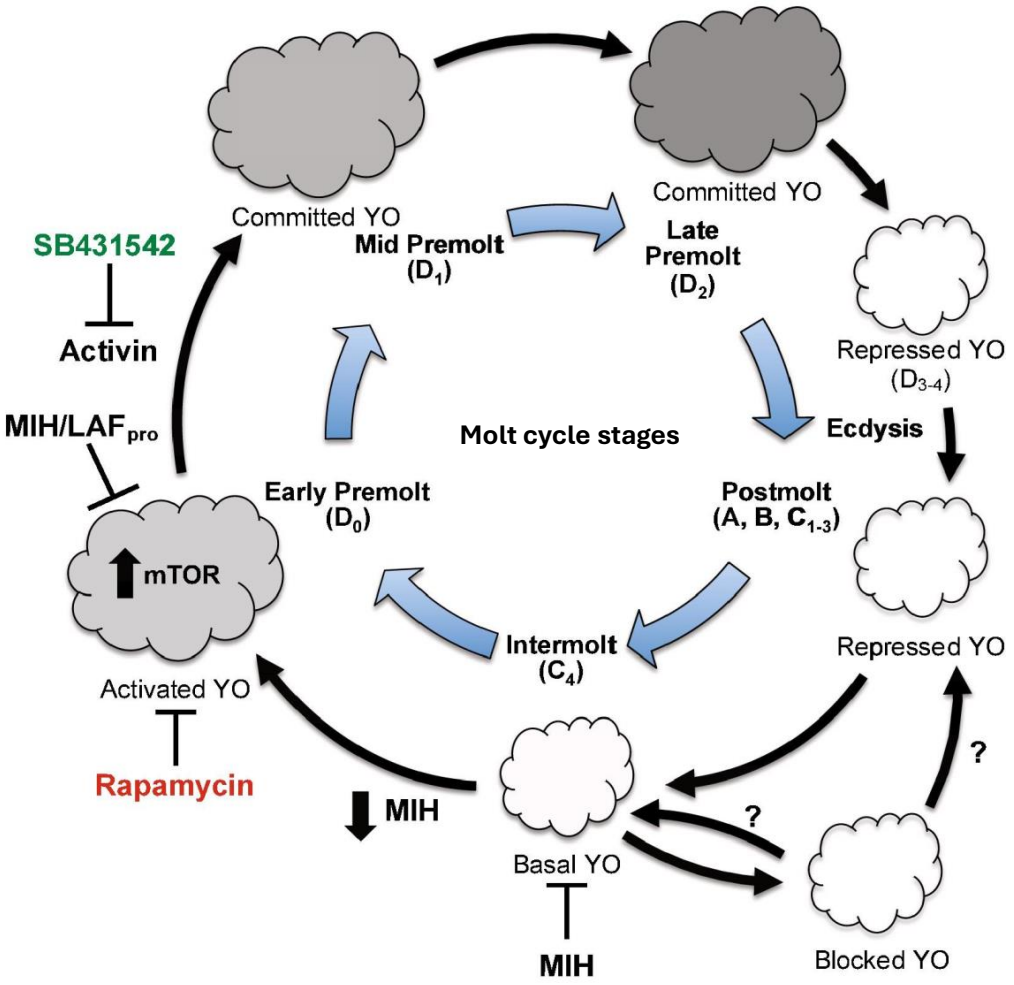

Figure 1.2. YO regulation over the molt cycle in *G. lateralis*. The YO transitions through basal, activated, committed, and repressed phenotypes at intermolt (stage C_4), early premolt (stage D_0), mid/late premolt (stages D_1 and D_2), and postmolt (stages A, B, and C_{1-3}), respectively. During intermolt, MIH release from the eyestalk X-organ/sinus gland complex maintains the YO in the basal state. Reduced MIH release activates the YO via mTOR, which is inhibited by rapamycin. TGFβ/Activin signaling, which is inhibited by SB431542, mediates YO transition from the activated to committed phenotype. Elevated ecdysteroid titers at the end of premolt are hypothesized to drive the transition to the repressed phenotype. Some animals enter a blocked state, in which animals are refractory to molt induction by multiple leg autotomy. Basal and activated YOs are sensitive to MIH, CHH, and limb autotomy factor-proecdysis (LAF_{pro}), which is secreted by limb regenerates; committed and repressed YOs are refractory to MIH, CHH, and LAF_{pro}. Size indicates YO hypertrophy and shading indicates relative ecdysteroidogenic activity (lowest in postmolt; highest in D2). From Mykles (2020).

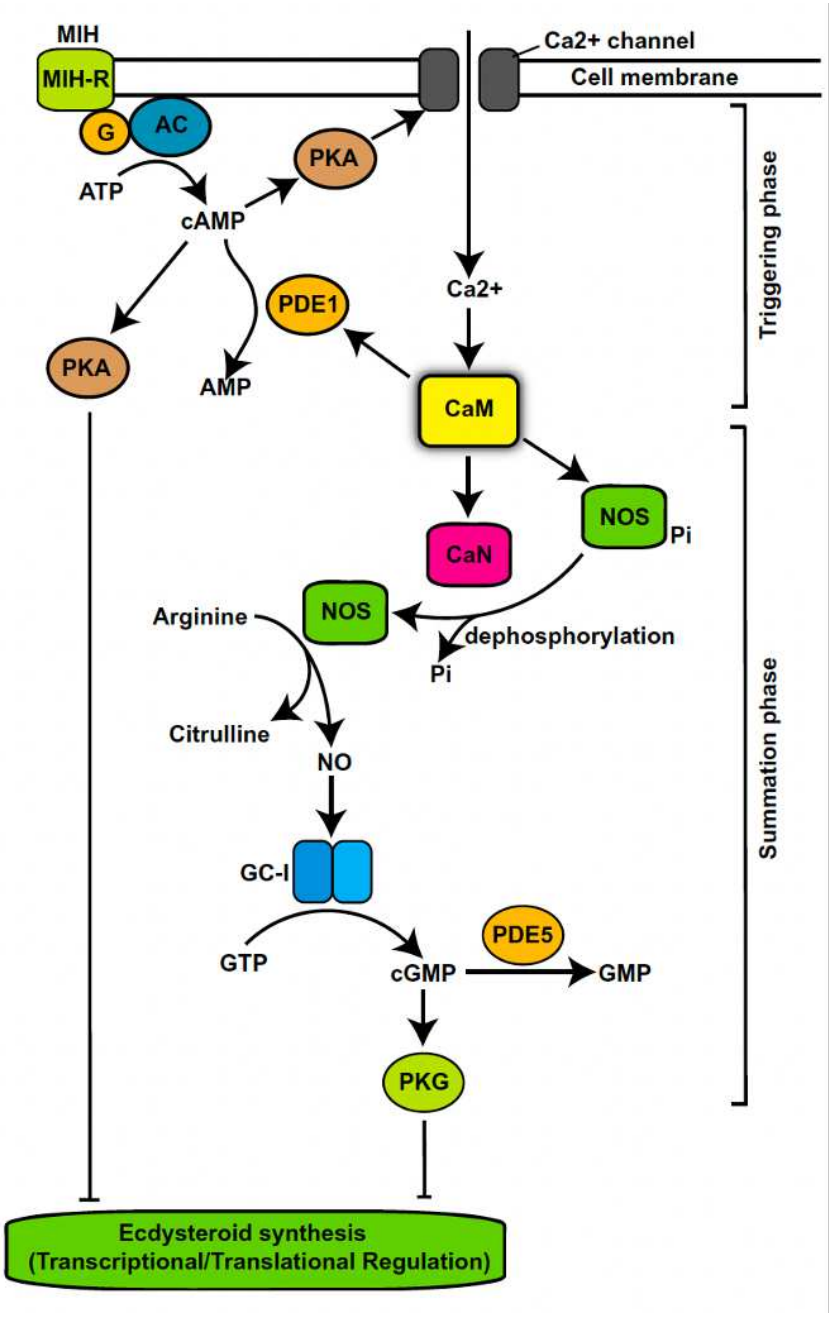

Figure 1.3. Proposed signaling pathway of MIH in the decapod YO. MIH binds to a G-protein coupled receptor, activating the production of cAMP by adenylyl cyclase (AC). cAMP-dependent protein kinase (PKA) binds cAMP and causes a transient Ca^{2+} influx. Calmodulin (CaM) bound to Ca^{2+} allosterically activates nitric oxide synthase (NOS) and activates the phosphatase calcineurin (CaN). Dephosphorylation and allosteric activation of NOS results in the synthesis of nitric oxide (NO)from the conversion of arginine to citrulline. A soluble NO-dependent guanylyl cyclase (GC) produces a sustained cGMP signal, activating cGMP-dependent protein kinase (PKG). Activation of PKG results in downstream inhibition of ecdysteroid synthesis, presumably through mTORC1 inhibition. Figure from Chang and Mykles (2011).

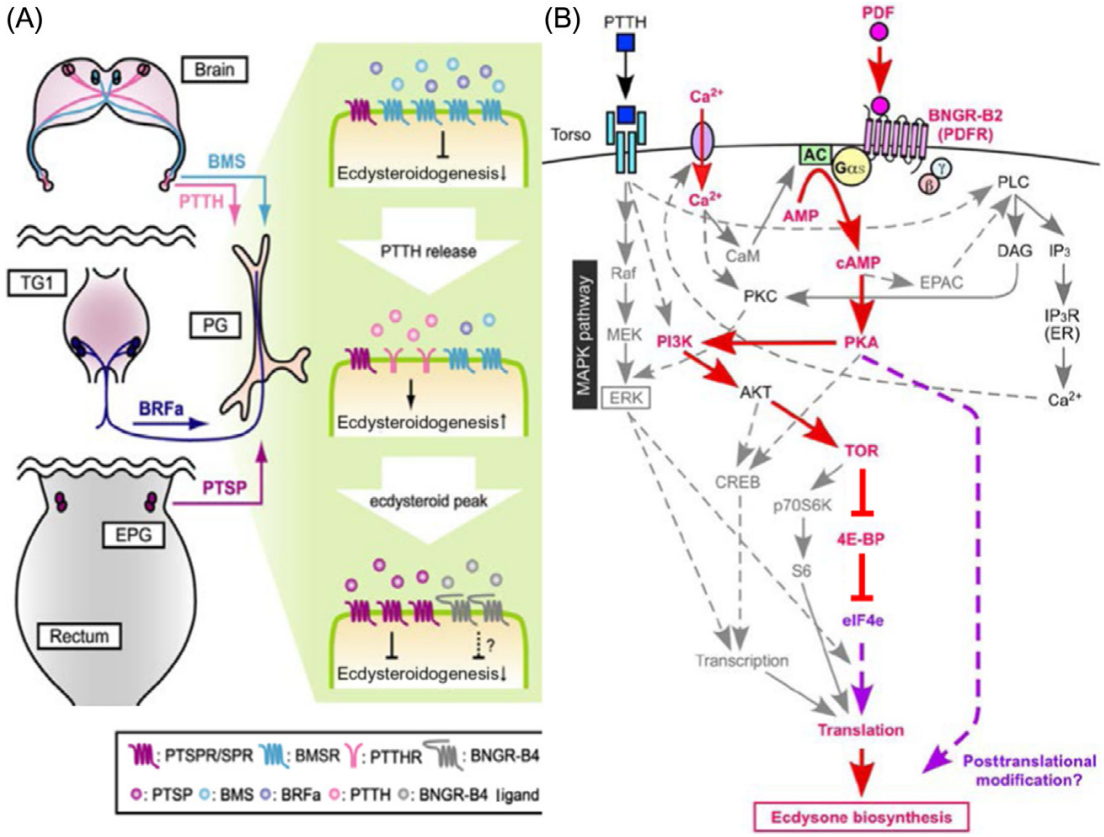

Figure 1.4. Regulation of ecdysteroid synthesis in the insect prothoracic gland. This figure is based on studies in the silk moth *Bombyx mori.* (A) Regulation of ecdysteroid synthesis in the PG is mediated by numerous neuropeptides. Bommo-myosuppressin (BMS), produced in the brain, and Bommo-FMRFamide (BRFa), produced in the prothoracic ganglion (TG1), inhibit ecdysteroidogenesis in the PG. Prothoracicotropic hormone (PTTH) release by the brain (specifically the corpora cardiaca) is temporally regulated and stimulates ecdysteroidogenesis. Following a peak in ecdysteroid secretion, prothoracicostatic peptide (PTSP) and the BNGR-B4 ligand suppress further ecdysteroidogenesis. (B) Multiple signaling pathways regulate ecdysteroid synthesis in the insect PG. PTTH activates numerous kinases including the mitogen-activated protein kinase (MAPK) pathway, protein kinase C (PKC), protein kinase A (PKA), and the target of rapamycin (TOR). Pigment-dispersing factor (PDF) also converges on TOR, although it has an inhibitory effect on ecdysteroidogenesis by inhibiting TOR. Abbreviations: 4E-BP, eIF4E-binding protein; AC, adenylate cyclase; AKT, protein kinase B; AMP, adenosine monophosphate; CaM, calmodulin; cAMP, cyclic AMP; CREB, cAMP response element-binding protein; DAG, diacylglycerol; eIF4e, eukaryotic translation initiation factor 4E; EPAC, exchange protein directly activated by cAMP; ERK, extracellular signal-regulated kinase; Gαs, G protein αs subunit; IP3, inositol 1,4,5-trisphosphate; IP3R, IP3 receptor; MAPK, mitogen-activated protein kinase; MEK, MAP kinase kinase; p70S6K , 70 kDa S6 kinase; PKA, protein kinase A; PKC, protein kinase C; PI3K, phosphatidylinositol 3-kinase; PLC, phospholipase C; Raf, MAP kinase kinase kinase; S6, ribosomal protein S6; TOR, target of rapamycin. From Belles (2020) Chapter 7.

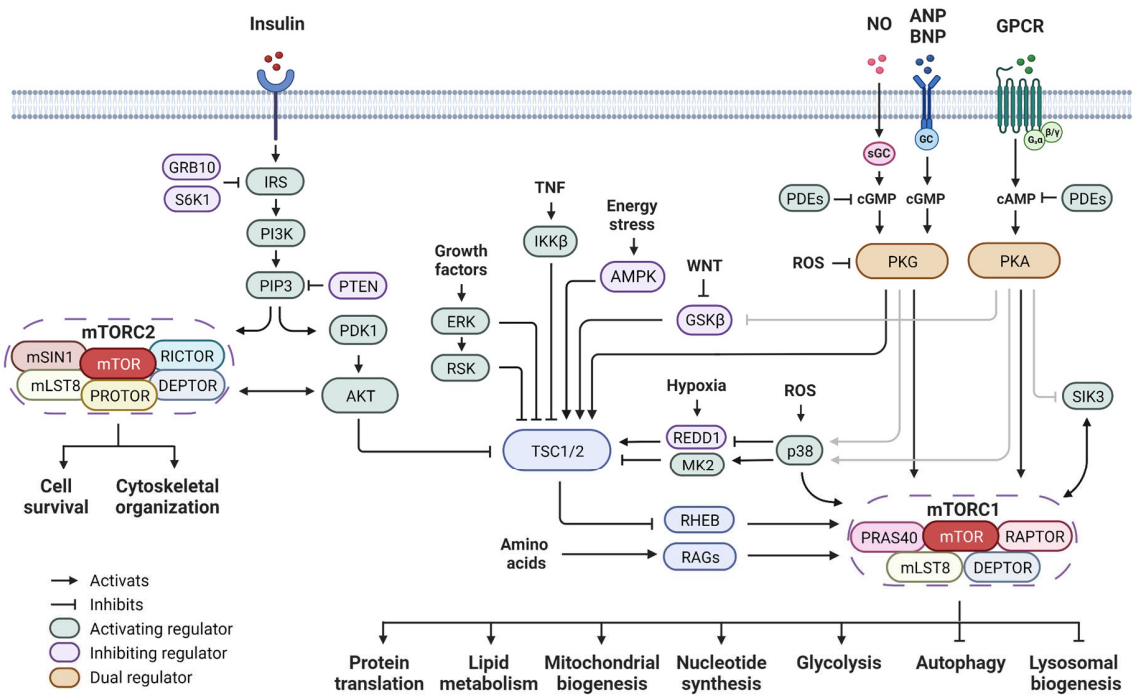

Figure 1.5. Canonical signaling pathways that activate or inhibit mTORC1 and mTORC2. mTORC1 activity is regulated by growth factors, tumor necrosis factor (TNF), metabolic stress, hypoxia, reactive oxygen species, nitric oxide, natriuretic peptides, and various ligands of GPCRs. cGMP-dependent protein kinase (PKG) can stimulate mTORC1 directly or inhibit it indirectly by phosphorylation and activation of the tuberous sclerosis complex (TSC1/2), depending on the cellular context. mTORC1 positively regulates protein translation, lipid metabolism, mitochondrial biogenesis, nucleotide synthesis, and glycolysis and inhibits autophagy and lysosomal biogenesis. mTORC2 primarily integrates insulin signaling to regulate cell survival and cytoskeletal organization. Abbreviations: AKT, protein kinase B; AMPK, AMP-activated protein kinase; ANP, atrial natriuretic peptide; BNP, B-type natriuretic peptide; cAMP, cyclic adenosine monophosphate; cGMP, cyclic guanosine monophosphate; DEPTOR, DEP domain-containing mTOR-interacting protein; ERK, extracellular signal-regulated kinase; GC, guanylyl cyclase; sGC, soluble guanylyl cyclase; GPCR, G protein-coupled receptor; GRB10, growth factor receptor bound protein 10; GSK , glycogen synthase kinase 3; IKK, inhibitor of nuclear factor kappa-B kinase subunit beta; MK2, MAPK activated protein kinase 2; mLST8, mammalian lethal with SEC13 protein 8; mSIN1, mammalian stress activated protein kinase-interaction protein 1; NO, nitric oxide; p38 MAPK, p38 mitogen-activated protein kinases; PDK1, phosphoinositide-dependent protein kinase 1; PI3K, phosphoinositide 3-kinase; PIP3, phosphatidylinositol 3,4,5-triphosphate; PKA, cAMP-dependent protein kinase; PKG, cGMP-dependent protein kinase; PRAS40, proline-rich AKT substrate of 40 kDa; PROTOR, protein observed with RICTOR; PTEN, phosphatase and tensin homolog; RAGs, Ras-related GTPases; REDD1, regulated in development and DNA damage responses 1; RHEB, Ras homolog mTORC1 binding; RICTOR, rapamycin-insensitive companion of mTOR; ROS, reactive oxygen species; RSK, ribosomal S6 kinase 1; SIK3, salt-inducible kinase 3; TNF, tumor necrosis factor; TSC1/2,tuberous sclerosis complex 1/2; WNT, wingless and lnt-1;IRS, insulin receptor substrate; mTOR, mechanistic target of rapamycin; PDEs, phosphodiesterases; RAPTOR, regulatory-associated protein of mTOR. From Shi and Collins (2023).

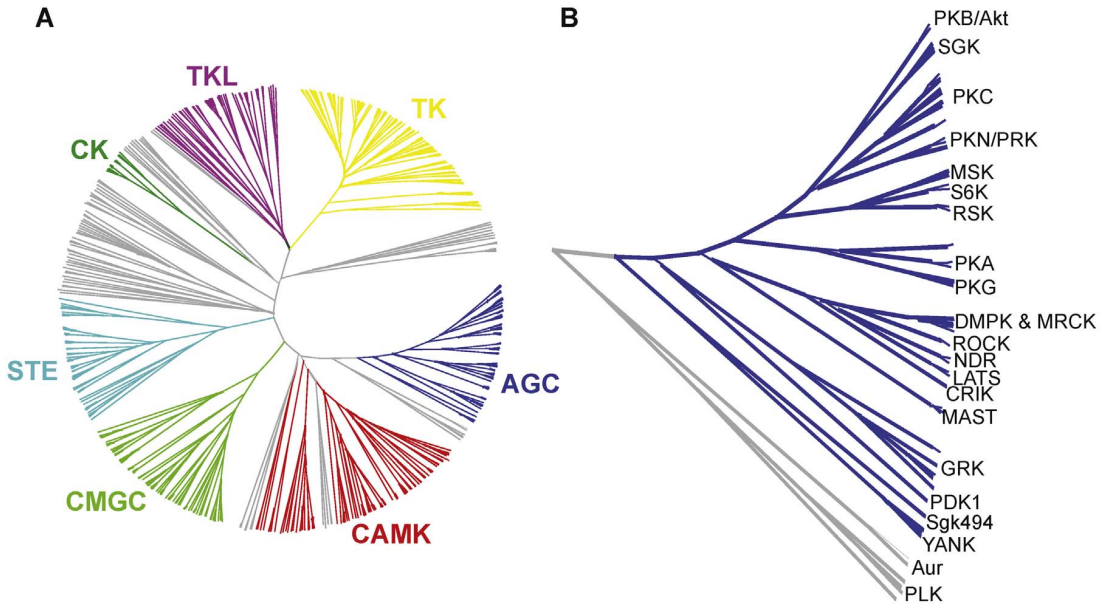

Figure 1.6. Relationship of protein kinases in seven major groups. (A) The evolutionary relationship of the catalytic domain(s) of protein kinases in the human kinome. (B) Within the AGC kinases, there are 19 different families. Abbreviations: ACG, protein kinase A/protein kinase C/ protein kinase G; CAMK, calcium/calmodulin-dependent protein kinase; CMGC, glycogen synthase kinase 3 and CDK2-like kinase; CK1, casein kinase 1; MAPK, mitogen activated protein kinase; STE, homologs of yeast Sterile 7, Sterile 11, and Sterile 20; TK, tyrosine kinase; TKL tyrosine kinase-like kinase. From Leroux (2018).

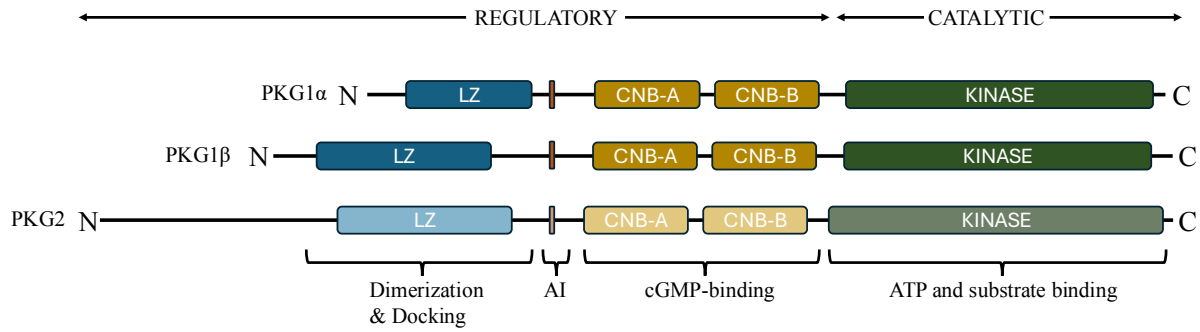

Figure 1.7. Domain organization of canonical PKG isoforms. PKG consists of an N-terminal regulatory region and a C-terminal catalytic region. The regulatory region consists of a leucine zipper (LZ) that facilitates homodimer formation as well as docking by PKG-interacting proteins, an autoinhibitory site (AI) which is a pseudosubstrate that maintains autoinhibition, and two cGMP-binding domains. The catalytic region consists of a kinase domain which binds ATP and phosphorylates kinase substrates. Two PKG1 isoforms, PKG1α and PKG1β, are encoded by alternative splicing in the N-terminus of the same gene. PKG2 is encoded by a different gene, indicated by different shading of the domains.

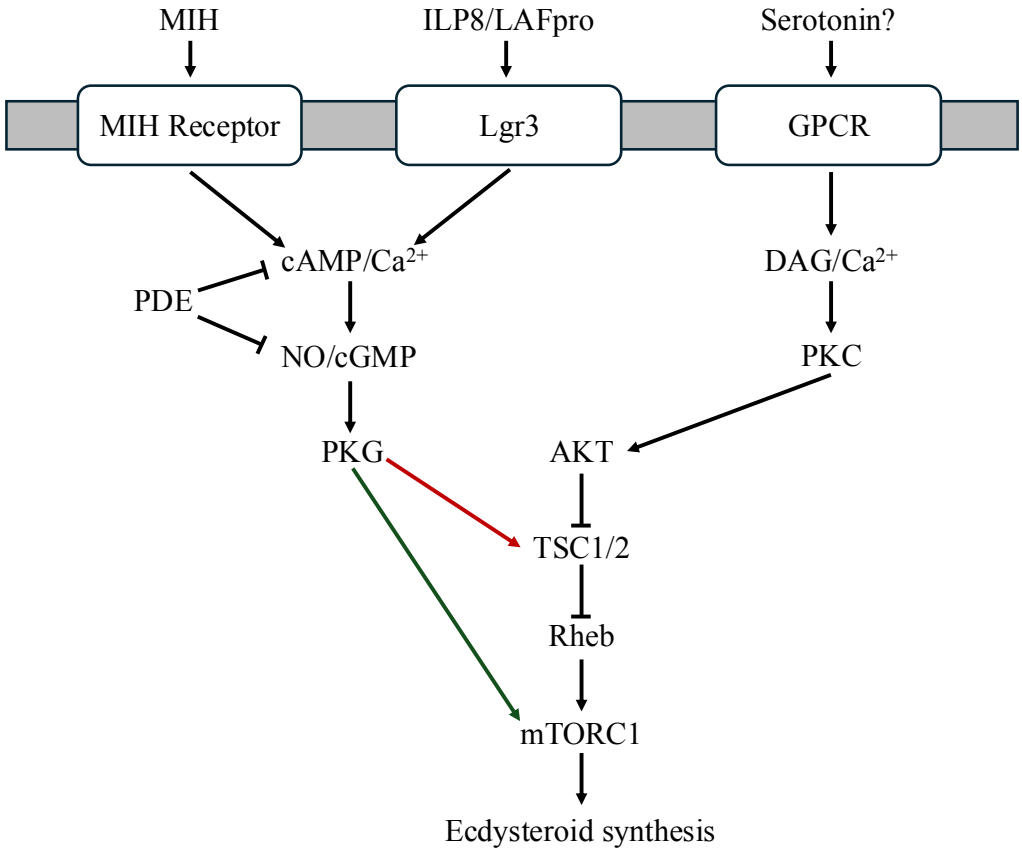

Figure 1.8. Proposed G protein coupled receptor signaling pathways in the YO that mediate ecdysteroid synthesis. MIH signaling stimulates a transient increase in cAMP, followed by production of nitric oxide and a sustained increase in cGMP. PKG is activated by cGMP and is hypothesized to inhibit mTORC1-dependent ecdysteroid synthesis indirectly through phosphorylation and activation of TSC1/2 (red arrow). Depending on the cellular context, PKG may also stimulate ecdysteroid synthesis by direct phosphorylation and activation of mTORC1 (green arrow). Other GPCR ligands are presumed to be ILP8, LAF_{pro}, and biogenic amines such as serotonin, which converge on mTORC1 to regulate ecdysteroid synthesis. Abbreviations: MIH, molt inhibiting hormone; ILP8, insulin like peptide 8; LAF_{pro}, limb autotomy factor proecdysis; PDE, phosphodiesterase; NO, nitric oxide; PKG, cGMP-dependent protein kinase; AKT, protein kinase B; TSC, tuberous sclerosis complex; Rheb, Ras homolog enriched in brain; mTORC1, mechanistic target of rapamycin complex 1; GPCR, G protein coupled receptor; Lgr3, leucine-rich repeat-containing GPCR; DAG, diacylglycerol. Figure modified from Mykles, (2021).

REFERENCES

Abdullah Al Balushi, K.S., Devi, G., Rashid Khamis Al Gharibi, A.S., Adeeb, M.A.S., Al Hudaifi, A.S.M. and Khalfan Al Shabibi, S.S. (2021). Extraction of Bio Polymers from Crustacean Shells and its Application in Refinery Wastewater Treatment. *WJST.* **18**, 11543.

Abuhagr, A.M., Blindert, J.L., Nimitkul, S., Zander, I.A., LaBere, S.M., Chang, S.A., MacLea, K.S., Chang, E.S. and Mykles, D.L. (2014a). Molt regulation in green and red color morphs of the crab *Carcinus maenas*: gene expression of molt-inhibiting hormone signaling components. *J. Exp. Biol.* **217**, 796-808.

Abuhagr, A.M., MacLea, K.S., Chang, E.S. and Mykles, D.L. (2014b). Mechanistic target of rapamycin (mTOR) signaling genes in decapod crustaceans: Cloning and tissue expression of mTOR, Akt, Rheb, and p70 S6 kinase in the green crab, *Carcinus maenas*, and blackback land crab, *Gecarcinus lateralis*. *Comp. Biochem. Physiol.* **168A**, 25-39.

Abuhagr, A.M., MacLea, K.S., Mudron, M.R., Chang, S.A., Chang, E.S. and Mykles, D.L. (2016). Roles of mechanistic target of rapamycin and transforming growth factor-β signaling in the molting gland (Y-organ) of the blackback land crab, *Gecarcinus lateralis*. *Comp. Biochem. Physiol.* **198A**, 15-21.

Adiyodi, K.G. and Adiyodi, R.G. (1970). Endocrine control of reproduction in decapod crustacea. *Biol. Rev. Camb. Philos. Soc.* **45**, 121-164.

Aiken, D.E. (1969). Photoperiod, endocrinology and the crustacean molt cycle. *AAAS.* **164**, 149-55.

Allen, A.M., Anreiter, I., Neville, M.C. and Sokolowski, M.B. (2017). Feeding-related traits are affected by dosage of the *foraging* gene in *Drosophila melanogaster*. *Genetics.* **205**, 761-773.

Allen, A.M., Anreiter, I., Vesterberg, A., Douglas, S.J. and Sokolowski, M.B. (2018). Pleiotropy of the *Drosophila melanogaster* foraging gene on larval feeding-related traits. *J. Neurogenetics.* **32**, 256-266.

Alverdi, V., Mazon, H., Versluis, C., Hemrika, W., Esposito, G., van den Heuvel, R., Scholten, A. and Heck, A.J.R. (2008). cGMP-binding Prepares PKG for Substrate Binding by Disclosing the C-terminal Domain. *J. Molec. Biol.* **375**, 1380-1393.

Anreiter, I., Kramer, J.M. and Sokolowski, M.B. (2017). Epigenetic mechanisms modulate differences in *Drosophila* foraging behavior. *PNAS.* **114**, 12518-12523.

Aranaz, I., Alcántara, A.R., Civera, M.C., Arias, C., Elorza, B., Heras Caballero, A. and Acosta, N. (2021). Chitosan: An Overview of Its Properties and Applications. *Polymers (Basel).* **13**, 3256.

Ardito, F., Giuliani, M., Perrone, D., Troiano, G. and Lo Muzio, L. (2017). The crucial role of protein phosphorylation in cell signaling and its use as targeted therapy *Int. J. Molec. Med.* **40**, 271-280.

Arvy, L., Gabe, M. and Scharrer, B. (1956). Scientific Meetings. *AAAS.* **123**, 382-384.

Baghdassarian, D., deBesse, N., Saidi, B., Somme, G. and Lachaise, F. (1996). Neuropeptide-induced inhibition of steroidogenesis in crab molting glands: Involvement of cGMP-dependent protein kinase. *Gen. Comp. Endocrinol.* **104**, 41-51.

Bauer, R.T. (1981). Grooming Behavior and Morphology in the Decapod Crustacea. *J. Crustacean Biol.* **1**, 153-173.

Bax, N., Williamson, A., Aguero, M., Gonzalez, E. and Geeves, W. (2003). Marine invasive alien species: a threat to global biodiversity. *Mar. Policy.* **27**, 313-323.

Belles, X. (2020). Chapter 7 - Molecular mechanisms regulating hormone production and action. *Insect Metamorphosis* (ed. X. Belles), pp. 131-176. Academic Press.

Benchmark Insights. (2019). Technologies shaping the future of shrimp production. *Benchmark* **11**, 1.

Benrabaa, S.A.M., Chang, S.A., Chang, E.S. and Mykles, D.L. (2023). Effects of molting on the expression of ecdysteroid biosynthesis genes in the Y-organ of the blackback land crab, Gecarcinus lateralis. *Gen. Comp. Endocrinol.* **340**, 114304.

Bertness, M.D. and Coverdale, T.C. (2013). An invasive species facilitates the recovery of salt marsh ecosystems on Cape Cod. *Ecol.* **94**, 1937-1943.

Blakeslee, A.M.H., McKenzie, C.H., Darling, J.A., Byers, J.E., Pringle, J.M. and Roman, J. (2010). A hitchhiker's guide to the Maritimes: anthropogenic transport facilitates long-distance dispersal of an invasive marine crab to Newfoundland. *Divers. Distrib.* **16**, 879-891.

Bliss, D.E. and Boyer, J.R. (1964). Environmental regulation of growth in the decapod crustacean *Gecarcinus lateralis*. *Gen. Comp. Endocrinol.* **4**, 15-41.

Bliss, D.E., Van Montfrans, J., Van Montfrans, M. and Boyer, J.R. (1978). Behavior and growth of the land crab *Gecarcinus lateralis* (Fréminville) in southern Florida. *Bull. Am. Mus. Nat. Hist.* **160**, 111-152.

Bliss, D.E. (1979). From Sea to Tree: Saga of a Land Crab. *Am. Zool.* **19**, 385-410.

Böcking, D. and Sedlmeier, D. (1994). Protein phosphorylation in the moulting gland of the crayfish, *Orconectes limosus*: Role of cyclic nucleotides, calcium, and moult inhibiting hormone (MIH). *Inv. Rep. Dev.* **26**, 237-245.

Boudreau, S.A. and Worm, B. (2012). Ecological role of large benthic decapods in marine ecosystems, a review. *Mar. Ecol. Prog. Ser.* **469**, 195-214.

Bracken, H.D., De Grave, S., Toon, A., Felder, D.L. and Crandall, K.A. (2010). Phylogenetic position, systematic status, and divergence time of the Procarididea (Crustacea: Decapoda). *Zool. Scr.* **39**, 198-212.

Bright, D.B. and Hogue, C.L. (1972). A synopsis of burrowing land crabs of the world and list of their arthropod symbionts and burrow associates. *Contrib. Sci.* **220**, 1-58.

Brown, F.A. and Cunningham, O.N.A. (1939). Influence of the sinus gland of crustaceans on normal viability and ecdysis. *Biol. Bull.* **77**, 104-114.

Bulut, E., Sargin, I., Arslan, O., Odabasi, M., Akyuz, B. and Kaya, M. (2017). In situ chitin isolation from body parts of a centipede and lysozyme adsorption studies. *Mater. Sci. Eng. C.* **70**, 552-563.

Carlisle, D.B. (1957). On the hormonal inhibition of moulting in decapod Crustacea II. The terminal anecdysis in crabs. *J. Mar. Biol. Assoc. U.K.* **36**, 291-307.

Carlisle, D.B. (1965). The effects of crustacean and locust ecdysons on moulting and proecdysis in juvenile shore crabs, Carcinus maenas. *Gen. Comp. Endocrinol.* **5**, 366-372.

Carlton, J.T. and Geller, J.B. (1993). Ecological roulette- The global transport of nonindigenous marine organisms. *AAAS.* **261**, 78-82.

Casteel, D.E., Boss, G.R. and Pilz, R.B. (2005). Identification of the interface between cGMP-dependent Protein Kinase Iβ and its interaction partners TFII-I and IRAG reveals a common interaction motif. *J. Biol. Chem.* **280**, 38211-38218.

Casteel, D.E., Zhang, T., Zhuang, S. and Pilz, R.B. (2008). cGMP-dependent protein kinase anchoring by IRAG regulates its nuclear translocation and transcriptional activity. **20**, 1392-1399.

Casteel, D.E., Smith-Nguyen, E.V., Sankaran, B., Roh, S.H., Pilz, R.B. and Kim, C. (2010). A crystal structure of the cyclic GMP-dependent protein kinase Iβ dimerization/docking domain reveals molecular details of isoform-specific anchoring. *J. Biol. Chem.* **285**, 32684-32688.

Chang, E.S. and O'Connor, J.D. (1977). Secretion of α-ecdysone by crab Y-organs in vitro. *PNAS.* **74**, 615-618.

Chang, E.S. and Mykles, D.L. (2011). Regulation of crustacean molting: A review and our perspectives. *Gen. Comp. Endocrinol.* **172**, 323-330.

Chassard-Bouchaud, C. and Hubert, M. (1976). On the fine structure of the regressing ecdysial glands of *Carcinus maenas* L. (Crustacea Decapoda) parasitized by *Sacculina carcini thompson*. *Cell Tissue Res.* **167**, 351-361.

Chen, J. and Roberts, J.D., Jr. (2014). cGMP-dependent protein kinase I gamma encodes a nuclear localization signal that regulates nuclear compartmentation and function. *J. Cell Sig.* **26**, 2633-44.

Chen, T., Ren, C., Jiang, X., Zhang, L., Li, H., Huang, W. and Hu, C. (2018). Mechanisms for type-II vitellogenesis-inhibiting hormone suppression of vitellogenin transcription in shrimp hepatopancreas: Crosstalk of GC/cGMP pathway with different MAPK-dependent cascades. *PLoS One.* **13**, e0194459.

Chung, J.S. and Webster, S.G. (2005). Dynamics of release of molt-inhibiting hormone and crustacean hyperglycemic hormone in the shore crab, *Carcinus maenas*. *J. Endocrinol.* **146**, 5545-5551.

Cordone, G., Galván, D.E. and Momo, F.R. (2023). Impacts of an invasion by green crab Carcinus maenas on the intertidal food web of a Patagonian rocky shore, Argentina. *Mar. Ecol. Prog. Ser.* **713**, 97-115.

Couch, J. (1837a). Exuviation in shrimps and lobsters. *Mag. Zool. Bot.* **1**, 170-173.

Couch, J. (1837b). Exuviation of the common crab. *Mag. Zool. Bot.* **1**, 341-344.

Couch, J. (1843a). On the process of exuviation and growth in crabs and lobsters, and other British species of stalk-eyes crustacean animals. *Ann. Rep. Roy. Cornwall Polytechnic Soc.* **11**, 1-15.

Couch, J. (1858). A particular description of some circumstances hiterto little known, connected with the process of exuviation in the common edible Crab. *Ann. Rep. Roy. Cornwall Polytechnic Soc.* . **26**, 39-45.

Couch, R.Q. (1843b). On the metamorphosis of the decapod crustaceans. *Ann. Rep. Roy. Cornwall Polytechnic Soc.* **11**, 28-43.

Couch, R.Q. (1856). New facts on the ecdysis or moulting of crustacea. *The Zoologist.* **14**, 4972.

Covi, J.A., Chang, E.S. and Mykles, D.L. (2009). Conserved role of cyclic nucleotides in the regulation of ecdysteroidogenesis by the crustacean molting gland. *Comp. Biochem. Physiol.* **152A**, 470-477.

Covi, J.A., Chang, E.S. and Mykles, D.L. (2012). Neuropeptide signaling mechanisms in crustacean and insect molting glands. *Invertebr. Reprod. Dev.* **56**, 33-49.

Das, S., Pitts, N.L., Mudron, M.R., Durica, D.S. and Mykles, D.L. (2016). Transcriptome analysis of the molting gland (Y-organ) from the blackback land crab, *Gecarcinus lateralis*. *Comp. Biochem. Physiol.* **17D**, 26-40.

Das, S., Vraspir, L., Zhou, W., Durica, D.S. and Mykles, D.L. (2018). Transcriptomic analysis of differentially expressed genes in the molting gland (Y-organ) of the blackback land crab, *Gecarcinus lateralis*, during molt-cycle stage transitions. *Comp. Biochem. Physiol.* **28D**, 37-53.

Davis, K.E., Grave, S.D., Delmer, C., Payne, A.R.D., Mitchell, S. and Wills, M.A. (2022). Ecological Transitions and the Shape of the Decapod Tree of Life. *Integr. Comp. Biol.* **62**, 332-344.

De Grave, S., Pentcheff, N.D., Ahyong, S.T., Chan, T.-Y., Crandall, K.A., Dworschak, P.C., Felder, D.L., Feldmann, R.M., Fransen, C.H.J.M., Goulding, L.Y.D., et al. (2009). A classification of living and fossil genera of decapod crustaceans. *RBZ.* **21**, 1-109.

de Vente, J., Asan, E., Gambaryan, S., Markerink-van Ittersum, M., Axer, H., Gallatz, K., Lohmann, S.M. and Palkovits, M. (2001). Localization of cGMP-dependent protein kinase type II in rat brain. *Neuroscience.* **108**, 27-49.

Drach, P. (1939). *Mue et cycle d'intermue chez les crustacés décapodes.* Paris: Masson.

Echalier, G. (1954). Recherches expérimentales sur le rôle de “l'organe Y” dans la mue de *Carcinus moenas* (L.) Crustacé Décapode. *C. R. Acad. Sci. Paris.* **238**, 523-525.

Echalier, G. (1955). Role de l’organe-Y dans le determinisme de la mue de *Carcinides*-(*Carcinus*) *moenas* (L.) (Crustacea, Decapode): experiences d’implantation. *C. R. Acad. Sci. D.* **240**, 1581-1583.

Echalier, G. (1959). L'organe Y et le déterminisme de la croissance et de la mue chez "Carcinus maenas" (L.), crustacé décapode.

FAO. (2024). *The state of world fisheries and aquaculture 2024- Blue transformation in action.* Rome, Italy: FAO.

Feijó, R.G., Braga, A.L., Lanes, C.F.C., Figueiredo, M.A., Romano, L.A., Klosterhoff, M.C., Nery, L.E.M., Maggioni, R., Wasielesky, W. and Marins, L.F. (2016). Silencing of gonad-inhibiting hormone transcripts in *Litopenaeus vannamei* females by use of the RNA interference technology. *Mar. Biotech.* **18**, 117-123.

Fisher, M.C., Grason, E.W., Stote, A., Kelly, R.P., Litle, K. and Sean McDonald, P. (2023). Invasive European green crab (*Carcinus maenas*) predation revealed with quantitative DNA metabarcoding. *bioRxiv.* 2023.11.27.568928.

Fowler, S.W., Small, L.F. and Kečkeš, S. (1971). Effects of temperature and size on molting of euphausiid crustaceans. *Mar. Biol.* **11**, 45-51.

Francis, S.H. and Corbin, J.D. (2013). Cyclic nucleotide-dependent protein kinases. *Encyclopedia of Biological Chemistry (Second Edition)* (ed. W. J. Lennarz and M. D. Lane), pp. 574-579. Waltham: Academic Press.

Frederich, M. and Lancaster, E.R. (2024). Chapter 1 - The European green crab, Carcinus maenas: Where did they come from and why are they here? *Ecophysiology of the European Green Crab (Carcinus Maenas) and Related Species* (ed. D. Weihrauch and I. J. McGaw), pp. 1-20. Academic Press.

Gabe, M. (1953a). Sur l'existence, chez quelques crustacés Malacostraces, d'un organe comparable a la glande de la mue des Insects. *C. R. Acad. Sci. D.* **327**, 1111-1113.

Gabe, M. (1953b). Quelques acquisitions récentes sur les glandes endocrines des Arthropodes. *Experientia.* **9**, 352-356.

Gabe, M. (1956). Histologie comparée de la glande de mue (organe Y) des Crustacés Malacostracés. *Ann. Sci. Nat. Zool.* **11**, 145-152.

Gamm, D.M., Francis, S.H., Angelotti, T.P., Corbin, J.D. and Uhler, M.D. (1995). The type II isoform of cGMP-dependent protein kinase is dimeric and possesses regulatory and catalytic properties distinct from the type I isoforms. *J. Biol. Chem.* **270**, 27380-8.

Garbary, D.J., Miller, A.G., Williams, J. and Seymour, N.R. (2014). Drastic decline of an extensive eelgrass bed in Nova Scotia due to the activity of the invasive green crab (Carcinus maenas). *Mar. Biol.* **161**, 3-15.

Garelli, A., Gontijo, A.M., Miguela, V., Caparros, E. and Dominguez, M. (2012). Imaginal Discs Secrete Insulin-Like Peptide 8 to Mediate Plasticity of Growth and Maturation. **336**, 579-582.

Gontijo, A.M. and Garelli, A. (2018). The biology and evolution of the Dilp8-Lgr3 pathway: A relaxin-like pathway coupling tissue growth and developmental timing control. *Mech. Dev.* **154**, 44-50.

Grosholz, E. (2002). Ecological and evolutionary consequences of coastal invasions. *TREE.* **17**, 22-27.

Gudi, T., Huvar, I., Meinecke, M., Lohmann, S.M., Boss, G.R. and Pilz, R.B. (1996). Regulation of gene expression by cGMP-dependent protein kinase. Transactivation of the c-fos promoter. *J. Biol. Chem.* **271**, 4597-600.

Gudi, T., Lohmann, S.M. and Pilz, R.B. (1997). Regulation of gene expression by cyclic GMP-dependent protein kinase requires nuclear translocation of the kinase: identification of a nuclear localization signal. *Molec. Cell Biol.* **17**, 5244-5254.

Gudi, T., Casteel, D.E., Vinson, C., Boss, G.R. and Pilz, R.B. (2000). NO activation of fos promoter elements requires nuclear translocation of G-kinase I and CREB phosphorylation but is independent of MAP kinase activation. *Oncogene.* **19**, 6324-33.

Harish Prashanth, K.V. and Tharanathan, R.N. (2007). Chitin/chitosan: modifications and their unlimited application potential—an overview. *Trends. Food Sci. Technol.* **18**, 117-131.

Harpaz, S., Kahan, D. and Galun, R. (1987). Variability in Feeding Behavior of the Malaysian Prawn *Macrobrachium rosenbergii* (De Man) during the Molt Cycle (Decapoda, Caridea). *Crustaceana.* **52**, 53-60.

Head, T.B., Mykles, D.L. and Tomanek, L. (2019). Proteomic analysis of the crustacean molting gland (Y-organ) over the course of the molt cycle. *Comp. Biochem. Physiol.* **29D**, 193-210.

Hikino, H. and Takemoto, T. (1974). Ecdysones of Plant Origin. *Invertebrate Endocrinology and Hormonal Heterophylly* (ed. W. J. Burdette), pp. 185-203. Berlin, Heidelberg: Springer Berlin Heidelberg.

Hochard, J.P., Hamilton, S. and Barbier, E.B. (2019). Mangroves shelter coastal economic activity from cyclones. *PNAS.* **116**, 12232-12237.

Hofmann, F. (2005). The biology of cyclic GMP-dependent protein kinases. *J. Biol. Chem.* **280**, 1-4.

Hofmann, F. (2018). A concise discussion of the regulatory role of cGMP kinase I in cardiac physiology and pathology. *Basic Res. Cardiol.* **113**, 31.

Hofmann, F. (2020). The cGMP system: components and function. *Biol. Chem.* **401**, 447-469.

Holland, C.A. and Skinner, D.M. (1976). Interactions between molting and regeneration in the land crab. *Biol. Bull.* **150**, 222-240.

Iga, M., Nakaoka, T., Suzuki, Y. and Kataoka, H. (2014). Pigment Dispersing Factor Regulates Ecdysone Biosynthesis via Bombyx Neuropeptide G Protein Coupled Receptor-B2 in the Prothoracic Glands of *Bombyx mori*. **9**, e103239.

Jaszczak, J.S., Wolpe, J.B., Bhandari, R., Jaszczak, R.G. and Halme, A. (2016). Growth Coordination During *Drosophila melanogaster* Imaginal Disc Regeneration Is Mediated by Signaling Through the Relaxin Receptor Lgr3 in the Prothoracic Gland. *Genetics.* **204**, 703-709.

Josefsson, L. and Kleinholz, L.H. (1964). Isolation and purification of hormones of the crustacean eyestalk. *Nature.* **201**, 301-2.

Kalderon, D. and Rubin, G.M. (1989). cGMP-dependent protein kinase genes in *Drosophila*. *J. Biol. Chem.* **264**, 10738-10748.

Kang, B.J., Bae, S.-H., Suzuki, T., Niitsu, S. and Wilder, M.N. (2019). Transcriptional silencing of vitellogenesis-inhibiting hormone (VIH) subtype-I in the whiteleg shrimp, Litopenaeus vannamei. *Aquaculture.* **506**, 119-126.

Kannangara, J.R., Mirth, C.K. and Warr, C.G. (2021). Regulation of ecdysone production in Drosophila by neuropeptides and peptide hormones. *Open Biol.* **11**, 200373.

Karlson, P. and Skinner, D.M. (1960). Attempted extraction of crustacean moulting hormone from isolated Y-organs. *Nature.* **185**, 543-4.

Karlson, P. and Sekeris, C.E. (1966a). Ecdysone, an insect steroid hormone, and its mode of action. *Recent Prog Horm Res.* **22**, 473-502.

Kashyap, N., Kumar, N. and Kumar, M.N. (2005). Hydrogels for pharmaceutical and biomedical applications. *Crit Rev Ther Drug Carrier Syst.* **22**, 107-49.

Katayama, H., Ohira, T., Nagata, K. and Nagasawa, H**.** (2001). A recombinant molt-inhibiting hormone of the kuruma prawn has a similar secondary structure to a native hormone: determination of disulfide bond arrangement and measurements of circular dichroism spectra. *Biosci. Biotechnol. Biochem.* **65**, 1832-9.

Kato, M., Blanton, R., Wang, G.R., Judson, T.J., Abe, Y., Myoishi, M., Karas, R.H. and Mendelsohn, M.E. (2012). Direct binding and regulation of RhoA protein by cyclic GMP-dependent protein kinase Iα. *J. Biol. Chem.* **287**, 41342-51.

Kato, S., Zhang, R. and Roberts, J.D. (2013). Proprotein convertases play an important role in regulating PKGI endoproteolytic cleavage and nuclear transport. *Am. J. Physiol. Lung Cell. Molec. Physiol.* **305**, L130-L140.

Kim, C. and Sharma, R. (2021). Cyclic nucleotide selectivity of protein kinase G isozymes. *Protein Sci.* **30**, 316-327.

Kim, H.W., Batista, L.A., Hoppes, J.L., Lee, K.J. and Mykles, D.L. (2004). A crustacean nitric oxide synthase expressed in nerve ganglia, Y-organ,gill and gonad of the tropical land crab, *Gecarcinus lateralis*. *J. Exp. Biol.* **207**, 2845-2857.

Knigge, T., LeBlanc, G.A. and Ford, A.T. (2021). A Crab Is Not a Fish: Unique Aspects of the Crustacean Endocrine System and Considerations for Endocrine Toxicology. *Front. Endocrinol. (Lausanne).* **12**, 587608.

Koolman, J. (1982). Ecdysone metabolism- Review. *Insect Biochem.* **12**, 225-250.

Kozma, M.T., Pérez-Moreno, J.L., Gandhi, N.S., Hernandez Jeppesen, L., Durica, D.S., Ventura, T. and Mykles, D.L. (2024). *In silico* analysis of crustacean hyperglycemic hormone family G protein-coupled receptor candidates. *Front. Endocrinol.* **14**, 1322800.

Lee, S.G. and Mykles, D.L. (2006). Proteomics and signal transduction in the crustacean molting gland. *Integr. Comp. Biol.* **46**, 965-977.

Leroux, A.E., Schulze, J.O. and Biondi, R.M. (2018). AGC Kinases, mechanisms of regulation and innovative drug development. *Semin. Cancer Biol.* **48**, 1-17.

Lipcius, R.N. and Herrnkind, W.F. (1982). Molt cycle alterations in behavior, feeding and diel rhythms of a decapod crustacean, the spiny lobster *Panulirus argus*. *Mar. Biol.* **68**, 241-252.

Liu, D., Ceddia, R.P. and Collins, S**.** (2018). Cardiac natriuretic peptides promote adipose 'browning' through mTOR complex-1. *Molec. Metab.* **9**, 192-198.

Liu, G.Y. and Sabatini, D.M. (2020). mTOR at the nexus of nutrition, growth, ageing and disease. *Nature Rev. Molec. Cell Biol.* **21**, 183-203.

Lorenz, R., Bertinetti, D. and Herberg, F.W. (2017). cAMP-Dependent Protein Kinase and cGMP-Dependent Protein Kinase as Cyclic Nucleotide Effectors. *Handb. Exp. Pharmacol.* **238**, 105-122.

MacPherson, M.R., Lohmann, S.M. and Davies, S.A. (2004). Analysis of Drosophila cGMP-dependent protein kinases and assessment of their in vivo roles by targeted expression in a renal transporting epithelium. *J. Biol. Chem.* **279**, 40026-34.

Mattson, M.P. and Spaziani, E. (1985a). Cyclic AMP mediates the negative regulation of Y-organ ecdysteroid production. *Molec. Cell Endocrinol.* **42**, 185-189.

Mattson, M.P. and Spaziani, E. (1985b). Functional relations of crab molt-inhibiting hormone and neurohypophysial peptides. *Peptides.* **6**, 635-640.

Mattson, M.P. and Spaziani, E. (1986a). Regulation of Y-organ ecdysteroidogenesis by molt-inhibiting hormone in crabs: involvement of cyclic AMP-mediated protein synthesis. *Gen. Comp. Endocrinol.* **63**, 414-423.

Mattson, M.P. and Spaziani, E. (1986b). Regulation of crab Y-organ steroidogenesis in vitro: evidence that ecdysteroid production increases through activation of cAMP-phosphodiesterase by calcium-calmodulin. *Molec. Cell Endocrinol.* **48**, 135-51.

Mattson, M.P. and Spaziani, E. (1987). Demonstration of protein kinase C activity in crustacean Y-organs, and partial definition of its role in regulation of ecdysteroidogenesis. *Mol. Cell Endocrinol.* **49**, 159-171.

McCarthy, J.F. and Skinner, D.M. (1977b). Interruption of proecdysis by autotomy of partially regenerated limbs in the land crab, *Gecarcinus lateralis*. *Dev. Biol.* **61**, 299-310.

McDonald, A.A., Chang, E.S. and Mykles, D.L. (2011). Cloning of a nitric oxide synthase from green shore crab, *Carcinus maenas*: A comparative study of the effects of eyestalk ablation on expression in the molting glands (Y-organs) of *C. maenas*, and blackback land crab, *Gecarcinus lateralis*. *Comp. Biochem. Physiol.* **158A**, 150-162.

Molnar, J.L., Gamboa, R.L., Revenga, C. and Spalding, M.D. (2008). Assessing the global threat of invasive species to marine biodiversity. *Front. Ecol. Environ.* **6**, 485-492.

Monteiro, J.N., Ovelheiro, A., Maia, F., Teodósio, M.A. and Leitão, F. (2025). Biological traits and population dynamics for sustainable harvesting of Carcinus maenas. *Fish. Res.* **281**, 107243.

Morton, D.B. and Hudson, M.L. (2002). Cyclic GMP regulation and function in insects. *Adv. Insect Physiol.* **29**, 1-54.

Mykles, D.L. and Skinner, D.M. (1981). Preferential loss of thin filaments during molt-induced atrophy in crab claw muscle. *Journal Ultrastruct. Res.* **75**, 314-325.

Mykles, D.L. and Skinner, D.M. (1982). Molt cycle-associated changes in calcium-dependent proteinase activity that degrades actin and myosin in crustacean muscle. *Dev. Biol.* **92**, 386-397.

Mykles, D.L. (1992). Getting out of a Tight Squeeze—Enzymatic Regulation of Claw Muscle Atrophy in Molting. *Am. Zool.* **32**, 485-494.

Mykles, D.L. (2001). Interactions Between Limb Regeneration and Molting in Decapod Crustaceans. *Am. Zool.* **41**, 399-406.

Mykles, D.L., Adams, M.E., Gäde, G., Lange, A.B., Marco, H.G. and Orchard, I. (2010). Neuropeptide action in insects and crustaceans. *Physiol. Biochem. Zool.* **83**, 836-846.

Mykles, D.L. (2011). Ecdysteroid metabolism in crustaceans. *J. Steroid Biochem. Molec. Biol.* **127**, 196-203.

Mykles, D.L. and Chang, E.S. (2020). Hormonal control of the crustacean molting gland: Insights from transcriptomics and proteomics. *Gen. Comp. Endocrinol.* **294**, 113493.

Mykles, D.L. (2021). Signaling pathways that regulate the crustacean molting gland. *Front. Endocrinol.* **12**, 113658.

Mykles, D.L. (2024). Molting physiology. *Frontiers in Invertebrate Physiology* (ed. S. P. L. S. Saleuddin, R.D. Roer, I. Wilkie), pp. 229-274. Palm Bay, FL: Apple Academic Press.

Nakatsuji, T., Sonobe, H. and Watson, R.D. (2006). Molt-inhibiting hormone-mediated regulation of ecdysteroid synthesis in Y-organs of the crayfish (*Procambarus clarkii*): involvement of cyclic GMP and cyclic nucleotide phosphodiesterase. *Molec. Cell Endocrinol.* **253**, 76-82.

Nakatsuji, T., Lee, C.-Y. and Watson, R.D. (2009). Crustacean molt-inhibiting hormone: Structure, function, and cellular mode of action. *Comp. Biochem. Physiol.* **152**, 139-148.

Neckles, H.A. (2015). Loss of Eelgrass in Casco Bay, Maine, Linked to Green Crab Disturbance. *Northeast. Nat.* **22**, 478-500.

O'Brien, J.J., Kumari, S.S. and Skinner, D.M. (1991). Proteins of Crustacean Exoskeletons: I. Similarities and Differences among Proteins of the Four Exoskeletal Layers of Four Brachyurans. *Biol. Bull.* **181**, 427-441.

O'Halloran, M.J. and O'Dor, R.K. (1988). Molt Cycle of Male Snow Crabs, *Chionoecetes Opilio*, from Observations of External Features, Setal Changes, and Feeding Behavior. *J. Crustacean Biol.* **8**, 164-176.

Oeing, C.U., Mishra, S., Dunkerly-Eyring, B.L. and Ranek, M.J. (2020). Targeting protein kinase G to treat cardiac proteotoxicity. *Front. Physiol.* **11**, 858.

Oeing, C.U., Nakamura, T., Pan, S., Mishra, S., Dunkerly-Eyring, B.L., Kokkonen-Simon, K.M., Lin, B.L., Chen, A., Zhu, G., Bedja, D., et al. (2020). PKG1α cysteine-42 redox state controls mTORC1 activation in pathological cardiac hypertrophy. *Circulat. Res.* **127**, 522-533.

Ørstavik, S., Natarajan, V., Taskén, K., Jahnsen, T. and Sandberg, M. (1997). Characterization of the human gene encoding the type I alpha and type I beta cGMP-dependent protein kinase (PRKG1). *Genomics.* **42**, 311-8.

Orth, R.J., Carruthers, T.J.B., Dennison, W.C., Duarte, C.M., Fourqurean, J.W., Heck, K.L., Hughes, A.R., Kendrick, G.A., Kenworthy, W.J., Olyarnik, S., et al. (2006). A Global Crisis for Seagrass Ecosystems. *Biosci.* **56**, 987-996.

Panwar, V., Singh, A., Bhatt, M., Tonk, R.K., Azizov, S., Raza, A.S., Sengupta, S., Kumar, D. and Garg, M. (2023). Multifaceted role of mTOR (mammalian target of rapamycin) signaling pathway in human health and disease. *STTT.* **8**, 375.

Passano, L.M. and Jyssum, S. (1963). The role of the Y-organ in crab proecdysis and limb regeneration. *Comp. Biochem. Physiol.* **9**, 195-213.

Pimentel, D., Zuniga, R. and Morrison, D. (2005). Update on the environmental and economic costs associated with alien-invasive species in the United States. *Ecol. Econ.* **52**, 273-288.

Pitts, N.L. and Mykles, D.L. (2017). Localization and expression of molt-inhibiting hormone and nitric oxide synthase in the central nervous system of the green shore crab, *Carcinus maenas*, and the blackback land crab, *Gecarcinus lateralis*. *Comp. Biochem. Physiol.* **203A**, 328-340.

Quackenbush, L.S. and Herrnkind, W.F. (1983). Partial Characterization of Eyestalk Hormones Controlling Molt and Gonadal Development in the Spiny Lobster *Panulirus argus*. *J. Crustacean Biol.* **3**, 34-44.

Ranek, M.J., Kokkonen-Simon, K.M., Chen, A., Dunkerly-Eyring, B.L., Pinilla Vera, M., Oeing, C.U., Patel, C.H., Nakamura, T., Zhu, G., Bedja, D., et al**.** (2019). PKG1-modified TSC2 regulated mTORC1 activity to counter adverse cardiac stress. *Nature.* **566**, 264-269.

Rao, K.R. (1965). Isolation and partial characterization of the moult-inhibiting hormone of the crustacean eyestalk. *Experientia.* **21**, 593-594.

Rato, L.D., Simões, T., Novais, S.C., Damasceno, J.M., Van der Meer, J., Thieltges, D.W., Marques, J.C. and Lemos, M.F.L. (2024). Thermal performance of native and invasive crab species: investigating the invasion potential of Hemigrapsus takanoi in southern European Carcinus maenas' habitats. *Biol. Invasions.* **26**, 3587-3601.

Réaumur, R. (1712). Sur les diverses reproductions qui se font dans les écrevisses, les homards, les crabes, et entre autres sur celles de leurs jambes et écailles. *Mem. Acad. Roy. Sci.* 223-245.

Réaumur, R. (1718). Aux observations sur la mue des ecrevisses, donnée dans les mémoires de 1712. *Hist. Acad. Roy. Sci.* 263-274.

Reese, T.C., Blakeslee, A.M.H., Crane, L.C., Fletcher, L.S., Repetto, M.F., Smith, N., Stancil, C., Tepolt, C.K., Toscano, B.J. and Griffen, B.D. (2024). Shift from income breeding to capital breeding with latitude in the invasive Asian shore crab Hemigrapsus sanguineus. *Sci. Reports.* **14**, 6654.

Rewitz, K.F., Yamanaka, N., Gilbert, L.I. and O'Connor, M.B. (2009). The insect neuropeptide PTTH activates receptor tyrosine kinase torso to initiate metamorphosis. *J. Sci.* **326**, 1403-5.

Ricciardi, A., Iacarella, J.C., Aldridge, D.C., Blackburn, T.M., Carlton, J.T., Catford, J.A., Dick, J.T.A., Hulme, P.E., Jeschke, J.M., Liebhold, A.M., et al. (2020). Four priority areas to advance invasion science in the face of rapid environmental change. *Environ. Rev.* **29**, 119-141.

Roman, J. (2006). Diluting the founder effect: cryptic invasions expand a marine invader's range. *Proc. Roy. Soc. London, Ser. B, Biol. Sci.* **273**, 2453-2459.

Ruth, P., Pfeifer, A., Kamm, S., Klatt, P., Dostmann, W.G. and Hofmann, F. (1997). Identification of the Amino Acid Sequences Responsible for High Affinity Activation of cGMP Kinase Iα. *J. Biol. Chem.* **272**, 10522-10528.

Saborowski, R., Bartolin, P., Koch, M. and Jungblut, S. (2023). Trophic ecophysiology of the native green shore crab, *Carcinus maenas*, and the invasive Asian shore crab, *Hemigrapsus sanguineus*, in the rocky intertidal of Helgoland (North Sea). *Front. Marine Sci.* **10**, 10:1247263.

Saidi, B., Debesse, N., Webster, S.G., Sedlmeier, D. and Lachaise, F. (1994). Involvement of cAMP and cGMP in the mode of action of molt-inhibiting hormone (MIH) a neuropeptide which inhibits steroidogenesis in a crab. *Molec. Cell Endocrinol.* **102**, 53-61.

Schröder, K. (2022). PKG, CXL, and HNO. Relax! *Hypertension.* **79**, 957-959.

Sedlmeier, D. and Fenrich, R. (1993). Regulation of ecdysteroid biosynthesis in crayfish Y-Organs: 1. Role of cyclic-nucleotides. *J. Exp. Zool.* **265**, 448-453.

Sekeris, C.E. and Karlson, P. (1964). On the mechanism of hormone action: II. Ecdysone and protein biosynthesis. *Arch. Biochem. Biophys.* **105**, 483-487.

Shi, F. and Collins, S. (2023). Regulation of mTOR signaling: Emerging role of cyclic nucleotide-dependent protein kinases and implications for cardiometabolic disease. *Int. J. Molec. Sci.* **24**, 11497.

Shyamal, S., Sudha, K., Gayathri, N. and Anilkumar, G**.** (2014). The Y-organ secretory activity fluctuates in relation to seasons of molt and reproduction in the brachyuran crab, Metopograpsus messor (Grapsidae): Ultrastructural and immunohistochemical study. *Gen. Comp. Endocrinol.* **196**, 81-90.

Shyamal, S., Das, S., Guruacharya, A., Mykles, D.L. and Durica, D.S. (2018). Transcriptomic analysis of crustacean molting gland (Y-organ) regulation via the mTOR signaling pathway. *Sci. Reports.* **8**, 7307.

Sin, Y.W., Kenny, N.J., Qu, Z., Chan, K.W., Chan, K.W.S., Cheong, S.P.S., Leung, R.W.T., Chan, T.F., Bendena, W.G., Chu, K.H., et al. (2015). Identification of putative ecdysteroid and juvenile hormone pathway genes in the shrimp. *Gen. Comp. Endocrinol.* **214,** 167-176.

Skinner, D.M. (1962). The structure and metabolism of a crustacean integumentary tissue during a molt cycle. *Biol. Bull.* **123**, 635-647.

Skinner, D.M. (1965). Amino acid incorporation into protein during the molt cycle of the land crab, *Gecarcinus lteralis*. *J. Exp. Biol.* **160**, 225-33.

Skinner, D.M. (1966). Breakdown and reformation of somatic muscle during the molt cycle of the land crab, *Gecarcinus lateralis*. *J. Exp. Biol.* **163**, 115-23.

Skinner, D.M. and Graham, D.E. (1972). Loss of limbs as a stimulus to ecdysis in brachyura (true crabs). *Biol. Bull.* **143**, 222-223.

Skinner, D.M. (1985a). Molting and Regeneration. *Integument, Pigments, and Hormonal Processes, Vol. 9* (ed. D. E. Bliss and L. H. Mantel), pp. 43-146. San Diego: Academic Press.

Skinner, D.M. (1985b). Interacting Factors in the Control of the Crustacean Molt Cycle. *Am. Zool.* **25**, 275-284.

Soumoff, C. and Skinner, D.M. (1983). Ecdysteroid titers during the molt cycle of the blue crab resemble those of other crustacea. *Biol. Bull.* **165**, 321-329.

Spaziani, E., Mattson, M.P., Wang, W.N.L. and McDougall, H.E. (1999). Signaling pathways for ecdysteroid hormone synthesis in crustacean Y-organs. *Am. Zool.* **39**, 496-512.

Spiessberger, B., Bernhard, D., Herrmann, S., Feil, S., Werner, C., Luppa, P.B. and Hofmann, F. (2009). cGMP-dependent protein kinase II and aldosterone secretion. *FEBS J.* **276**, 1007-13.

Styrishave, B., Rewitz, K. and Andersen, O. (2004). Frequency of moulting by shore crabs Carcinus maenas (L.) changes their colour and their success in mating and physiological performance. *J. Exp. Mar. Bio. Ecol.* . **313**, 317-336.

Subramoniam, T. (2000). Crustacean ecdysteriods in reproduction and embryogenesis. *Comp. Biochem. Physiol.* **125C**, 135-156.

Szwed, A., Kim, E. and Jacinto, E. (2021). Regulation and metabolic functions of mTORC1 and mTORC2. *Physiol. Rev.* **101**, 1371-1426.

Taher, T.B., Althaus, C.E., Tranter, P.J. and Evans, M.C. (2023). Impacts of shrimp aquaculture on the local communities and conservation of the world's largest protected mangrove forest. *Environ. Sci. Policy.* **147**, 351-360.

Tamm, G.R. and Cobb, J.S. (1978). Behavior and the Crustacean Molt Cycle: Changes in Aggression of *Homarus americanus*. *AAAS.* **200**, 79-81.

Tamone, S.L., Adams, M.M. and Dutton, J.M. (2005). Effect of Eyestalk-Ablation on Circulating Ecdysteroids in Hemolymph of Snow Crabs, *Chionoecetes opilio*: Physiological Evidence for a Terminal Molt. *Integr. Comp. Biol.* **45**, 166-171.

Tang, Y., Liu, F., Lu, L., Liu, A. and Ye, H. (2024). Identification of ETH receptor and its possible roles in the mud crab *Scylla paramamosain*. *Comp. Biochem. Physiol.* **297A**, 11.

Tarrant, M.K. and Cole, P.A. (2009). The chemical biology of protein phosphorylation. *Ann. Rev. Biochem.* **78**, 797-825.

Tepolt, C.K. and Somero, G.N. (2014). Master of all trades: thermal acclimation and adaptation of cardiac function in a broadly distributed marine invasive species, the European green crab, *Carcinus maenas*. *J. Exp. Biol.* **217**, 1129-38.

Tepolt, C.K. and Palumbi, S.R. (2020). Rapid Adaptation to Temperature via a Potential Genomic Island of Divergence in the Invasive Green Crab, *Carcinus maenas*. *Front. Ecol. Evol.* **8**, 580701.

Till, R., Barth, A., Tschirner, M., Patrick, S., Marius, W., André, B., Thomas, W. and Andreas, V. (2023). Insect feed in sustainable crustacean aquaculture. *JIFF.* **9,** 1115-1138l.

Tran, N.M., Mykles, D.L., Elizur, A. and Ventura, T. (2019). Characterization of G-protein coupled receptors from the blackback land crab *Gecarcinus lateralis* Y organ transcriptome over the molt cycle. *BMC Genom.* **20**, 74.

Truman, J.W. (2019). The Evolution of Insect Metamorphosis. *Curr. Biol.* **29**, R1252-R1268.

Tsang, L.M., Schubart, C.D., Ahyong, S.T., Lai, J.C.Y., Au, E.Y.C., Chan, T.-Y., Ng, P.K.L. and Chu, K.H. (2014). Evolutionary History of True Crabs (Crustacea: Decapoda: Brachyura) and the Origin of Freshwater Crabs. *Molec. Biol. Evol.* **31**, 1173-1187.

Vasquez, O.E., Allen, A.M., So, A.K.-C., Nguyen, Q., H., Krause, H.M., Levine, J.D. and Sokolowski, M.B. (2023). Characterizing the protein isoforms of foraging (for), the PKGI ortholog in *Drosophila melanogaster*. *Int. J. Molec. Sci.* **24**, 10219.

Vongliscynski, U. and Sedlmeier, D. (1993). Regulation of ecdysteroid biosynthesis in crayfish Y-Organs: 2. Role of cyclic nucleotide-dependent protein-kinases. *J. Exp. Zool.* **265**, 454-458.

Wall, M.E., Francis, S.H., Corbin, J.D., Grimes, K., Richie-Jannetta, R., Kotera, J., Macdonald, B.A., Gibson, R.R. and Trewhella, J. (2003). Mechanisms associated with cGMP binding and activation of cGMP-dependent protein kinase. *PNAS.* **100**, 2380-2385.

Wang, R., Kwon, I.K., Singh, N., Islam, B., Liu, K., Sridhar, S., Hofmann, F. and Browning, D.D. (2014). Type 2 cGMP-dependent protein kinase regulates homeostasis by blocking c-Jun N-terminal kinase in the colon epithelium. *Cell Death Diff.* **21**, 427-437.

Washburn, B.E., Bernhardt, G.E., Kutschbach-Brohl, L., Chipman, R.B. and Francoeur, L.C. (2013). Foraging Ecology of Four Gull Species at a Coastal-Urban Interface: Ecología de Forrajeo de Cuatro Especies de Gaviota en una Interface Costera-Urbana. *Condor.* **115**, 67-76.

Watson-Zink, V.M. (2021). Making the grade: Physiological adaptations to terrestrial environments in decapod crabs. *Arthropod Struct. Dev.* **64**, 101089.

Webster, S.G. (1986). Neurohormonal control of ecdysteroid biosynthesis by *Carcinus maenas* Y-organs *in vitro*, and preliminary characterization of the putative molt-inhibiting hormone (MIH). *Gen. Comp. Endocrinol.* **61**, 237-247.

Webster, S.G., Keller, R. and Dircksen, H. (2012). The CHH-superfamily of multifunctional peptide hormones controlling crustacean metabolism, osmoregulation, moulting, and reproduction. *Gen. Comp. Endocrinol.* **175**, 217-233.

Webster, S.G. (2015). Endocrinology of molting. *The Natural History of the Crustacea: Physiology* (ed. E. S. Chang and M. Thiel), pp. 1-35. Oxford: Oxford Press.

Weis, J.S. (1976). Effects of environmental factors on regeneration and molting in fiddler crabs. *Biol. Bull.* **150**, 152-162.

Willems, K.A. (1982). Larval Development of the Land Crab *Gecarcinus Lateralis Lateralis* (Fréminville, 1835) (Brachyura: Gecarcinidae) Reared in the Laboratory. *J. Crustacean Biol.* **2**, 180-201.

Willig, A. (1974). Die rolle der ecdysone em haeutungszuklus der crustacean, Translated 1976. *Fortschr. Zool.* **22**, 55-74.

Wolcott, D.L. and Wolcott, T.G. (1984). Food Quality and Cannibalism in the Red Land Crab, *Gecarcinus lateralis*. *Physiol. Zool.* **57**, 318-324.

Wolcott, T.G. and Wolcott, D.L. (1982). Larval loss and spawning behavior in the land crab *Gecarcinus lateralis* (Fréminville). *J. Crustacean Biol.* **2**, 477-485.

Wolfe, J.M., Brieinholt, J.W., Crandall, K.A., Lemmon, A.R., Lemmon, E.M., Timm, L.E., Siddall, M.E. and Bracken-Grisson, H.D. (2019). A phylogenomic framework, evolutionary timeline and genomic resources for comparative studies of decapod crustaceans. *Proc. Roy. Soc. London, Ser. B, Biol. Sci.* **286**, 20190079.

Wolfe, J.M., Ballou, L., Luque, J., Watson-Zink, V.M., Ahyong, S.T., Barido-Sottani, J., Chan, T.-Y., Chu, K.H., Crandall, K.A., Daniels, S.R., et al. (2024). Convergent Adaptation of True Crabs (Decapoda: Brachyura) to a Gradient of Terrestrial Environments. *Syst. Biol.* **73**, 247-262.

Yee Kuen, C. and Masarudin, M.J. (2022). Chitosan Nanoparticle-Based System: A New Insight into the Promising Controlled Release System for Lung Cancer Treatment. *MOL.* **27**, 473.

Yorio, P., Suárez, N., Kasinsky, T., Pollicelli, M., Ibarra, C. and Gatto, A. (2020). The introduced green crab (*Carcinus maenas*) as a novel food resource for the opportunistic kelp gull (*Larus dominicanus*) in Argentine Patagonia. *Aquat. Invasions* **15**, 140-159.

Young, A.M. and Elliott, J.A. (2020). Life History and Population Dynamics of Green Crabs (*Carcinus maenas*). *Fishes.* **5**, 1-44.

Yu, X.L., Chang, E.S. and Mykles, D.L. (2002). Characterization of limb autotomy factor-proecdysis (LAFpro), isolated from limb regenerates, that suspends molting in the land crab *Gecarcinus lateralis*. *Biol. Bull.* **202**, 204-212.

Zacarias, S., Carboni, S., Davie, A. and Little, D.C. (2019). Reproductive performance and offspring quality of non-ablated Pacific white shrimp (*Litopenaeus vannamei*) under intensive commercial scale conditions. *Aquaculture.* **503**, 460-466.

Zhang, X., Pan, L., Wei, C., Tong, R., Li, Y., Ding, M. and Wang, H. (2020). Crustacean hyperglycemic hormone (CHH) regulates the ammonia excretion and metabolism in white shrimp, *Litopenaeus vannamei* under ammonia-N stress. *Sci. Total Environ.* **723**, 138128.

Zhong, Q., Xiao, X., Qiu, Y., Xu, Z., Chen, C., Chong, B., Zhao, X., Hai, S., Li, S., An, Z., et al. (2023). Protein posttranslational modifications in health and diseases: Functions, regulatory mechanisms, and therapeutic implications. *MedComm.* **4**, e261.

CHAPTER TWO

TWO cGMP-DEPENDENT PROTEIN KINASES HAVE OPPOSING EFFECTS ON MOLT-INHIBITING HORMONE REGULATION OF Y-ORGAN ECDYSTEROIDOGENESIS[1]

SUMMARY

Decapod crustaceans regulate molting through steroid molting hormones, ecdysteroids, synthesized by the molting gland (Y-organ, YO). Molt-inhibiting hormone (MIH), a neuropeptide synthesized and secreted by the eyestalk ganglia, negatively regulates YO ecdysteroidogenesis. MIH signaling is mediated by cyclic nucleotide second messengers. cGMP-dependent protein kinase (PKG) is the presumed effector of MIH signaling by inhibiting mechanistic Target of Rapamycin Complex 1 (mTORC1)-dependent ecdysteroidogenesis. Phylogenetic analysis of PKG contiguous sequences in CrusTome as well as 35 additional species in NCBI RefSeq, identified 206 PKG1 sequences in 108 species and 59 PKG2 sequences in 53 species. These included four *PKG1α* splice variants in the N-terminal region that were unique to decapods, as well as *PKG1β* and *PKG2* homologs. *In vitro* assays using YOs from the blackback land crab (*Gecarcinus lateralis*) and green shore crab (*Carcinus maenas*) determined the effects of MIH ± PKG inhibitors on ecdysteroid secretion. A general PKG inhibitor, Rp-8-Br-PET-cGMPS, countered the effects of MIH, as ecdysteroid secretion increased in PKG-inhibited YOs compared to *C. maenas* YOs incubated with MIH alone. By contrast, a PKG2-specific inhibitor, AP-C5 (4-[4-(1*H*-Imidazol-1-yl)phenyl]-*N*-2-propyn-1-yl-2-pyrimidinamine),

[1] This chapter was published in the Journal of Experimental Biology in January 2025: Head, T.B., Pérez-Moreno, J.L., Ventura, T., Durica, D.S., Mykles, D.L. (2025). Two cGMP-dependent protein kinases have opposing effects on molt-inhibiting hormone regulation of Y-organ ecdysteroidogenesis. *J. Exp. Biol.* DOI 10.1242/jeb.249739.

enhanced the effects of MIH, as ecdysteroid secretion decreased in *G. lateralis* and *C. maenas* YOs incubated with AP-C5 and MIH compared to YOs incubated with MIH alone. These data suggest that both PKG1 and PKG2 are activated by MIH, but have opposing effects on mTORC1-dependent ecdysteroidogenesis. A model is proposed in which the dominant role of PKG1 is countered by PKG2, resulting in low ecdysteroid production by the basal YO during intermolt.

INTRODUCTION

Growth in decapod crustaceans is restricted by the presence of a chitin-based exoskeleton that must be periodically shed through the process of molting. Molting is regulated primarily by the neuropeptide molt-inhibiting hormone (MIH) produced in the X-organ/sinus gland complex in the eyestalk ganglia (ESG), and ecdysteroids produced by a pair of molting glands or Y-organs (YOs) located in the cephalothorax (reviewed in Mykles, 2024; Fehsenfeld, 2024). The YO transitions through four physiological states over the molt cycle. These are the basal state during intermolt (stage C_4), activated state during early premolt (stage D_0), committed state during mid- and late premolt (stages D_1 and D_{2-3}, respectively), and repressed state during postmolt (stages A, B, and C_{1-3}; reviewed in Mykles, 2011; Mykles and Chang, 2020). Ecdysteroid synthesis in the basal YO is attenuated by the action of MIH, resulting in low levels of YO ecdysteroid secretion and low titers of ecdysteroid in the hemolymph (Mykles, 2011; Mykles and Chang, 2020). The activated YO is characterized by an increase in ecdysteroid synthesis and secretion that initiates premolt processes in peripheral tissues, but the YO itself remains sensitive to MIH (Mykles, 2024). Increased ecdysteroidogenesis by the activated YO requires mechanistic Target of Rapamycin Complex 1 (mTORC1)-dependent protein synthesis (reviewed in Mykles and Chang, 2020; Mykles, 2021). Once the YO reaches the committed

state, the YO becomes insensitive to MIH; ecdysteroid synthesis increases to a peak in late premolt, which ultimately triggers ecdysis (Mykles and Chang, 2020; Mykles, 2024). During postmolt, the repressed YO has low ecdysteroidogenic activity, resulting in the lowest hemolymph ecdysteroid titers of the molt cycle stages (Mykles, 2011). Transcriptional down-regulation of MIH and mTORC1 signaling genes suggests that the repressed YO is refractory to endocrine factors until the YO transitions back to the basal state (Mykles and Chang, 2020).

MIH signaling involves cyclic nucleotide second messengers organized into a transient cAMP/Ca^{2+}-dependent triggering phase linked to a sustained NO/cGMP-dependent summation phase (reviewed in Webster et al., 2012; Webster, 2015; Mykles and Chang, 2020). The transient increase in cAMP and sustained increase in cGMP together with the *in vitro* inhibition of ecdysteroid secretion by analogs of either cyclic nucleotide suggest that MIH binding stimulates cyclic AMP-dependent kinase (PKA) activity, which, in turn, stimulates prolonged cGMP-dependent protein kinase (PKG) activity (reviewed in Covi et al., 2009; Webster et al., 2012; Mykles and Chang, 2020). Pulsatile release of MIH from the sinus gland inhibits YO ecdysteroidogenesis and maintains the YO in the basal state (Mykles and Chang, 2020). In the proposed model, binding of MIH to a G protein-coupled receptor (GPCR) activates PKA activity, which leads to activation of a Ca^{2+}-dependent NO synthase, NO-dependent guanylyl cyclase, and PKG (Mykles and Chang, 2020). Although the identity of the MIH receptor has not been established with any certainty, it is hypothesized that it is homologous to insect ion transport peptide GPCRs (Kozma et al., 2024).

PKG activity is the primary effector regulating mTORC1-dependent YO ecdysteroidogenesis by MIH (Mykles, 2021). As proposed, PKG mediates mTORC1 activity via the tuberous sclerosis complex (TSC; Mykles, 2021). TSC is a heterotrimeric GTPase-activating

protein that inactivates the small G protein Ras homolog enriched in brain (Rheb), an activator of mTORC1, by promoting the hydrolysis of GTP to GDP (reviewed in Shi and Collins, 2023; Wang et al., 2024). In mammalian cardiomyocytes, PKG1 phosphorylation of the TSC2 subunit activates TSC, resulting in inhibition of mTORC1 (Ranek et al., 2019; Oeing et al., 2020).

PKGs are members of AGC (PKA, PKG, PKC) subfamily of serine/threonine protein kinases (reviewed in Leroux et al., 2018). PKGs occur as homodimers in the native state. Each subunit has an N-terminal regulatory region consisting of a leucine/isoleucine-zipper (LZ) domain and a cGMP-binding domain with two cyclic nucleotide binding sites, and a C-terminal region containing a protein kinase domain; an autoinhibitory site is located between the LZ and cGMP-binding domains (Kim and Sharma, 2021). The LZ domain mediates dimerization and docking with G-kinase anchoring proteins (GKAPs) that facilitate sub-cellular localization (Vo et al., 1998; Casteel et al., 2010).

In mammals, PKGs are encoded by two genes, designated *prkg1* and *prkg2* (Kim and Sharma, 2021). Alternative splicing produces two PKG1 isoforms, designated PKG1α and PKG1β, which differ in the N-terminal region that includes the LZ domain (Hofmann, 2020; Kim and Sharma, 2021). By contrast, PKG2 occurs as a single gene product (Hofmann, 2020; Kim and Sharma, 2021). PKG2 is known to localize to the plasma membrane by myristoylation of the N-terminus, whereas mammalian PKG1 isoforms are cytosolic (Vaandrager et al., 2005; Yuasa et al., 2008; and reviewed in Hofmann, 2020). In *Drosophila*, PKGs are also encoded by two genes, *foraging* (*for*) or *dg2* is homologous to PKG1 and encodes 21 alternatively spliced transcripts, while *dg1* is homologous to PKG2, encoding only one protein product (Kalderon and Rubin, 1989; Allen et al., 2017). PKG1 homologs have been linked to functional changes in

food-related behaviors in fruit flies, honeybees, and nematodes (Fitzpatrick and Sokolowski, 2004).

The decapod YO expresses all the components of the MIH signaling pathway, including PKG (Das et al., 2016; Mykles, 2021). In the blackback land crab, *Gecarcinus lateralis*, PKG1 transcript expression in the YO is molt-stage dependent with the highest expression occurring in the basal YO (Das et al., 2018). Here we report a comprehensive analysis of crustacean PKGs using bioinformatic tools and biochemical assays. Taking advantage of the CrusTome database (Pérez-Moreno et al., 2023), phylogenetic analysis identified contiguous sequences encoding four PKG1 isoforms and PKG2 in decapod crustaceans. Multiple sequence alignments identified conserved motifs that distinguished PKG1 isoforms. *In vitro* assays of YOs from *G. lateralis* and green shore crab (*Carcinus maenas*) determined the effects of PKG inhibitors on MIH control of ecdysteroid secretion. Surprisingly, the results indicate that PKG1 and PKG2 had opposing effects, which may explain how the basal YO maintains low ecdysteroid secretion rates in the presence of MIH in intermolt animals.

MATERIALS AND METHODS

Animals and ecdysteroid quantification

Adult male *G. lateralis* (Fréminville 1835) were collected in the Dominican Republic and shipped overnight via air cargo to Colorado, USA. Animals were housed in group cages containing 10-15 animals each with an aspen bedding substrate moistened with 5 ppt Instant Ocean at 27 ºC and 80% relative humidity on a 12 h:12 h light:dark schedule as described (Covi et al., 2010). Animals were fed lettuce, carrots, and raisins twice a week. Molt stage was determined by limb regenerate growth, condition of the membranous layer of the exoskeleton,

and hemolymph ecdysteroid titer (Covi et al., 2010). For the YO assays, intermolt animals were eyestalk-ablated (ESA) 3 days prior to the assay to activate the YOs (Lee et al., 2007a).

Adult male *Carcinus maenas* (Linnaeus 1758) were collected from Bodega Harbor, Bodega Bay, California, USA and maintained at the Bodega Marine Laboratory in a flow-through seawater system at ambient sea water temperatures (12-16 ºC). Crabs were fed weekly with fish.

Ecdysteroid concentrations in hemolymph and YO media samples were quantified by a competitive enzyme-linked immunosorbent assay (ELISA; Kingan, 1989) as modified by Abuhagr et al. (2014).

Synthesis of Gl-MIH

The full-length mature *G. lateralis* MIH (Gl-MIH, without the signal peptide) was synthesized using the solid phase Fmoc (FluorenylMethylOxyCarbonyl) methodology by Pepmic Co., Ltd (Suzhou, China). The specific synthesis steps followed previously established procedures (Mosco et al., 2012) and chemical synthesis took into account the three disulfide bridges through the use of semi-synthetic tethers (Thalluri et al., 2018). The Gl-MIH amino acid sequence is as follows:

AVINDE**C**PNVIGNRDIFKKVDWI**C**ED**C**ANIFRIDGLATL**C**RKN**C**FRNIDFLW**C**VYASERQ AEKDELTRYVSILRAGSV with three disulfide bridges (Cys7:Cys44, Cys24:Cys40, and Cys27:Cys53; indicated by bold font). The mature *G. lateralis* MIH sequence shares 67% AA identity and 84% similarity with *C. maenas*.

Y-organ assay

An *in vitro* assay quantified the effects of MIH with or without PKG inhibitors on YO ecdysteroid secretion. YOs from adult male intermolt *C. maenas* or from 3-day post-ESA *G.*

lateralis were used. The *G. lateralis* physiological saline consisted of 316 mM NaCl, 5.4 mM KCl, 8.8 mM $CaCl_2$, 6.8 mM $MgSO_4$, and 1 mM Na_3PO_4 and 10 mM HEPES-NaOH (pH 7.4). The *C. maenas* physiological saline consisted of 430 mM NaCl, 5 mM K_2SO_4, 7 mM $MgCl_2$, 4.5 mM $CaCl_2$, and 10 mM HEPES-NaOH (pH 7.2). A general PKG inhibitor, Rp-8-Br-PET-cGMPS (2-Bromo-3,4-dihydro-3-[3,5-*O*-[(*R*)-mercaptophosphinylidene]-β-D-ribofuranosyl]-6-phenyl-9*H*-Imidazo[1,2-*a*]purin-9-one; Cayman Chemical, Ann Arbor, MI, USA) and a PKG2-specific inhibitor, AP-C5 (4-[4-(1*H*-Imidazol-1-yl)phenyl]-*N*-2-propyn-1-yl-2-pyrimidinamine; R&D Systems Inc., Minneapolis, MN, USA), were dissolved in dimethyl sulfoxide (DMSO) and diluted 100-fold in crab saline to achieve final inhibitor concentrations of 1, 10, or 100 µM for *C. maenas* and 100 µM for *G. lateralis* (one concentration was used due to a limited number of animals).

One set of experiments determined the biological activity of MIH. YO pairs were incubated with either saline control or 50 nM MIH. A second set of experiments tested the effects of PKG inhibitors ± 50 nM MIH. Hemolymph samples were taken for each animal before dissection to assess molt stage based on circulating ecdysteroid titers. One YO in the pair from each animal served as the MIH control treatment, while the other YO served as the MIH and PKG inhibitor experimental treatment. YOs were preincubated for 30 min at room temperature in 0.5 ml saline containing either 1% DMSO (control treatment) or PKG inhibitor and 1% DMSO (experimental treatment) on an orbital shaker at 100 rpm. After preincubation, YOs were transferred to 0.5 ml saline containing either 50 nM MIH and 1% DMSO (control) or 50 nM MIH, PKG inhibitor, and 1% DMSO (experimental) for 4.5 h at 100 rpm at room temperature. Hemolymph (100 µl) and a subset of media (200 µl) samples were combined with three volumes of methanol and stored at -15 ˚C until quantification with the competitive ELISA. In *C. maenas*

animals determined to be in premolt (>100 pg/µl) or postmolt (<20 pg/µl) based on hemolymph 20E were excluded from analysis. Data are expressed as percent of control [(experimental 20E secretion/control 20E secretion) *100]. Statistical significance between the means was determined by a two-tailed paired t-test in RStudio (v. 2024.4.1.748; Rstudio Team, 2024).

Bioinformatics and phylogenetic analyses

Protein reference sequences were obtained from the NCBI Reference Sequence Database (RefSeq; O'leary et al., 2016), GenBank (Sayers et al., 2020), and UniProtKB (Consortium, 2022) and used as the query for four iterative BLAST searches against the CrusTome database (v.0.1.0) to ensure broad phylogenetic representation among crustaceans (Altschul et al., 1990; Pérez-Moreno et al., 2023). Protein sequences, including reference sequences and BLAST results, were aligned using MAFFT-DASH with the flag "-originalseqonly" (v7.508; Rozewicki et al., 2019). MSAs were trimmed using ClipKit with the smart-gap parameter to trim alignment gaps while maintaining phylogenetically informative sites (Steenwyk et al., 2020). Phylogeny was inferred using IQ-TREE (v1.6.12; Trifinopoulos et al., 2016) to construct a maximum likelihood phylogenetic tree and evolutionary models were estimated using ModelFinder (Kalyaanamoorthy et al., 2017) as optimized in IQ-TREE.

Initial trees were refined by removing partial sequences with 200 or fewer amino acids, those that did not contain at least two of the conserved domains found in PKGs (leucine-zipper, two cGMP binding domains, and a kinase domain), sequences with ambiguous residues, those that appeared to be other related proteins (e.g., those containing kinase or cyclic-nucleotide binding domains), and those that were contamination from nematodes which often infect crustaceans. Nematode contamination was initially identified by long branch lengths and erroneous position within phylogenies, and subsequently validated with NCBI BLAST. Final

trees were constructed with the refined dataset using the above parameters and rooted at the midpoint. Branch support for phylogenetic relationships was estimated with UltraFast Bootstrap approximation (UFBoot; Minh et al., 2013) with 1000 iterations, as well as an approximate Bayes test. Final tree files, input files, and multiple sequence alignments are deposited on Dryad at https://doi.org/10.5061/dryad.1g1jwsv7b.

CD-Search in the NCBI Conserved Domain Database (CDD, v3.20; Wang et al., 2023) and EMBL-EBI's InterProScan (IPS, v5.69-101.0; Paysan-Lafosse et al., 2023) were used to predict and annotate the position of conserved domains and essential residues in *G. lateralis* and *C. maenas* sequences. MSAs were generated using MAFFT and visualized using the *plot_msa.py* script (Kozma et al., 2024) available at https://github.com/invertome/scripts/tree/main/plots.

Relative expression of PKG1 and PKG2 in the Y-organ

Relative transcript expression in transcripts per million reads (TPM) of intermolt YOs was determined for *G. lateralis* using RNAseq data from Das et al. (2018). PKG1 isoforms were not distinguished in this dataset due to the method of transcript assembly available at that time. Therefore, PKG1 transcript expression was assumed to be pooled expression of all reads from PKG1 sequences that mapped to the PKG1β contig sequence. Relative transcript expression for *C. maenas* YOs was obtained from the intermolt YO RNAseq data generated by Oliphant et al. (2018), assembled in the CrusTome database, and quantified into TPM using Salmon (v.1.7.0). Salmon quantifications were run with the following flags "*--seqBias --gcBias –validateMappings*" to ensure accurate quantification by avoiding potential biases. Expression was graphed as mean ± standard error of the mean (SEM) in RStudio (v.2024.04.1.748).

PKG sequence validation

Sequencing of PCR products was used to validate the identities of the *G. lateralis* and *C. maenas* PKGs. Combined cDNA from YO, heart, and claw muscle was used as template for PCR using sequence-specific primers directed to the N-terminal region (Table A1). As the primers for the four PKG1 (α1-3, β) isoforms identified in these species spanned the putative alternative splicing site, the same reverse primer was used for each isoform; the forward primer was isoform-specific. PCR conditions were as follows: initial denaturation at 95 ºC for 2 min, followed by 35 cycles of denaturation at 95 ºC for 30 sec, annealing at 55 ºC for 30 sec, and extension at 72 ºC for 45 sec, and a final extension cycle at 72 ºC for 10 min. PCR products were purified from agarose gels using the QIAEX II Gel Extraction Kit (QIAGEN, Hilden, Germany) and sequenced by GeneWiz (Azenta Life Sciences, South Plainfield, NJ, USA).

RESULTS

Effects of Gl-MIH and PKG inhibitors on Y-organ ecdysteroid secretion

The biological activity of the synthetic Gl-MIH was tested by incubating YOs in media without (control) or with 50 nM Gl-MIH. The synthetic peptide was more effective on *C. maenas* YOs. In *C. maenas*, MIH significantly inhibited ecdysteroid secretion by 63% (37% of control ± 8%, n = 7; $p = 0.006$). In *G. lateralis*, ecdysteroid secretion with MIH was 51% lower than the control. However, the difference in the means did not reach significant levels (49% of control ± 11%, n = 8; $p = 0.054$).

A general PKG inhibitor, Rp-8-Br-PET-cGMPS, countered the inhibitory effect of MIH on YO ecdysteroid secretion in *C. maenas* (Fig. 2.1A). YO secretion in media containing 10 µM or 100 µM Rp-8-Br-PET-cGMPS and 50 nM MIH was significantly higher than that of the paired control YOs incubated with 50 nM MIH alone (217% and 311% of control; $p = 0.017$ and

$p = 0.006$, respectively). In *G. lateralis*, 100 µM Rp-8-Br-PET-cGMPS had no effect on YO ecdysteroid secretion (101% of MIH control; $p = 0.92$; Fig. 2.1B).

A PKG2-specific inhibitor, AP-C5, enhanced the inhibitory effect of MIH on ecdysteroid secretion in both *C. maenas* and *G. lateralis* YOs (Fig. 2.1C, D). In *C. maenas*, AP-C5 showed a concentration-dependent effect on YO secretion (Fig. 2.1C). In media containing 1 µM, 10 µM, or 100 µM AP-C5 and 50 nM MIH, YO secretion was significantly lower than that of the paired control YOs incubated with 50 nM MIH alone (60%, 24%, and 10% of the control; $p = 0.04$, $p = 0.0002$ and $p = 0.0002$, respectively). In *G. lateralis*, 100 µM AP-C5 and 50 nM MIH significantly lowered ecdysteroid secretion with respect to 50 nM MIH alone (Fig. 2.1D; 24% of the control; $p = 0.0004$).

Phylogenetic analysis and classification of PKG sequences

Phylogenetic analysis of pancrustacean and tardigrade sequences from CrusTome and selected vertebrate sequences from RefSeq (NCBI), GenBank (NCBI), and UniProtKB showed that PKG sequences partitioned into PKG1 and PKG2 clades (Fig. 2.2). PKG1 formed a monophyletic group consisting of 206 sequences among 108 species, with subclades in vertebrates and decapods distinguishing PKG1α and PKG1β isoforms (Fig. 2.2). PKG2 formed a monophyletic group consisting of 60 sequences among 53 species (Fig. 2.2). The distribution of PKG1 and PKG2 sequences in the Ecdysozoa in the CrusTome database is summarized in Table 2.1. In 42 decapod species, 107 sequences were identified; PKG1α sequences were more common than PKG1β and PKG2 sequences. Copepoda had 20 sequences in 8 species and Isopoda had 19 sequences in 14 species (Table 2.1). The number of PKG sequences ranged between one and nine in the other ten taxa.

Within decapods, PKG1 isoforms were classified as alpha or beta based upon homology with annotated reference sequences and the position in the phylogenetic tree, as well as identification of the leucine zipper as either DD_cGKI-alpha (cd12085) or DD_cGKI-beta (cd12086) by NCBI CDS software. Importantly, predicted PKG1 sequences deduced from the NCBI Eukaryotic Genome Annotation Pipeline (accession numbers beginning with XP) match transcripts found in CrusTome (Table 2.2). Phylogenetic analysis identified four alpha (PKG1α1, PKG1α2, PKG1α3, and PKG1α4) isoforms and one beta (PKG1β) isoform in decapod species (Fig. 2.3). The naming convention used here provides clear annotation of PKG1 isoforms as either alpha or beta, as well as subtypes of alpha, rather than the vague "isoform X1" used in reference sequence databases.

PKG2 was identified in all decapod taxa, except penaeid shrimp (Fig. 2.4; Table 2.2). A single PKG2 transcript was identified in each of the decapod species, including identical transcripts in dactyl and lateral flagella (E) and YO in the blue crab, *Callinectes sapidus* (Fig. 2.4). The *Procambarus clarkii* PKG2 sequence predicted from genomic data matched that of the *Pc-PKG2* contig sequence assembled in CrusTome (Table 2.2). The *Eriocheir sinensis* PKG2 sequence predicted from genomic data contained a full-length ORF, while the *Es-PKG2* contig sequence assembled in CrusTome is missing a portion of the N-terminal (Table 2.2).

Domain organization and sequence analysis of decapod PKGs

The domain organization of PKGs was highly conserved in metazoan species (Kim and Sharma, 2021). Figure 2.5 shows the functional domains of *G. lateralis* PKGs as representative of the decapod sequences. The N-terminal regulatory region contained a leucine zipper (LZ) domain, an autoinhibitory (AI) site, and two cyclic nucleotide binding (CNB) domains in the cGMP-binding domain. The C-terminal catalytic region contained a kinase domain with ATP

and substrate binding sites. The PKG1 isoforms differed in the N-terminal sequence that included the LZ domain and AI site (Fig. 2.5).

Multiple sequence alignment of decapod sequences identified four PKG1α isoforms, designated PKG1α1, PKG1α2, PKG1α3, and PKG1α4 (Fig. 2.6). PKG1α isoforms differed in the N-terminal sequence that included the LZ domain. The isoforms were first distinguished by the length and amino acid sequence upstream from the LZ domain (Fig. 2.6A-D). PKG1α1 sequences in Anomura and Brachyura began with MPL[P/S] (reference positions #1-4) and ranged from 14 to 20 amino acids in length before the beginning of the LZ domain (Fig. 2.6A). PKG1α2 was identified in all decapod taxa. This isoform began with MPQ[L/F] (reference positions #1-4) and was 14 to 15 amino acids in length (Fig. 2.6B). PKG1α3 was identified in Anomura, Astacidea, Brachyura, and Caridea. The protein began at the LZ domain sequence MGS[L/M] (Fig. 2.6C; reference positions #21-24). PKG1α4 was identified only in Achelata, Astacidea, and Caridea. This isoform began with MS[E/L/K/Q] (Fig. 2.6D; reference positions #1-3). The LZ domain commonly began with MES (reference positions #19-21), rather than MGS found in the other alpha isoforms (Fig. 2.6D). Other PKG1α sequences that occurred in Astacidea and Caridea could not be assigned to the four isoforms. These sequences were designated "PKG1α-", as they appeared to be an additional isoform unique to Astacidea and Caridea (Fig. 2.3). Sequences for Gl-PKG1α and Cm-PKG1α isoforms were validated by direct sequencing of purified PCR products (see Materials and Methods).

Multiple sequence alignment of decapod sequences identified one PKG1β isoform. Compared to PKG1α isoforms, the PKG1β sequences had an extended N-terminal sequence rich in glycine residues that ranged in length between 33 and 47 amino acids upstream of the LZ domain (Fig. 2.6E). The PKG1β LZ domain sequence began with LRDT (reference positions

#63-65) and diverged significantly from the alpha isoforms until the 3' end of the LZ domain, in which all the PKG1 isoforms ended with LDKxxSV[I/M/L]P (Fig. 2.5). Sequences for Gl-PKG1β and Cm-PKG1β isoforms were validated by direct sequencing of purified PCR products (see Materials and Methods).

Sequence analysis of the *G. lateralis* and *C. maenas* contigs indicated that the PKG1α1, PKG1α2, PKG1α3, and PKG1β isoforms in CrusTome were alternatively spliced mRNA products of the same gene. The PKG1 isoforms in each species had identical 3'-untranslated regions (UTRs) but varied in 5'-UTR sequences. The open reading frames (ORFs) differed in the DNA sequence of the 5' region encoding the LZ domain and much of the region before the first CNB site (Fig. 2.7). A conserved serine (reference position #180; indicated by a star) marked the beginning of DNA and protein sequence identity in all four isoforms in each species (Fig. 2.7). Conserved amino acids predicted to be important for function were identified in the LZ, cGMP-binding, and kinase domains (Fig. 2.7).

Analysis of the Gl-PKG2 and Cm-PKG2 sequences indicated that the contigs were products of a single gene. The sequences were validated by direct sequencing of purified PCR products (see Materials and Methods). Both proteins had a long N-terminal extension consisting of a ~190-amino acid sequence rich in glycine, proline, and a consecutive stretch of histidine (Fig. 2.8; reference positions #150-162). An annotated LZ sequence, including conserved residues, for PKG2 was identified through IPS as CDD did not identify the LZ domain in these sequences. Conserved amino acids predicted to be important for function were identified in the LZ, cGMP-binding, and kinase domains (Fig. 2.8).

GKAP-docking residues in the LZ domain predicted by CDD and IPS were unique to each isoform. The four predicted GKAP-docking residues were [R/K]DxExK in PKG1α1;

[R/H]RxExK in PKG1α2; KQxExV in PKG1α3; and [Q/K]RxExE in PKG1β (Fig. 2.7; reference positions #55, #56, #58, and #60). The predicted GKAP-docking residues in PKG2 were DVxExQ (Fig. 2.8; reference positions #209, #210, #212, and #221). The location of putative decapod GKAP-docking residues within the leucine zipper aligns with that of annotated reference sequences in human and mouse (alignment available on Dryad). Glutamic acid (E) is the third amino acid was conserved in all human, mouse, and decapod GKAP-docking sites for PKG1 and PKG2. However, the first, second, and fourth GKAP-docking residues varied between mammalian and decapod sequences.

Novel PKG1ins isoform in crustaceans

Unexpectedly, PKG1 sequences with a 14- to 17-amino acid insertion located in the kinase domain were identified in ten decapod and one stomatopod species (Fig. 2.6F; Table A2). For all but two species, a matching transcript was identified for the same isoform that did not contain the insertion (Fig. 2.6F). This conserved insertion was identified in several different PKG1 isoforms, including PKG1α2, PKG1α3, PKG1α4, the ungrouped PKG1α-, and PKG1β (Fig. 2.3). Sequences containing this insertion were denoted with 'ins' to differentiate them from the corresponding isoform sequence lacking the insertion (Fig. 2.6F). The insertion appeared to be unique to crustaceans and was located upstream of the activation loop in the catalytic site. It added amino acids in the region between conserved residues involved in substrate binding, ATP binding, and the active site (Fig. 2.6F). The insertion did not contain additional functional residues annotated by NCBI CDS.

PKG expression in the Y-organ

The relative expression of PKG1 and PKG2 in *G. lateralis* and *C. maenas* YOs was calculated using transcriptomic data from intermolt animals. In *G. lateralis* only the PKG1β

isoform was identified (Das et al., 2018), which was likely due to the assembly methods used that did not distinguish between isoforms. Therefore, we assume that the expression of PKG1α isoforms were also included in PKG1β, resulting in an overall quantification of PKG1 expression in the *G. lateralis* YO. For *C. maenas*, all PKG1α isoforms were identified in the CrusTome database. However, *Cm-PKG1α1* and *Cm-PKG1α2* were expressed in both the YO and central nervous system (CNS), while PKG1α3 was only expressed in the CNS (Table 2.2). Regardless of isoform, PKG1 transcript expression in the intermolt YO far exceeded that of PKG2 in both species. PKG1 expression was two orders of magnitude greater than that of PKG2 in the *G. lateralis* intermolt YO (Fig. 2.9A). PKG1 expression was three orders of magnitude greater than that of PKG2 in the *C. maenas* intermolt YO (Fig. 2.9B).

DISCUSSION

Phylogenetic analysis established that ecdysozoan species have two PKG genes, designated *PKG1* and *PKG2*. These were homologous to the *prkg1*/*PKG I* and *prkg2*/*PKG II* genes in chordates (Fig. 2.2), which indicates a remarkable conservation of *PKG* genes across metazoan taxa. It appears that there has been no gene duplication since the protostome and deuterostome lineages split over 500 million years ago. The crustacean and vertebrate PKGs have the same domain organization (Fig. 2.5; Leroux et al., 2018; Kim and Sharma, 2021). Moreover, the similarity extends to the major *PKG1*/*PKG I* isoforms produced by alternative mRNA splicing. Two *PKG1* and *PKG I* isoforms, designated as alpha and beta, have identical cGMP-binding and C-terminal regions, but differ in the N-terminal region (Figs. 2.2, 2.5; Kim and Sharma, 2021). An exception is *Drosophila*, in which four alternative promoters and alternative mRNA splicing of the *foraging* (*PKG1*) gene produce 21 isoforms (Allen et al., 2017). These isoforms share the same kinase domain but differ in the N-terminal region and

cGMP-binding domain (Allen et al., 2017). By contrast, *PKG2*/*PKG II* is expressed as a single sequence, indicating that alternative mRNA splicing does not occur (Fig. 2.5; Kim and Sharma, 2021). It is notable that the representation of annotated PKG2 sequences is scarce even in repositories, such as RefSeq (NCBI) and UniProtKB, as much of the research has focused on PKG1 and its role in cardiac function (reviewed in Hofmann, 2018; Leroux et al., 2018; Adler et al., 2020; Cuello and Nikolaev, 2020).

Decapod PKGs are likely encoded by two genes, *PKG1* and *PKG2*, that are orthologous to the two corresponding single-copy genes found in humans, mice, *Drosophila*, and other model organisms (Fitzpatrick and Sokolowski, 2004; Kim and Sharma, 2021). Although genomic sequences for *G. lateralis* or *C. maenas* are not available, analyses of the mRNA and amino acid sequences are consistent with transcripts that were generated from two distinct PKG genes. First, the *G. lateralis* or *C. maenas PKG1* mRNAs shared a common 3'-UTR but differed in the 5'-UTRs. Human and mouse *prkg1*/*PKG I* transcripts also share a common 3'-UTR but differ in the 5'-UTR sequences between the α and β isoforms (Sellak et al., 2013). Second, the splice site that joins either the α or β N-terminal sequence to the C-terminal human and mouse *prkg1*/*PKG I* sequences (Sandberg et al., 1989) aligns at the same position in both nucleotide and amino acid sequences with all *G. lateralis* and *C. maenas* PKG1 isoforms. Third, PKG2 is likely a single and separate gene, as only one sequence was identified for *G. lateralis* and *C. maenas* and in 10 other decapod species (Fig. 2.4) and model organisms (Hofmann, 2020). Moreover, PKG1 and PKG2 transcripts differed in both the 3'-UTR and 5'-UTR sequences. The absence of PKG2 in penaeid shrimps was likely a factor of low transcript expression, as opposed to loss of the gene.

Crustacean species express numerous PKG1 isoforms. Identification of multiple isoforms was made possible by taking advantage of the CrusTome RNA sequence database, which

consists of reassembled transcriptomes representing different tissue types and 189 species from the major crustacean taxonomic groups (Pérez-Moreno et al., 2023). Five PKG1α isoforms, designated α-, α1, α2, α3, and α4, and one PKG1β isoform were identified in decapod species (Fig. 2.3). Sequencing of PCR products from the sequences that spanned the LZ domain and putative splice site in the *Gl-PKG1* and *Cm-PKG1* isoforms confirmed that the isoforms were alternatively spliced products of the same gene. In addition, a novel alternatively spliced variant was identified. Designated "ins" this *PKG1* isoform had a 14- to 17-amino acid insertion in the kinase domain (Fig. 2.6F). In most cases, corresponding PKG1α and PKG1β isoforms without the insertion were identified (Fig. 2.3, 2.6F). This suggests that alternative splicing occurs outside of the amino-terminal region in crustaceans. Although located in a highly conserved region between residues involved in substrate binding, ATP binding, and kinase activity (Fig. 2.6F), the functional signification of this insertion in unknown.

PKG1 isoforms and PKG2 sequences differed in the N-terminal region, which has structural and regulatory functions. The LZ domain mediates isoform-specific homodimer formation and subcellular localization (Francis and Corbin, 2013; Kim and Sharma, 2021; Sharma et al., 2022; Hofmann, 2020). The length and amino acid sequences of the LZ domains differed among the PKGs, suggesting that dimerization only occurs between the same proteins (Fig. 2.6). The LZ domain also had four amino acid residues responsible for binding GKAPs, which are isoform-specific and mediate subcellular localization (Casteel et al., 2010). Variation among the predicted GKAP-docking residues for decapod isoforms suggests that each isoform selectively interacts with different GKAPs and may therefore have a unique subcellular localization, which mirrors PKG isoform-specific differences in mammalian cells (Corradini et al., 2015). The specificity of GKAP interactions with individual PKG isoforms is mainly

mediated by the physiochemical properties of the amino acid residues in each isoform. For example, negatively-charged residues in human PKG1β interact with positively-charged residues on associated GKAPs (Casteel et al., 2005; Corradini et al., 2015). A positively-charged lysine in PKG1α mediates the formation of the PKG1α-GKAP complex (Sharma et al., 2008). On the other hand, the LZ of PKG2 interacts with a characterized GKAP through van der Waals forces (Corradini et al., 2015). The physiochemical properties of decapod GKAP-docking sites are unique to each isoform, such as charged amino acids in PKG1α1, PKG1α2, PKG1α4, and PKG1β and hydrophobic or uncharged polar amino acids in PKG1α3 and PKG2 (Fig. 2.6, 2.7, 2.8).

The AI site is a six amino acid motif located between the LZ and CNB-A domains (Fig. 2.5). AI sites are pseudo-substrate motifs that block substrate binding within the catalytic core (Francis and Corbin, 2013; Sharma et al., 2022). The AI sites characterized in human PKG sequences are largely conserved in the decapod sequences (Francis and Corbin, 2013; Sharma et al., 2022). The AI motif sequence (RAQGIS) in human PKG1α is nearly identical in all the decapod PKG1α isoforms (Fig. 2.7). For PKG1β, the human and selected decapod AI sequences differ by one residue (KRQAIS and KRTAIS, respectively; Fig. 2.7). For PKG2, the human and selected decapod AI sequences differ at two resides (AKAGVS and KKQGVS, respectively; Fig. 2.8; Francis and Corbin, 2013; Sharma et al., 2022). These differences in the LZ domain and AI site determine isozyme-specific activation constants and affinities for cGMP (Sharma et al., 2022). Given the strong similarities between decapod and mammalian PKGs, it is likely that the biological properties of these proteins are retained in decapods. These data suggest that expressing multiple PKG1 isoforms broadens its function by expanding the subcellular localization of the protein and/or allowing for activity across a range of cGMP concentrations.

PKG1 and PKG2 had opposite effects on MIH-dependent YO ecdysteroid synthesis and secretion. Experiments using PKG inhibitors ± Gl-MIH showed that PKG1 inhibits ecdysteroidogenesis, while PKG2 stimulates ecdysteroidogenesis (Fig. 2.1). Inhibition of both PKG1 and PKG2 with a cGMP analog reversed the effects of MIH in the *C. maenas* YO, but not in the *G. lateralis* YO (Fig. 2.1 A, B). In addition, Gl-MIH alone was more effective in inhibiting YO ecdysteroid secretion in *C. maenas* than in *G. lateralis* (see Results). Although PKG1 had a dominant role in both species, these data suggest that the two species differed in the relative contributions of PKG1 and PKG2 activity to MIH signaling. RNAseq data showed that PKG1 was expressed at levels about two- and three-orders of magnitude greater than PKG2 in *G. lateralis* and *C. maenas*, respectively (Fig. 2.10). Assuming that protein levels are correlated with transcript levels, the PKG1:PKG2 ratio is estimated to be about 10-fold greater in *C. maenas* than in *G. lateralis*. As MIH activates both PKGs, a lower PKG1:PKG2 ratio would lessen the effect of Gl-MIH ± cGMP analog on the *G. lateralis* YO ecdysteroid secretion. In other words, PKG2 counters the inhibitory effect of PKG1, and the greater the PKG2 activity, the greater the countering effect would be. Consequently, Gl-MIH would have a greater inhibitory effect on *C. maenas* YO than on *G. lateralis* YO. Moreover, the cGMP analog inhibitor would be more effective in reversing the effect of Gl-MIH on the *C. maenas* YO than on the *G. lateralis* YO, which is supported by the results (Fig. 2.1). This data is supported by previous studies in which ecdysteroid secretion by activated YOs was inhibited by the cGMP analog 8-Br-cGMP to 50% in *G. lateralis* and 34% in *C. maenas* (reviewed in Covi et al., 2009). Notably, a difference in which PKG1 isoform predominates in the YO may also contribute to species-specific differences in responsiveness to MIH, although at this time we do not know

which isoforms are dominant or how differences in the alternatively spliced regions may affect cellular location and affinity for cGMP binding.

This study has revealed a fascinating example of paralogs that have opposing, rather than redundant, effects. It also raises the possibility that PKG1 and PKG2 have opposing roles in vertebrates. Three separate paralogous gene pairs associated with Huntington's disease have opposing effects and interact with a similar network of proteins (Vagonia et al., 2022). One such pair is inhibitor of nuclear factor kappa B kinase subunit beta (IKBKB) and inhibitor of nuclear factor kappa-B subunit alpha (IKKA). DNA damage has opposite effects on the paralogs: increased IKBKB activity and decreased IKKA activity promotes cleavage of the huntingtin protein (HTT; Khoshnan et al., 2009; Vagonia et al., 2022). Conversely, increased IKKA activity and decreased IKBKB activity blocks HTT cleavage, which protects against the neurodegenerative effects of Huntington's disesase (Khoshnan et al., 2009; Vagonia et al., 2022).

The discovery that PKG2 inhibitor AP-C5 enhanced the inhibitory effect of Gl-MIH on YO ecdysteroidogenesis answers a longstanding question in decapod endocrinology. The magnitudes of the synergistic effect of Gl-MIH and AP-C5 on *C. maenas* and *G. lateralis* YO secretion (90% and 76% inhibition compared to Gl-MIH controls; Fig. 2.1) are larger than those reported for MIH alone (Mattson and Spaziani, 1985b; Webster, 1986; Saidi et al., 1994; and reviewed in Lachaise et al., 1993; Mykles, 2021). Numerous studies have shown that YOs incubated with high concentrations of MIH or sinus gland extract reach a maximum of 60-70% inhibition, depending upon the species (Lachaise et al., 1993; Covi et al., 2012). The opposing effects of PKG1 and PKG2 explain how MIH prevents molting, while allowing for basal ecdysteroidogenesis in the intermolt YO. As PKG1 is expressed at much higher levels than

PKG2, PKG1 has the dominant role in MIH suppression of ecdysteroid synthesis, while PKG2 counteracts that suppression and allows for basal ecdysteroid secretion during intermolt.

CONCLUSIONS

MIH signaling controls mTORC1-dependent ecdysteroid synthesis in the decapod YO. Mykles (2021) proposed a model in which PKG activates the TSC complex by phosphorylating the TSC2 subunit; TSC inactivates Rheb by promoting the hydrolysis of GTP to GDP, resulting in mTORC1 inhibition. TSC2 is regulated by various protein kinases, such as PKG, AKT, and AMP kinase (Ranek et al., 2019; Oeing et al., 2020; reviewed in Shi and Collins, 2023). The effects of protein kinases are determined by which target sites in TSC2 are phosphorylated. In mammals, PKG1 and AMP kinase activate TSC2, while AKT inhibits TSC2 (reviewed in Shi and Collins, 2023; Da Silva et al., 2022; Yin et al., 2021). As decapod PKG1 and PKG2 have opposite effects on MIH-dependent ecdysteroidogenesis, a revised model is proposed, in which PKG1 and PKG2 activate and inhibit TSC, respectively, by phosphorylating TSC2 at different sites (Fig. 2.10). Although MIH activates both PKG1 and PKG2, PKG1 has the dominant role, as it is expressed at two to three orders of magnitude greater than PKG2 (Fig. 2.9). This leads to inhibition of mTORC1-dependent ecdysteroid synthesis. However, PKG2 activity prevents total inhibition of ecdysteroid synthesis in the basal YO, resulting in low hemolymph ecdysteroid titer in intermolt animals (Mykles, 2011). Further, oxidation of PKG1α at Cys42 tempers PKG1 inhibition of mTORC1 by reducing phosphorylation and activation of TSC2 (Oeing et al., 2020). Oxidation of Cys117 and Cys195 in the cGMP-binding domains of PKG1α modulates subcellular localization and protein activity, thereby conferring a redox-responsive function in mammalian cells (Cuello and Nikolaev, 2020). This may also have implications for PKG1 in the YO during premolt when increased cytochrome p450 activity, which supports increased

ecdysteroid synthesis, may increase production of radical oxygen species (ROS; Mykles and Chang, 2020). This is consistent with increases in anti-ROS proteins during premolt (Head et al., 2019).

G. lateralis and *C. maenas* have been used for decades as models for the study of molting physiology (reviewed in Mykles and Chang, 2020; Mykles, 2024; Webster et al., 2012, 2013; Fehsenfeld, 2024). Although decapods share the same endocrine system that controls molting, the two species show notable differences in the effects of experimental treatments on the MIH signaling pathway. Acute withdrawal of MIH by eyestalk ablation (ESA) results in YO activation in *G. lateralis*; this method was used here and in previous studies to determine the effects of MIH and reagents on ecdysteroid secretion (Mykles and Chang, 2020; Mykles, 2024). By contrast, adult *C. maenas* are refractory to ESA, which was attributed to extra-eyestalk sources of MIH in the central nervous system (McDonald et al., 2011; Abuhagr et al., 2014; Pitts et al., 2017). However, when removed from the animal, the YOs are activated and begin secreting ecdysteroids immediately (Fig. 2.1). MIH and compounds that inhibit ecdysteroid secretion, such as PKG agonist (8-Br-cGMP), phosphodiesterase inhibitor (IBMX), NO donors (SNAP and SE175), and NO-dependent guanylyl cyclase agonist (YC-1), have a greater effect on the *C. maenas* YO than the *G. lateralis* YO *in vitro* (this study; Covi et al., 2009; Mykles et al., 2010). These data suggest that the cGMP turnover rate is higher in the *C. maenas* YO than in the *G. lateralis* YO. Consequently, the *C. maenas* YO would be more responsive to changes in MIH level in the hemolymph and would explain the immediate activation of *C. maenas* YO *in vitro*. The difference in cGMP turnover would also contribute to the differential effect of Rp8-Br-PET-cGMPs on MIH-dependent inhibition between the two species (Fig. 2.1).

Future studies should be directed toward identifying the substrates of PKG1 and PKG2 in the decapod YO, to determine how MIH and mTORC1 signaling pathways are linked. In human and mouse cardiomyocytes, PKG1 activates the TSC complex by phosphorylating TCS2 at Ser1365 and Ser1366 (Ranek et al., 2019; Oeing et al., 2020), resulting in Rheb inactivation and mTORC1 inhibition (Shi and Collins, 2023). Furthermore, quantifying PKG mRNA and protein levels over the molt cycle may elucidate the roles of PKG1 and PKG2 as the YO transitions through the basal, activated, committed, and repressed states.

DATA AVAILABILITY

Tables A1, A2, and A3 presented in this study can be found in the appendix of this dissertation, and online in the supplementary material associated with this publication at DOI 10.1242/jeb.249739. Fasta files of all sequences and alignments presented in this study, sequence metadata, raw data from *in vitro* YO assays, and sanger sequencing have been deposited on Dryad: https://doi.org/10.5061/dryad.1g1jwsv7b.

Table 2.1. Taxonomic distribution of pancrustacean and tardigrade PKG sequences in the CrusTome database.

Taxon	# Species	PKG1[2]	PKG1α[3]	PKG1β	PKG2	Total
Decapoda	42	-	76	18	13	107
Amphipoda	7	5	3	-	1	9
Anomopoda	1	1	6	-	1	8
Copepoda	8	3	7	1	9	20
Euphausiacea	2	-	3	1	4	8
Eutardigrada	2	2	-	-	2	4
Insecta	3	2	2	1	2	7
Isopoda	14	1	8	-	10	19
Pycnogonida	2	2	-	-	-	2
Remipedia	1	-	1	-	-	1
Sessilia	1	-	1	-	1	2
Stomatopoda	1	-	2	1	-	3
Trombidiformes	2	1	1	-	-	2

[2] PKG1 sequences where alpha or beta isoforms were not distinguished are identified as PKG1
[3] All PKG1α isoforms are grouped together for simplicity. Sequences deposited on Dryad at https://doi.org/10.5061/dryad.1g1jwsv7b.

Table 2.2. PKG sequences in selected decapod species. Contigs encoding PKG isoforms in the CrusTome (v.0.1.0) database (Pérez-Moreno et al., 2023) and previously identified PKG sequences in other decapods. Gene names are the proposed classification, based on clades and subclades from taxonomically comprehensive phylogenetic analyses. Tissue abbreviations: B, brain; D, dactyl; E, eyestalk; Eye, whole eye; LF, lateral flagellum; MD, multiple developmental stages of whole larvae; MT, multiple tissues; N, neural tissue; PWO, pooled whole organisms; SG, supraesophageal ganglia; U, unspecified; WO, whole organism; YO, Y-organ. RefSeq accession numbers included, if known. Asterisk (*) indicates partial sequence, open reading frame incomplete.

Gene Name	Species	Tissue	Transcript ID	Accession #
Gl-PKG1α1	*G. lateralis*	YO	GeclaM_EVm002389t2	PQ196148
Cm-PKG1α1	*C. maenas*	CNS	CarmaC_EVm005181t3*	
		YO	CarmaY_EVm003118t2	PQ196153
Es-PKG1α1	*E. sinensis*	MD	Erisi1_EVm002590t6*	
Ca-PKG1α1	*C. antillensis*	Eye	Cliant_EVm006358t1*	
Lp-PKG1α1	*L. pugilator*	LB	Minpug_EVm002714t3	
Gl-PKG1α2	*G. lateralis*	YO	GeclaM_EVm002389t3	PQ196149
Cm-PKG1α2	*C. maenas*	CNS	CarmaC_EVm005181t2*	
		YO	CarmaY_EVm003118t1	PQ196152
Es-PKG1α2	*E. sinensis*	MD	Erisi1_EVm002590t3	
Cq-PKG1α2	*C. quadricarinatus*	MT	ChequaEVm001918t2	
Lv-PKG1α2	*L. vannamei*	PWO	PenvanEVm001303t1	
Mm-PKG1α2	*M. magister*	YO	MetmagEVm001747t1	
Gl-PKG1α3	*G. lateralis*	YO	GeclaM_EVm002389t4	PQ196150
Cm-PKG1α3	*C. maenas*	CNS	CarmaC_EVm005181t4_Merge14[4]	PQ196154
Es-PKG1α3	*E. sinensis*	MD	Erisi1_EVm002590t4	XP_050687427
Cq-PKG1α3	*C. quadricarinatus*	MT	ChequaEVm001918t3	
Pc-PKG1α3	*P. clarkii*	E	Procl1_EVm001493t4	
Pc-PKG1α4	*P. clarkii*	E	Procl1_EVm001493t3	
Pa-PKG1α4	*P. argus*	D, LF, B, SG	Panar2_EVm001962t4	
Gl-PKG1β	*G. lateralis*	YO	GeclaM_EVm002389t1	PQ196147
Cm-PKG1β	*C. maenas*	CNS	Cmae_CNS_GFXF01063191[5]	PQ196156
Ha-PKG1β	*H. americanus*	D, LF, B, SG	HomameEVm003066t1	XP_042243236.1[6]
Pa-PKG1β	*P. argus*	D, LF, B, SG	Panar1_EVm002735t1	
		U	Panar2_EVm001962t1	
Pc-PKG1β	*P. clarkii*	E	Procl1_EVm001493t2	XP_045597802.1
Pc-PKG1βins			Procl1_EVm001493t1	XP_045597794.1

[4] Combination of two partial and overlapping contigs: CarmaC_EVm005181t4 and CarmaC_EVm005181t1

[5] From Oliphant et al. (2018).

[6] RefSeq sequence is slightly different from the *Ha-PKG1β* sequence from CrusTome.

Cq-PKG1β	*C. quadricarinatus*	MT	ChequaEVm001918t1	
Cs-PKG1β	*C. sapidus*	D, LF	CalsaE_EVm002791t1	
Cs-PKG2	*C. sapidus*	D, LF	CalsaE_EVm002757t1*	
		YO	CalsaY_EVm002578t1*	
Cm-PKG2	*C. maenas*	YO	CarmaY_EVm001907t1	PQ196151
		CNS	CarmaC_EVm003011t1*	
Cq-PKG2	*C. quadricarinatus*	MT	ChequaEVm001934t1*	
Es-PKG2	*E. sinensis*	MD	Erisi1_EVm002854t1*	XP_050728644.1[7]
Gl-PKG2	*G. lateralis*	YO	GeclatEVm001732t1[8]	PQ196155
			GeclaM_EVm002889t1*	
Ha-PKG2	*H. americanus*	D, LF, B, SG	HomameEVm002972t1*	
Pc-PKG2	*P. clarkii*	E	Procl2_EVm003235t1*	XP_045598842.1

[7] RefSeq sequence has complete ORF while *Es-PKG2* sequence from CrusTome is incomplete

[8] From Kozma et al. (2023)

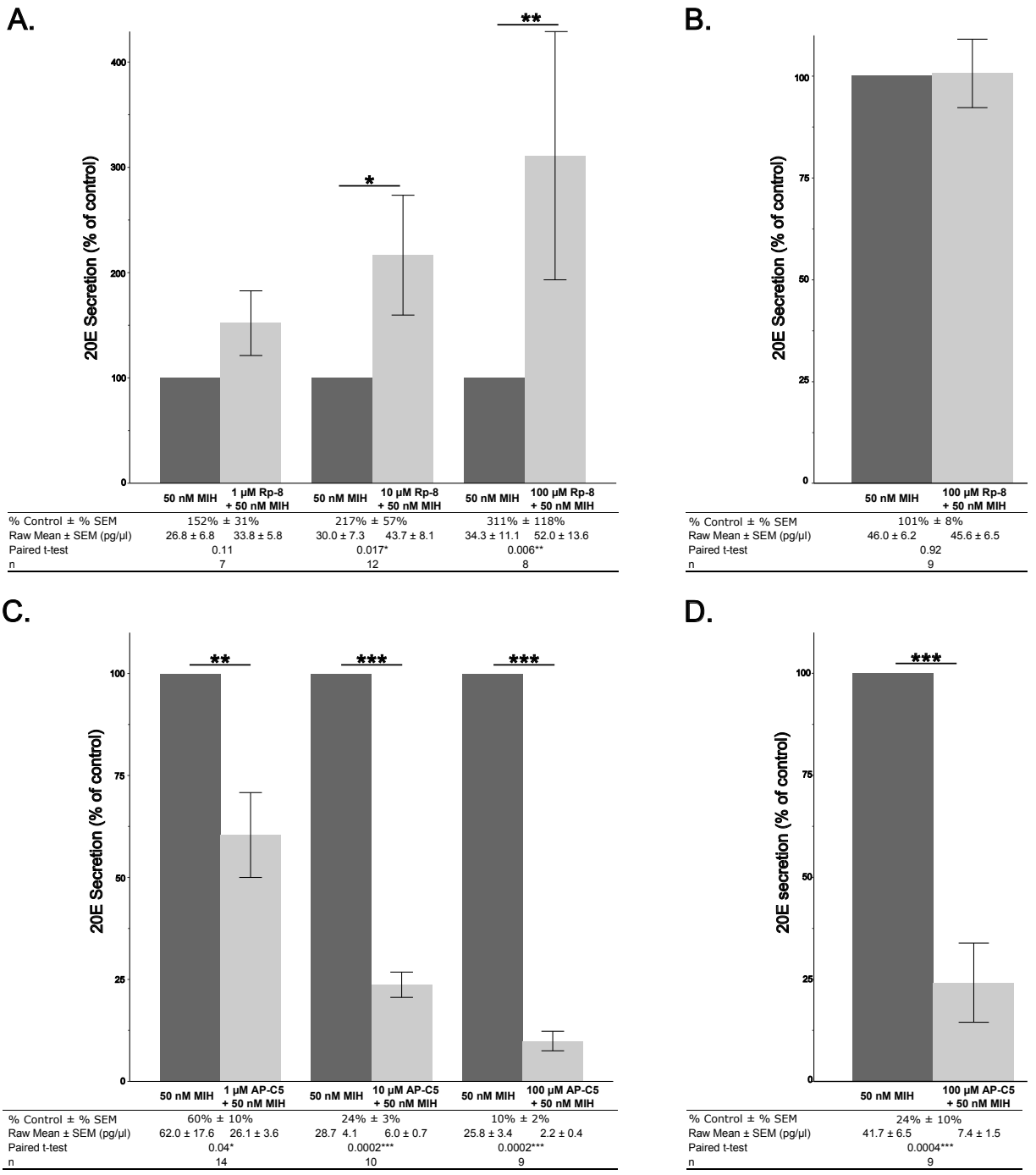

Figure 2.1. Effects of MIH ± PKG inhibitors on *in vitro* ecdysteroid secretion by Y-organs from *G. lateralis* and *C. maenas*. Bar plots of ecdysteroid secretion (20E equivalents) from *in vitro* YO assays. Y-axis represents ecdysteroid secretion from YOs as a percentage of the secretion from the paired control YO [(experimental secretion/control secretion) *100]. Control YOs represent 100% of the secretion rate of YOs inhibited by 50 nM MIH. Percent of the control (% Control) is reported as the mean percent change in secretion of experimentally treated YOs compared to the paired control YOs. Standard error of the mean is reported for the percent change in secretion (% SEM) and plotted as error bars. Mean ± SEM is given for the raw data as

pg/µl 20E equivalents. Paired t-tests represent the effects of the treatment as compared to the paired control. (A) *C. maenas* ecdysteroid secretion at 1, 10, and 100 µM Rp-8-Br-PET-cGMPS + 50 nM MIH increased secretion to 152%, 217%, and 314% of the control, respectively. (B) *G. lateralis* ecdysteroid secretion at 100 µM Rp-8 + 50 nM MIH did not change secretion (mean of 101%) relative to the MIH control. (C) *C. maenas* ecdysteroid secretion at 1, 10, and 100 µM AP-C5 + 50 nM MIH reduced secretion to 60%, 24%, and 10% of the control, respectively. (D) *G. lateralis* secretion at 100 µM AP-C5 + 50 nM MIH reduced secretion to 24% of the control.

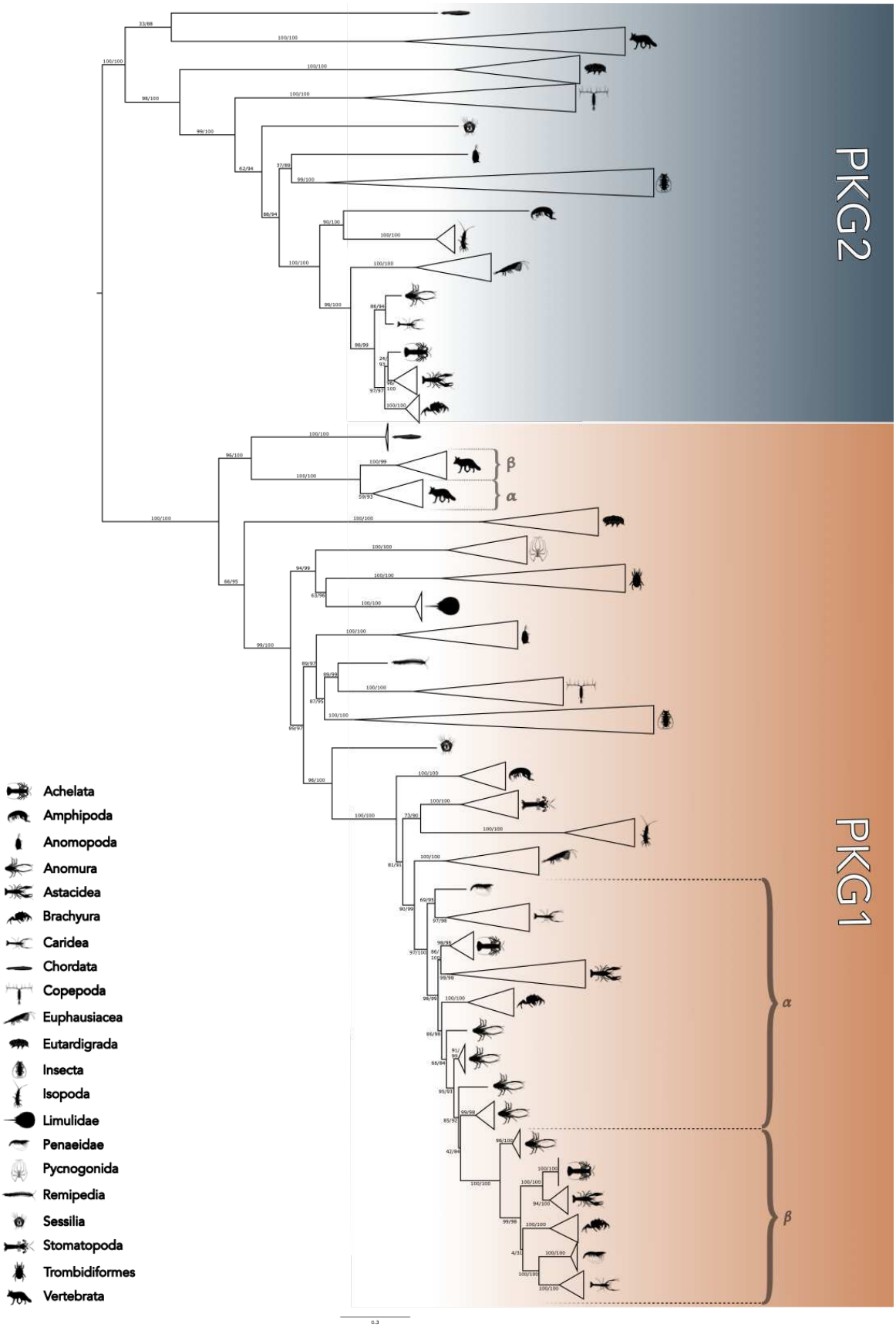
PKG2
PKG1
β
α
α
β
Achelata
Amphipoda
Anomopoda
Anomura
Astacidea
Brachyura
Caridea
Chordata
Copepoda
Euphausiacea
Eutardigrada
Insecta
Isopoda
Limulidae
Penaeidae
Pycnogonida
Remipedia
Sessilia
Stomatopoda
Trombidiformes
Vertebrata

Figure 2.2. Phylogenetic tree of metazoan cGMP-dependent protein kinases (PKGs). Midpoint-rooted phylogenetic tree (JTT+I+G4) of PKGs in chordates and invertebrates, with an emphasis on crustaceans. The tree had two large clades representing PKG1 (orange shading) and PKG2 (blue shading) sequences. PKG1α and PKG1β isoforms formed subclades in vertebrate and decapod groups. Branch support is indicated by Ultra-Fast Boostrap approximation/approximate Bayes Test. Ultra-Fast Bootstrap values are rounded to the nearest whole number for visual clarity. Taxa images from PhyloPic.org (credits in Table A3).

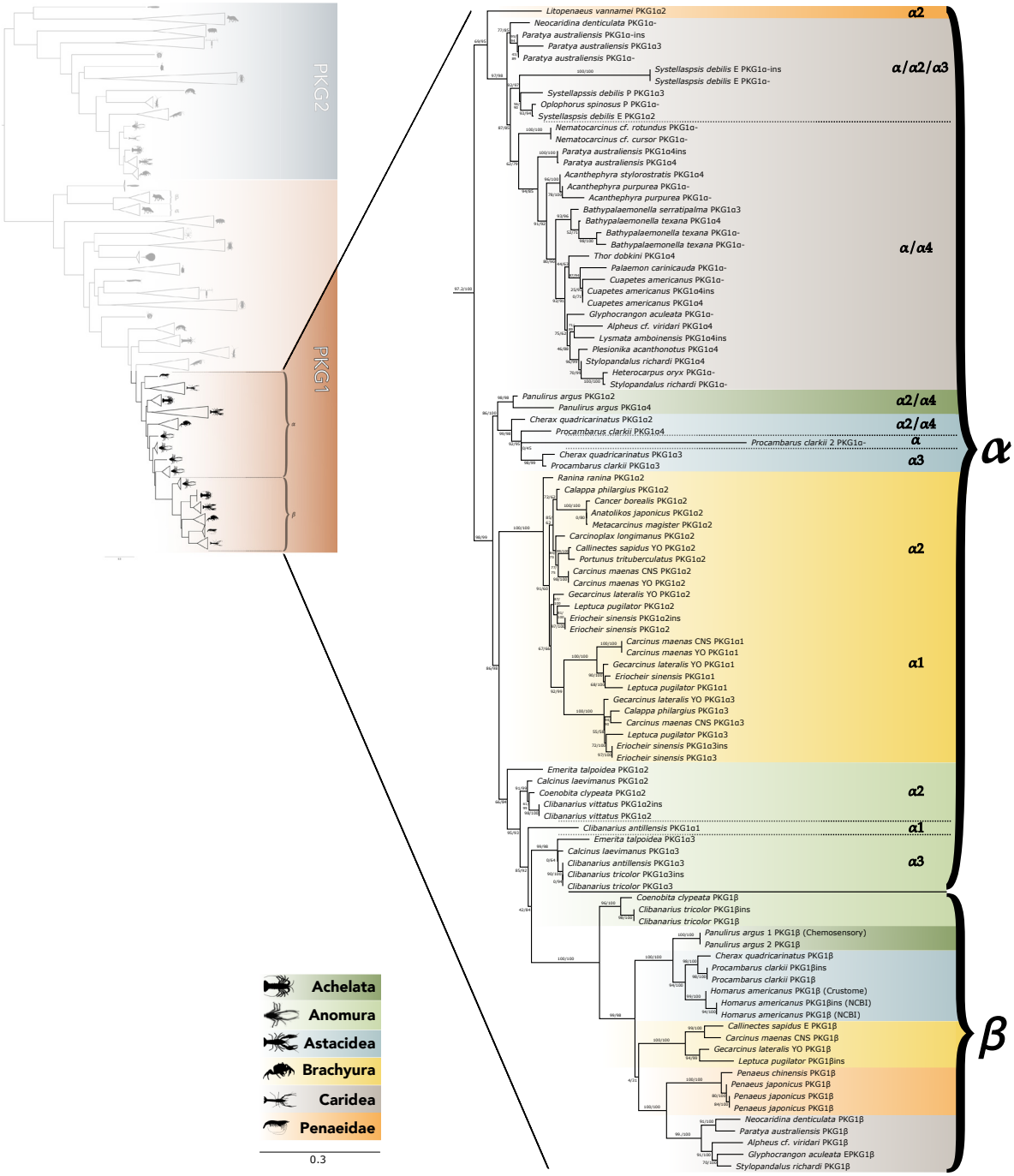

Figure 2.3. PKG1 phylogeny in decapods. Expanded phylogeny of the decapod branches within the PKG1 clade in Figure 2.2. Alternatively spliced PKG1α1, PKG1α2, PKG1α3, and PKG1α4 isoforms are indicated with dotted lines that separate groupings for each isoform. PKG1α and PKG1β sequences with a 14- to 17-amino acid insertion in the kinase domain are indicated with 'ins'. Branch support is indicated by Ultra-Fast Boostrap approximation/approximate Bayes Test. Ultra-Fast Bootstrap values are rounded to the nearest whole number. Shading is as follows: Achelata, dark green; Anomura, light green; Astacidea, blue; Brachyura, yellow; Caridea, gray; Penaeidae, orange. Taxa images from PhyloPic.org (credits in Table A3).

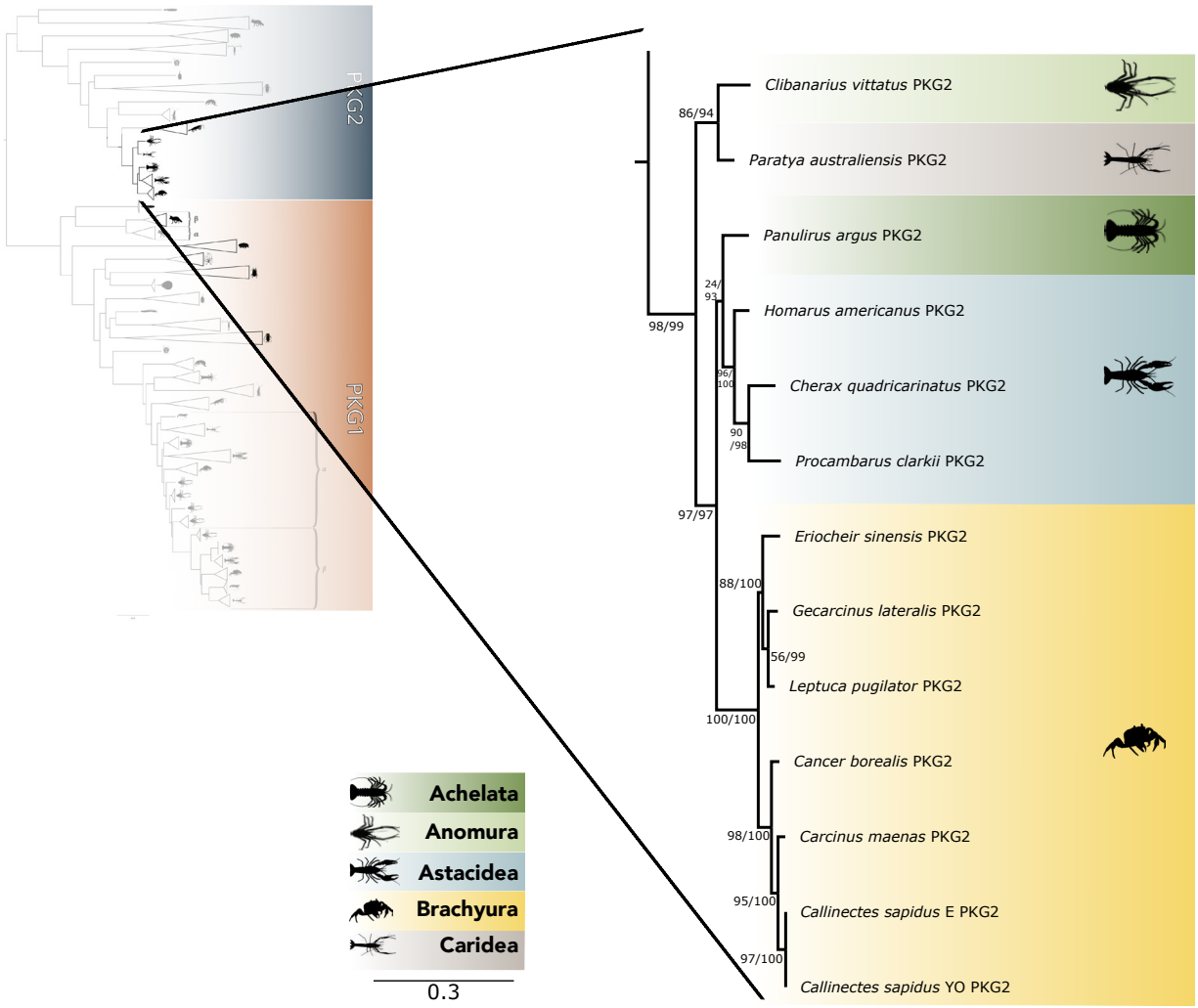

Figure 2.4. PKG2 phylogeny in decapods. Expanded phylogeny of the decapod branches within the PKG2 clade in Figure 2.2. Branch support is indicated by Ultra-Fast Boostrap approximation/approximate Bayes Test. Ultra-Fast Bootstrap values are rounded to the nearest whole number. Shading is as follows: Achelata, dark green; Anomura, light green; Astacidea, blue; Brachyura, yellow; Caridea, gray. Taxa images from PhyloPic.org (credits in Table A3).

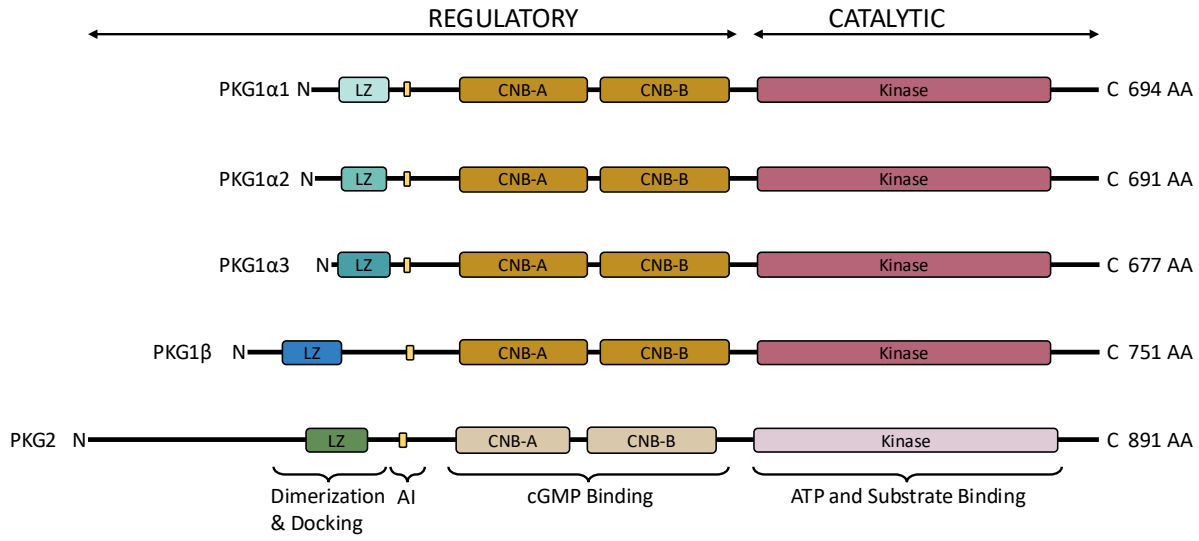

Figure 2.5. Domain organization of *G. lateralis* PKG1 and PKG2 proteins. Schematic diagrams of the five identified PKG proteins encoded by YO transcripts in *G. lateralis*. Sequences are represented to scale. Functional domains were identified using NCBI CD-Search and EBML-InterProScan. The autoinhibitory (AI) region was identified based on homology with human sequences (Sharma et al., 2022). The regulatory region consisted of leucine zipper (LZ), AI, and cGMP-binding (CNB-A and CNB-B) domains (CNB = cyclic nucleotide binding). The catalytic region contained the kinase domain. The PKG1 isoforms differed only in the N-terminal region that included distinct LZ sequences, which are distinguished by different shading. The DNA and amino acid sequences of the regions that included the cGMP-binding and kinase domains were identical among the four PKG1 isoforms.

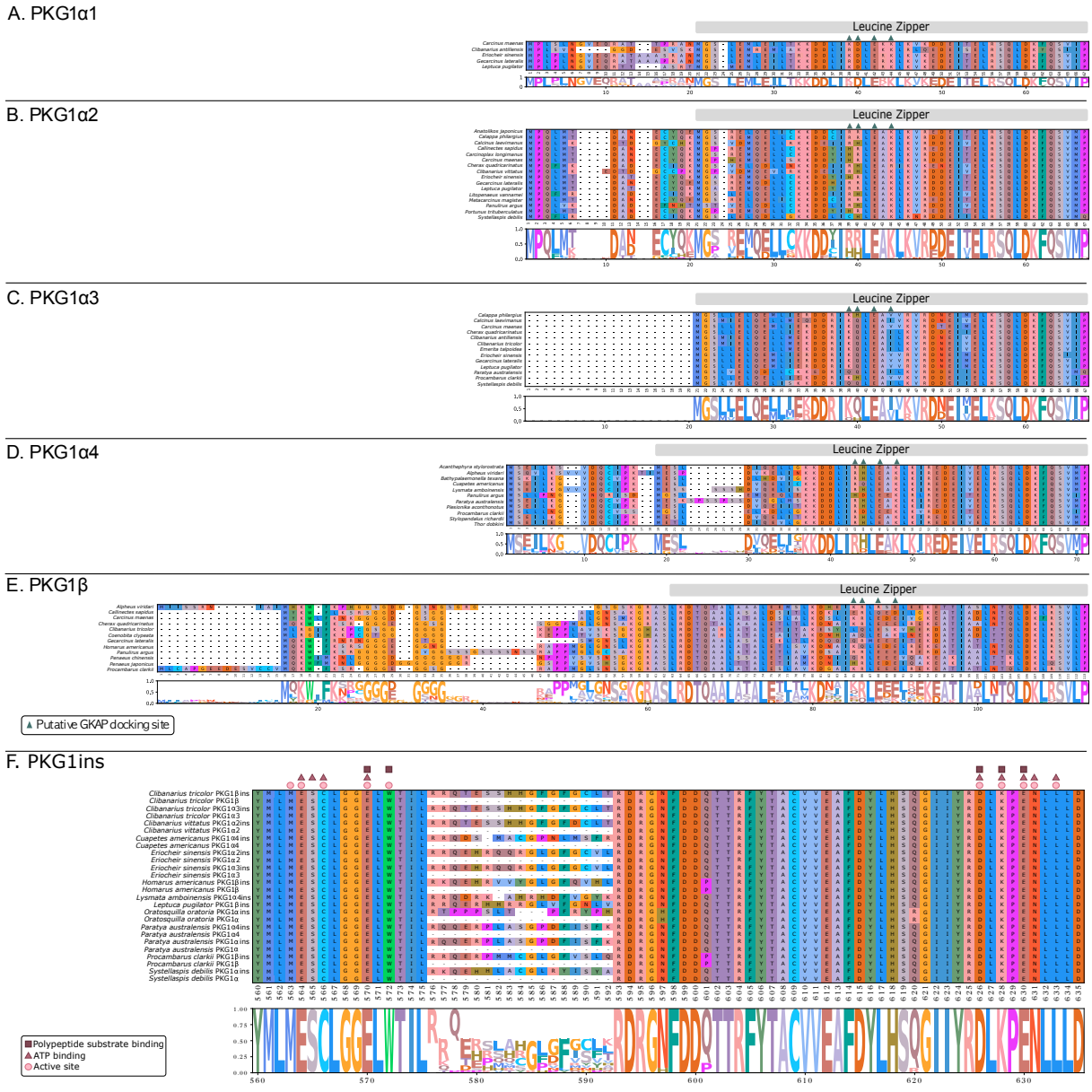

Figure 2.6. Alternatively spliced PKG1 isoform motifs in decapods. Multiple sequence alignments (MSAs) and logo plots of the N-terminal regions of the PKG1α isoforms, PKG1β, and PKG1ins isoforms in decapod species. MSA color scheme corresponds to similarities in amino acid physiochemical properties. (A-E) Sequences for each isoform began with the first methionine in the open reading frame and continue until the end of the LZ domain, indicated by a grey bar for each isoform. Gaps in MSAs were retained to aid in overall comparison among the isoforms. Partial sequences lacking a complete sequence from the start codon to the end of the LZ domain were excluded from the analysis. (A) PKG1α1 began with MPL[PS] motif (reference positions #1-4). (B) PKG1α2 began with MPQ[LF] motif (reference positions #1-4).

(C) PKG1α3 began with the LZ domain with a MGS[LM] motif (reference positions #21-24). (D) PKG1α4 began with a MS[ELKQ] motif (reference positions #1-3). The LZ domain commonly began with MES (reference positions #19-21), rather than MGS (reference positions #21-23) in the PKGα1-α3 isoforms. (E) PKG1β had an extended N-terminal sequence rich in glycine residues and a LZ that began with LRD (reference positions #63-65). (F) PKG1ins isoforms with a 14- to 17-amino acid insertion in the kinase domain. Paired sequences lacking the insertion were identified for all species except *Lysmata ambionensis* and *Leptuca pugilator*. Residues predicted to be important in polypeptide substrate binding, ATP binding, and the kinase active site are indicated in the legend. The insertion does not add residues predicted to be important by NCBI-CDS.

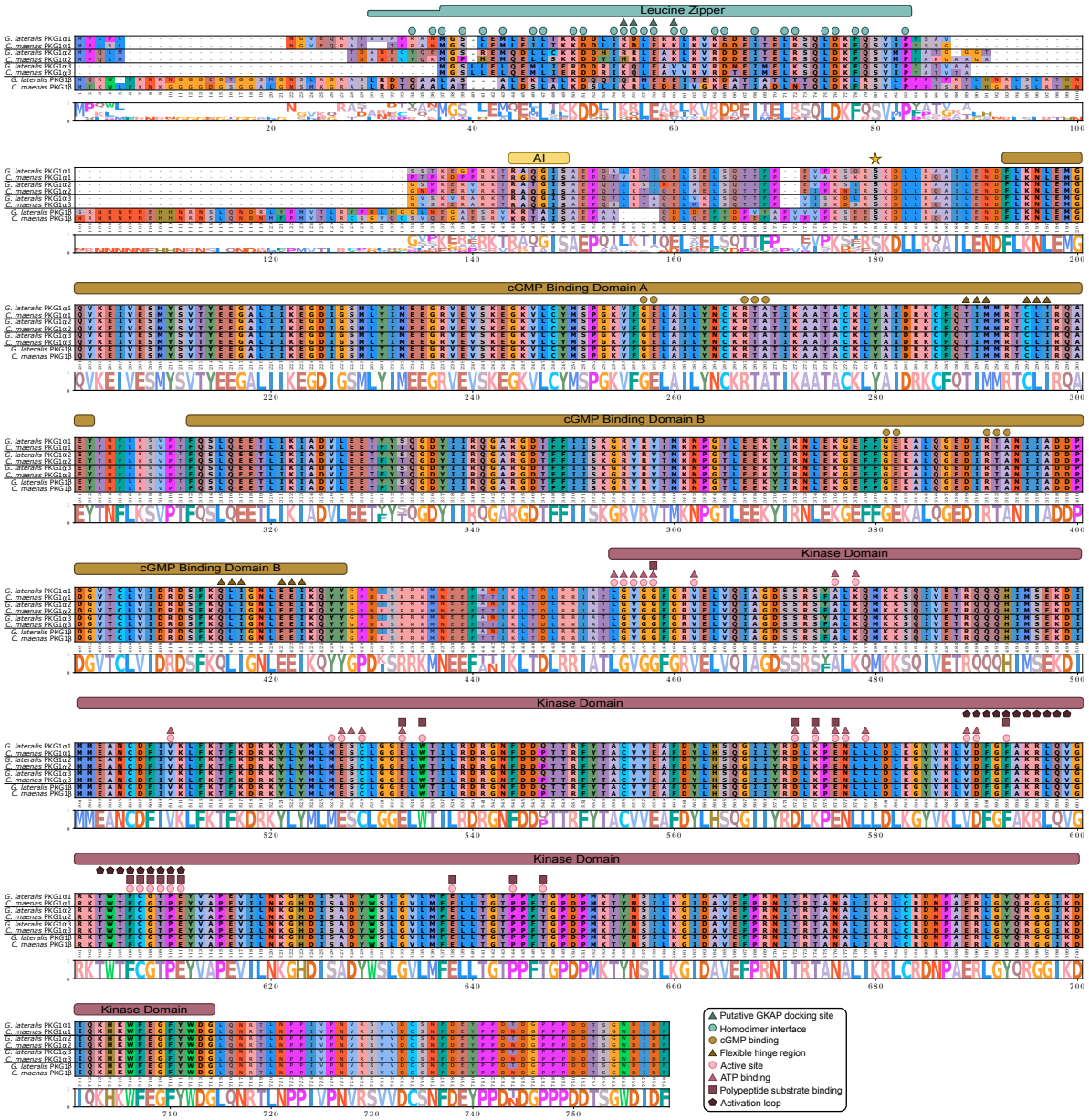

Figure 2.7. Conserved motifs in PKG1 isoforms in *G. lateralis* and *C. maenas*. MSA and logo plot of the PKG1α1, PKG1α2, PKG1α3, and PKG1β sequences. Predicted domains are annotated above each line; the domain color scheme corresponds with that in Figure 2.2. Residues predicted to be important in homodimer formation, GKAP-docking, cGMP-binding, kinase active site, ATP-binding, polypeptide substrate binding, and the activation loop are identified in the legend. A conserved serine residue that marks the putative splice site (reference position #180) is indicated by a star. MSA color scheme corresponds to similarities in amino acid physiochemical properties. AI, autoinhibitory region.

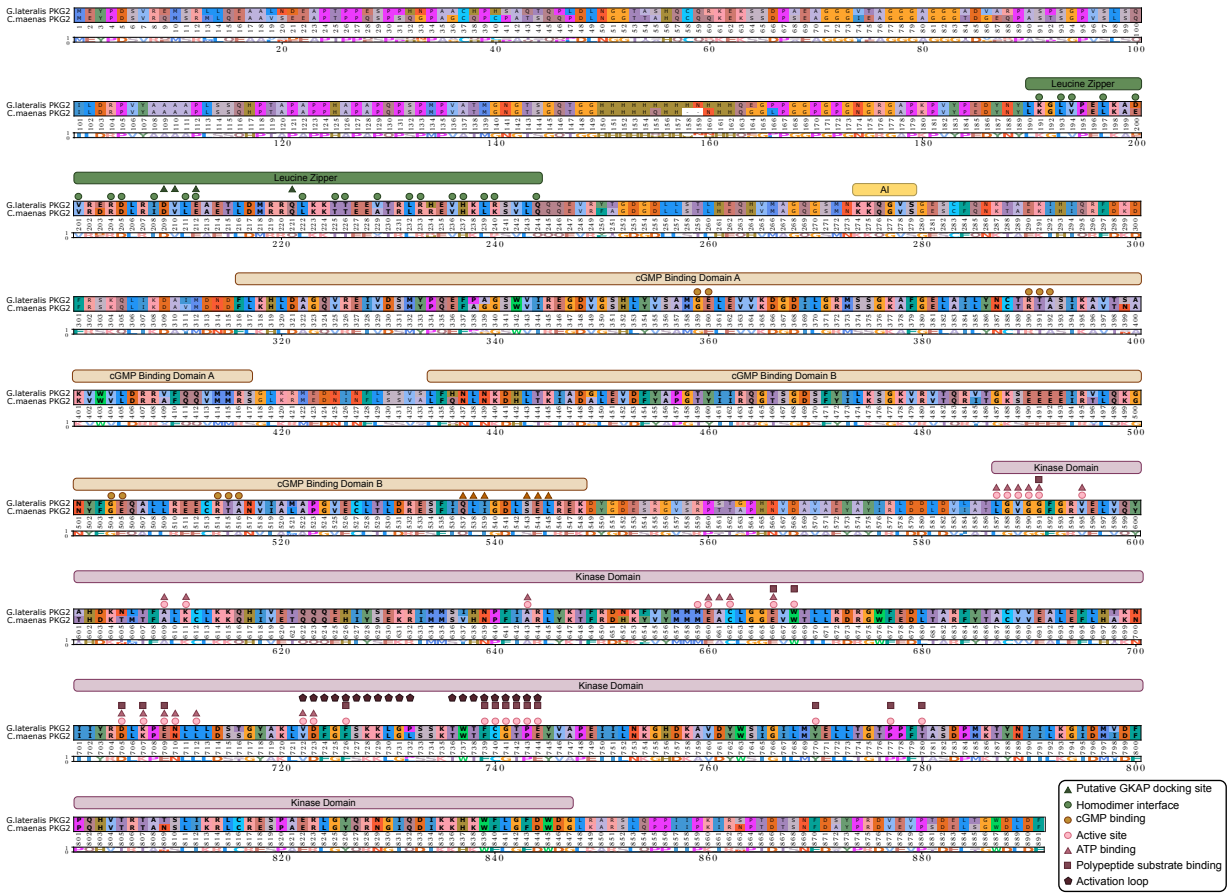

Figure 2.8. Conserved motifs in PKG2 in *G. lateralis* and *C. maenas*. MSA and logo plot of the PKG2 sequences. Predicted domains are annotated above each line; the domain color scheme corresponds with that in Figure 2.2. Residues predicted to be important in homodimer formation, GKAP-docking, cGMP-binding, kinase active site, ATP-binding, polypeptide substrate binding, and the activation loop are identified in the legend. MSA color scheme corresponds to similarities in amino acid physiochemical properties. AI, autoinhibitory region.

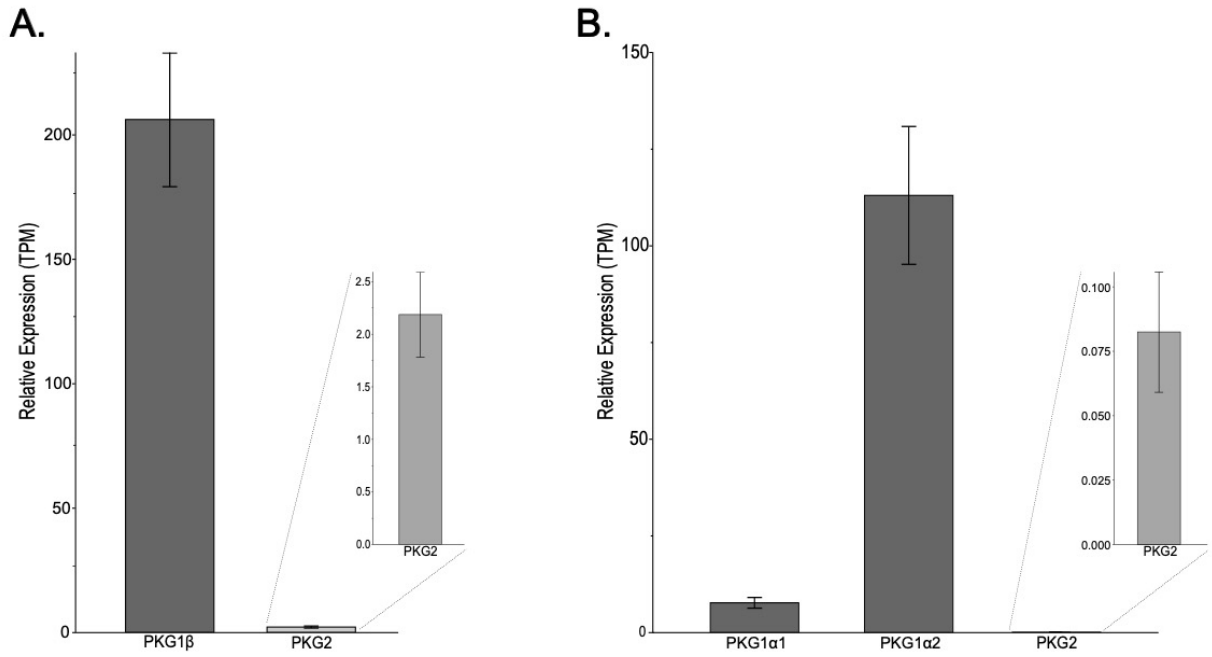

Figure 2.9. Relative expression of PKGs in intermolt Y-organs. mRNA levels are expressed as mean transcripts per million reads (TPM) ± standard error of the mean (SEM). (A) Relative expression of PKG1β and PKG2 in the *G. lateralis* intermolt YO; inset provides scaled resolution of PKG2 expression. PKG1β transcript expression represents pooled expression of PKG1 isoforms. Raw RNAseq data from Das et al., 2018 (n = 3 pooled replicates of 3 animals each) was quantified with Salmon (v.1.7.0). (B) Relative expression of PKG1α1, PKG1α2, and PKG2 in the *C. maenas* intermolt YO; inset provides scaled resolution of PKG2 expression. Raw RNAseq data was obtained from Oliphant et al. (2018; n = 5 biological replicates of paired YOs) and quantified with Salmon (v.1.7.0) using the *C. maenas* YO transcriptome assembly included in CrusTome (v.0.1.0). Other PKG1 isoforms were not identified in these datasets.

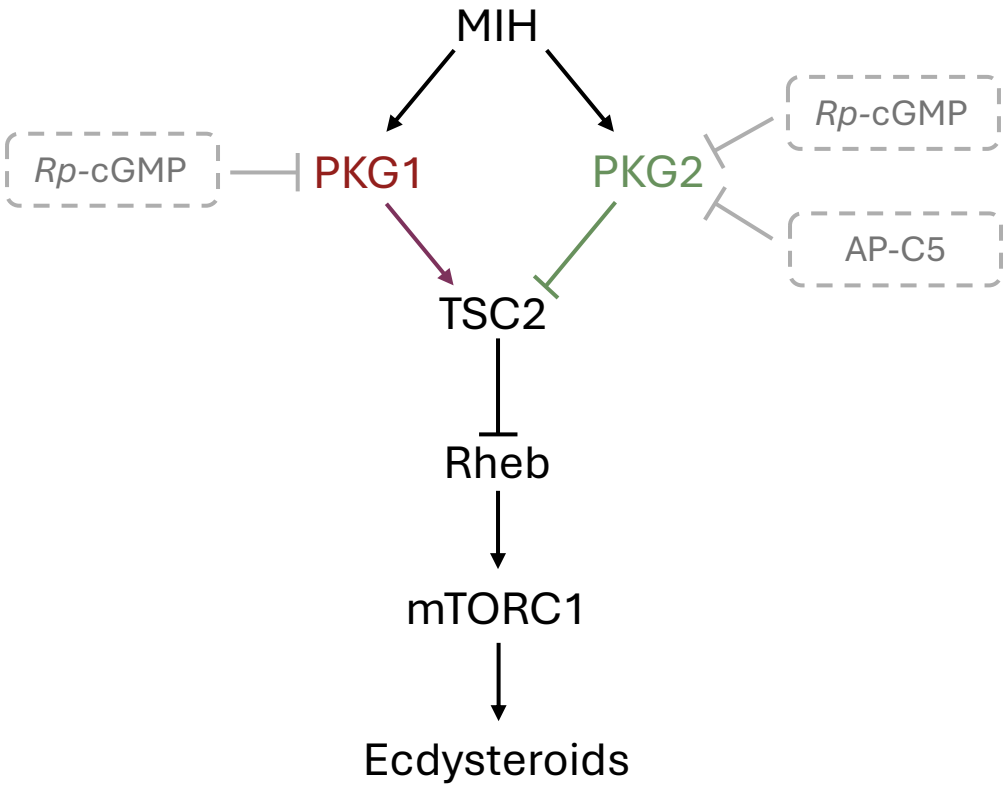

Figure 2.10. Proposed model for linking the MIH/PKG signaling pathway with mTORC1-dependent ecdysteroid synthesis in the YO. MIH activates both PKG1 and PKG2 via nitric oxide-dependent synthesis of cGMP (not shown; see Mykles, 2024). We hypothesize that both PKG1 and PKG2 converge on TSC2, with opposing effects. TSC inhibits mTORC1 activation through stimulating the GTPase activity of Rheb. Inhibition of mTORC1 suppresses ecdysteroid synthesis, whereas mTORC1 activation initiates increased translation of ecdysteroidogenic enzymes, including cytochrome p450 enzymes, leading to increased ecdysteroid synthesis. Based on *in vitro* YO assays (Fig. 2.1), inhibition of both PKGs with Rp-8-Br-PET-cGMPS (Rp-cGMPS) reverses the effects of MIH in *C. maenas* but not in *G. lateralis* (see Discussion). Inhibition of PKG2 alone with AP-C5 enhances the effects of MIH by PKG1 in both species. In effect, PKG1 activation by MIH suppresses ecdysteroid synthesis presumably by activating TSC2. Conversely, PKG2 activation by MIH stimulates ecdysteroid synthesis presumably by inhibiting TSC2 via phosphorylation of different residues than those of PKG1. In this model, PKG1 is dominant over PKG2, allowing the YO to maintain basal levels of ecdysteroid synthesis during intermolt.

REFERENCES

Abuhagr, A.M., Blindert, J.L., Nimitkul, S., Zander, I.A., LaBere, S.M., Chang, S.A., MacLea, K.S., Chang, E.S. and Mykles, D.L. (2014). Molt regulation in green and red color morphs of the crab *Carcinus maenas*: gene expression of molt-inhibiting hormone signaling components. *J. Exp. Biol.* **217**, 796-808.

Adler, J., Kuret, A., Langst, N. and Lukowski, R. (2020). Targets of cGMP/cGKI in cardiac myocytes. *J. Cardiovasc. Physiol.* **75**, 494-507.

Allen, A.M., Anreiter, I., Neville, M.C. and Sokolowski, M.B. (2017). Feeding-related traits are affected by dosage of the *foraging* gene in *Drosophila melanogaster*. *Genetics* 205, 761-773.

Altschul, S.F., Gish, W., Miller, W., Myers, E.W. and Lipman, D.J. (1990). Basic local alignment search tool. *J. Molec. Biol.* **215**, 403-410.

Casteel, D.E., Boss, G.R. and Pilz, R.B. (2005). Identification of the interface between cGMP-dependent Protein Kinase Iβ and its interaction partners TFII-I and IRAG reveals a common interaction motif. *J. Biol. Chem.* **280**, 38211-38218.

Casteel, D.E., Smith-Nguyen, E.V., Sankaran, B., Roh, S.H., Pilz, R.B. and Kim, C. (2010). A crystal structure of the cyclic GMP-dependent protein kinase Ibeta dimerization/docking domain reveals molecular details of isoform-specific anchoring. *J. Biol. Chem.* **285**, 32684-32688.

Corradini, E., Burgers, P.P., Plank, M., Heck, A.J.R. and Scholten, A. (2015). Huntingtin-associated Protein 1 (HAP1) Is a cGMP-dependent kinase anchoring protein (GKAP) specific for the cGMP-dependent protein kinase Iβ isoform *J. Biol. Chem.* **290**, 7887-7896.

Covi, J.A., Chang, E.S. and Mykles, D.L. (2009). Conserved role of cyclic nucleotides in the regulation of ecdysteroidogenesis by the crustacean molting gland. *Comp. Biochem. Physiol.* 1**52A**, 470-477.

Covi, J.A., Bader, B.D., Chang, E.S. and Mykles, D.L. (2010). Molt cycle regulation of protein synthesis in skeletal muscle of the blackback land crab, *Gecarcinus lateralis*, and the differential expression of a myostatin-like factor during atrophy induced by molting or unweighting. *J. Exp. Biol.* **213**, 172-183.

Covi, J.A., Chang, E.S. and Mykles, D.L. (2012). Neuropeptide signaling mechanisms in crustacean and insect molting glands. *Invertebr. Reprod. Dev.* **56**, 33-49.

Cuello, F. and Nikolaev, V.O. (2020). Cardiac cGMP signaling in health and disease: Location, location, location. *J. Cardiovasc. Physiol.* **75**, 399-409.

da Silva, E.F., Fong, J., Roye-Azar, A., Nadi, A., Drouillard, C., Pillon, A. and Porter, L.A. (2022). Beyond protein synthesis; The multifaceted roles of tuberin in cell cycle regulation. *Front. Cell. Dev. Biol.* **9**, 806521.

Das, S., Vraspir, L., Zhou, W., Durica, D.S. and Mykles, D.L. (2018). Transcriptomic analysis of differentially expressed genes in the molting gland (Y-organ) of the blackback land crab, *Gecarcinus lateralis*, during molt-cycle stage transitions. *Comp. Biochem. Physiol.* **28D**, 37-53.

Fehsenfeld, S. (2024). Endocrinology. In: *Ecophysiology of the European Crab Crab (Carcinus maenas) and Related Species: Mechanisms Behind the Success of a Global Invader* (ed. D. Weihrauch and I. J. McGaw), pp. 159-178. London: Academic Press.

Fitzpatrick, M.J. and Sokolowski, M.B. (2004). In search of food: Exploring the evolutionary link between cGMP-dependent protein kinase (PKG) and behaviour. *Int. Comp. Biol.* **44**, 28-36.

Francis, S.H. and Corbin, J.D. (2013). Cyclic nucleotide-dependent protein kinases. In: *Encyclopedia of Biological Chemistry (Second Edition)* (ed. W. J. Lennarz and M. D. Lane), pp. 574-579. Waltham: Academic Press.

Head, T.B., Mykles, D.L. and Tomanek, L. (2019). Proteomic analysis of the crustacean molting gland (Y-organ) over the course of the molt cycle. *Comp. Biochem. Physiol.* **29D**, 193-210.

Hofmann, F. (2018). A concise discussion of the regulatory role of cGMP kinase I in cardiac physiology and pathology. *Basic Res. Cardiol.* **113**, 31.

Hofmann, F. (2020). The cGMP system: components and function. *Biol. Chem.* **401**, 447-469.

Kalderon, D. and Rubin, G.M. (1989). cGMP-dependent protein kinase genes in *Drosophila*. *J. Biol. Chem.* **264**, 10738-10748.

Kalyaanamoorthy, S., Minh, B.Q., Wong, T.F.K., von Haeseler, A. and Jermiin, L.S. (2017). ModelFinder: fast model selection for accurate phylogenetic estimates. *Nature Meth.* **14**, 587-589.

Khoshnan, A., Ko, J., Tescu, S., Brundin, P. and Patterson, P. (2009). IKKα and IKKβ regulation of DNA damage-induced cleavage of Huntingtin. *PLoS One.* **4**, e5768.

Kim, C. and Sharma, R. (2021). Cyclic nucleotide selectivity of protein kinase G isozymes. *Protein Sci.* **30**, 316-327.

Kingan, T.G. (1989). A competitive Enzyme-Linked Immunosorbent-Assay - Applications in the assay of peptides, steroids, and cyclic-nucleotides. *Anal. Biochem.* **183**, 283-289.

Kozma, M.T., Pérez-Moreno, J.L., Gandhi, N.S., Hernandez Jeppesen, L., Durica, D.S., Ventura, T. and Mykles, D.L. (2024). *In silico* analysis of crustacean hyperglycemic hormone family G protein-coupled receptor candidates. *Front. Endocrinol.* **14**, 1322800.

Lachaise, F., Leroux, A., Hubert, M. and Lafont, R. (1993). The molting gland of crustaceans - Localization, activity, and endocrine control (a review). *J. Crustacean Biol.* **13**, 198-234.

Lee, K.J., Kim, H.W., Gomez, A.M., Chang, E.S., Covi, J.A. and Mykles, D.L. (2007a). Molt-inhibiting hormone from the tropical land crab: Cloning, tissue expression, and expression of biologically active recombinant peptide in yeast. *Gen. Comp. Endocr.* **150**, 505-513.

Lee, S.G., Kim, H.W. and Mykles, D.L. (2007b). Guanylyl cyclases in the tropical land crab, *Gecarcinus lateralis*: Cloning of soluble (NO-sensitive and -insensitive) and membrane receptor forms. *Comp. Biochem. Physiol.* **2D**, 332-344.

Leroux, A.E., Schulze, J.O. and Biondi, R.M. (2018). AGC Kinases, mechanisms of regulation and innovative drug development. *Semin. Cancer Biol.* **48**, 1-17.

Mattson, M.P. and Spaziani, E. (1985). Functional relations of crab molt-inhibiting hormone and neurohypophysial peptides. *Peptides* **6**, 635-640.

McDonald, A.A., Chang, E.S. and Mykles, D.L. (2011). Cloning of a nitric oxide synthase from green shore crab, *Carcinus maenas*: A comparative study of the effects of eyestalk ablation on expression in the molting glands (Y-organs) of *C. maenas*, and blackback land crab, *Gecarcinus lateralis*. *Comp. Biochem. Physiol.* **158A**, 150-162.

Minh, B.Q., Nguyen, M.A.T. and von Haeseler, A. (2013). Ultrafast approximations for phylogenetic bootstrap. *Molec. Biol. Evol.* **30**, 1188-1195.

Mosco, A., Zlatev, V., Guarnaccia, C., Pongor, S., Campanella, A., Zahariev, S. and Giulianini, P.G. (2012). Novel protocol for the chemical synthesis of crustacean hyperglycemic hormone analogues — An efficient experimental tool for studying their functions. *PLoS One.* **7**, e30052.

Mykles, D.L., Adams, M.E., Gäde, G., Lange, A.B., Marco, H.G. and Orchard, I. (2010). Neuropeptide action in insects and crustaceans. *Physiol. Biochem. Zool.* **83**, 836-846.

Mykles, D.L. (2011). Ecdysteroid metabolism in crustaceans. *J. Steroid Biochem. Molec. Biol.* **127**, 196-203.

Mykles, D.L. and Chang, E.S. (2020). Hormonal control of the crustacean molting gland: Insights from transcriptomics and proteomics. *Gen. Comp. Endocrinol.* **294**, 113493.

Mykles, D.L. (2021). Signaling pathways that regulate the crustacean molting gland. *Front. Endocrinol.* **12**, 113658.

Mykles, D.L. (2024). Molting physiology. In: *Frontiers in Invertebrate Physiology* (ed. S. P. L. S. Saleuddin, R.D. Roer, I. Wilkie), pp. 229-274. Palm Bay, FL: Apple Academic Press.

O'Leary, N.A., Wright, M.W., Brister, J.R., Ciufo, S., Haddad, D., McVeigh, R., Rajput, B., Robbertse, B., Smith-White, B., Ako-Adjei, D., et al. (2016). Reference sequence (RefSeq) database at NCBI: current status, taxonomic expansion, and functional annotation. *Nucleic Acids Res.* **44**, D733-D745.

Oeing, C.U., Mishra, S., Dunkerly-Eyring, B.L. and Ranek, M.J. (2020). Targeting protein kinase G to treat cardiac proteotoxicity. *Front. Physiol.* **11**, 858.

Oeing, C.U., Nakamura, T., Pan, S., Mishra, S., Dunkerly-Eyring, B.L., Kokkonen-Simon, K.M., Lin, B.L., Chen, A., Zhu, G., Bedja, D., et al. (2020). PKG1α cysteine-42 redox state controls mTORC1 activation in pathological cardiac hypertrophy. *Circulat. Res.* **127**, 522-533.

Oliphant, A., Alexander, J.L., Swain, M.T., Webster, S.G. and Wilcockson, D.C. (2018). Transcriptomic analysis of crustacean neuropeptide signaling during the moult cycle in the green shore crab, *Carcinus maenas*. *BMC Genomics.* **19**, 711.

Paysan-Lafosse, T., Blum, M., Chuguransky, S., Grego, T., Pinto, B.L., Salazar, G.A., Bileschi, M.L., Bork, P., Bridge, A., Colwell, L., et al. (2023). InterPro in 2022. *Nucleic Acids Res.* **51**, D418-D427.

Pérez-Moreno, J.L., Kozma, M.T., DeLeo, D.M., Bracken-Grisson, H.D., Durica, D.S. and Mykles, D.L. (2023). CrusTome: a transcriptome database resource for large-scale analyses across Crustacea. *G3-Genes Genomes Genet.*. **13**, jkad098.

Pitts, N.L. and Mykles, D.L. (2017). Localization and expression of molt-inhibiting hormone and nitric oxide synthase in the central nervous system of the green shore crab, *Carcinus maenas*, and the blackback land crab, *Gecarcinus lateralis*. *Comp. Biochem. Physiol.* **203A**, 328-340.

Ranek, M.J., Kokkonen-Simon, K.M., Chen, A., Dunkerly-Eyring, B.L., Pinilla Vera, M., Oeing, C.U., Patel, C.H., Nakamura, T., Zhu, G., Bedja, D., et al. (2019). PKG1-modified TSC2 regulated mTORC1 activity to counter adverse cardiac stress. *Nature.* **566**, 264-269.

Rozewicki, J., Li, S.L., Amada, K.M., Standley, D.M. and Katoh, K. (2019). MAFFT-DASH: integrated protein sequence and structural alignment. *Nucleic Acids Res.* **47**, W5-W10.

Saidi, B., Debesse, N., Webster, S.G., Sedlmeier, D. and Lachaise, F. (1994). Involvement of cAMP and cGMP in the mode of action of molt-inhibiting hormone (MIH) a neuropeptide which inhibits steroidogenesis in a crab. *Molec. Cell Endocrinol.* **102**, 53-61.

Sandberg, M., Natarajan, V., Ronander, I., Kalderon, D., Walter, U., Lohmann, S.M. and Jahnsen, T. (1989). Molecular cloning and predicted full-length amino acid sequence of the type Iβ isozyme of cGMP-dependent protein kinase from human placenta. *FEBS Lett.* **255**, 321-329.

Sayers, E.W., Cavanaugh, M., Clark, K., Pruitt, K.D., Schoch, C.L., Sherry, S.T. and Karsch-Mizrachi, I. (2020). GenBank. *Nucleic Acids Res.* **49**, D92-D96.

Sellak, H., Choi, C.S., Dey, N.B. and Lincoln, T.M. (2013). Transcriptional and post-transcriptional regulation of cGMP-dependent protein kinase (PKG-I): pathophysiological significance. *Cardiovasc. Res.* **97**, 200-207.

Sharma, A.K., Zhou, G., Kupferman, J., Surks, H.K., Christensen, E.N., Chou, J.J., Mendelsohn, M.E. and Rigby, A.C. (2008). Probing the Interaction between the coiled coil leucine zipper of cGMP-dependent protein kinase Iα and the C terminus of the myosin binding subunit of the myosin light chain phosphatase *J. Biol. Chem.* **283**, 32860-32869.

Sharma, R., Kim, J., Qin, L., Henning, P., Akimoto, M., VanSchouwen, B., Kaur, G., Sankaran, B., MacKenzie, K.R., Melacini, G., et al. (2022). An auto-inhibited state of protein kinase G and implications for selective activation. *eLife* **11**, e79530.

Shi, F. and Collins, S. (2023). Regulation of mTOR signaling: Emerging role of cyclic nucleotide-dependent protein kinases and implications for cardiometabolic disease. *Int. J. Molec. Sci.* **24**, 11497.

Steenwyk, J.L., Buida III, T.J., Li, Y., Shen, X. and Rokas, A. (2020). ClipKIT: A multiple sequence alignment trimming software for accurate phylogenomic inference. *PLoS Biol.* **18**, e3001007.

Thalluri, K., Mayer, J.P., Chabenne, J.R., Gelfanov, V. and DiMarchi, R.D. (2018). Synthesis of disulfide-rich heterodimeric peptides through an auxiliary N, N-crosslink. *Commun. Chem.* **1**, 36.

The UniProt Consortium. (2022). UniProt: the Universal Protein Knowledgebase in 2023. *Nucleic Acids Res.* **51**, D523-D531.

Trifinopoulos, J., Nguyen, L.T., von Haeseler, A. and Minh, B.Q. (2016). W-IQ-TREE: a fast online phylogenetic tool for maximum likelihood analysis. *Nucleic Acids Res.* **44**, W232-W235.

Vaandrager, A., Hogema, B. and de Jonge, H. (2005). Molecular properties and biological functions of cGMP-dependent protein kinase II. . *Front. Biosci.* **10**, 2150-2164.

Vagonia, A.C., Mier, P., Petrakis, S. and Andrade-Navarro, M.A. (2022). Analysis of Huntington's disease modifiers using the hyperbolic mapping of the protein interaction network. *Int. J. Mol. Sci.* **23**, 5853.

Vo, N.K., Gettemy, J.M. and Coghlan, V.M. (1998). Identification of cGMP-dependent protein kinase anchoring proteins (GKAPs). *Biochem. Bioph. Res. Commun.* **246**, 831-835.

Wang, J., Chitsaz, F., Derbyshire, M.K., Gonzales, N.R., Gwadz, M., Lu, S., Marchler, G.H., Song, J.S., Thanki, N., Yamashita, R.A., et al. (2023). The conserved domain database in 2023. *Nucleic Acids Res.* **51**, D384-D388.

Wang, Y.M., Vandewalle, N., De Veirman, K., Vanderkerken, K., Menu, E. and De Bruyne, E. (2024). Targeting mTOR signaling pathways in multiple myeloma: Biology and implication for therapy. *Cell Commun. Signal.* **22**, 320.

Webster, S.G. (1986). Neurohormonal control of ecdysteroid biosyntheiss by *Carcinus maenas* Y-organs *in vitro*, and preliminary characterization of the putative molt-inhibiting hormone (MIH). *Gen. Comp. Endocr.* **61**, 237-247.

Webster, S.G., Keller, R. and Dircksen, H. (2012). The CHH-superfamily of multifunctional peptide hormones controlling crustacean metabolism, osmoregulation, moulting, and reproduction. *Gen. Comp. Endocrinol.* **175**, 217-233.

Webster, S.G., Wilcockson, D.C., Mrinalini and Sharp, J.H. (2013). Bursicon and neuropeptide cascades during the ecdysis program of the shore crab, *Carcinus maenas*. *Gen. Comp. Endocrinol.* **182**, 54-64.

Webster, S.G. (2015). Endocrinology of molting. *The Natural History of the Crustacea: Physiology* (ed. E. S. Chang and M. Thiel), pp. 1-35. Oxford: Oxford Press.

Yin, S., Liu, L. and Gan, W. (2021). The roles of post-translational modifications on mTOR signaling. *Int. J. Molec. Sci.* **22**, 1784.

Yuasa, K., Yamagami, S., Nagahama, M. and Tsuji, A. (2008). Trafficking of cGMP-dependent protein kinase II via interaction with Rab11. *Biochem. Bioph. Res. Commun.* **374**, 522-526.

CHAPTER THREE

TRANSCRIPT EXPRESSION OF PROTEIN KINASE G GENES IN THE MOLTING GLAND OF DECAPOD CRUSTACEANS

SUMMARY

Ecdysteroid production is negatively regulated by the neuropeptide molt-inhibiting hormone (MIH) synthesized and secreted by the X-organ/sinus gland complex (XO/SG) in the eyestalk ganglia. MIH signaling in the YO stimulates a cAMP-dependent triggering phase, followed by a cGMP-dependent summation phase modulated by cGMP-dependent protein kinase (protein kinase G, PKG). Two PKG isoforms are activated by MIH but have opposing effects of ecdysteroidogenesis. PKG1 inhibits mTORC1-dependent ecdysteroidogenesis in the YO, while PKG2 stimulates mTORC1-dependent ecdysteroidogenesis. Differences in YO expression of PKG1 and PKG2 may explain how the YO maintains basal levels of ecdysteroid secretion during intermolt. Transcripts of *PKG1* isoforms and *PKG2* are differentially expressed in the YO throughout the molt cycle. *PKG1α2* is the dominant isoform expressed in the YO by both *G. lateralis* and *C. maenas.* Increased transcript abundance of *PKG1* isoforms in late premolt, postmolt and blocked *G. lateralis* YOs and in mid premolt, late premolt, and postmolt *C. maenas* YOs suggest that the inhibitory role of PKG1 may be involved in repression of the YO.

INTRODUCTION

Regulation of growth in crustaceans is a highly coordinated process between environmental inputs, endocrine signaling, and the physical state of the animal. Ultimately, the output of ecdysteroids by the YO is the deciding factor in whether an animal proceeds towards

molting. Therefore, the signaling pathways that regulate ecdysteroid synthesis are under tight control. Ecdysteroid synthesis in the crustacean YO relies on mTORC1-dependent regulation of transcription and translation. MIH signaling in the intermolt YO activates two cGMP-dependent protein kinases, PKG1 and PKG2, which have opposing effects on ecdysteroid synthesis. A temporary drop in MIH causes the YO to enter the activated state in early premolt. The initial increase in ecdysteroid synthesis results from increased translation of transcripts encoding steroidogenic enzymes (Abuhagr et al., 2016; Benrabaa et al., 2023). Transition of the YO from the activated to the committed state results from increased expression of myostatin, a member of the transforming growth factor-beta (TGF-β) family of proteins (Abuhagr et al., 2016; Mykles, 2021). TGF-β signaling is believed to induce the committed state by increasing expression of ecdysteroid synthetic genes directly via SMAD signaling, and indirectly via sustained mTORC1 activation (Abuhagr et al., 2016; Mykles, 2021). Just before ecdysis, the late premolt YO becomes repressed which is characterized by a drop in ecdysteroidogenesis (Mykles and Chang, 2020).

The transitions of the YO from basal to activated to committed to repressed are important phenotypes characterized by changes in expression of transcript, proteins, or both, of signaling pathways that regulate the expression of ecdysteroid synthetic genes (Benrabaa et al., 2023). Transcriptional characterization of these pathways has led to further physiological characterization and validation of their role in ecdysteroidogenic regulation in the YO (Covi et al., 2009; Abuhagr et al., 2014b; Abuhagr et al., 2016; Mykles, 2021; Black et al., 2024; Kozma et al., 2024). However, a complete investigation of transcriptional expression of PKG remains incomplete. Given the opposing roles of PKG1 and PKG2 in the MIH signaling pathway

presented in Chapter 2, transcriptional characterization of the genes may provide additional insights as to their roles at different stages of the molting cycle.

Molting in decapods can be induced by multiple leg autotomy (MLA) or eyestalk ablation (ESA). MLA involves the loss of five or more walking legs, in laboratory practice all eight walking legs are typically removed (Skinner and Graham, 1972). While animals can and do autotomize limbs in their natural environment, the loss of all walking legs and survival to molting is likely rare. Limb regenerates, called limb buds, can produce peptide factors that influence regeneration. Limb autotomy factor anecdysis (LAF_{an}), produced by primary limb buds, is presumed to be a stimulatory factor for growth within the limb buds and may also exert some stimulatory influence on the YO (Skinner and Graham, 1972; Skinner, 1985a; 1985b; Mykles, 2001). The loss of a limb bud before a YO has transitioned to the committed state can halt further progression of molting until the growth of the secondary limb regenerate catches up to that of other limb buds through the action of a second peptide factor called limb autotomy proecdysis (LAF_{pro}; Skinner and Graham, 1972; Mccarthy and Skinner, 1977; Yu et al., 2002). While limb bud autotomy, and therefore LAF_{pro}, is not a component of typical MLA in laboratory animals, LAF_{an} may influence the YO in ways that are not typical of a "natural molt". Despite this, molting induced by MLA is presumed to most closely resemble that of a natural molt between the two induction methods available.

ESA involves the removal of one or both eyestalks to stimulate molting. In aquaculture methods unilateral ESA is used to stimulate ovarian maturation in shrimps and crabs, in turn increasing the rate of reproduction and production of stock animals (Meng et al., 2020; Ruan et al., 2024; Urdes et al., 2024). In the laboratory, ESA typically involves removal of both eyestalks to stimulate the transition of the YO from the basal to the activated state by the acute withdrawal

of MIH (Skinner and Graham, 1972; Skinner, 1985b). While *G. lateralis* animals subjected to ESA appear to progress quickly toward molting, they are not able to survive ecdysis itself (Skinner, 1985b). Further the removal of eyestalks results in the acute withdrawal of numerous neuropeptides in addition to MIH (Webster et al., 2012). Other neuropeptides synthesized in the eyestalk regulate vital processes such as carbohydrate metabolism, gonad development, and reproduction and the acute withdrawal of these neuropeptides certainly results in systemic dysregulation (Skinner, 1985b; Webster et al., 2012). While the results of ESA experiments should be interpreted with the broader context of systemic endocrine disruption, they can also uncover nuanced regulatory pathways by means of that disruption.

To date, deep RNA sequencing of YOs has been completed for six species of crabs: *G. lateralis* (Das et al., 2016; Das et al., 2018; Shyamal et al., 2018), *C. maenas* (Oliphant et al., 2018), *Callinectes sapidus* (Roegner and Watson, 2020), *Eriochier sinensis* (Wang et al., 2020), *Paralithodes camtschaticus*, and *Chionoecetes opilio* (Andersen et al., 2022). Transcriptomic analysis of the YO at each stage of the molt cycle (intermolt, early-, mid-, and late- premolt, and postmolt) has been assessed for *G. lateralis* (Das et al., 2018) and *C. maenas* (Oliphant et al., 2018). The transcriptomic response of the YO to ESA has only been assessed for *G. lateralis* (Shyamal et al., 2018). In the blue crab *C. sapidus* RNA sequencing of YOs from two intermolt animals and two premolt animals provides some capacity for comparative analysis, although the dataset is highly limited by the small sample size (Roegner and Watson, 2020).

In *G. lateralis*, *PKG* expression in the YO is significantly upregulated in intermolt relative to each of the premolt and postmolt stages (Das et al., 2018). The MLA transcriptome contained 94 cGMP-PKG signaling related contigs identified by KEGG analysis, 51 (54%) of which were differentially expressed between the molt stages (Das et al., 2018). In response to

ESA, one PKG-encoding transcript was identified in the *G. lateralis* YO and expression decreased sequentially at days 1, 3, and 7 following ESA relative to intermolt (Shyamal et al., 2018). Both assemblies of YO transcriptomes (MLA and ESA) only identified one PKG-encoding transcript, however both occurred before the identification and characterization of multiple PKG1 isoforms as well as PKG2 presented in Chapter 2. Subsequent reassembly of the 2018 *G. lateralis* transcriptomes in combination with transcriptomic data from the eyestalk ganglia (Kozma et al., 2023) improved identification of gene isoforms and paralogs, allowing for the identification of multiple *PKG* transcripts (see Chapter 2).

In the *C. sapidus* YO transcriptome, one PKG-encoding transcript was identified along with 49 other PKG-pathway genes identified by KEGG analysis (Roegner and Watson, 2020). Of these, five PKG-pathway genes were upregulated in YOs from the two premolt animals, although the identity of those transcripts was not stated (Roegner and Watson, 2020). The *C. maenas* transcriptome included not only YO samples, but also central nervous system (CNS), and the motivation of the analysis was to examine neuropeptides and their receptors. As such, PKG and related genes in the *C. maenas* YO transcriptome were not assessed. Raw reads from the *C. maenas* CNS and YO, as well as the *C. sapidus* YO were reassembled in the pancrustaceans transcriptomic database, CrusTome (Pérez-Moreno et al., 2023), which aided in the identification and characterization of crustacean PKG isoforms in Chapter 2.

In this chapter, the sequencing and assembly of a new YO transcriptome in *G. lateralis* in response to both MLA and ESA is reported. This transcriptome includes 125 animals, the largest sample size of a crustacean YO transcriptome to date. Motivation for generating this large dataset includes the ability to more accurately quantify changes in transcriptional expression that were previously limited by small sample size. Further, co-assembly of RNAseq data from both

MLA and ESA experiments aids in the assembly and identification of transcripts that may have incomplete reads or be more lowly expressed under some conditions but not others. Additionally, identification of peptides and proteins by LC-MS/MS is dependent upon the quality of the database to which the data is matched. One major goal of this dissertation includes identifying differentially phosphorylated proteins in response to PKG inhibition in the YO, an undertaking that requires an extensive reference dataset.

Here, quantitative patterns of transcript expression for *PKG1* and *PKG2* isoforms in the YO is presented for both *G. lateralis* and *C. maenas* over the course of the molt cycle. Additionally, the response of *PKG* transcript expression to ESA over the course of 19 days is also presented for *G. lateralis*. Finally, expression of each *PKG* isoform in ten different tissues was assessed for both *G. lateralis* and *C. maenas* to expand insights into potential roles of PKG beyond molt regulation that may be tissue and/or isoform specific. Our hypothesis is that PKG expression in the YO is both molt-stage and isoform dependent. As PKG isoforms are presumably trafficked to different subcellular locations (Vo et al., 1998; Casteel et al., 2010; Corradini et al., 2015), different isoforms are likely mediators of different cellular signals in different locations and at different times. Preliminary quantification of transcripts presented in Chapter 2 suggest that PKG activity in the YO may be transcriptionally mediated.

MATERIALS AND METHODS

Animal husbandry and tissue collection

Adult *G. lateralis* were collected in the Dominican Republic and shipped overnight via air cargo to Colorado, Usa. Animals were housed in group enclosures of 10-15 animals with an aspen bedding substrate moistened with 5 ppt Instant Ocean, and fed a diet of lettuce, carrots, and raisins coated in calcium powder twice a week. Animal enclosures were kept in an

environmental chamber maintained at 27ºC and 80% relative humidity with a 12 h: 12 h light:dark schedule as described (Covi et al., 2010). The third walking leg on the right side was autotomized from each animal, and molt stage was determined by limb regenerate growth (R index; [length of limb regenerate * 100/carapace width]), as well as the condition of the membranous layer upon dissection, and subsequent quantification of hemolymph ecdysteroid titer (Covi et al., 2010).

Adult male *C. maenas* were collected from Bodega Harbor, Bodega Bay, California, USA and housed at the UC David Bodega Marine Laboratory in a flow-through seawater system at ambient seawater temperatures (12-16ºC). Animals were fed weekly with fish. Molt stage was determined by the condition of the membranous layer upon dissection and subsequent quantification of hemolymph ecdysteroid titer. Prior to tissue harvesting, animals were anesthetized on ice for 5-15 minutes.

Hemolymph samples (100 µl) from *G. lateralis* were immediately combined with 300 µl methanol prior to animal dissection. Hemolymph samples (100 µl) from *C. maenas* were immediately combined with 100 µl marine anticoagulant (0.45 M NaCl, 0.1 M glucose, 30 mM trisodium citrate, 26 mM citric acid, 10 mM EDTA; pH 4.6; Banks et al., 2020) at the time of tissue harvest, and subsequently diluted 3-fold in methanol immediately prior to ecdysteroid quantification. Ecdysteroid concentration in hemolymph was quantified by a competitive enzyme-linked immunosorbent assay (ELISA; Kingan, 1989) as modified by Abuhagr et al. (2014a). Tissues were harvested from 1 intermolt adult male *G. lateralis* and 1 intermolt adult male *C. maenas* to assess transcript expression of PKG isoforms by end-point PCR. Tissues harvested were as follows: YO, ESG, gill, hepatopancreas, heart, thoracic ganglia, midgut, hindgut, brain, claw muscle, and testis. Tissues were stored in 0.5 mL RNA Later (Invitrogen,

Waltham, MA, USA) upon dissection and stored at 4ºC overnight to allow infiltration into the tissue before storing the samples at -20ºC until RNA isolation.

Multiple leg autotomy and eyestalk ablation

Molting was stimulated in intermolt adult male *G. lateralis* (carapace width = 44.1 - 63.7 mm) by multiple leg autotomy (MLA) of the eight walking legs. MLA animals were housed in individual enclosures with sand hydrated with 10 ppt Instant Ocean and fed as above. Environmental chambers were maintained at 27ºC and 80% relative humidity, and light was blocked from MLA animals with a curtain to simulate burrows in their native environment. Molt stage was estimated by measuring the R index, assessing the condition of the membranous layer upon dissection, and quantification of hemolymph ecdysteroid titer (Yu et al., 2002; Covi et al., 2010). YOs were harvested from animals in each molt stage: intermolt (C_4; n = 12), early premolt (D_0; n = 10), mid premolt (D_1; n = 6), late premolt ($D_{2\text{-}3}$; n = 7), and 10 days postmolt (B; n = 12). Additionally, animals with an R index ≤ 12 at 12 weeks post-MLA were considered blocked from molting and were harvested (n = 7; Pitts et al., 2017). One YO per animal was stored in 0.5 mL RNA Later (Invitrogen, Waltham, MA, USA) upon dissection and stored at 4ºC overnight to allow infiltration into the tissue before storing the samples at -20ºC until RNA isolation. The second YO from each pair was frozen in liquid nitrogen and stored at -80ºC for proteomic analysis, the results of which will be in a separate publication. Left and right YOs were alternated for transcriptomic or proteomic analysis.

Eyestalk ablation (ESA) was used to activate YOs in intermolt adult male *G. lateralis* (carapace width = 33.1 - 63.5 mm). ESA animals were housed and fed in group cages as described above. Animals were injected with a volume of 10 mM dimethylsulfoxide (DMSO) equal to 30% body weight at the time of ESA as a control treatment for part of a larger study.

The injection of 10 mM DMSO does not affect molting or gene expression in the YO (Abuhagr et al., 2016; (Benrabaa and Mykles, 2025). YOs were harvested at 0 (intact; n = 19), 1 (n = 7), 3 (n = 8), 5 (n = 10), 7 (n = 10), 14 (n = 10), and 19 (n = 7) days post-ESA. Both YOs were stored in 0.5 mL RNA Later (Invitrogen, Waltham, MA, USA) upon dissection and stored at 4ºC overnight to allow infiltration into the tissue before storing the samples at -20ºC until RNA isolation.

RNA isolation

Total RNA was isolated using TRIzol reagent (Invitrogen, Waltham, MA, USA) with modifications to the manufacturer's protocol optimized for crustacean samples. Briefly, samples were thawed on ice and tissues were transferred to RNAse free tubes containing 1 mL TRIzol reagent and a sterilized 5 mm stainless steel bead. Tissues were homogenized at RT for 60 seconds at 30 Hz using a TissueLyser II (Qiagen, Hilden, NRW, Germany), then held at RT for 5 minutes.

For phase separation, 0.2 mL of chloroform was added to each sample and shaken vigorously by hand for 20 seconds. Samples sat at RT for 3 minutes then were centrifuged at 12,000 g for 15 minutes at 4ºC. The upper aqueous phase was transferred to a new tube and RNA was precipitated by adding 4 µl of molecular grade glycogen (Invitrogen, Waltham, MA, USA) and a volume of ice-cold isopropanol equal to the volume of aqueous phase recovered. Samples were gently inverted then sat at RT for 10 minutes. Samples were centrifuged at 12,000 g for 15 minutes at 4ºC. Supernatant was discarded and 1 mL of 70% EtOH was added, samples were centrifuged at 7,500 g for 5 minutes at 4ºC. Supernatant was again removed, and samples were air-dried until no visible droplets remained (approximately 10 minutes).

RNA was resuspended in 0.04 mL DEPC RNase-free water on ice. DNA was digested using the rDNase Set according to the manufacturer's protocol (Macherey-Nagel, Düren, NRW, Germany). RNA was cleaned using RNAclean XP magnetic beads according to the manufacturer's single-tube format protocol (Beckman Coulter Life Sciences, Indianapolis, IN, USA). Final RNA quality and quantity was assessed with the Qubit™ RNA HS Assay Kit (Invitrogen, Waltham, MA, USA).

RNA sequencing & transcript assembly

G. lateralis YO RNA samples from MLA and ESA experiments were shipped on dry ice to the Clinical Genomics Center, Oklahoma Medical Research Foundation (OMRF), Oklahoma City, OK, USA. Library preparation was completed at OMRF using New England Biolabs (Ipswich, MA, USA) poly-A selection along with the Watchmaker Genomics (Boulder, CO, USA) RNA library prep kit. Illumina HiSeq™ 3000 was used for paired-end sequencing of the cDNA libraries.

Transcript assembly was completed using the same assembly methods as CrusTome, as previously described (Pérez-Moreno et al., 2023). Quality of raw reads was assessed with FastQC (Andrews, 2010) and reads were trimmed with Trimmomatic (Bolger et al., 2014) was used to trim raw reads and remove adapter sequences. Rcorrecter was used for *k*-mer based error correction of Illumina reads (Song and Florea, 2015). The quality-filtered, trimmed, and corrected reads were then assembled into *de novo* transcriptomes by merging multiple assemblies. The Trinity pipeline (version 2.13.2; Grabherr et al., 2011; Haas et al., 2013) and rnaSPAdes (Bankevich et al., 2012) were used with various *k*-mer, normalization, minimum contig length, and quality filtering thresholds as described in Pérez-Moreno, 2023. Resulting assemblies were merged and filtered with the EvidentialGene pipeline (Gilbert, 2019) into the

final *G. lateralis* MLA and ESA YO transcriptome. The transcriptome was also translated into amino acid sequences, and both the nucleotide and amino acid versions were filtered for contamination using Kraken (version 2.1.2; Wood et al., 2019; Wright et al., 2023).

Differential expression analysis

Relative transcript expression was quantified as transcripts per million reads (TPM) for the *G. lateralis* MLA and ESA YO transcriptome using Salmon (v.1.7.0; Patro et al., 2017) in *quasi-mapping mode*. Salmon quantifications were run with the following flags "--seqBias --gcBias --validateMappings" to ensure accurate quantification by avoiding potential biases. Expression was graphed as mean ± standard error of the mean (SEM) in RStudio (v.2024.04.1.748; Rstudio Team, 2024). A one-way ANOVA with Tukey's Honestly Significant Difference (HSD) post-hoc test was used to evaluate differential expression of the transcripts across the molt cycle.

Tissue distribution of PKG transcripts

Purified RNA from one intermolt male *G. lateralis* and *C. maenas* tissues were reverse transcribed using qScript™ XLT cDNA SuperMix (Quantabio, Beverly, MA, USA) using 500 ng RNA input per tissue according to the manufacturer's protocols. Tissue distribution of PKG isoforms for *G. lateralis* and *C. maenas* were determined by end-point PCR. Translation elongation factor 2 (EF2) is highly expressed in all tissues and each molt stage and was used as a positive control for RNA isolation and cDNA synthesis. Reactions were assembled with 1 µl cDNA, 2 µl nuclease-free water, 5 µl GoTaq Green Master Mix (Promega, Madison, WI, USA), and 1 µl each of 20 µM forward and 20 µM reverse primers (Table 3.1). A negative control consisted of 3 µl nuclease-free water, 5 µl GoTaq Green Master Mix, and 1 µl each of the forward and reverse primers for each primer set. Products were stored at -20ºC until visualization

with gel electrophoresis. Products were separated on a 1% agarose gel containing 40 mM Tris base (tris [hydroxymethyl] aminomethane), 20 mM glacial acetic acid, and 1 mM disodium EDTA at 100 volts for 50 minutes. Gels were stained with ethidium bromide and visualized with UV light.

RESULTS

Transcriptome assembly

Circulating *G. lateralis* ecdysteroid (20E) levels increased exponentially with R-index (Fig. 3.1). R-index ranges for molt stages (IM: 5.3-10.8; EP: 12.2-15.5; MP: 16.2-17.8; LP: 18.2-20.4) correspond with those previously described (Skinner and Graham, 1972; Mykles, 2024). Condition of the membranous layer distinguished molt stage between mid premolt and late premolt, mid premolt membranous layers were thin and stringy, while the membranous layer in late premolt animals was absent, and a new cuticle was present and easily separated from the existing exoskeleton. Ecdysteroid titers in late premolt animals had the widest range, with a minimum of 624 pg/µl and a maximum of 1485 pg/µl. A trend toward increasing hemolymph ecdysteroid levels was observed in animals after ESA (Fig. 3.2). The largest range in circulating ecdysteroid titers was observed in late premolt animals, with a minimum of 72 pg/µl and maximum of 431 pg/µl.

Sequencing of 125 libraries prepared from *G. lateralis* YOs generated a total of 252,274,255 raw reads. Of those, 136,830,000 reads were from the 71 ESA-induced libraries generated, and 115,444,255 were from the 54 MLA-induced libraires. Transcriptome assembly resulted in 324,297 unique contigs from 125 animals in response to either MLA or ESA. Just over 22% (72,333 contigs) of those contigs were annotated by either BLAST homology with the UniProt brachyuran database, or identification of conserved domains and residues using

InterProScan. Complete PKG contigs for all 5 isoforms were identified in the *G. lateralis* MLA and ESA (MLA/ESA) transcriptome.

PKG1 expression across the molt cycle

In *G. lateralis*, *PKG1* expression was isoform-dependent over the course of the molt cycle (Fig. 3.3). *Gl-PKG1α1* was consistently lowly expressed at each molt stage, while expression of the *Gl-PKG1α2* isoform was more highly expressed than any other isoform at each molt stage (Fig. 3.3A, B). Expression of *Gl-PKG1α1* and *Gl-PKG1α2* did not change significantly with molt stage (Fig. 3.3A, B). Expression of *Gl-PKG1α3* gradually increased with progression toward ecdysis, and expression was significantly upregulated in the late premolt YO relative to intermolt ($p_{adj} = 0.035$) and postmolt ($p_{adj} = 0.036$; Fig. 3.3C). *Gl-PKG1β* transcript expression was significantly higher in the blocked YO than that of intermolt YOs ($p_{adj} = 0.046$) and postmolt YOs ($p_{adj} = 0.039$; Fig. 3.3D).

In *G. lateralis*, *PKG1* expression was isoform dependent in response to ESA (Fig. 3.4). Expression of *Gl-PKG1α1*, *Gl-PKG1α2*, and *Gl-PKG1β* followed a similar trend with an initial up-down-up-down during the first 7 days after ESA (Fig. 3.4A-C), whereas *Gl-PKG1α3* gradually increased in expression until day 7 then decreased at 14 and 19 days post-ESA (Fig 3.4D). *Gl-PKG1α2* transcript expression was roughly an order of magnitude greater than the expression of other *Gl-PKG1* isoforms (Fig. 3.4B). *PKG1α1* expression did not change significantly in response to ESA (Fig. 3.4A). *Gl-KG1α2* expression was significantly increased at 1 day post-ESA relative to days 0, 3, 7, and 14 ($p_{adj} = 0.013$, 0.049, 0.004, and 0.002 respectively; Fig. 3.4B). *Gl-PKG1α3* expression showed an increasing trend up to 7 days post-ESA, followed by a decrease at 14 and 19 days (Fig. 3.4C). Expression of *Gl-PKG1α3* was significantly upregulated at 3 and 7 days post-ESA relative to day 0 ($p_{adj} = 0.027$ and 0.013

respectively). *Gl-PKG1β* expression peaks at 3 days post-ESA where expression is significantly higher than days 0 and 14 (p_{adj} = *0.005* and *0.026* respectively; Fig. 3.4D).

In *C. maenas*, *PKG1* expression was not statistically associated with molt stage (Fig. 3.5). *Cm-PKG1α2* was the dominant *PKG1* isoform, in that transcript expression was higher than that of *Cm-PKG1α1* at each stage (Fig. 3.5A, B). *Cm-PKG1α3* and *Cm-PKG1β* isoforms were not identified in the *C. maenas* YO transcriptome.

PKG2 expression across the molt cycle

In *G. lateralis*, *PKG2* expression peaked during late premolt, although the transcript was lowly expressed among all molt stages (Fig. 3.6A). In response to ESA, *Gl-PKG2* gradually increased until day 7 and slightly decreasing at 14 and 19 days post-ESA, although these changes were not significantly different between molt stages (Fig. 3.6B). *Gl-PKG2* expression was lowly expressed in the *G. lateralis* YO in response to both MLA and ESA (Fig. 3.6).

In *C. maenas*, *PKG2* was expressed at lower levels at each molt stage with respect to *Cm-PKG1* isoforms (Fig. 3.6C). *Cm-PKG2* expression peaked during mid premolt and was significantly higher in expression than intermolt YOs (p_{adj} = *0.0197*). *Cm-PKG2* transcript expression remained elevated, although not significantly, in late premolt and postmolt YOs.

EF2 expression across the molt cycle

In *G. lateralis* expression of *Gl-EF2* was associated with molt stage in response to MLA and ESA (Fig. 3.7). In MLA animals, *Gl-EF2* was highly expressed at all molt stages relative to the PKG isoforms. EF2 expression peaked in YOs from late premolt animals relative to other stages ($p_{adj} < 0.001$ for all molt stages, Fig. 3.7A). In response to ESA, *Gl-EF2* expression increased until day 5, dropped at days 7 and 14, then began to rise again at 19 days post-ESA (Fig. 3.7B). Changes in expression were significantly different between days 0 and 3 (p_{adj} =

0.0001), 0 and 5 ($p_{adj} < 0.0001$), 1 and 5 ($p_{adj} = 0.006$), 3 and 7 ($p_{adj} = 0.034$), 3 and 14 ($p_{adj} = 0.0008$), 5 and 7 ($p_{adj} = 0.003$), and 5 and 14 ($p_{adj} = 0.0001$). In *C. maenas*, *Cm-EF2* was also highly expressed at each molt stage. *Cm-EF2* transcript was increased in YOs from mid premolt animals relative to late premolt animals ($p_{adj} = 0.004$; Fig. 3.7C).

Tissue distribution

PKG isoform expression is tissue-dependent in both *G. lateralis* and *C. maenas* (Fig. 3.8). Additionally, species-level differences in expression of *PKG* isoforms in various tissues is also observed. Quantifiable conclusions about transcript expression cannot be drawn from end-point PCR, however it is notable that expression for various *Gl-PKG* isoforms appears to be absent in certain *G. lateralis* tissues. Additionally, it is important to note that *G. lateralis* YO and hepatopancreas (Hp) cDNA appeared to be of slightly lower quality than other tissues, as evidenced by amplification of *Gl-EF2* (Fig. 3.8A). However, *Gl-EF2* still served as a reasonable positive control, as the transcript was expressed and amplified in all tissues.

In *G. lateralis*, amplification of all *Gl-PKG* isoforms was detected in the brain, thoracic ganglion, heart, and claw muscle; expression of *Gl-PKG1α2* was only detected in these tissues (Fig. 3.8A). Of the *Gl-PKG1* isoforms, only *Gl-PKG1α2* and *Gl-PKG1α3* were observed in the YO. *Gl-PKG1β* expression was similar to that of *Gl-PKG1α2* and *Gl-PKG1α*. However, it was absent in YO and only faint bands were observed in claw muscle and gill. *Gl-PKG2* was expressed in all tissues except the hindgut.

In *C. maenas* all *Cm-PKG1* isoforms were amplified and detected in the YO (Fig. 3.8B). Further, expression of all *Cm-PKG1* isoforms was observed in all tissues, although the bands were faint for all isoforms in the gill, *Cm-PKG1α2* in the eyestalk ganglia, and *Cm-PKG1α3* in the hepatopancreas. Interestingly, Cm-PKG2 was faintly detected in the brain and thoracic

ganglion but was not amplified in any of the other tissues. Amplification of *Cm-EF2* indicated that the cDNA libraries from all tissues were of good quality.

DISCUSSION

Based on circulating ecdysteroid titers, animals at 1, 3, and 5 days post-ESA were in early premolt, animals at 7 and 14 days were in mid premolt, and animals at 19 days after ESA were in late premolt. However, the changes in transcript expression for *PKG* and *EF2* emphasize that the physiological response to ESA is much different than MLA. The XO is not only the site of MIH production, but numerous other neuropeptides that regulate a range of physiological processes are also synthesized by the XO and secreted by the SG (Quackenbush and Herrnkind, 1983; Pitts et al., 2017; Mykles and Chang, 2020; Mykles, 2021; Pan et al., 2024). Other neuropeptides synthesized in the eyestalk include crustacean hyperglycemic hormone, gonad-inhibiting hormone, and pigment-dispersing hormone which regulate metabolism, reproduction, and pigment dispersion of chromatophores (Webster et al., 2012).

ESA appears to induce an initial upregulation of *PKG* and *EF2* transcripts. The same changes in *Gl-EF2* transcript in response to ESA have previously been reported in *G. lateralis* (Abuhagr et al., 2016; Shyamal et al., 2018). However, Shyamal and others (2018) previously found that transcript expression of MIH-signaling genes in the YO, including *Gl-PKG*, decreased over 7 days in response to ESA. Notably, in that analysis only one *Gl-PKG* isoform was identified and analyzed. The raw reads from Shyamal 2018, along with those from the MLA experiment by Das et al. (2018) were previously re-assembled and quantified by Drs. Jorge Pérez-Moreno and Mihika Kozma, former post-docs in the Mykles lab (data not published). In this reassembled *G. lateralis* YO transcriptome in response to ESA, two *PKG* isoforms were identified, a complete *Gl-PKG1β* sequence and an 82% complete *Gl-PKG2* isoform, which is

missing 164 amino acids from the N-terminus, as reported in Chapter 2. Quantification of this dataset reveals a pattern of transcript expression similar to that observed for *PKG1* isoforms in this chapter (Fig. 3.9A). That is, transcript expression of *Gl-PKG1β* increased from day 0 to 1 day post-ESA, decreased by day 3, and decreased further by day 7, although it remains higher than that at day 0. In the same reassembled dataset *Gl-PKG2* expression showed a similar trend, but the actual magnitude of change at each time point was small and consistent with the changes observed here (Figs. 9B and 6B. respectively). Differences in expression between the original assembly and that assembled by Pérez-Moreno and Kozma were likely a result of new assembly and quantification software. Assembly methods available today are better at merging short or incomplete reads to a single contig, as well as identifying and quantifying isoforms and paralogs (Patro et al., 2017). Further, quantification Pérez-Moreno and Kozma used TPM, rather than Fragments Per Kilobase of transcript per Million mapped reads (FPKM). Identifying a second *PKG* isoform and therefore separating abundance between the two, as well as differences in quantification methods likely explain the differences between the reassembly and original assembly of *G. lateralis* YO transcripts in response to ESA.

More broadly, differences in expression patterns between the MLA/ESA transcriptome and the 2018 datasets (Das et al.; Shyamal et al.) may be explained by a combination of factors. First, the transcriptome assembled in this chapter included individual libraries for between 7 and 19 animals at 0, 1, 3, 5, 7, 14, and 19 days after ESA, whereas the transcriptome assembled in 2018 included three biological replicates of six YOs pooled from three animals at days 0, 1, 3, and 7 days after ESA. The individual sequencing and larger sample size used here resulted in an increase in accuracy of transcript quantification. Second, timepoints at days 5, 14, and 19 allowed us to identify nuances in expression changes. For example, the increase in transcript

expression for *Gl-PKG1α1* and *Gl-PKG1α2* at day 5 is missing in the original dataset. Third, all five *PKG* isoforms were identified in the MLA/ESA transcriptome, allowing for finer identification of transcript abundance changes between isoforms that may otherwise mask those patterns.

Focusing on the data from the MLA/ESA transcriptome presented here, it is clear that gene regulation in the YO in response to ESA is very different than the response to MLA. The vacillating increases and decreases observed primarily between days 1 and 7 after ESA indicate disorder and dysregulation of YO signaling in response to the sudden absence of MIH and other neuropeptides. Given that the complete absence of MIH and other neuropeptides does not occur over the course of a natural or MLA-induced molt cycle, it would make sense that many signaling pathways would fall apart and make the underlying molecular responses to ESA convoluted. Yet, understanding the effects of ESA is a high priority as it is the most effective and widely used method to induce ovarian maturation in aquaculture decapod species (Urdes et al., 2024). In the swimming crab *Portunus trituberculatus*, ESA induces upregulation of 132 proteins and differential expression of 31 microRNAs in the ovary, although RNAseq to compare differential transcript expression was not performed (Meng et al., 2020). While functional analysis did reveal changes in expected pathways that regulate ovarian maturation, such as vitellogenesis and methyl farnesoate metabolism, most differentially expressed proteins and miRNAs regulate metabolism (Meng et al., 2020).

Changes in transcript expression of *PKG1* isoforms followed surprising patterns over the course of the molt cycle in both *G. lateralis* (Fig. 3.3) and *C. maenas* (Fig. 3.5). In both species, transcript expression of *PKG1α1* and *PKG1α2* did not change significantly over the course of the molt cycle. *Gl-PKG1α2* expression is the most highly expressed of all the *PKG1* isoforms at

each molt stage in the *G. lateralis* YO. In response to ESA, *Gl-PKG1α2* expression increased nearly 4-fold after 1 day (Fig. 3.4). In *C. maenas*, *Cm-PKG1α2* expression exceeded that of *Cm-PKG1α3* at each molt stage. Taken together, these data indicate the *PKG1α2* is the primary isoform expressed in the YO of both species.

High expression of *PKG1* transcripts in intermolt YOs were expected relative to premolt stages, given that PKG1 has an inhibitory effect on ecdysteroid synthesis (Head et al., 2025). Increased expression of *Gl-PKG1* isoforms in *G. lateralis* YOs from late premolt, postmolt, and blocked animals was initially unexpected, but upon further consideration is consistent with the known role of PKG1 in the YO. During late premolt, ecdysteroid synthesis peaks, then abruptly drops as the YO transitions to the repressed phenotype (Mykles, 2021; 2024). These data indicate that *Gl-PKG1*, most notably *Gl-PKG1α2* and *Gl-PKG1α3*, may be part of the transition from the committed to repressed YO, and might also maintain low ecdysteroid titers during postmolt. Upregulation of *Gl-PKG1* in the blocked phenotype also complies with the role of PKG1, as blocked animals remain refractory to MLA even after 12 weeks, likely due to increased MIH synthesis in the eyestalk (Pitts et al., 2017). Expression of MIH signaling genes, including PKG, guanylyl cyclase, nitric oxide synthase, adenylyl cyclase, and cAMP-dependent protein kinase are upregulated in the YO of blocked *G. lateralis* relative to intact intermolt control animals (Pitts et al., 2017). *Cm-PKG1* isoforms expression in the YO of *C. maenas* is also consistent with PKG1-dependent inhibition of ecdysteroid synthesis in the basal intermolt YO, as well as the repressed state in late premolt and postmolt, although the peak in expression occurred in the mid-premolt (Fig. 3.5). Transcript "priming", or expression of transcripts in molt stages just prior to their expected role, has been observed for mTOR pathway and ecdysteroid synthetic genes in the *G. lateralis* YO (Abuhagr et al., 2014b; Abuhagr et al., 2016; Benrabaa et al., 2023). Increased

expression of *PKG1* isoforms in the mid-premolt YO may be a case of transcript priming in *C. maenas*.

Transcript expression of *PKG2* was substantially lower than all the *PKG1* isoforms at each molt stage in both *G. lateralis* and *C. maenas* and the days post-ESA in *G. lateralis*. The difference in expression of *Gl-PKG1α2* and *Gl-PKG2* in the *G. lateralis* intermolt YO was nearly a 100-fold. Previously, a roughly 10-fold difference in *Gl-PKG1β* relative to *Gl-PKG2* was reported, although *Gl-PKG1β* was the only identified *PKG1* isoform identified in that dataset and presumed to represent cumulative expression of PKG1 isoforms (Head et al., 2025). Again, the differences observed are likely due to the limited sample size of the previous data set and the ability to more accurately separate and quantify isoforms. Intriguingly, *PKG2* transcript was significantly upregulated in late premolt in *G. lateralis* and mid premolt in *C. maenas*, following a similar trend to that observed for *PKG1* in the premolt YOs of both species. Given the opposing roles of PKG1 and PKG2, perhaps the genes are co-regulated to some degree as a mechanism to maintain balance of ecdysteroid secretion and prevent complete inhibition.

Expression of *PKG* isoforms may indicate both tissue and species-specific differences. Most notably, all isoforms of *Cm-PKG1* were strongly amplified in the *C. maenas* YO, while only *Gl-PKG1α2* and *Gl-PKG1α3* were amplified in the *G. lateralis* YO, and the bands are weak. Further, *Gl-PKG2* was strongly amplified in the *G. lateralis* YO, but not amplified in the *C. maenas* YO. This data is contrary to that discussed in the previous paragraphs. An important consideration is that the end-point PCR used here represents only one individual from each species. Further, as end-point PCR is not quantitative, differences in the intensity of bands may not represent true quantitative differences in transcript expression. Factors such as the quality of RNA isolation, cDNA synthesis, and primers can dramatically affect the results of end-point

PCR. The absence of PKG2 amplification in *C. maenas* was probably a result of cDNA library preparation for this individual rather than a true absence of transcript expression. All *PKG* primers had previously been tested using pooled cDNA from YO, heart, and claw muscle and sequencing of the PCR product extracted from agarose gels validated their specificity (Head et al., 2025).

Similarly, the absence of *Gl-PKG1α1* and *Gl-PKG1β* PCR products in the *G. lateralis* YO is likely a result of individual variation and/or library-based errors, as all *PKG* isoforms were amplified and sequenced previously from *G. lateralis* and *C. maenas* YOs (Head et al., 2025).

While gene expression is certainly regulated at the transcriptional level, post-transcriptional and post-translational regulation adds complexity to the interpretation of "gene expression". Expression of transcript and protein levels are not 1:1, and frequently are gene-specific (Sellak et al., 2013; Edfors et al., 2016; Gleason et al., 2023; Xing et al., 2024). Nevertheless, transcript-level quantification provides insight into one important component of gene expression. Regulation of *PKG* expression in mammals, primarily in vascular smooth muscle cells (VSMCs), involves changes in gene transcription, mRNA stability, protein synthesis, and post-translational modifications that all affect *PKG* "expression" (reviewed in Sellak et al., 2013). For example, the half-life of *PKG1* mRNA in VSMCs is around 10-12 hours, which is relatively long for that cell type (Sellak et al., 2011). This may explain the low copy number of *PKG1* mRNA typically identified in mammalian VSMC, despite the protein playing vital roles in maintaining vascular homeostasis (Browner et al., 2004). Notably, the 5'- and 3'-UTRs also contribute to differences in transcript stability and protein expression between mammalian *PKG1α* and *PKG1β*. Alternative splicing of *PKG1* results in transcript isoforms that have the same 3'-UTR, but have different 5'-UTRs (Sellak et al., 2011; Sellak et al., 2013), an

element that was key to determining that *PKG1* isoforms are alternatively spliced products of a single gene in crustaceans (Head et al., 2025). Evidence suggests that differences in the 5'-UTR influence isoform-specific translation (Sellak et al., 2011; Sellak et al., 2013). In short, this means that changes in transcript abundance do not give the full picture of gene expression, and definitive conclusions cannot be drawn from transcript expression alone.

CONCLUSIONS

Transcript expression of *PKG* isoforms is differentially regulated in the YO across the molt cycle in both *G. lateralis* and *C. maenas*. Upregulation of *PKG1* isoform transcripts during late premolt, postmolt, and in blocked YOs in *G. lateralis* and in mid- and late premolt and postmolt YOs in *C. maenas* suggest that PKG may mediate transition to the repressed state. Further, transcript expression after ESA indicates a disordered response in signaling pathways resulting from the acute withdrawal of MIH and other ESG neuropeptides. While the changes in transcript expression presented here are not conclusive evidence, these findings provide direction for further studies assessing protein expression and activity of PKG1 and PKG2 in the YO over the course of a complete molt cycle. Proteomic analysis to quantify protein abundance and isoform-specific knockdown using RNAi are suggested approaches to further investigating the roles of individual PKG isoforms, and whether protein abundance and activity influence YO phenotypes.

Table 3.1. Primers used for amplification and sequencing of *G. lateralis* and *C. maenas PKG* and *EF2*.

Gene	Sequence (5' - 3')	Annealing Temperature (ºC)	Amplicon Size (bp)
Gl-PKG1α1	F: TGCTGGAGATCCTCACCAAGAAG	56.7	307
	R: AAGTCATTCTCCAGGATCG	51.4	
Gl-PKG1a2	F: CCGCAGCTAATGACAGAT	52.1	371
	R: AAGTCATTCTCCAGGATCG	51.4	
Gl-PKG1α3	F: GGACAATGAGATAATGGAGC	50.6	249
	R: AAGTCATTCTCCAGGATCG	51.4	
Gl-PKG1β	F: CTACACAACCGCCTCTC	52.4	299
	R: AAGTCATTCTCCAGGATCG	51.4	
Gl-PKG2	F: GTGTGATAGCCTGAGAACTGG	55.1	505
	R: GCACGTAGTTACAAAGCAAGG	54.2	
Gl-EF2	F: TTCTATGCCTTTGGCCGTGTC	57.8	227
	R: ATGGTGCCCGTCTTAACCA	56.6	
Cm-PKG1α1	F: TGCTGGAGATTCTCACCAAGAAG	56.7	305
	R: GTCATTCTCCAGGATCGC	52.8	
Cm-PKG1a2	F: CAGATGCCAACGAGTGC	54.0	359
	R: GTCATTCTCCAGGATCGC	52.8	
Cm-PKG1α3	F: CAGTTGGAGGCTGTAGTGAAAG	55.5	273
	R: GTCATTCTCCAGGATCGC	52.8	
Cm-PKG1β	F: CCTTCGCACTCACAATAACC	53.7	280
	R: GTCATTCTCCAGGATCGC	52.8	
Cm-PKG2	F: AGGACTTCAGGTCCAAGC	54.3	377
	R: GTCTTCCATACGCTTCAGTCC	55.3	
Cm-EF2	F: CCATCAAGAGCTCCGACAATGAGCG	61.6	278
	R: CATTTCGGCACGGTACTTCTGAGCG	61.8	

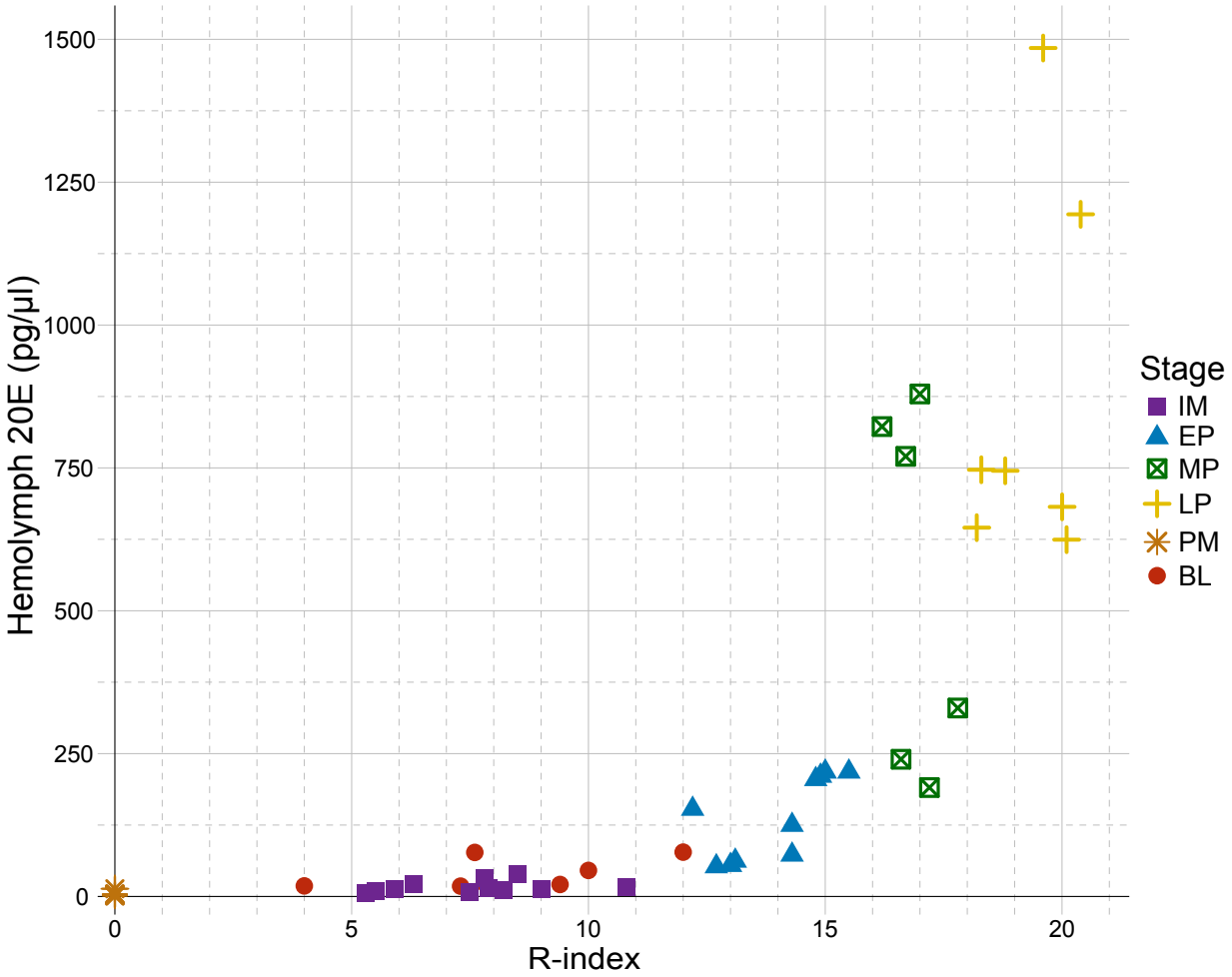

Figure 3.1. Relationship between circulating hemolymph ecdysteroid (20E) titer and R-index of *G. lateralis* in response to MLA. Molt stage was determined by the relationship between R-index (x-axis), hemolymph ecdysteroid titer (20E pg/µl; y-axis), and condition of the membranous layer (not shown). Postmolt animals has R-index of zero as the missing appendages were regenerated, blocked animals had R-index ≤ 12 after 12 weeks from the date of MLA. Legend is as follows: IM = intermolt, purple square, EP = early premolt, blue triangle; MP = mid premolt, green boxed X; LP = late premolt, yellow plus sign; PM = postmolt, orange asterisk; BL = blocked, red circle.

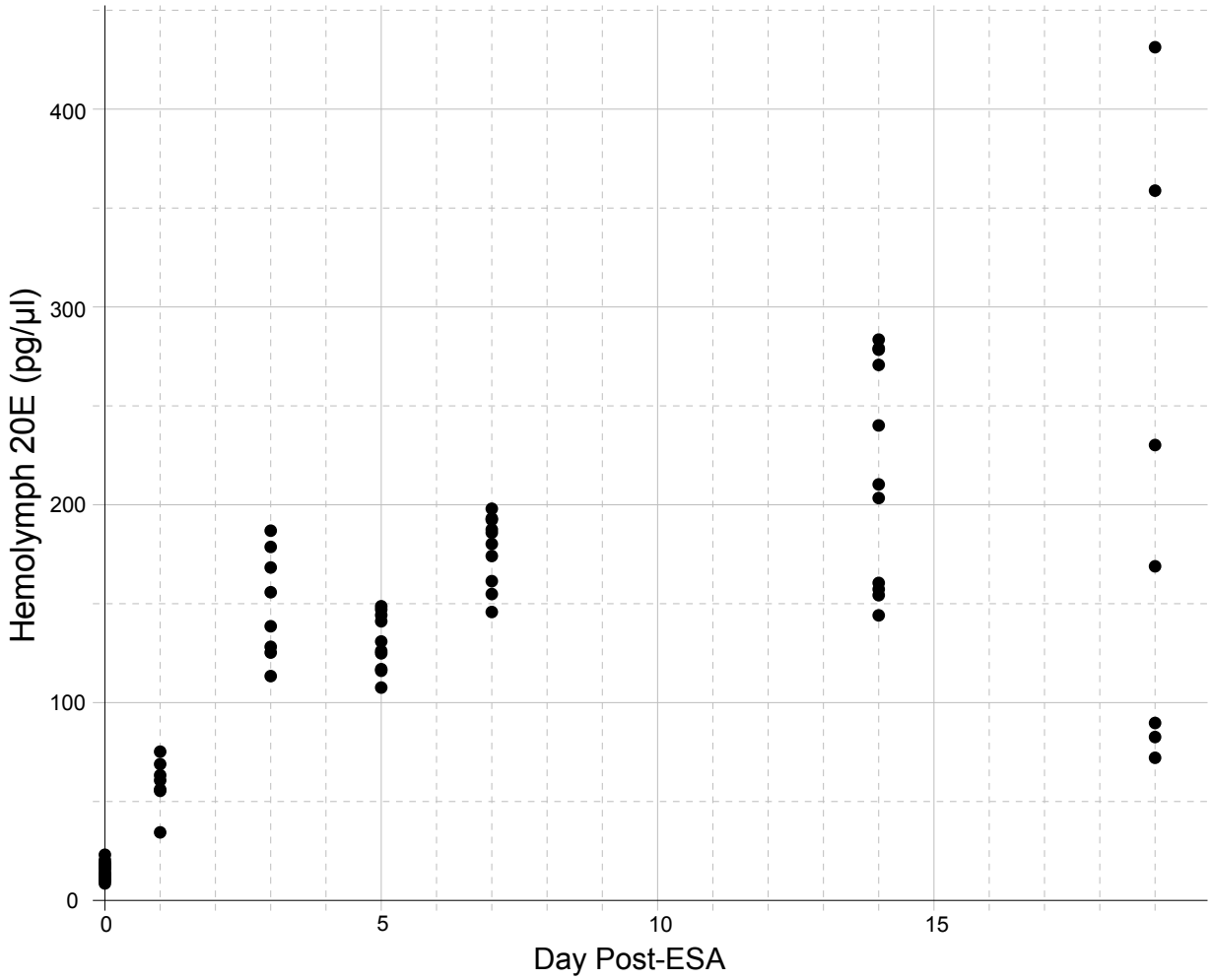

Figure 3.2. Relationship between circulating ecdysteroid (20E) titer and days post-ESA of *G. lateralis* used for transcriptomic analysis. Hemolymph ecdysteroid titers (20E pg/µl; y-axis), in male *G. lateralis* at 0 (n = 19), 1 (n = 7), 3 (n = 8), 5 (n = 10), 7 (n = 10), 14 (n = 10), and 19 (n = 7) days post-ESA.

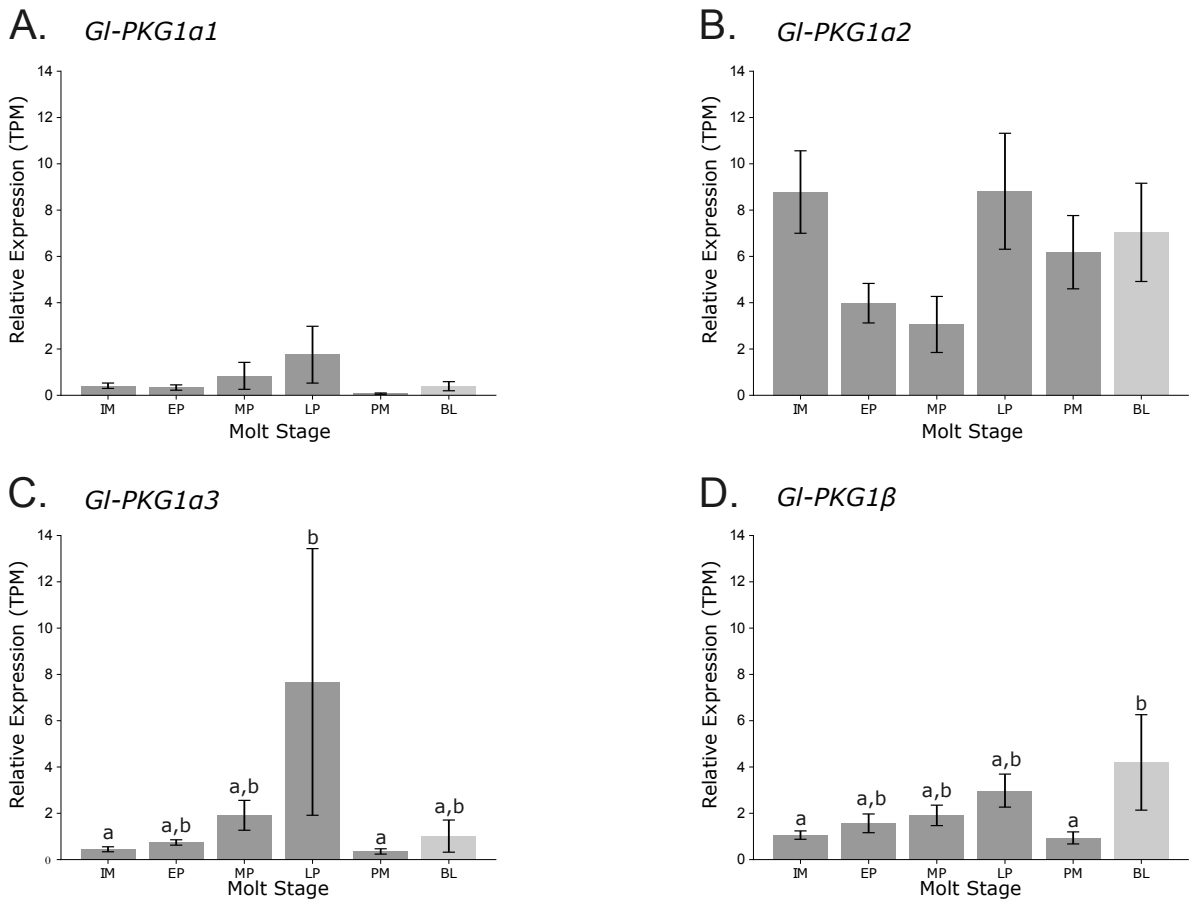

Figure 3.3. Expression of PKG1 isoforms in the *G. lateralis* YO across the molt cycle. Relative transcript expression (transcripts per million reads, TPM) of (A) PKG1α1, (B) PKG1α2, (C) PKG1α3, and (D) PKG1β in the *G. lateralis* YO in response to MLA, plotted as mean ± SEM. Molt stages are as follows: intermolt, IM; early premolt, EP; mid premolt, MP; late premolt, LP; postmolt, PM; blocked, BL. Statistically significant differences in transcript expression are indicated by groups that do not share a letter; one-way ANOVA with Tukey HSD $p_{adj} \leq 0.05$.

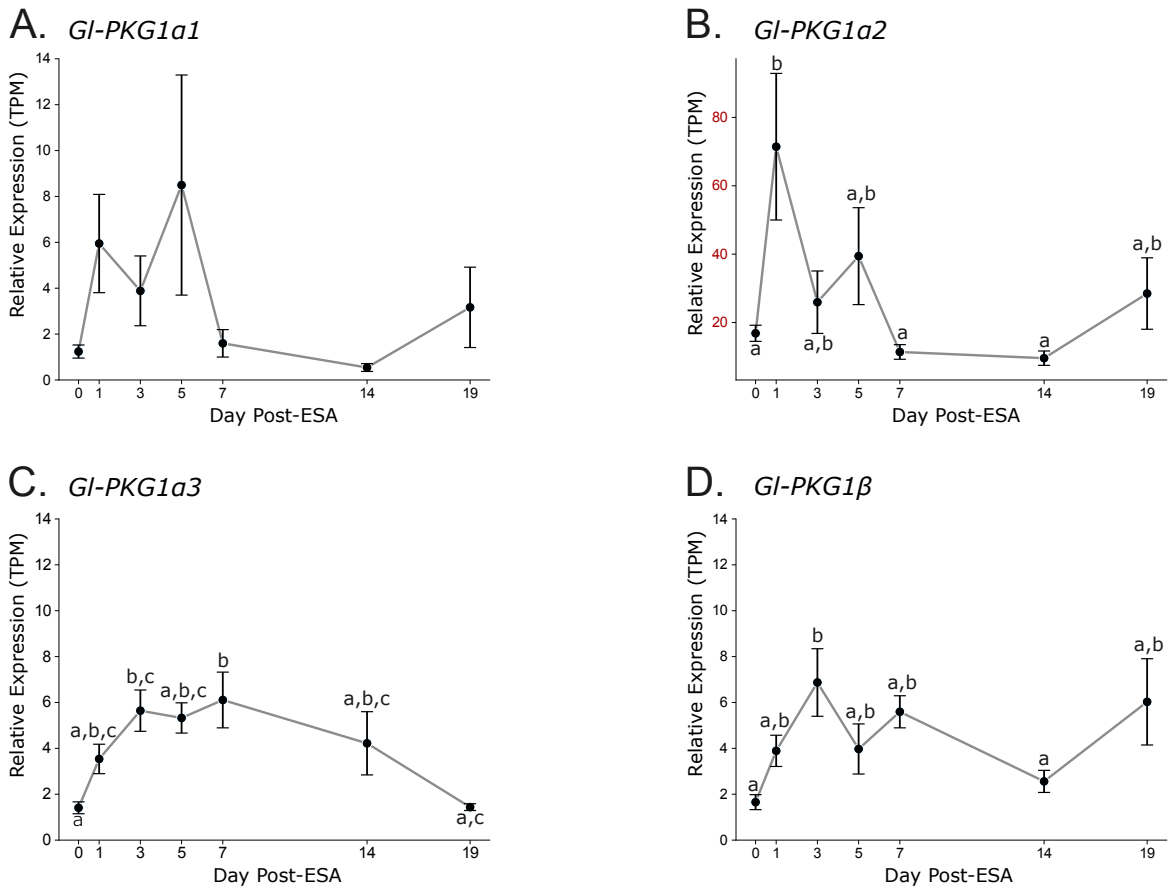

Figure 3.4. Expression of PKG1 isoforms in the *G. lateralis* YO in response to ESA. Relative transcript expression (transcripts per million reads, TPM) of (A) PKG1α1, (B) PKG1α2, (C) PKG1α3, and (D) PKG1β in the *G. lateralis* YO in response to ESA, plotted as mean ± SEM. The y-axis is plotted in red for (B) PKG1α2 to distinguish the difference in scale. Statistically significant differences in transcript expression are indicated by groups that do not share a letter; one-way ANOVA with Tukey HSD $p_{adj} \leq 0.05$.

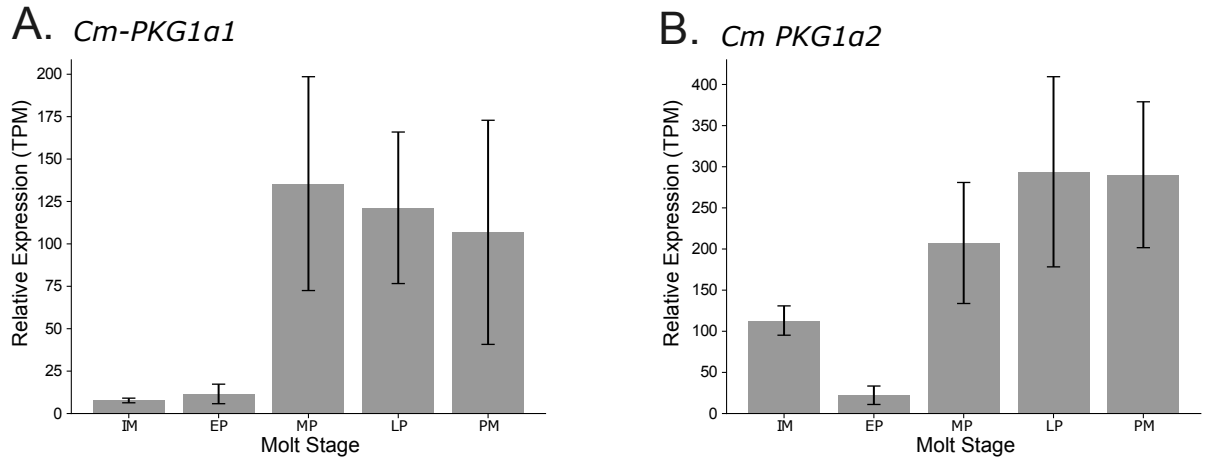

Figure 3.5. Expression of PKG1 isoforms in the *C. maenas* YO across the molt cycle. Relative transcript expression (transcripts per million reads, TPM) of (A) PKG1α1 and (B) PKG1α2 in the *C. maenas* YO, plotted as mean ± SEM. Molt stages are as follows: intermolt, IM; early premolt, EP; mid premolt, MP; late premolt, LP; postmolt, PM. Statistically significant differences in transcript expression were assessed with one-way ANOVA with Tukey HSD $p_{adj} \leq 0.05$, no significant differences were found.

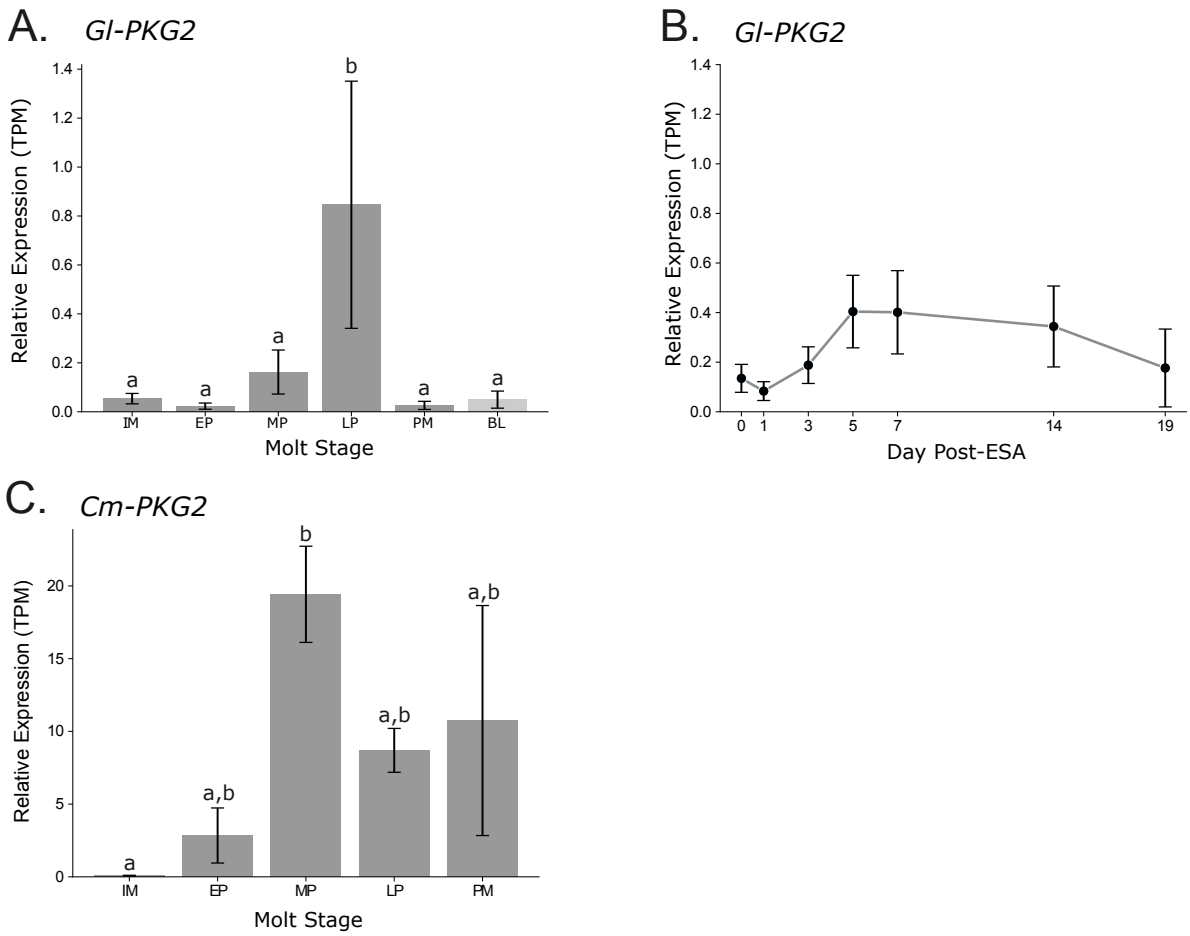

Figure 3.6. Expression of PKG2 in the *G. lateralis* YO in response to MLA and ESA and the *C. maenas* YO over the molt cycle. Relative transcript expression (transcripts per million reads, TPM) of *G. lateralis* PKG2 in response to (A) MLA and (B) ESA, and *C. maenas* (C) over the molt cycle, plotted as mean ± SEM. Molt stages are as follows: intermolt, IM; early premolt, EP; mid premolt, MP; late premolt, LP; postmolt, PM; blocked, BL. Statistically significant differences in transcript expression are indicated by groups that do not share a letter; one-way ANOVA with Tukey HSD $p_{adj} \leq 0.05$.

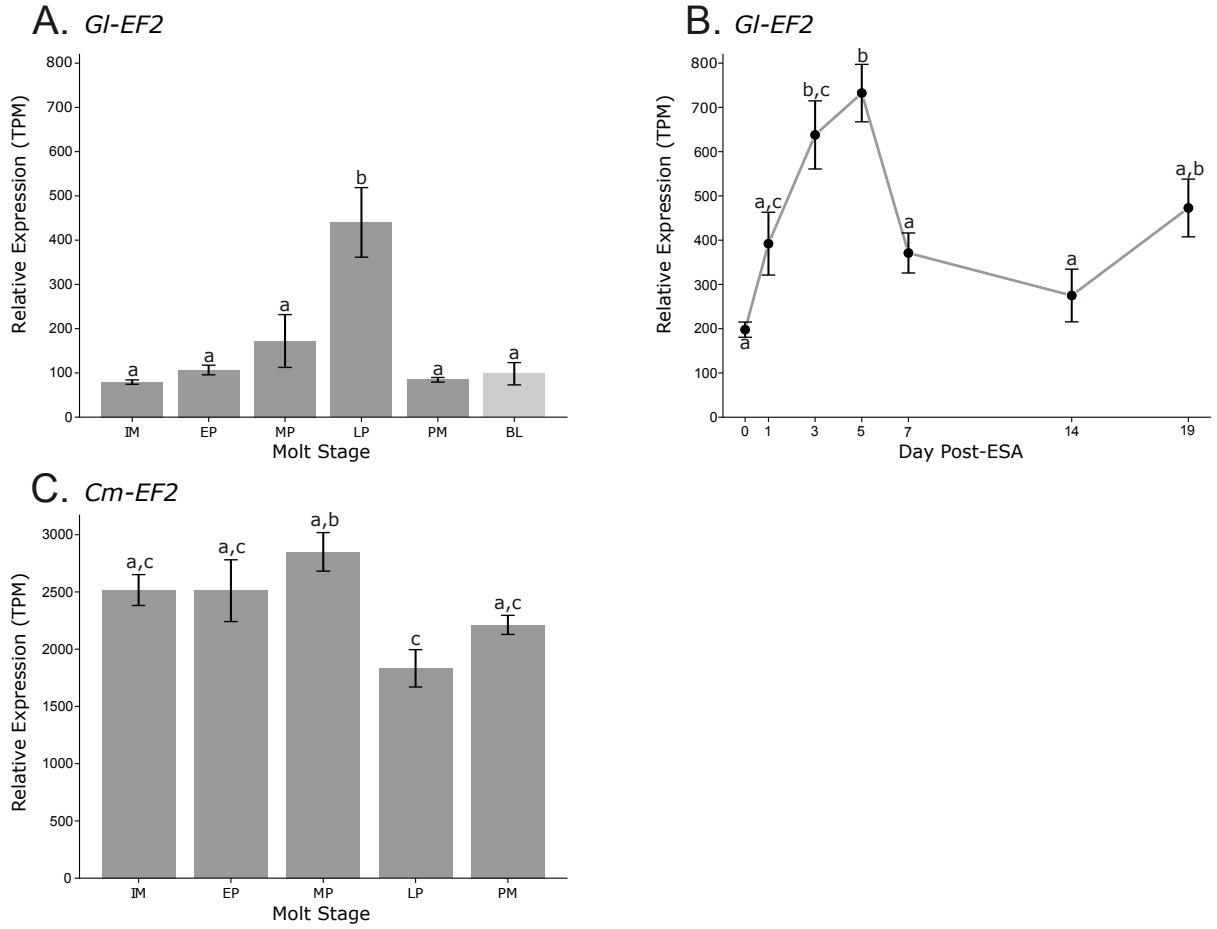

Figure 3.7. Expression of EF2 in the *G. lateralis* YO in response to MLA and ESA and the *C. maenas* YO over the molt cycle. Relative transcript expression (transcripts per million reads, TPM) of *G. lateralis* EF2 in response to (A) MLA and (B) ESA, and *C. maenas* (C) over the molt cycle. Molt stages are as follows: intermolt, IM; early premolt, EP; mid premolt, MP; late premolt, LP; postmolt, PM; blocked, BL. Statistically significant differences in transcript expression are indicated by groups that do not share a letter; one-way ANOVA with Tukey HSD $p_{adj} \leq 0.05$.

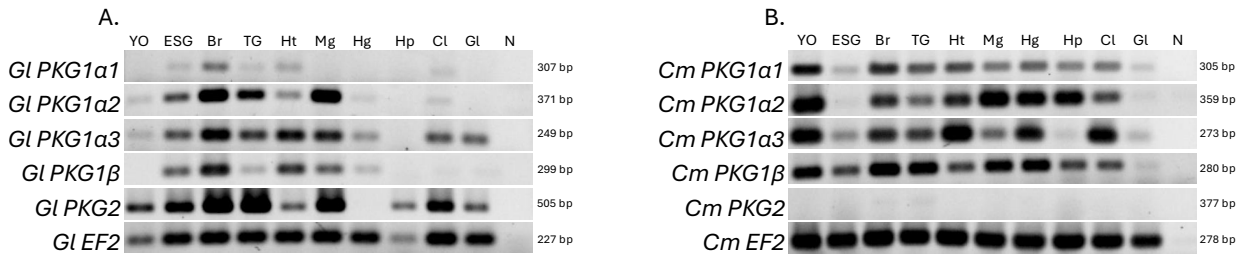

Figure 3.8. Expression of PKG isoforms in *G. lateralis* and *C. maenas* tissues. Transcript expression of each PKG isoform was assessed using end-point PCR in one male intermolt animal for *G. lateralis* (A) and *C. maenas* (B). Translation elongation factor 2 (EF2) was used as a positive control as it is expressed in all tissues and all molt stages. Tissues are as follows: YO, Y-organ; ESG, eyestalk ganglia; Br, brain; TG, thoracic ganglia; Ht, heart; Mg, midgut; Hg, hindgut; Hp, hepatopancreas; Cl, claw; Gl, gill; N, negative control.

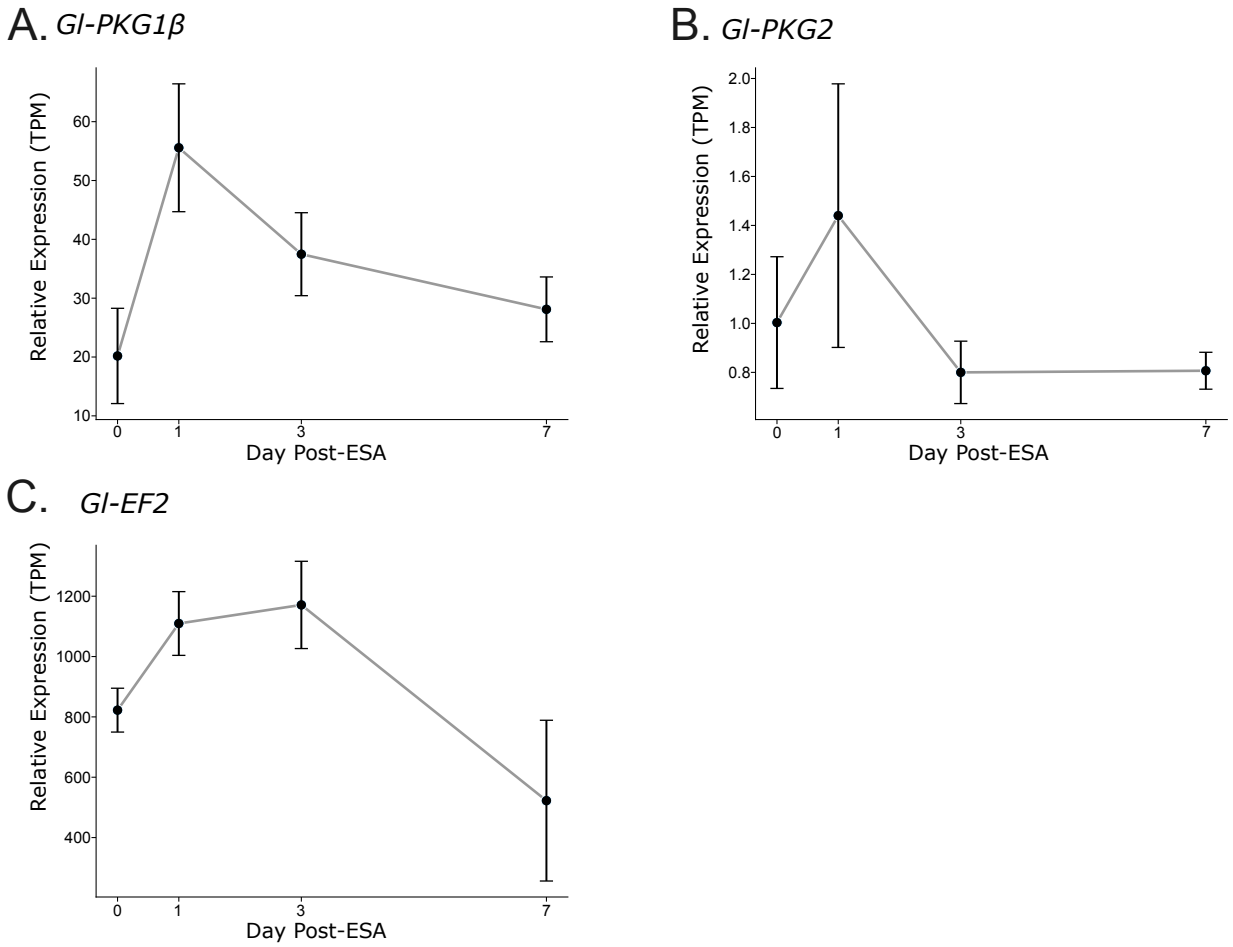

Figure 3.9. Expression of PKG and EF2 in the *G. lateralis* YO in response to ESA, from reassembled RNAseq data. Relative transcript expression (transcripts per million reads, TPM) of (A) PKG1β, (B) PKG2, and (C) EF2 in the *G. lateralis* YO in response to ESA from data originally published by Shyamal et al. 2018 and reassembled by JPM and MK. Data expressed as mean ± SEM. Statistically significant differences in transcript expression were assessed with one-way ANOVA with Tukey HSD $p_{adj} \leq 0.05$, no significant differences were found.

REFERENCES

Abuhagr, A.M., Blindert, J.L., Nimitkul, S., Zander, I.A., LaBere, S.M., Chang, S.A., MacLea, K.S., Chang, E.S. and Mykles, D.L. (2014a). Molt regulation in green and red color morphs of the crab *Carcinus maenas*: gene expression of molt-inhibiting hormone signaling components. *J. Exp. Biol.* **217**, 796-808.

Abuhagr, A.M., MacLea, K.S., Chang, E.S. and Mykles, D.L. (2014b). Mechanistic target of rapamycin (mTOR) signaling genes in decapod crustaceans: Cloning and tissue expression of mTOR, Akt, Rheb, and p70 S6 kinase in the green crab, *Carcinus maenas*, and blackback land crab, *Gecarcinus lateralis*. *Comp. Biochem. Physiol.* **168A**, 25-39.

Abuhagr, A.M., MacLea, K.S., Mudron, M.R., Chang, S.A., Chang, E.S. and Mykles, D.L**.** (2016). Roles of mechanistic target of rapamycin and transforming growth factor-β signaling in the molting gland (Y-organ) of the blackback land crab,. *Comp. Biochem. Physiol.* **198A**, 15-21.

Andersen, Ø., Johnsen, H., Wittmann, A.C., Harms, L., Thesslund, T., Berg, R.S., Siikavuopio, S. and Mykles, D.L. (2022). De novo transcriptome assemblies of red king crab (*Paralithodes camtschaticus*) and snow crab (*Chionoecetes opilio*) molting gland and eyestalk ganglia - Temperature effects on expression of molting and growth regulatory genes in adult red king crab. *Comp. Biochem. Physiol.* **257B**, 110678.

Bankevich, A., Nurk, S., Antipov, D., Gurevich, A.A., Dvorkin, M., Kulikov, A.S., Lesin, V.M., Nikolenko, S.I., Pham, S., Prjibelski, A.D., et al. (2012). SPAdes: A New Genome Assembly Algorithm and Its Applications to Single-Cell Sequencing. *J. Comput. Biol.* **19**, 455-477.

Banks, T.M., Wang, T., Fitzgibbon, Q.P., Smith, G.G. and Ventura, T. (2020). Double-Stranded RNA Binding Proteins in Serum Contribute to Systemic RNAi Across Phyla-Towards Finding the Missing Link in Achelata. *Int. J. Molec. Sci.* **21**, 6967.

Benrabaa, S.A.M., Chang, S.A., Chang, E.S. and Mykles, D.L. (2023). Effects of molting on the expression of ecdysteroid biosynthesis genes in the Y-organ of the blackback land crab, Gecarcinus lateralis. *Gen. Comp. Endocrinol.* **340**, 114304.

Benrabaa, S.A.M. and Mykles, D.L. (2025). Effects of blocking transforming factor-b/activin signaling on the expression of ecdysteroid metabolism and responsive genes in the crustacean molting gland (Y-organ). *Gen. Comp. Endocrinol.* **Submitted**.

Black, N., Banks, T.M., Glendinning, S., Chowdhury, G., Mykles, D.L. and Ventura, T. (2024). Silencing Multiple Crustacean Hyperglycaemic Hormone-Encoding Genes in the Redclaw Crayfish *Cherax quadricarinatus* Induces Faster Molt Rates with Anomalies. *Int. J. Molec. Sci.* **25**, 18.

Bolger, A.M., Lohse, M. and Usadel, B. (2014). Trimmomatic: a flexible trimmer for Illumina sequence data. *Bioinformatics.* **30**, 2114-2120.

Browner, N.C., Sellak, H. and Lincoln, T.M. (2004). Downregulation of cGMP-dependent protein kinase expression by inflammatory cytokines in vascular smooth muscle cells. *Am. J. Physiol.-Cell Physiol.* **287**, C88-96.

Casteel, D.E., Smith-Nguyen, E.V., Sankaran, B., Roh, S.H., Pilz, R.B. and Kim, C. (2010). A crystal structure of the cyclic GMP-dependent protein kinase Iβ dimerization/docking domain reveals molecular details of isoform-specific anchoring. *J. Biol. Chem.* **285**, 32684-32688.

Corradini, E., Burgers, P.P., Plank, M., Heck, A.J.R. and Scholten, A. (2015). Huntingtin-associated Protein 1 (HAP1) Is a cGMP-dependent kinase anchoring protein (GKAP) specific for the cGMP-dependent protein kinase Iβ isoform *J. Biol. Chem.* **290**, 7887-7896.

Covi, J.A., Chang, E.S. and Mykles, D.L. (2009). Conserved role of cyclic nucleotides in the regulation of ecdysteroidogenesis by the crustacean molting gland. *Comp. Biochem. Physiol.* **152A**, 470-477.

Covi, J.A., Bader, B.D., Chang, E.S. and Mykles, D.L. (2010). Molt cycle regulation of protein synthesis in skeletal muscle of the blackback land crab, *Gecarcinus lateralis*, and the differential expression of a myostatin-like factor during atrophy induced by molting or unweighting. *J. Exp. Biol.* **213**, 172-183.

Das, S., Pitts, N.L., Mudron, M.R., Durica, D.S. and Mykles, D.L. (2016). Transcriptome analysis of the molting gland (Y-organ) from the blackback land crab, *Gecarcinus lateralis*. *Comp. Biochem. Physiol.* **17D**, 26-40.

Das, S., Vraspir, L., Zhou, W., Durica, D.S. and Mykles, D.L. (2018). Transcriptomic analysis of differentially expressed genes in the molting gland (Y-organ) of the blackback land crab, *Gecarcinus lateralis*, during molt-cycle stage transitions. *Comp. Biochem. Physiol.* **28D**, 37-53.

Edfors, F., Danielsson, F., Hallström, B.M., Käll, L., Lundberg, E., Pontén, F., Forsström, B. and Uhlén, M. (2016). Gene-specific correlation of RNA and protein levels in human cells and tissues. *Molec. Syst. Biol.* **12**, 883.

Gilbert, D.G. (2019). Longest protein, longest transcript or most expression, for accurate gene reconstruction of transcriptomes? *bioRxiv.* 829184.

Gleason, L.U., Fekete, F.J., Tanner, R.L. and Dowd, W.W. (2023). Multi-omics reveals largely distinct transcript- and protein-level responses to the environment in an intertidal mussel. *J. Exp. Biol.* **226**, jeb245962.

Grabherr, M.G., Haas, B.J., Yassour, M., Levin, J.Z., Thompson, D.A., Amit, I., Adiconis, X., Fan, L., Raychowdhury, R., Zeng, Q., et al. (2011). Full-length transcriptome assembly from RNA-Seq data without a reference genome. *Nat. Biotechnol.* **29**, 644-652.

Haas, B.J., Papanicolaou, A., Yassour, M., Grabherr, M., Blood, P.D., Bowden, J., Couger, M.B., Eccles, D., Li, B., Lieber, M., et al. (2013). De novo transcript sequence reconstruction from RNA-seq using the Trinity platform for reference generation and analysis. *Nature Protoc.* **8**, 1494-1512.

Head, T.B., Pérez-Moreno, J.L., Ventura, T., Durica, D.S. and Mykles, D.L. (2025). Two cGMP-dependent protein kinases have opposing effects on molt-inhibiting hormone regulation of Y-organ ecdysteroidogenesis. *J. Exp. Biol.*

Kingan, T.G. (1989). A competitive Enzyme-Linked Immunosorbent-Assay - Applications in the assay of peptides, steroids, and cyclic-nucleotides. *An. Biochem.* **183**, 283-289.

Kozma, M.T., Pérez-Moreno, J.L., Durica, D.S. and Mykles, D.L. (2023). *Gecarcinus lateralis* - Eyestalk ganglia transcriptome *Zenodo*. https://doi.org/10.5281/zenodo.7987266

Kozma, M.T., Pérez-Moreno, J.L., Gandhi, N.S., Hernandez Jeppesen, L., Durica, D.S., Ventura, T. and Mykles, D.L. (2024). *In silico* analysis of crustacean hyperglycemic hormone family G protein-coupled receptor candidates. *Front. Endocrinol.* **14**, 1322800.

McCarthy, J.F. and Skinner, D.M. (1977). Interruption of proecdysis by autotomy of partially regenerated limbs in the land crab, *Gecarcinus lateralis*. *Dev. Biol.* **61**, 299-310.

Meng, X., Zhang, M., Gao, B., Lv, J., Li, J. and Liu, P**.** (2020). Integrative Proteomic and MicroRNA Analysis: Insights Into Mechanisms of Eyestalk Ablation-Induced Ovarian Maturation in the Swimming Crab *Portunus trituberculatus*. *Front. Endocrinol.* **11**,

Mykles, D.L. (2001). Interactions Between Limb Regeneration and Molting in Decapod Crustaceans. *Am. Zool.* **41**, 399-406.

Mykles, D.L. and Chang, E.S. (2020). Hormonal control of the crustacean molting gland: Insights from transcriptomics and proteomics. *Gen. Comp. Endocrinol.* **294**, 113493.

Mykles, D.L. (2021). Signaling pathways that regulate the crustacean molting gland. *Front. Endocrinol.* **12**, 113658.

Mykles, D.L. (2024). Molting physiology. *Frontiers in Invertebrate Physiology* (ed. S. P. L. S. Saleuddin, R.D. Roer, I. Wilkie), pp. 229-274. Palm Bay, FL: Apple Academic Press.

Oliphant, A., Alexander, J.L., Swain, M.T., Webster, S.G. and Wilcockson, D.C. (2018). Transcriptomic analysis of crustacean neuropeptide signaling during the moult cycle in the green shore crab, *Carcinus maenas*. *BMC Genomics.* **19**, 711.

Pan, T.S., Yang, M., Li, T., Jiang, H. and Ling, J. (2024). Integrate Analysis of Eyestalk Proteome and Metabolome in Precocious and Formal Juvenile Female *Eriocheir sinensis*. *Fishes.* **9**, 468.

Patro, R., Duggal, G., Love, M.I., Irizarry, R.A. and Kingsford, C. (2017). Salmon provides fast and bias-aware quantification of transcript expression. *Nature Meth.* **14**, 417-419.

Pérez-Moreno, J.L., Kozma, M.T., DeLeo, D.M., Bracken-Grisson, H.D., Durica, D.S. and Mykles, D.L. (2023). CrusTome: a transcriptome database resource for large-scale analyses across Crustacea. *G3-Genes Genomes Genet.* **13**, jkad098.

Pitts, N.L., Schulz, H.M., Oatman, S.R. and Mykles, D.L. (2017). Elevated expression of neuropeptide signaling genes in the eyestalk ganglia and Y-organ of *Gecarcinus lateralis* individuals that are refractory to molt induction. *Comp. Biochem. Physiol.* **214A**, 66-78.

Quackenbush, L.S. and Herrnkind, W.F. (1983). Partial Characterization of Eyestalk Hormones Controlling Molt and Gonadal Development in the Spiny Lobster *Panulirus argus*. *J. Crustacean Biol.* **3**, 34-44.

Roegner, M.E. and Watson, R.D. (2020). De novo transcriptome assembly and functional annotation for Y-organs of the blue crab (*Callinectes sapidus*), and analysis of differentially expressed genes during pre-molt. *Gen. Comp. Endocrinol.* **298**, 113567.

Ruan, X.H., Cheng, H.T., Shan, J.H., Li, L.H., Xuan, Z.J., Liang, K.S., Jia, X.Z., Yu, J., Li, Z.Y., Luo, L.Y., et al. (2024). Effect of eyestalk ablation and water temperature on the gonadal transcriptome of greasyback shrimp (*Metapenaeus ensis*). *Aquacult. Rep.* **39**, 14.

Sellak, H., Lincoln, T.M. and Choi, C.S. (2011). Stabilization of cGMP-dependent protein kinase G (PKG) expression in vascular smooth muscle cells: contribution of 3'UTR of its mRNA. *J. Biochem.* **149**, 433-41.

Sellak, H., Choi, C.S., Dey, N.B. and Lincoln, T.M. (2013). Transcriptional and post-transcriptional regulation of cGMP-dependent protein kinase (PKG-I): pathophysiological significance. *Cardiovasc. Res.* **97**, 200-207.

Shyamal, S., Das, S., Guruacharya, A., Mykles, D.L. and Durica, D.S. (2018). Transcriptomic analysis of crustacean molting gland (Y-organ) regulation via the mTOR signaling pathway. *Sci. Reports.* **8**, 7307.

Skinner, D.M. and Graham, D.E. (1972). Loss of limbs as a stimulus to ecdysis in brachyura (true crabs). *Biol. Bull.* **143**, 222-223.

Skinner, D.M. (1985a). Molting and Regeneration. *Integument, Pigments, and Hormonal Processes, Vol. 9* (ed. D. E. Bliss and L. H. Mantel), pp. 43-146. San Diego: Academic Press.

Skinner, D.M. (1985b). Interacting Factors in the Control of the Crustacean Molt Cycle. *Am. Zool.* **25**, 275-284.

Song, L. and Florea, L. (2015). Rcorrector: efficient and accurate error correction for Illumina RNA-seq reads. *GigaScience.* **4**, s13742-015-0089-y.

Urdes, L., Walster, C., Tepper, J. and Foyle, L. (2024). How one health and one welfare can strengthen the evidence of a management procedure- A case study of eyestalk ablation in farmed shrimp. *Sci. Pap.* **67D**, 818-829.

Vo, N.K., Gettemy, J.M. and Coghlan, V.M. (1998). Identification of cGMP-dependent protein kinase anchoring proteins (GKAPs). *Biochem. Bioph. Res. Commun.* **246**, 831-835.

Wang, B., Yang, J., Gao, C., Hao, T., Li, J. and Sun, J. (2020). Reconstruction of *Eriocheir sinensis* Y-organ Genome-Scale Metabolic Network and Differential Analysis After Eyestalk Ablation. *Front. Genet.* **11**, 532492.

Webster, S.G., Keller, R. and Dircksen, H. (2012). The CHH-superfamily of multifunctional peptide hormones controlling crustacean metabolism, osmoregulation, moulting, and reproduction. *Gen. Comp. Endocrinol.* **175**, 217-233.

Wood, D.E., Lu, J. and Langmead, B. (2019). Improved metagenomic analysis with Kraken 2. *Genome Biol.* **20**, 257.

Wright, R.J., Comeau, A.M. and Langille, M.G.I. (2023). From defaults to databases: parameter and database choice dramatically impact the performance of metagenomic taxonomic classification tools. *Microb. Genom.* **9**, 000949.

Xing, K., Yan, C., Feng, D., Wu, Z., Sun, Y. and J., Z. (2024). Integrated analysis of transcriptome and proteome reveals the key genes and processes involved in ovarian development in *Exopalaemon carinicauda*. *Aquacult. Rep.* **37**, 102248.

Yu, X.L., Chang, E.S. and Mykles, D.L. (2002). Characterization of limb autotomy factor-proecdysis (LAFpro), isolated from limb regenerates, that suspends molting in the land crab *Gecarcinus lateralis*. *Biol. Bull.* **202**, 204-212.

CHAPTER FOUR

ANALYSIS OF THE GLOBAL AND PHOSPHO-PROTEOME OF THE MOLTING GLAND OF DECAPOD CRUSTACEANS

SUMMARY

Ecdysteroid production is a highly coordinated and regulated process involving input from a range of pathways and systems. The molt-inhibiting hormone (MIH) is produced and secreted by the X-organ/sinus gland complex located in the eyestalk ganglia and negatively regulates the production of ecdysteroids in the molting gland (Y-organ, YO). MIH signaling begins with a cAMP-dependent triggering phase followed by a cGMP-dependent summation phase which ultimately leads to inhibition of mTORC1. This pathway is highly reliant on phosphorylation to mediate activation or repression of signaling proteins. The previous chapters establish that two cGMP-dependent protein kinases (PKG1 and PKG2) have opposing roles in modulating ecdysteroidogenesis via MIH signaling in YOs. The inhibitory role of MIH signaling is carried out by PKG1, which inhibits ecdysteroid synthesis. PKG2 counters that inhibition and maintains basal ecdysteroidogenesis in the intermolt YO. Differences in expression between PKG1 and PKG2 likely lead to the ability of MIH to primarily inhibit ecdysteroidogenesis, while allowing for the production of ecdysteroids needed for peripheral metabolic and reproductive processes.

This chapter uses isobaric labeling of YO peptides and phosphopeptide enrichment in liquid chromatography/tandem mass spectrometry (LC-MS/MS) to identify potential substrates of PKG in the YO. PKG1α1 and PKG1α2 isoforms were distinguished by the identification of

unique peptides from the alternatively spliced amine-terminus of the proteins, and PKG2 was not identified. This data supports the notion that differences between PKG1 and PKG2 expression allow for their opposing roles in the YO. No proteins were differentially expressed at the global level, although strong batch effects between TMT sets within the same experimental treatment were observed which may mask differential expression at both the protein and the peptide level. Therefore, the present results should be interpreted with caution, and correcting for batch effects in future analyses of this dataset will strengthen confidence in the results and unmask additional differentially expressed proteins and likely phosphopeptides.

Phosphopeptides from several signaling pathways including the mitogen-activated protein kinase (MAPK) and phosphoinositide 3-kinase/protein kinase B (PI3K/Akt) pathways are identified as possible substrates of PKG signaling in the YO. Additionally, pathways that regulate cytoskeletal organization and RNA processing were highly upregulated in the global and phosphoproteomes. Together, these data indicate crosstalk between multiple signaling pathways, as well as cytoskeletal mediated regulation of signaling pathways that impede or facilitate protein-protein interactions, as components of YO ecdysteroidogenic regulation.

INTRODUCTION

Signaling pathways that regulate the decapod Y-organ (YO) are intricate and interlinked. Molting is a tightly controlled process, as ecdysis and the postmolt period leave the animal vulnerable to predation. Additionally, molting is coupled with oocyte maturation and reproduction in many species (Subramoniam, 2000; Supriya et al., 2017; Fukasawa and Yasuda, 2024; Lu et al., 2024). Many environmental factors also influence or control the timing of molting, such as temperature, seasonality, photoperiod, salinity, and the presence or absence of

other crabs (Bliss and Boyer, 1964; Nagaraju, 2011; Kim et al., 2024; Luo et al., 2024; Gray et al., 2025).

Early studies on the regulation of molting in decapods established that the molt cycle is under regulatory control of neuropeptides, and that these neuropeptides are synthesized and secreted by cells in different parts of the body, depending on their action (Brown and Cunningham, 1939; Hanström, 1939; Bliss and Welsh, 1952; Gabe, 1953a; 1953b; Bliss et al., 1954; Echalier, 1954; Carlisle, 1957; Karlson and Skinner, 1960; Welsh, 1961). While we know that multiple signals regulate YO activation and ecdysteroidogenesis, our understanding of the signaling pathways involved becomes more complex with each new finding. In the *Gecarcinus lateralis* YO transcriptome, 99 G-protein coupled receptors (GPCRs) were identified (Tran et al., 2019). These GPCRs include representatives from Class A (rhodopsin-like receptors), Class B (secretin-like receptors), and Class C (metabotropic glutamate and pheromone receptors). These GPCRs bind ligands from biogenic amines, such as serotonin and dopamine, arthropod neuropeptides molt-inhibiting hormone (MIH), crustacean hyperglycemic hormone (CHH), corazonin, and proctolin, and insulin-like peptides (ILPs), such as relaxin (Tran et al., 2019). The YO also expresses four types of receptor tyrosine kinases, which bind ILPs and growth factors (Flores et al., 2024). The effects of each of these regulatory ligands are integrated to coordinate ecdysteroid synthesis, the only known role of the YO (Mykles, 2021).

MIH plays the predominant role in YO regulation during intermolt (Webster, 1986; Webster and Keller, 1986; Saidi et al., 1994; Baghdassarian et al., 1996; Chung and Webster, 2003; Nakatsuji et al., 2006; Nakatsuji et al., 2009; Pitts et al., 2017; and reviewed in Covi et al., 2012; Mykles, 2021; 2024). MIH signaling inhibits ecdysteroid synthesis primarily through the inhibition of mechanistic target of rapamycin (mTOR) and associated increases in transcription

of ecdysteroid biosynthetic enzymes (Abuhagr et al., 2014b; Abuhagr et al., 2016; Benrabaa et al., 2023; Shyamal et al., 2018; Mykles and Chang, 2020; Hou et al., 2021; Mykles, 2021; Li et al., 2023). Dysfunctional regulation of mTOR is implicated in various cancers and other human diseases, as it is a critical and central regulator of gene expression (Shahbazian et al., 2006; Ballou and Lin, 2008; Arif et al., 2017; Szwed et al., 2021; Basnet et al., 2023; Martinez-Lopez et al., 2023; Panwar et al., 2023; Shi and Collins, 2023; Mehta et al., 2024; Stanciu et al., 2024; Wang et al., 2024). Our current hypothesis is that the signaling pathways that regulate ecdysteroidogenesis in the YO, including, but not limited to MIH, converge on mTOR (Mykles, 2021).

mTOR is a serine/threonine protein kinase that is a central component of two different complexes, mTOR complex 1 (mTORC1) and mTOR complex 2 (mTORC2; Liu and Sabatini, 2020; Panwar et al., 2023; Shi and Collins, 2023; Liu et al., 2024). mTORC1 stimulates translation, lipid metabolism, mitochondrial biogenesis, nucleotide synthesis, and glycolysis and inhibits catabolic processes such as autophagy and lysosomal biogenesis (Shi and Collins, 2023). mTORC2 stimulates cytoskeletal stability and organization, as well as cell proliferation and survival (Panwar et al., 2023; Shi and Collins, 2023). The regulation of mTOR activation is highly dependent upon phosphorylation. Upstream regulators protein kinase B (Akt), and the tuberous sclerosis complex (TSC) are highly regulated by phosphorylation and have a number of phosphosites that can either stimulate or inhibit their activation (Liu and Sabatini, 2020; Panwar et al., 2023; Shi and Collins, 2023; Liu et al., 2024).

In this dissertation it has been established that cGMP-dependent protein kinase (PKG), a serine/threonine kinase, regulates ecdysteroid synthesis in the YO (Head et al., 2025; see also Chapter 2). The primary goal of this chapter is to identify potential substrates of PKG in the YO.

Mammalian PKG1 has previously been characterized as a stimulatory kinase of TSC2, which results in the inactivation of mTORC1 (Ranek et al., 2019; Oeing et al., 2020). PKG may also directly phosphorylate the regulatory-associated protein of mTOR (RAPTOR), leading to mTORC1 inhibition (Bordicchia et al., 2012; Liu et al., 2018; reviewed in Shi and Collins, 2023). PKG may also regulate mTOR indirectly by MAPK signaling pathways (Komalavilas et al., 1999; Doronzo et al., 2011; Bordicchia et al., 2012), and/or glycogen synthase kinase 3β (GSK3B; Shi and Collins, 2023). Identification of dynamically phosphorylated proteins in the YO may help to clarify the involvement and interconnection of multiple signaling pathways.

Advances in proteomics using highly sensitive tandem mass spectrometry coupled with high performance liquid chromatography dramatically increases the number of peptides that can be identified in a sample (Muneer et al., 2024). Additionally, isobaric mass tags can be used to distinguish samples from different treatments or biological replicates, which allows samples to be pooled together in a manner similar to multiplexing in DNA and RNA sequencing (Myers et al., 2019). This capability can increase peptide identification for small samples, as it enables higher peptide input. Affinity chromatography can be used offline (prior to MS/MS) or online (coupled with MS/MS) to enrich samples for post-translational modifications, including phosphorylation and glycosylation (Brandi et al., 2022).

Using the YOs from MIH ± PKG-inhibitor assays presented in Chapter 2, liquid chromatography and tandem mass spectrometry (LC-MS/MS)-based phosphoproteomics was used to examine the dynamic role of phosphorylation in the YO. Additionally, paired profiling of the global YO proteome was used to survey protein expression in the intermolt YOs of *C. maenas* and the activated YOs of *G. lateralis*. Previous proteomic analysis of the crustacean molting gland using 2-dimensional gel electrophoresis (2D-GE) and MALDI-ToF/ToF mass

spectrometry identified broad changes over the molt cycle in both *C. maenas* (Hamer, 2015) and *G. lateralis* (Head, 2017); Head et al., 2019). In both species, the identification of proteins primarily consisted of hemocyanins, actin, and tubulin, as the use of 2D-GE inherently limits protein identification to the most abundant proteins in a given sample. Cytoskeletal organization was associated with changes in the molt cycle, corresponding with the hypertrophy of the YO associated with premolt. Additionally, changes in energy metabolism and oxidative stress responses were associated with ecdysteroid production (Hamer, 2015; Head, 2017; Head et al., 2019). This chapter presents the results of high-throughput LC-MS/MS profiling of the global and phosphoproteome of YOs from *C. maenas* and *G. lateralis.*

MATERIALS AND METHODS

PKG-inhibited YO sample collection

In vitro assays quantified the effects of MIH with or without PKG inhibitors on YO ecdysteroid secretion as previously described in Chapter 2. Briefly, the competitive PKG inhibitor Rp-8-Br-PET-cGMPs (2-Bromo-3,4-dihydro-3-[3,5-*O*-[(*R*)-mercaptophosphinylidene]-β-D-ribofuranosyl]-6-phenyl-9*H*-Imidazo[1,2-*a*]purin-9-one; Cayman Chemical, Ann Arbor, MI, USA) and a PKG2-specific inhibitor, AP-C5 (4-[4-(1*H*-Imidazol-1-yl)phenyl]-*N*-2-propyn-1-yl-2-pyrimidinamine; R&D Systems Inc., Minneapolis, MN, USA), were dissolved in dimethyl sulfoxide (DMSO) and diluted 100-fold in crab saline to achieve final inhibitor concentration of 100 μM. Synthetic Gl-MIH was used as previously described (Head et al., 2025).

Paired YOs from adult male intermolt *C. maenas* or 3-day post-ESA *G. lateralis* were used. One YO from each pair served as the MIH control and the other received the experimental PKG inhibitor in addition to MIH. YOs were preincubated for 30 minutes at room temperature in 0.5 ml saline media with 1% DMSO (control treatment) or PKG inhibitor and 1% DMSO

(experimental treatment) to allow the PKG inhibitor to permeate the YO. After preincubation, YOs were transferred to 0.5 ml saline media containing either 50 nM MIH and 1% DMSO (control treatment) or 50 nM MIH, PKG inhibitor [1, 10, or 100 µM], and 1% DMSO and incubated at 100 rpm at room temperature for 4.5 hours. Media samples were combined with 3 volumes of methanol, and 20E was quantified with a competitive enzyme-linked immunosorbent assay (ELISA; Kingan, 1989) as modified by Abuhagr et al. (2014). YOs were frozen in liquid nitrogen and stored at -80ºC. Samples were shipped overnight on dry ice to California Polytechnic State University, San Luis Obispo, CA, USA and again stored at -80ºC until preparation for LC-MS/MS analysis as described below.

Protein precipitation

The workflow for LC-MS/MS sample preparation is presented in Fig. 4.1. Sample preparation from cell lysis to peptide cleanup was completed with the EasyPep 96 MS Sample Prep Kit (Thermo Scientific, Waltham, MA, USA) with modifications to increase crustacean peptide recovery. Reagents were included with the EasyPep kit unless otherwise noted. YOs were thawed on ice and transferred to 0.2 ml of lysis buffer containing 1% universal nuclease and 1% Halt™ Phosphatase Inhibitor Cocktail (100X; Thermo Scientific, Waltham, MA, USA) in 2 ml low-protein binding (LPB) tubes. Tissues were sonicated (20 Hz) three times for 5 s each with intermittent cooling on ice using a Fisherbrand Model 50 sonic dismembrator. Lysates were centrifuged at 16,000 xg for 10 minutes at 4ºC. Protein concentration of the supernatant was quantified using the Pierce BCA Protein Assay Kit. The *G. lateralis* YOs were larger than *C. maenas* YOs, resulting in higher protein yields. For *G. lateralis*, 100 µg of each sample was transferred into a 1.3-ml 96-well plate and sample volume was adjusted to 100 µl with lysis

buffer. For *C. maenas*, 30 µg of each sample was transferred into a 1.3 ml 96-well plate and sample volume was adjusted to 100 µl with lysis buffer.

Trypsin/LysC protein digestion

Fifty µl of reduction solution was added and gently mixed, followed by 50 µl of alkylation solution and gently mixed. The sample plate was sealed and incubated at 95ºC for 10 minutes. Once the samples had returned to room temperature, 7.5 µg of Trypsin/Lys-C protease was added to each sample, the plate was sealed and incubated at 75 rpm at 37ºC for 3.5 hours. Samples were then acidified by adding 50 µl of digestion stop solution and gently mixing.

Peptide cleanup and quantification

Protein digest samples (~300 µl) were transferred to the peptide clean-up plate and secured on top of a 2 ml collection plate. The sample plate was centrifuged at 250 x *g* for 10 min. Flow-through solution was re-applied to each well and the centrifugation step was repeated; the second flow-through was discarded. To each sample well, 300 µl of wash solution A was added and the plate was centrifuged at 1000 x *g* for 2 minutes and the flow-through was discarded. To each sample well, 300 µl of wash solution B was added and the plate was centrifuged at 1000 x *g* for 2 minutes, flow-through was discarded, and the wash with solution B was repeated. The peptide cleanup plate was transferred to a new 2 ml collection plate and 300 µl of elution solution was added to each sample and peptides were eluted by centrifugation at 1000 x *g* for 2 minutes.

Peptide samples were transferred to 2-ml LPB tubes and dried using a vacuum centrifuge. Dried peptide samples were reconstituted in 100 µl 0.1% formic acid (FA). To ensure peptides were completely solubilized, samples placed on an orbital rocker at room temp for 15 minutes and were briefly vortexed. Peptide concentration was determined using the Pierce Quantitative

Colorimetric Peptide Assay (Thermo Scientific, Waltham, MA, USA). Fifteen µg aliquots of each sample were dried in a vacuum centrifuge for Tandem Mass Tag (TMT) labeling and sample multiplexing.

Tandem mass tag (TMT) labeling of total peptides

Peptide aliquots (15 µg) were reconstituted in 40 µl 100 mM triethylammonium bicarbonate on an orbital rocker at room temperature for 30 minutes. The pH of each sample was verified as ~8.5 using pH paper. TMT isobaric label reagents were reconstituted to 10 µg/µl in anhydrous acetonitrile at room temperature for 10 minutes with occasional vortexing (TMT10-plex; Thermo Scientific, Waltham, MA, USA). To label each sample, 120 µg TMT label was added (final ratio of 8:1 w:w TMT to peptide) and samples were placed on an orbital rocker at room temperature for 1 hour. Labeling reactions were quenched by adding 5% hydroxylamine (0.67% final), gently mixing, and incubating at room temperature for 15 minutes. As experiments used eight to ten animals with two YOs each, two sets ('Set A' and 'Set B') of TMT-labeled peptides were created for each experiment (Fig. 4.1). Each TMT set consisted of 13 µg peptide from both YOs from four or five animals.

SMOAC phosphopeptide enrichment

Sequential enrichment using metal oxide affinity chromatography (SMOAC; Choi et al., 2018) was used to enrich phosphopeptides from 90% of each TMT set using the High-Select TiO_2 Phosphopeptide Enrichment kit and Fe-NTA Phosphopeptide Enrichment kit (Thermo Scientific, Waltham, MA, USA), according to the manufacturer's protocol. Briefly, TMT sets were rehydrated in 150 µl binding/equilibration buffer from the TiO_2 kit. TiO_2 spin tips were used to bind phosphorylated proteins from 135 µl (93.6 µg) of each TMT set, while the remaining 15 µl (10.4 µg) of each TMT set was dried using a vacuum centrifuge for

fractionation and global proteome analysis. Unbound TiO_2 flow-through and TiO_2 wash fractions were pooled for each TMT set, dried using a vacuum centrifuge, and used for Fe-NTA phosphopeptide enrichment according to the SMOAC protocol. Eluate from TiO2 and Fe-NTA phosphopeptide enrichment steps were each rehydrated in 40 µl of 0.1% FA, then pooled together for total phosphoproteome LC-MS/MS analysis (Fig. 4.1).

High pH reversed-phase off-line peptide fractionation

The dried 10.4 µg total proteome aliquot of each TMT set was reconstituted in 300 µl 0.1% trifluoroacetic acid (TFA). Peptides were loaded onto an equilibrated high-pH reversed phase spin column (Thermo Scientific, Waltham, MA, USA) and desalted by washing with water. Unreacted TMT label was removed by washing the column with 5% acetonitrile (ACN)/0.1% triethylamine (TEA). Peptides were eluted into 8 fractions with an increasing ACN gradient dissolved in 0.1% TEA (Fig. 4.1). The percentage of ACN in each fraction was increased by 2.5% beginning with 10% ACN in fraction 1 through 25% ACN in fraction 7; fraction 8 was eluted with 50% ACN. Fractions were dried by vacuum centrifuge, then resuspended in 70 µl 0.1% FA prior to LC-MS/MS analysis.

LC-MS/MS data acquisition

Sample fractions and phosphopeptide-enriched samples were separated using liquid chromatography (UltiMate 3000 HPLC, Thermo Scientific) and run on a Q Exactive™ Plus Hybrid Quadrupole Orbitrap™ Mass Spectrometer equipped with Nanospray Flex (Thermo Scientific) for nano-electrospray ionization. A 4µl-volume of each fraction and 5-µl volume of each phosphopeptide-enriched sample were used for proteomic analysis. Samples were separated by reverse-phase chromatography on a 5 mm x 300 µm C18 pre-column and then on a 25 cm x 75 µm Acclaim PepMap™ RSLC C18 column (particle size 2 µm; Thermo Scientific). Buffer A

consisted of LCMS grade water with 0.1% FA, Buffer B consisted of 99.9% LCMS grade acetonitrile with 0.1% FA, and the loading buffer consisted of 98% LCMS grade water and 2% ACN with 0.08% TFA. For fractionated samples, peptides were eluted over a 185-min gradient that began with 2% Buffer B and increased to 4% in 17 min, then increased to 25% over the next 128 min. Any remaining peptides on the column were then "flushed" with 85% Buffer B for 12 min and the column was equalized at 4% Buffer B for 15 min before the next sample was loaded. Phosphopeptide-enriched samples were eluted over a 245-min gradient beginning with 2% Buffer B for 10 min, an increase to 15% Buffer B in 170 min, a further increase to 30% Buffer B over the next 30 min, followed by a flush with 90% Buffer B for 8 min and column equalization at 2% Buffer B for 17 min.

The Q Exactive Plus was operated in 'Full MS' mode for MS scans and data-dependent acquisition (DDA) mode for MS/MS (MS^2) scans. The nanospray source was used with a spray voltage of 1.8 kV, a capillary temperature of 250ºC, and S-lens radio frequency (RF) level of 50. Full MS scans were performed with a range of 350 to 1575 m/z, a nominal resolution of 70,000, automated control gain (AGC) target at 3×10^6, and a 50 msec maximum injection time. Higher energy collisional dissociation (HCD) MS^2 scans were collected for fractionated samples with a resolution of 35,000, AGC at 1×10^5, maximum injection time of 120 msec with a loop count of 15, a 0.7 m/z isolation window, fixed first mass of 110 m/z, normalized collision energy (NCE) of 32%, and dynamic exclusion for 30 sec. The polarity mode for MS and MS^2 scans was positive, and the default charge state was 2. For phosphopeptide enriched samples, MS^2 scans were collected for a scan range between 350 to 1500 m/z, maximum injection time of 100 msec, a loop count of 10, isolation window of 1.2 m/z, fixed first mass of 110 m/z, stepped NCE of 32-34%. Only charge states from 2+ to 6+ were selected for MS^2 scans for all samples.

Functional annotation of RNAseq reference databases

All translated *C. maenas* accessions were extracted from the CrusTome AA database (Pérez-Moreno et al., 2023) and saved as a single fasta file (protein databases). The translated *G. lateralis* transcriptome assembled and described in Chapter 3 of this dissertation was used as the *G. lateralis* protein database. The protein databases were uploaded to the Galaxy web platform (The Galaxy Community, 2024) to run computationally lengthy BlastP and InterProScan searches for the entirety of the transcriptomes. For each species, the protein databases were searched against the UniProtKB Brachyuran database (Taxonomy ID 6752; 148,143 protein sequences downloaded on 30 Oct. 2024) using BlastP. Expectation value (e-value) cutoff was set to 1e-12 and minimum query coverage was 20%. Each protein database was also used to identify conserved domains, motifs, and GO terms using InterProScan. A custom code was written to create an annotation file concatenating the BlastP and InterProScan results with the contig IDs from the *G. lateralis* and *C. maenas* protein databases. The Gene_Annotation.py code was uploaded to GitHub at https://github.com/crabomics/Annotation.

Peptide and protein identification and quantification

Raw data files collected from the Q Exactive Plus were processed using Proteome Discoverer™ (PD; version 3.1.0.638; Thermo Scientific). Raw files from all fractions and the phospho-enriched samples for both PKG inhibition experiments for a given species were processed in the same workflow within PD. A custom workflow was designed for the identification of phosphorylation across samples, the details of each node used are available (Appendix Table B1). Briefly, CHIMERYS, Sequest HT, and Comet search nodes included the species-specific annotated protein database and a UniProt Brachyura protein database (taxon ID 6752; 148,147sequences; downloaded 2024/10/30). TMT6plex labeling (+229.163 Da) of all

peptide N-termini and lysine (K) residues, and carbamidomethyl (+57.021 Da) of all cysteine (C) residues were set as static modifications. Phosphorylation (+79.966 Da) of serine (S), threonine (T), and tyrosine (Y), and oxidation (+15.995 Da) of all methionine (M) residues, were set as variable modifications. Each peptide could have a maximum of three equal modifications. The PTM-specific search node IMP-ptmRS was used to in Phospho-RS mode. Only phosphosites with a confidence score ≥ 0.75 were used. A protein database from *Homo sapiens* (UniProt taxon ID 9606) was used to remove contaminants, and reversed protein databases were used as decoy databases to reduce false positive identifications.

A strict false discovery rate (FDR) of 0.01 and a relaxed FDR of 0.05 was used to identify peptides and proteins with high-confidence and medium confidence, respectively. Protein grouping used strict parsimony, and a minimum of 1 peptide per protein was used for protein identification (Gupta and Pevzner, 2009). Quantification of reporter ion intensity from MS2 scans used isobaric mass correction factors for TMT6plex labels based on specifications from Lot# YE367339. Quantification included both unique and razor peptides, which are peptides that are shared between proteins, such as isoforms, that are also identified by unique peptides. Normalization used the total peptide amount and included TMT6plex and phosphorylation modifications. Protein groups are collections of proteins that include a shared set of peptides.

Data processing and statistical analysis

Differential expression (DE) of proteins and peptides identified in PD were processed and analyzed using Differential Enrichment Analysis of Proteomics data 2 (DEP2) in R (Feng et al., 2023). Analysis of the global proteome was completed by removing quantification data of the phospho-enriched sample. Peptides from the global proteomic dataset with more than 4 missing

intensity values in a least one condition were removed. Missing values were then imputed with the MinProb function to assign values based on a random draw of the left-centered Gaussian distribution based on the minimum observed intensity for a given peptide (Harris et al., 2023). After imputation, the data was normalized using variance stabilized normalization (vsn) to correct for batch effects and variance stabilization (Välikangas et al., 2018). Tukey's median polish was used to aggregate unique and razor peptides based on an overall median to correct for sample and batch effects (Tukey, 1977). After peptide aggregation, a moderated t-test was used to assess DE between the global proteome of control and PKG-inhibited samples. Within DEP2, the moderated t-test uses the *limma* R-package (Ritchie et al., 2015). The Benjamini-Hochberg (BH) procedure was used to correct FDR of protein-level differential expression (Haynes, 2013). Protein-level DE was assessed based on an adjusted p-value of 0.05 and log2-fold change (logFC) of one.

Peptides identified from the phospho-enriched fractions were then assessed with protein-level normalization of the global proteome to account for any background changes in protein or peptide level. Peptides with 5 or more missing intensity values in at least one condition were removed. This setting was slightly more liberal than that used for the global peptide due to the low overall abundance of phosphopeptides detected across all samples between the two different phospho-enriched runs for each experiment. After filtering, missing values were imputed with the MinProb function as described above. Phosphopeptide intensities were then normalized by protein-level quantification used in the global proteome. FDR was controlled with Strimmer's *t*-score (Strimmer, 2008). Phosphopeptide intensity was aggregated to the protein level using Tukey's median polish, and phosphoprotein DE was assessed with an adjusted p-value of 0.05 and a logFC of 0.5.

Characterization of identified proteins and peptides

Differentially expressed phosphoproteins were characterized using BLAST homology with the NCBI RefSeq (O'Leary et al., 2016) and UniProtKB (The UniProt Consortium, 2023) databases. NCBI's conserved domain search (Wang et al., 2023) and InterProScan (Paysan-Lafosse et al., 2023) were used to identify functional sites and domains. KEGG mapping of all identified proteins in both species was used to identify pathways that have nearly complete expression (Kanehisa and Sato, 2020).

RESULTS

Global protein and peptide abundance in MIH ± PKG inhibited YOs

For simplicity, the experiments in which YOs were incubated with MIH ± AP-C5 will be referred to as *Cm*-AP-C5 and *Gl*-AP-C5 for *C. maenas* and *G. lateralis* respectively. Experiments in which YOs were incubated with MIH ± Rp-8-Br-PET-cGMP will be referred to as *Cm*-Rp8 and *Gl*-Rp8.

A total of 1,788 global proteins were identified in *Cm*-AP-C5 YOs, and a total of 2175 global proteins were identified in *Cm*-Rp8 YOs. Of these, 1,606 proteins were identified in the global proteome of YOs from both treatments, 175 proteins were identified only in the global proteome of the *Cm*-AP-C5 experiment, and 541 were identified only in the global proteome of the *Cm*-Rp8 experiment (Fig. 4.2).

A total of 2,505 global proteins were identified in *Gl*-AP-C5 YOs, and a total of 864 proteins were identified in *Gl*-Rp8 YOs. Of these, 816 proteins were identified in the YOs from both experiments, 1,653 proteins were identified only in the global proteome of the *Gl*-AP-C5 experiment, and 47 were identified only in the global proteome of *Gl*-Rp8 (Fig. 4.3).

Among the global proteomes for both species, no proteins were differentially expressed (Fig. 4.4). In both the *Gl*-Rp8 and *Cm*-AP-C5 global proteomes there is one gene that initially appeared to be differentially expressed. However, after FDR correction using the BH procedure, the change was no longer significant. Strong batch effects were observed between TMT sets. Principle component 1 (PC1) explains between 45.3% and 69.6% of the variability seen in each experiment and is primarily due to the batch effects between Set A and Set B for each experiment (Fig. 4.5).

Differential phosphorylation between MIH ± PKG-inhibitor YOs

In phosphopeptide-enriched samples, 300 unique phosphopeptides belonging to 247 proteins were identified in *Cm*-AP-C5 YOs. A total of 130 unique phosphopeptides belonging to 121 different proteins were identified in *Cm-Rp8* YOs. Between the phosphopeptide samples, 113 identified proteins were found in both groups (Fig. 4.2). In *Cm*-AP-C5 YOs, nine phosphopeptides were differentially expressed (Fig. 4.6). Of these, five were upregulated in the control (MIH alone) samples relative to MIH plus AP-C5. In *Cm*-Rp8 YOs, seven phosphopeptides were differentially expressed. Of these, four were upregulated in the MIH control relative to MIH plus Rp-8-Br-PET-cGMP (Fig. 4.6).

In phosphopeptide-enriched samples, 103 unique phosphopeptides belonging to 92 different proteins were identified in *Gl*-AP-C5 YOs (Fig. 4.3). Of these, three phosphopeptides were differentially expressed. Two phosphopeptides were upregulated in the MIH control and one phosphopeptide was upregulated in the MIH plus AP-C5 treatment (Fig. 4.6). A total of eight unique phosphopeptides belonging to eight different proteins were identified in *Gl*-Rp8 YOs. Between the phosphopeptide samples, five identified proteins were found in both groups

(Fig. 4.3). Due to the low number of enriched phosphopeptides detected in the *Gl*-Rp8 samples, statistical analysis was not possible.

Proteins containing the differentially expressed phosphopeptides, as well as phosphopeptides that had a significant adjusted p-values but not logFC ($-0.5 \leq \text{logFC} \geq 0.5$), were characterized. The proteins primarily have functions in cell signaling pathways, cytoskeleton, and transcription (Table 4.1). Several proteins were identified that regulate cell signaling pathways through cytoskeletal organization and structure. Additionally, five proteins were identified that interact with mTOR signaling pathways. In *C. maenas,* five proteins were unable to be confidently identified. Where possible, the functional domains identified by CDD, IPR, pfam, and Panther were included. In *Gl*-Rp8 YOs, four of the eight proteins were confidently identified (Table 4.1). The other four proteins were uncharacterized and did not contain functional domains that were identified by any functional domain databases; these proteins were excluded from the table.

Characterization of the YO proteome

Components of the mTOR pathway were expressed in both the *G. lateralis* and *C. maenas* YOs (Fig. 4.7). Major components of both mTORC1 and mTORC2 were expressed, including mTOR and mammalian lethal with SEC13 protein 8 (mLST8). Additionally, Raptor, unique to the mTORC1 complex, was identified in *C. maenas*. Upstream of mTOR, amino acid-sensing, MAPK, PI3K-Akt, and AMPK pathways were well represented (Fig. 4.7). Rheb, the direct regulator of mTORC1, was identified in the YO global proteome of both *C. maenas* and *G. lateralis*. Downstream of mTOR, pathways involved in protein synthesis and cytoskeletal organization were identified. Phosphopeptides from mitogen-activated protein kinase kinase 1 (MAP2K1; MEK in KEGG) were identified in both *Gl*-AP-C5 and *Cm*-AP-C5 YOs. MAP2K1

was significantly upregulated in *C. maenas* MIH plus AP-C5 YOs relative to the MIH control, although the logFC did not exceed the 0.5 threshold (Table 4.1, Fig. 4.6). MAP2K1was not differentially expressed in phosphopeptides from *Gl*-AP-C5. Phosphopeptides from Rapidly Accelerated Fibrosarcoma (RAF) were identified in *Cm*-AP-C5 and *Cm*-Rp8, although they were not differentially expressed. Glycogen synthase kinase 3β (GSK3B) was identified in the phosphoproteome of *Cm*-AP-C5 and was not differentially expressed between treatments. Eukaryotic translation initiation factor 4B (eIF4B) was identified in the phosphoproteomes of *Cm*-AP-C5 and *Cm*-Rp8, and was not differentially expressed between either set of treatments. Eukaryotic initiation factor 4E-binding protein (4E-BP) and ribosomal protein S6 kinase (S6K) were not identified by KEGG mapping, but were identified manually using BLAST homology with blue crab *Callinectes sapidus* and mud crab *Scylla olivacea*.

The phosphoinositide 3-kinase (PI3K) - AKT pathway is also well represented and an upstream regulator of mTOR signaling. Phosphopeptides for MAP2K1, GSK3B, and eIF4B identified in the mTOR pathway are also components of PI3K-AKT signaling (Figs. 4.7, 4.8). AKT was identified in the YO global proteome of both *C. maenas* and *G. lateralis* (Fig. 4.8). GSK3B is a substrate of AKT and identified in the phosphoproteome of *Cm*-AP-C5 as previously mentioned. Glycogen synthase is a substrate of GSK3B and was identified in the phosphoproteome of *Gl*-AP-C5, although it was not differentially expressed. A phosphopeptide for heat shock protein 90 (Hsp90) was identified in *Cm*-AP-C5, *Cm*-Rp8, and *Gl*-AP-C5 and was not differentially expressed.

Proteins related to cytoskeletal organization were highly represented in the global and phosphoproteome in both the *G. lateralis* and *C. maenas* YOs (Fig. 4.9). Phosphopeptides associated with the regulation of the actin cytoskeleton were differentially expressed in *Gl*-AP-

C5, *Cm*-AP-C5, and *Cm*-Rp8 (Table 4.1; Fig. 4.6). A phosphopeptide arising from protein-enabled like (Enah; in KEGG called Mena) was significantly upregulated in *G. lateralis* YOs treated with MIH plus AP-C5 compared to the paired MIH control. Enah phosphopeptides were identified in YOs from *C. maenas*, although they were not differentially expressed in either experiment. Phosphopeptides from plexin A3 (plxna3; PXN in KEGG) were identified in *Cm*-AP-C5 and *Cm*-Rp8, and were significantly upregulated in the MIH control relative to MIH plus Rp8-Br-PET-cGMP (Table 4.1; Fig. 4.9).

Proteins and phosphopeptides involved controlling gene expression via transcriptional and translational regulation were also well represented in the YOs of both species (Table 4.1; Figs. 4.10, 4.11). Components of the mRNA surveillance pathway were identified in global proteomes of both species, including cap-binding proteins, exon-junction complex, spliceosome, nuclear export, nonsense-mediated decay, and no-go decay (Figs. 4.10, 4.11). Acinus (Acn, ACIN1 in KEGG), signal recognition (SR), and THO complex (THOC) were identified through phosphopeptides in *Cm*-AP-C5 and *Cm*-Rp8. An Acn phosphopeptide was upregulated in the MIH control relative to MIH plus Rp8-Br-PET-cGMP in *C. maenas* (Table 4.1).

mRNA processing is a complex pathway and not all details are shown in Figs. 4.10 and 4.11. Components involving additionally identified phosphopeptides are indicated with red stars in Fig. 4.11. Although not shown in Fig. 4.11, THOC is a nuclear component of the transcription-export complex. Not shown in Fig. 4.11, the pre-mRNA processing factor 39 (PRPF39) is part of the spliceosome involved in 5'-splice site recognition. Phosphorylation of PRPF39 is upregulated in MIH control YOs relative to MIH plus AP-C5 in *G. lateralis* (Table 4.1). Also in the spliceosome, phosphorylation of Bud13 homolog (BUD13) was significantly increased in YOs from the MIH control relative to MIH plus AP-C5 in *C. maenas* (Table 4.1).

Phosphorylation of polypyrimidine-tract binding protein 1 (PTBP1), involved in multiple aspects of mRNA maturation, was upregulated in MIH plus AP-C5 YOs relative to the MIH control in *C. maenas* (Table 4.1). LARK is an RNA-binding protein involved in post-transcriptional regulation of gene expression and organization of actin. A LARK phosphopeptide was identified in *Gl*-Rp8 YOs (Table 4.1). Additionally, poly(A)-specific ribonucleases PAN3 and PARN, as well as 5'-3' exoribonuclease 2 (XRN2) are part of the RNA degradation pathways and were phosphorylated in *Cm*-AP-C5 YOs, although they were not differentially expressed between treatments.

MIH signaling genes in the YO proteome

Components of the putative MIH signaling pathway were well represented in YOs from both species (Fig. 4.12). Alpha and gamma subunits of guanine nucleotide-binding proteins (G proteins) were identified in both species. As previously mentioned, mTORC1 components including mLST8, mTOR, and Raptor, as well as upstream mTORC1 activator Rheb and downstream proteins S6K and 4E-BP were identified. Calmodulin (CaM) and calcineurin (CaN) were identified in both species, although nitric oxide synthase (NOS) and soluble guanylyl cyclase (GC-I) were not identified.

In both *C. maenas* and *G. lateralis* YOs, peptides unique to the N-terminus of PKG were able to distinguish PKG1α1 and PKG1α2 isoforms. Members of other pathways that converge on mTOR and are postulated to regulate ecdysteroid synthesis in the YO were also represented, including phosphoinositide-dependent kinase (PDK), protein kinase C (PKC), and AKT. Although PI3K was not identified, other phosphoinositide kinases were, including PI4K and PI5K. Finally, a leucine-rich repeat GPCR, Lgr4, was identified in *G. lateralis* YOs. In both *C. maenas* and *G. lateralis* YOs, ecdysteroid synthetic enzymes that convert cholesterol to ecdysone

were identified (Fig. 4.13). Additionally, enzymes in the juvenile hormone biosynthetic pathway were identified in both *C. maenas* and *G. lateralis* YOs.

DISCUSSION

The number of proteins detected in the decapod YO using LC-MS/MS was 5.5-fold greater than the number detected from a previous analysis using 2D-gel electrophoresis and MALDI-ToF/ToF, which detected 457 total proteins (Head et al., 2019). The identification of these detected proteins increased by 11-fold relative to the manual identification of 191 proteins using BLAST homology alone (Head et al., 2019). Detection of 541 phosphopeptides belonging to 468 unique proteins between the *C. maenas* and *G. lateralis* YOs provides a significant look into the mechanisms that regulate ecdysteroid synthesis in decapods.

Assessment of the data analysis pipeline

It should be noted here that while the results identified within this chapter are important, batch effects between TMT sets in each experiment may mask differential expression between treatments, particularly for phosphopeptides, which had lower identification among biological replicates. Batch effects can be corrected with multiple rounds of normalization. First, mean-normalizing the intensity of global peptides in each TMT set to correct for differences in sample loading. Next, trimmed mean of M values (TMM) can be used to correct for compositional bias due to differences in intensity between fractions, as fractions at the low and high end of the range tend to contain fewer peptides and skew intensity. Finally, a pseudo-internal reference channel can be used to normalize the intensity of individual proteins identified between TMT sets. Phosphopeptide-enriched samples should first be normalized for sample loading, then normalization factors used for global peptides from the respective TMT set applied to the phosphopeptides to correct for differences between TMT sets. Applying the global normalization

factor to the phosphopeptide data also accounts for changes in global protein intensity that may explain observed differences in phosphopeptide intensity for individual proteins.

While numerous programs have been developed to analyze large proteomic datasets (Huang et al., 2020; Feng et al., 2023; Kohler et al., 2023; Kohler et al., 2024; Muneer et al., 2024) and phosphoproteomic datasets (Storey et al., 2020; Hong et al., 2022; Feng et al., 2023; Kohler et al., 2023; Schraink et al., 2023; Tong et al., 2024), there is not a single workflow for analyzing experiments that incorporates all aspects necessary for proper normalization of the data. A custom workflow can be pieced together from individual components of these programs. However, each program is only compatible with input from certain platforms. For example, TMT analyst only uses data in the format given by Proteome Discoverer. However, the PTM workflow of the same software, PhosphoAnalyst, only accepts data from MaxQuant (Zhang et al., 2023). MSstats can convert input data from a range of programs, but can only incorporate a single global normalization step. PhosphoDisco promises the ability to customize normalization steps, however the program has not been maintained and now requires step-by-step reformatting to use updated Python and R programs (Schraink et al., 2023). Output from Proteome Discoverer can be easily reformatted to be used by DEP2, and DEP2 allows for normalization of phosphopeptides relative to the global proteome (Feng et al., 2023). However, several issues with DEP2 still persist. First, DEP2 can only incorporate a single global normalization, leaving batch effects uncorrected as seen here. Second, although DEP2 applies global normalization at the phosphopeptide level, quantification of phosphopeptides is still aggregated to the protein level. Further, to take advantage of phosphosite-specific identification within phosphopeptides, an output exclusive to MaxQuant is required.

Phosphoproteome of the decapod molting gland

As expected, differential expression of proteins was not observed at the global level. At the 4.5-hour timescale, differences in ecdysteroid output seen between MIH ± PKG-inhibition are expected to result from altered activity of proteins that are already present, rather than the result of changes in translation. Prolonged activation of the YO and entry into early premolt is the effect of prolonged activation of mTORC1 activation that results in an increase in translation of ecdysteroid biosynthetic enzymes (Mykles and Chang, 2020; Mykles, 2021; Benrabaa et al., 2023; Mykles, 2024).

The biological functions of phosphoproteins that are differentially expressed in the YO paints a picture of ecdysteroid regulation through cytoskeletal organization, as well as signaling pathways that ultimately control gene expression and RNA processing. Previous proteomic analysis of the *G. lateralis* YO over the course of the molt cycle was characterized by large changes in cytoskeletal organization associated with activation of the YO and increased ecdysteroid synthesis (Head et al., 2019). Changes in protein synthesis and reactive oxygen species (ROS) was associated with increased ecdysteroidogenesis and supported by an increase in metabolic pathway proteins, as well as reactive oxygen species (ROS) scavengers (Head et al.,2019). While the previous provided insight into broad metabolic and homeostatic activities, cell signaling proteins were not identified. High throughput analysis using LC-MS/MS has yielded a large dataset that includes a web of signaling pathways within the YO. Many of the identified pathways are interconnected and complex. The following discussion will focus on broad functions and interpretations of their potential roles in regulating YO ecdysteroidogenesis.

Interactions between cytoskeletal organization and cell signaling

Slit-Robo signaling involves a complex of proteins that is typically associated with regulating axon guidance and directional cell growth (Guzmán-Palma et al., 2021; Bhosle et al., 2023; Li et al., 2023). Slit is a secreted ligand and Robo is a transmembrane protein receptor that, when bound to Slit, activates a signaling cascade that revolves around actin polymerization (Guzmán-Palma et al., 2021). Slit-Robo binding activates two proteins identified through phosphopeptides in the YOs, slit-robo Rho-GTPase activating protein (srGAP) and enabled protein (Enah; Lee et al., 2004; Bhosle et al., 2023; Li et al., 2023).

srGAP activation occurs through the binding of srGAP to the CC3 domain on the intracellular tail of the Slit-Robo complex (Li et al., 2023; Bhosle et al., 2023). srGAP then negatively regulates actin polymerization by activating the GTPase activity of various GTPases including cell division control protein 42 (Cdc42) and Ras-related C3 botulinum toxin substrate 1 (Rac1; Bhosle et al., 2023). srGAP activation induces cell polarity and repulsion from the slit ligand by activating actin depolymerization near the Slit-Robo complex (Li et al., 2023). In mammalian cell cultures, phosphorylation of srGAP2 at Ser206 is associated with increased srGAP activity and polarization of the cells (Li et al., 2023). Cdc42 is an activator of mTORC1 by both directly binding to mTOR, as well as by maintaining AKT activity (Teran Pumar et al., 2024). Slit-Robo binding is also implicated in mTORC1 inhibition by acute binding of Slit2 and downstream inactivation of Rac1 by srGAP, as well as through constitutive expression of Slit and Robo (Bhosle et al., 2023). srGAP2 deactivation of mTORC1 was also associated with increased autophagy (Bhosle et al., 2023).

In *C. maenas* YOs, the srGAP phosphopeptide was upregulated in cells treated with MIH relative to those treated with MIH plus Rp-8-Br-PET-cGMP (Table 4.1, Fig. 4.6). Phosphorylation of srGAP has been attributed to PKCα (Bhosle et al., 2023), and implication of

PKGs in this pathway has not been reported. These results may indicate that Slit-Robo signaling may be implicated in MIH inhibition by PKG1 phosphorylation of srGAP and subsequent inhibition of mTORC1.

In addition to activating srGAP, the Slit-Robo complex also induces binding of enabled homolog (Enah; Döppler and Storz, 2013; Benz et al., 2023). Enah is a homolog of mammalian-enabled (Mena), which belongs to the Ena/VASP (vasodilator-stimulated phospho-protein) family (Loureiro et al., 2002; Benz et al., 2023). Ena/VASP proteins act as links between cellular signaling pathways involving Rho GTPases and actin polymerization (Loureiro et al., 2002; Döppler and Storz, 2013). In mammalian cells, Mena and VASP are well characterized substrates of PKG, and their phosphorylation induces relaxation in vascular smooth muscle cells, and is also integral in platelets and endothelial cells (Butt et al., 1994; Loureiro et al., 2002; Döppler and Storz, 2013; Benz et al., 2023). Interestingly, serine and tyrosine phosphosites on Enah in *Drosophila* have been identified, but *Drosophila* Enah lacks a highly conserved motif for PKG and PKA phosphorylation that is found in vertebrates (Ahern-Djamali et al., 1998; Loureiro et al., 2002).

In *G. lateralis,* an Enah phosphopeptide was upregulated in MIH plus AP-C5 treated YOs relative to the MIH control. Although the PKG phosphosite characterized in vertebrates is lacking in invertebrates, phosphorylation of Enah still regulates its activity (Ahern-Djamali et al., 1998; Loureiro et al., 2002). Together with the phosphorylation of srGAP in *C. maenas*, Slit-Robo is implicated in YO ecdysteroid regulation, although the effects of the identified phosphosites remains to be determined.

In addition to the regulation of the actin cytoskeleton, microtubules are also implicated in YO ecdysteroidogenesis. Futsch in arthropods is homolgous to microtubule associated protein

1B (MAP1B). Interestingly, phosphorylation of Futsch was upregulated in the *C. maenas* YO treated with MIH plus AP-C5 relative to the MIH control, and the opposite pattern was identified in *G. lateralis* although the fold-change was not significant (Fig. 4.6; Table 4.1). Futsch in *Drosophila* is associated with neuronal growth (Da Cruz et al., 2005; Shi et al., 2019). Phosphorylation of Futsch in *Drosophila* occurs at a residue conserved with vertebrate MAP1B, and is the substrate of GSK3B (Gögel et al., 2006). In its unphosphorylated state MAP1B stabilizes microtubules, but phosphorylation by GSK3B switches its role and leads to increased depolymerization of microtubules (Halpain and Dehmelt, 2006).

GSK3B has been characterized as a substrate of PKG (Zhao et al., 2005; Sanyal et al., 2013). In human neuroblastoma cells, phosphorylation of GSK3B by both PKG1α and PKG2 is induced by insulin or by cGMP analogs that activate PKGs (Sanyal et al., 2013). While both PKG isoforms independently phosphorylated GSK3B, only PKG1α phosphorylation was associated with reduced accumulation of amyloid-β plaques as a result of GSK3B inhibition (Sanyal et al., 2013). In mouse and rat cardiomyocytes, cardioprotective effects were induced by activation of overexpressed PKG1α, which increased phosphorylation of both GSK3B and extracellular signal-regulated kinase (ERK; Das et al., 2008; Hoffmeister et al., 2020). GSK3B is highly regulated by phosphorylation, and phosphorylation at Ser9 in human GSK3B is inhibitory (Shi and Collins, 2023). PI3K/AKT, cAMP/PKA, and MAPK/ERK signaling pathways have also been implicated in GSK3B inhibition, indicating that GSK3B regulation of mTORC1 can be modulated by growth factors that stimulate PI3K/AKT and MAPK/ERK pathways, or GPCR stimulation that induces changes in intracellular cyclic nucleotides (Das et al., 2008; Hoffmeister et al., 2020; Shi and Collins, 2023). GSK3B negatively regulates mTORC1 activation by

phosphorylating TSC2 at Thr1329, Ser1333, Ser1336, and Ser1341, activating TSC (Inoki et al., 2006).

Intriguingly, phosphopeptides from GSK3B, Ras, and MAP2K1 (aka MEK) were identified in the *C. maenas* YO (Figs. 4.7, 4.8). Phosphorylation of GSK3B specifically was identified in the *Cm*-AP-C5 experiment, and nine phosphopeptides corresponding to unique phosphosites were identified. However, quantification at the protein level did not indicate differential expression. MAP2K1, the kinase of ERK, was phosphorylated in both *Cm*-AP-C5 and *Cm*-Rp-8 experiments. MAP2K1 was not differentially expressed in *Cm*-Rp8, and was upregulated in *C. maenas* MIH plus AP-C5 YOs relative to the MIH control, although the FC was not significant (Table 4.1). Together, these data indicate a complex web of signaling pathways that are mediated by phosphorylation in the decapod YO. Re-analysis of this phosphoproteomic data with proper normalization may help to clarify some of these relationships.

Interactions between FKBP5 and Hsp90

Hsp90 is a molecular chaperone that aids in the proper folding and maturation of roughly 10% of the eukaryotic proteome (Zhao et al., 2005). Among heat shock proteins, Hsp90's substrates are enriched in signaling proteins and, in particular, steroid hormone receptors ß (SHRs; Daneri-Becerra et al., 2019; Noddings et al., 2023). FKBP5 and FKBP4 (aka FKBP51 and FKBP52, respectively) are members of the FK506 binding protein family that also includes the mTORC1 inhibitor FKBP12 (Daneri-Becerra et al., 2019). Both FKBP5 and FKBP4 have co-chaperone activity with Hsp90, although their activities are antagonistic (Daneri-Becerra et al., 2019; Noddings et al., 2023). In human cells, a chaperone complex consisting of FKBP5/Hsp90 or FKBP4/Hsp90 interact with the glucocorticoid receptor (GR) in an antagonistic manner.

FKBP5/Hsp90 reduces affinity of GR for its ligand, inhibiting translocation of the GR to the nucleus, where it induces transcriptional activity. On the other hand, FKBP4/Hsp90/GR potentiates both the affinity for ligand binding and nuclear translocation of the complex by recruiting dynein/dynactin motors (Daneri-Becerra et al., 2019; Noddings et al., 2023). Translocation of the steroid receptor to the nucleus is dependent upon microtubule stability, implicating crosstalk between FKBP/Hsp90/SHRs and the previously describe cytoskeletal pathways.

FKBP5/Hsp90 also forms a complex with the PH domain and leucine rich repeat protein phosphatase (PHLPP), recruiting the phosphatase to AKT where it is subsequently dephosphorylated and inactivated (Wang, 2011; Daneri-Becerra et al., 2019). Inhibition of AKT prevents it from inhibiting TSC1/2, resulting in activation of Rheb GTPase activity and mTORC1 inactivation (Shi and Collins, 2023). Phosphorylation of FKBP5 has been identified in a stimulus-dependent manner, and phosphorylation at different residues may either enhance or inhibit its activity, although specific phosphosites are yet to be characterized (Daneri-Becerra et al., 2019). Phosphorylation of numerous residues on Hsp90 have been identified, including a serine residue that can be phosphorylated by both PKA and PKG (Backe et al., 2020).

Phosphorylated Hsp90 was identified in YOs of *Cm*-Ap-C5, *Cm*-Rp8, and *Gl*-AP-C5, although the phosphorylated protein isoform was not differentially expressed (Figs. 4.6, 4.8). Phosphorylation of FKBP5 was upregulated in *C. maenas* YOs from the MIH control relative to MIH plus AP-C5 (Table 4.1). Additionally, the phosphorylation of the ecdysteroid receptor EcR-3 was identified in *C. maenas* YOs treated with MIH plus AP-C5, potentially indicative of ecdysteroid-mediated feedback within the YO. Given these results, further characterization of the specific phosphosites identified in Hsp90 and FKBP5 may reveal an interesting and unexpected

path for PKG-mediated inhibition of mTORC1. Given the opposing roles of PKG1 and PKG2, and the ability of FKBP5 to be phosphorylated at multiple sites, resulting in either inhibition or activation, FKBP5 as a substrate for both PKG1 and PKG2 is a reasonable hypothesis. Phosphorylation of FKBP5 by PKG1 may enhance translocation of FKBP5/Hsp90/PHLPP to AKT, which would result in downstream inhibition of mTOR. Conversely, phosphorylation of FKBP5 by PKG2 could presumably attenuate its antagonistic role, maintaining phosphorylation and activation of AKT and mTORC1. These interactions could be further regulated by cytoskeletal stability and signaling elements including MAP1B, srGAP, GSK3B, and Enah.

N-myc downstream regulated gene 3

Another interesting player identified through phosphoproteomic analysis of the decapod YO is N-myc downstream regulated gene 3 (NDRG3). The NDRG protein family consists of NDRGs 1 through 4, all of which are implicated carcinogenesis although whether they act as tumor suppressors or oncogenes is dependent on the tissue, NDRG protein, and environmental conditions involved (Melotte et al., 2010; Yang et al., 2013; Lee et al., 2016; Lee et al., 2018). Of the NDRGs, NDRG3 is the least well characterized. It is implicated as a tumor suppressor and a tumor promoter under hypoxic conditions through regulating expression of hypoxia-inducible factor 1α (HIF1α; Yang et al., 2013; Lee et al., 2016; Lee et al., 2018). In the nervous system, NDRG3 is localized to the nucleus (Schonkeren et al., 2019). Subcellular localization of NDRG3 in other cell types has not been reported. PKG1α has been reported to localize to the nucleus upon binding to cGMP and proteolysis into a constitutively active kinase domain called PKG1γ (Chen and Roberts, 2014). While there is no evidence to link PKG1γ with NDRG3, there is also no evidence against their interaction as their cellular level functions remain relatively unexplored.

As previously mentioned, the ability to analyze phosphoproteomic data leaves much to be desired. A manual investigation of NDRG3 revealed two hypothetical phosphosites linked to PKG1 and PKG2 (Fig. 4.13). The *C. maenas* NDRG3 protein sequence was identified by four unique peptides (Fig. 4.13A). Of these peptides, phosphorylation was detected on two neighboring serine residues within one peptide. The *C. maenas* protein sequence was uploaded to the Group-based Prediction System (GPS6.0; Chen et al., 2023) for prediction of phosphorylation sites for PKG1 and PKG2. Three predicted phosphorylation sites were identified, two associated with PKG1 and one associated with PKG2 (Fig. 4.13B). The predicted phosphosites correspond to the phosphosites identified in the *Cm*-AP-C5 phosphoprotein. Specifically, PKG1 was predicted to phosphorylate both serine residues (S473 and S474), while PKG2 was only predicted to phosphorylate S473. The identification of phosphorylation on S473 was of lower confidence than S474. Looking at the expression data for this phosphoprotein, it was upregulated in MIH control YOs relative to MIH plus AP-C5 ($p_{adj} = 0.005$; Fig. 4.6, Table 4.1). Taken together, PKG2 phosphorylation of NDRG3 at S473 may have been inhibited by AP-C5, while PKG1 phosphorylation of S473 and S474 may have occurred in both treatments.

CONCLUSIONS

Signaling pathways that regulate ecdysteroid synthesis in the decapod molting gland are intricate and likely the result of integrating information from multiple stimuli, environmental and biological in nature, to precisely control the process of molting. Importantly, the putative MIH signaling pathway was near completely represented in the YO proteomes. The identification of both PKG1α1 and PKG1α2 protein isoforms is consistent with findings in Chapters 2 and 3, which indicate that PKG1α2 is the primary isoform expressed in the YO, followed by PKG1α1. Further, PKG2 was not identified in the YO proteome for either species, which is also consistent

with the dramatic difference in transcript expression presented in Chapters 1 and 2. The lack of identification of PKG2 in the YO proteome is not an assertion that the protein is not present, but rather it is likely lowly expressed and the resulting peptide spectra may have been masked by peptides from more abundant proteins. Additionally, these data are consistent with the opposing roles of PKG1 and PKG2 in regulating ecdysteroidogenesis (Head et al., 2025). That is, both PKG1 and PKG2 are activated by MIH, and PKG1 plays the predominate role of inhibiting ecdysteroid synthesis, while PKG2 stimulates ecdysteroid synthesis at low levels to maintain basal secretion in the intermolt YO.

In addition to the identification of MIH pathway genes, the identification of ecdysteroid biosynthesis genes in both species provides confidence in the quality of the dataset and peptide and protein identification. Searching for the presence of ecdysteroid synthetic genes led to the exciting discover that the juvenile hormone biosynthetic pathway was also well represented in the molting gland proteome of both *C. maenas* and *G. lateralis*. This biosynthetic pathway produces methyl farnesoate (MF) in the mandibular organ of decapods, which regulates development, reproduction, and molting (Borst et al., 2015).

Re-analysis of this data using methods to correct for batch effects, quantify phosphorylation at the peptide level, and identify consensus motifs of phosphosites will strengthen the conclusions that can be drawn. Additionally, other factors should be considered when interpreting phosphoproteomic data on a broad scale. For example, PKA, PKG, and PKC all share some overlap in substrates. However, compartmentalization of proteins through association with G-kinase anchoring proteins (GKAPs), scaffolding proteins (Hsp90), co-chaperones (FKBP5), proteolysis (PKG1γ), and numerous other PTMS or associated protein complexes determine what protein-protein interactions can occur at any given time. The

importance of cytoskeletal organization and stability in YO signaling pathways is apparent, and these insights provide new interpretations of the role of the cytoskeleton beyond mechanisms for cell hypertrophy and vesicular trafficking associated with premolt (Head et al., 2019). A further examination of components that mediate subcellular localization including cytoskeletal elements, proteolytic factors, and binding and anchoring proteins will also provide new insights into regulatory mechanisms in the YO.

Phosphopeptide identification in YOs in response to MIH and PKG inhibition has identified an abundance of potential substrates of both PKG1 and PKG2. Further characterization of these phosphosites and future experiments to identify direct interactions between the kinase and substrate(s) are necessary to fully interpret the results of this dataset. Importantly, the lack of identification of TSC2 in this dataset does not rule it out as a substrate of PKG in the YO. *In silico* digestion of the TSC2 protein suggests that TSC2 peptides, particularly those associated with presumed phosphosites, would be hard to detect using LC-MS/MS as they are long (48-61 amino acids), large (~4950 – 5730 kDa), and phosphorylation would result in two to four missed cleavages, as phosphorylated residues near cleavage sites can block trypsin digestion (Bubis et al., 2020). In fact, phosphorylation by PKG resulted in more missed cleavages than phosphorylation by PKA in a phosphoproteomic analysis of rat uteri (Huang et al., 2007). While direct phosphorylation of TSC2 by PKG remains a plausible hypothesis, several other potential substrates were identified in the YO phosphoproteomes. Namely, the MAPK signaling pathway as well as GSK3B are characterized regulators of mTORC1 (Shi and Collins, 2023). Identification of GSK3B phosphorylation in *C. maenas* as well as phospho-MAP2K1 in both *C. maenas* and *G. lateralis* make both proteins candidates for future characterization as potential

PKG substrates in the YO. Additionally, FKBP5 warrants further examination as a potential substrate given its identified interactions with Hsp90, AKT, and cytosolic steroid receptors.

Table 4.1. Differentially expressed phosphopeptides in *C. maenas* and *G. lateralis* YOs. The condition column identifies the condition in which the phosphopeptide was upregulated. Proteins listed in italic grey font were not differentially expressed, but had a significant logFC (±0.5) or a significant adjusted p-value (≤ 0.05). Phosphopeptides from a protein that could not be characterized are marked with a symbol, where applicable domains or other identifying information is included in the Protein Name column. Phosphopeptides from *Gl*-Rp8 were not numerous enough for reliable statistical testing.

Species	Experiment	Condition	Gene Symbol	Protein Name	Function		*padj*
C. maenas	MIH ± AP-C5	AP-C5	MAST3	Microtubule associated serine/threonine kinase 3	Cytoskeleton	Cell signaling	0.007
		AP-C5	IF-2	Translation initiation factor 2	Translation		0.025
		AP-C5	Futsch / MAP1B	Microtubule associated protein futsch-like	Cytoskeleton		0.004
		AP-C5	PTB / PTBP1	Polypyrimidine tract-binding protein 1	Transcription	mTOR	0.032
		AP-C5	*MAP2K1*	*Dual specificity mitogen-activated protein kinase kinase 1*	Cell signaling		*0.028*
		AP-C5	*EPRS1*	*Bifunctional glutamate/proline tRNA ligase*	*Translation*		*0.003*
		AP-C5	*EcR-3*	*Ecdysteroid receptor 3*	*Cell signaling*	*Ecdysteroid*	*0.006*
		AP-C5	*‡*	*Hypothetical protein E2C01_096008*			*0.034*
		MIH	BUD13	Bud13 homolog	Transcription	mTOR	0.003
		MIH	FKBP5	FK506-binding protein 5	Cell signaling	mTOR	0.045
		MIH	*	Zinc finger C3H1 domain (IPR000571) and U1-C zinc finger (IPR003604)	Predicted - Transcription		0.008
		MIH	NDRG3	N-myc downstream regulated gene	Cell signaling		0.005
		MIH	†	Peptidase c19 domain (cd02257) and SMC_N superfamily (cl47134)	Predicted - Transcription		0.015
		MIH	*Scrib*	*Scribble homolog*	*Cytoskeleton*	*Cell signaling*	*0.016*
	MIH ± Rp-8-Br-PET-cGMP	RP8	Titin	Titin	Cytoskeleton	Cell signaling	0.013
		RP8	¶	Zinc finger C3H1 domain (IPR000571) and Muscleblind-like (PTHR12675)	Predicted - Transcription		0.000
		RP8	H1f0	Histone family member 0	Cell cycle		0.013
		MIH	srGAP	SLIT-ROBO Rho GTPase-activating protein	Cell signaling		0.001
		MIH	§	Beta helix (pfam13229)			0.020
		MIH	FAT1	Protocadherin FAT1	Cell signaling		0.007
		MIH	plxna3	Plexin A3	Cytoskeleton	Cell signaling	0.015
		MIH	*Acn*	*Acinus*	Transcription	Cell signaling	*0.003*
G. lateralis	MIH ± AP-C5	AP-C5	Enah	Protein-enabled like	Cytoskeleton		0.032
		AP-C5	*TP53BP1*	*P53 binding protein*	Cell cycle	mTOR	*0.053*
		MIH	Wasf3	Wiskott-Aldrich syndrome family member 3	Cytoskeleton	Cell cycle	0.032
		MIH	PRPF39	Pre-mRNA processing factor 39	Transcription		0.032
		MIH	*Futsch / MAP1B*	*Microtubule associated protein futsch-like*	Cytoskeleton		*0.059*
	MIH ± Rp-8-Br-PET-cGMP	NA	LARK	RNA-binding protein LARK	Translation		NA
		NA	Titin	Titin	Cytoskeleton	Cell signaling	NA
		NA	B4GAT1	Beta-1,4-glucuronyltransferase 1	Protein metabolism		NA
		NA	SLC7A8	Solute carrier family 7 member 8	AA Transport	mTOR	NA

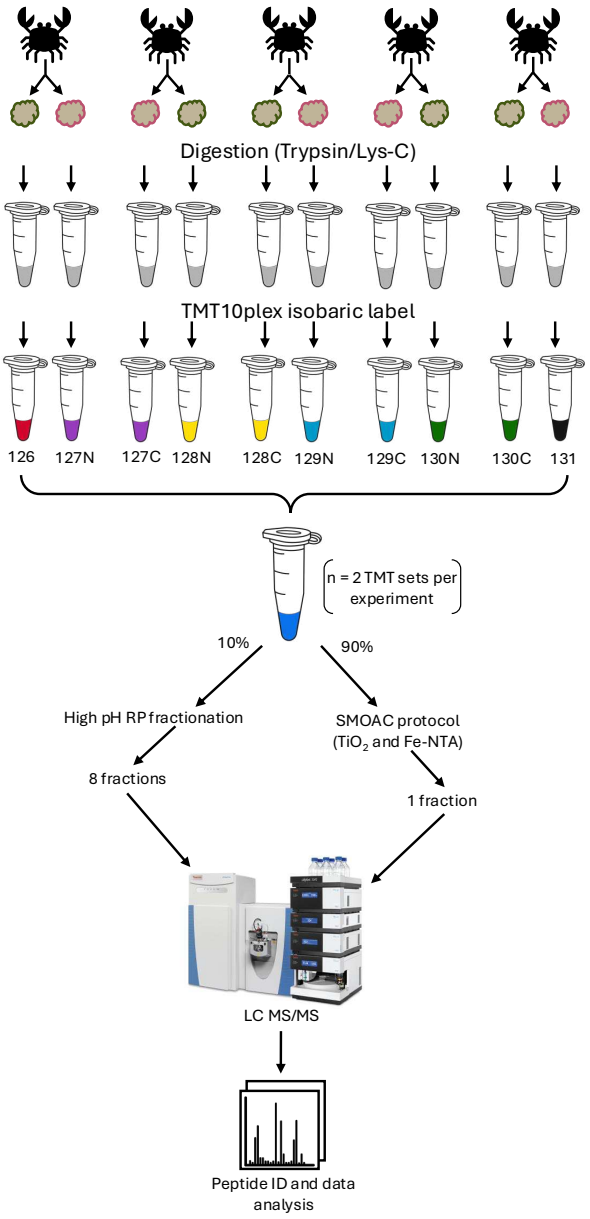

Figure 4.41. Proteomic workflow from tissue to data analysis. Paired YOs from each animal had been treated with 50 nM MIH (control) or 50 nM MIH + 100 µM PKG inhibitor (either AP-C5 or Rp-8-Br-PET-cGMP). Proteins were extracted and digested into peptides with trypsin and Lys-C protease. Each YO sample was labeled with an isobaric tandem mass tag (TMT). An equal amount of peptide from each sample was pooled to make a 'TMT set'. Two TMT sets were made for each experiment (*Cm*-AP-C5 n = 10 animals / 20 YOs; *Cm*-Rp8 n = 8 animals; *Gl*-AP-C5 n = 9 animals; *Gl*-Rp8 n = 10 animals). From each TMT set, 10% of the sample was fractionated offline using high pH reversed phase fractionation to a total of 8 fractions. The remaining 90% of sample was enriched for phosphopeptides using the SMOAC protocol. Each fraction was separately fractionated using HPLC and analyzed with tandem mass spectrometry.

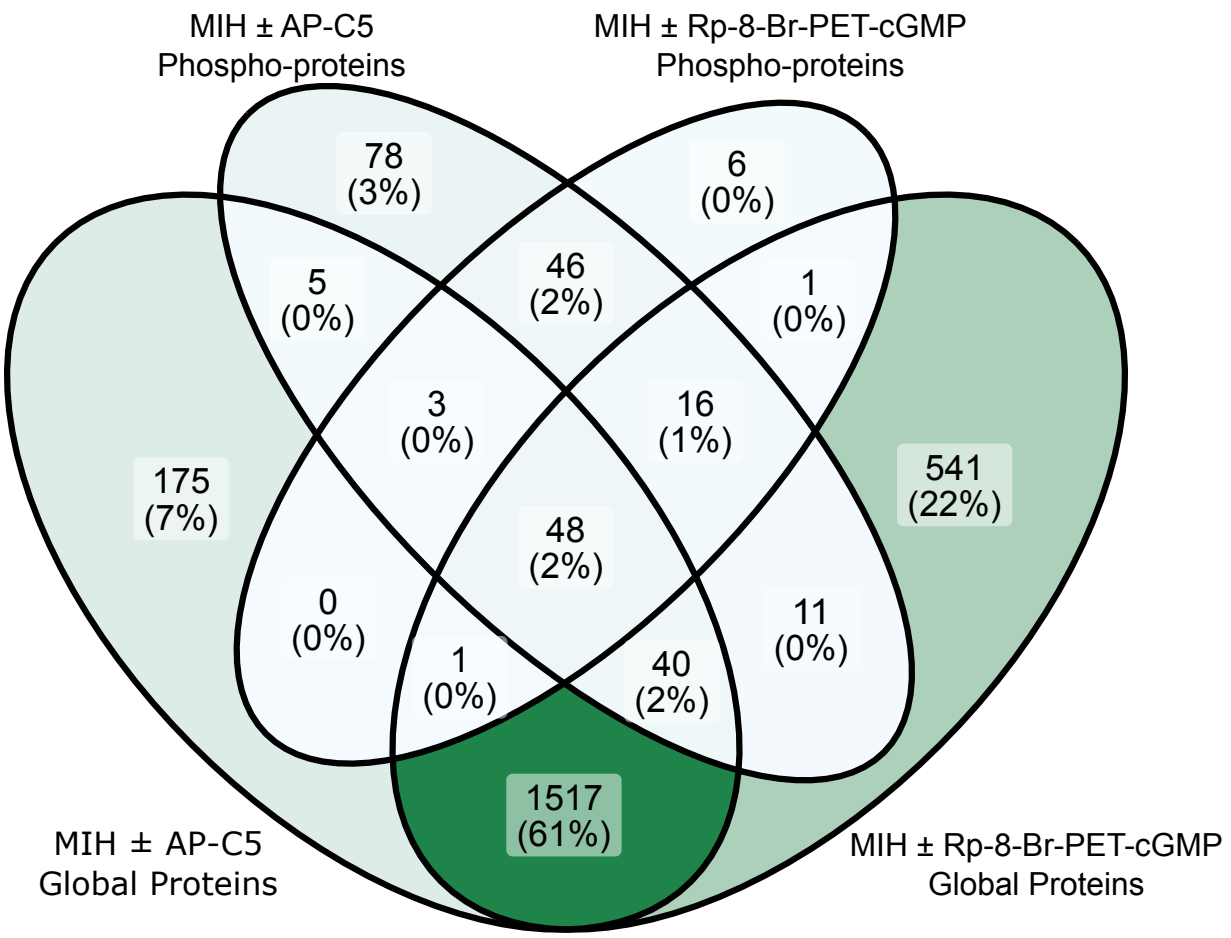

Figure 4.2. Shared proteins between treatments in *C. maenas*. Counts of proteins identified in *C. maenas* YOs treated with MIH ± AP-C5 or MIH ± Rp-8-Br-PET-cGMP. The phosphopeptide-enriched and the global proteome samples are represented for both treatments. Counts represent the number of unique proteins identified by at least 1 unique peptide.

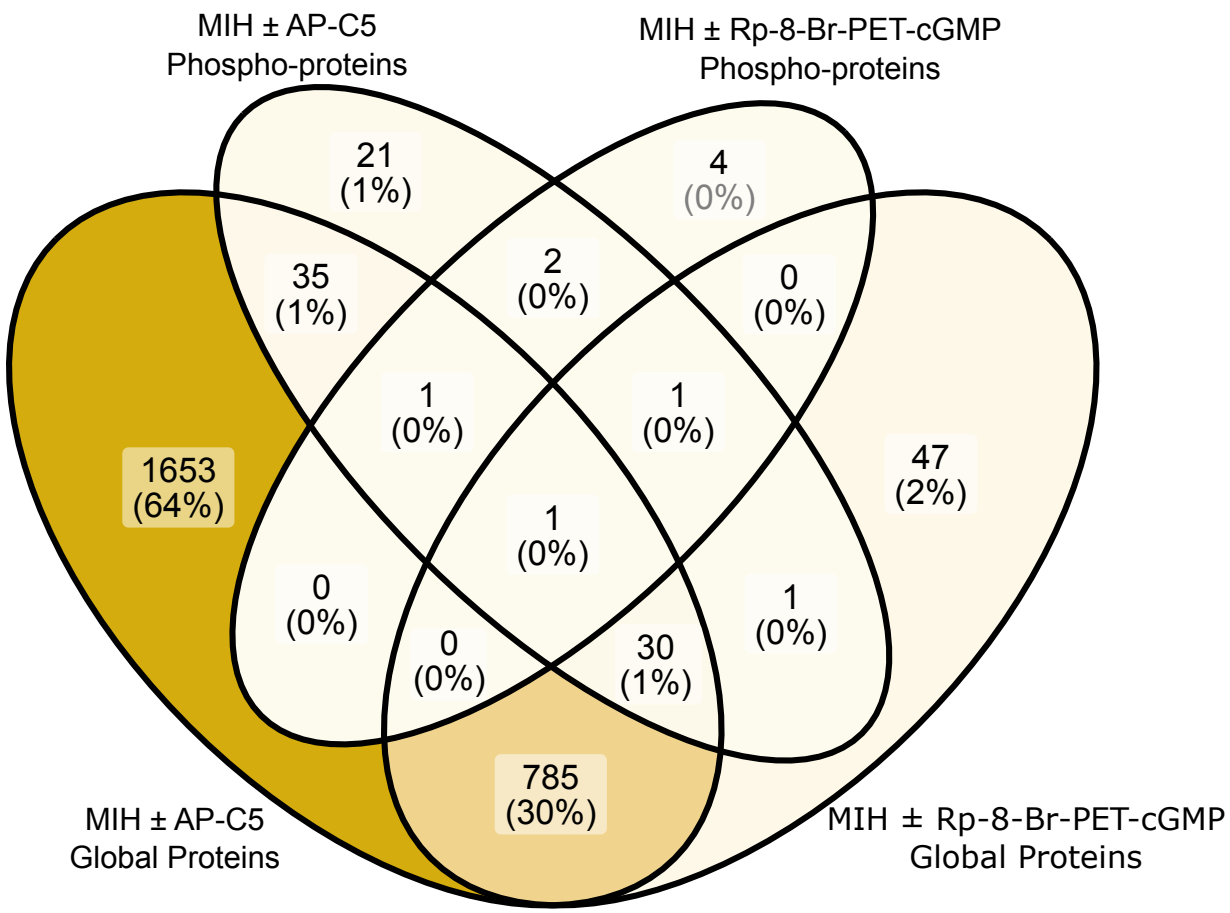

Figure 4.3. Shared proteins between treatments in *G. lateralis.* Counts of proteins identified in *G. lateralis* YOs treated with MIH ± AP-C5 or MIH ± Rp-8-Br-PET-cGMP. The phosphopeptide-enriched and the global proteome samples are represented for both treatments. Counts represent the number of unique proteins identified by at least 1 unique peptide.

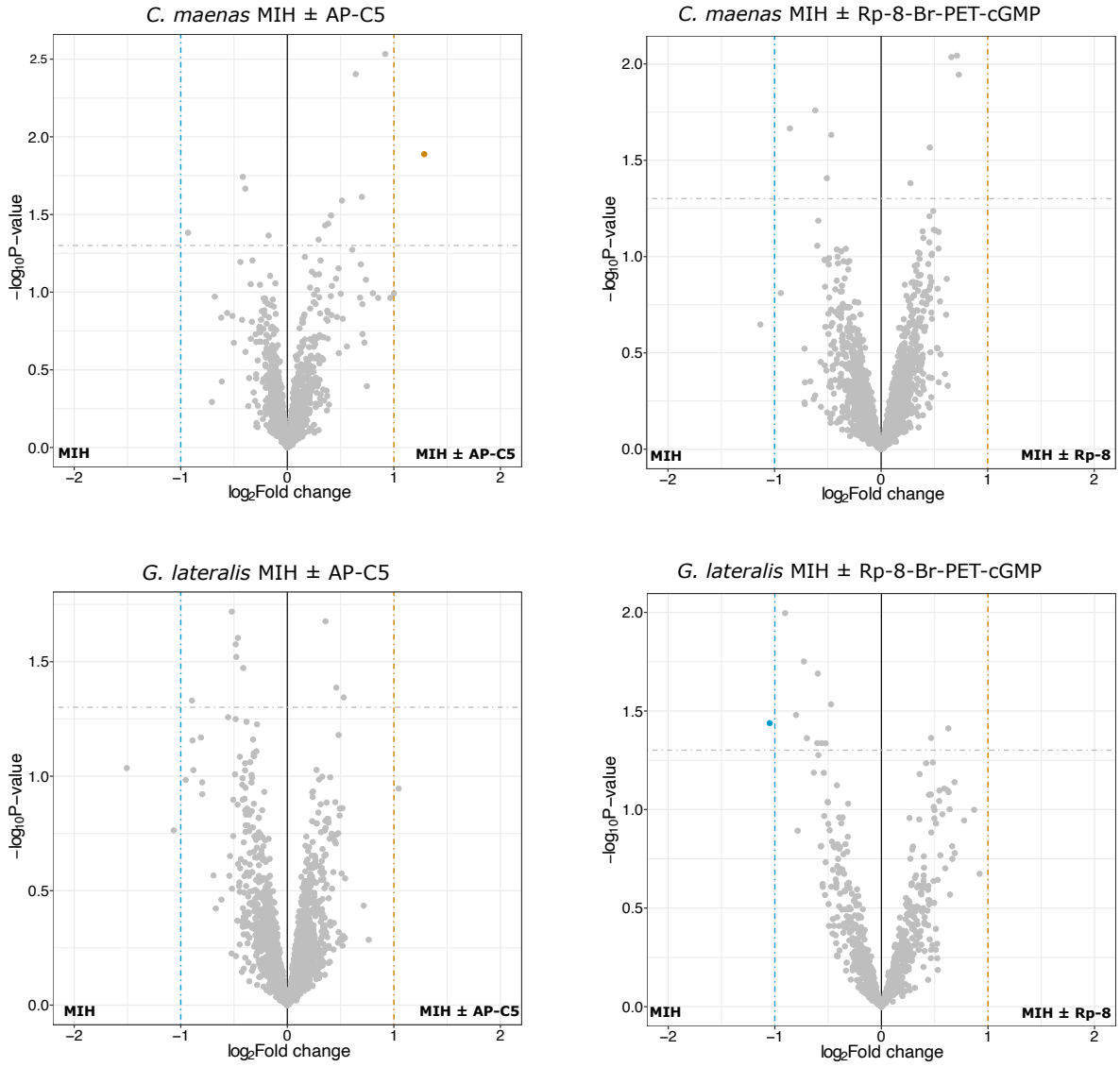

Figure 4.4. Volcano plot of global proteome for *G. lateralis* and *C. maenas*. Differential expression was assessed with a logFC cutoff of ± 1, and an adjusted p-value ≤ 0.05. The y-axis represents $\log_{10}$ of the unadjusted p-value to aid in visualization of the data. After correcting for multiple comparisons with the Benjamini-Hochberg (BH) protocol no proteins were identified as being differentially expressed.

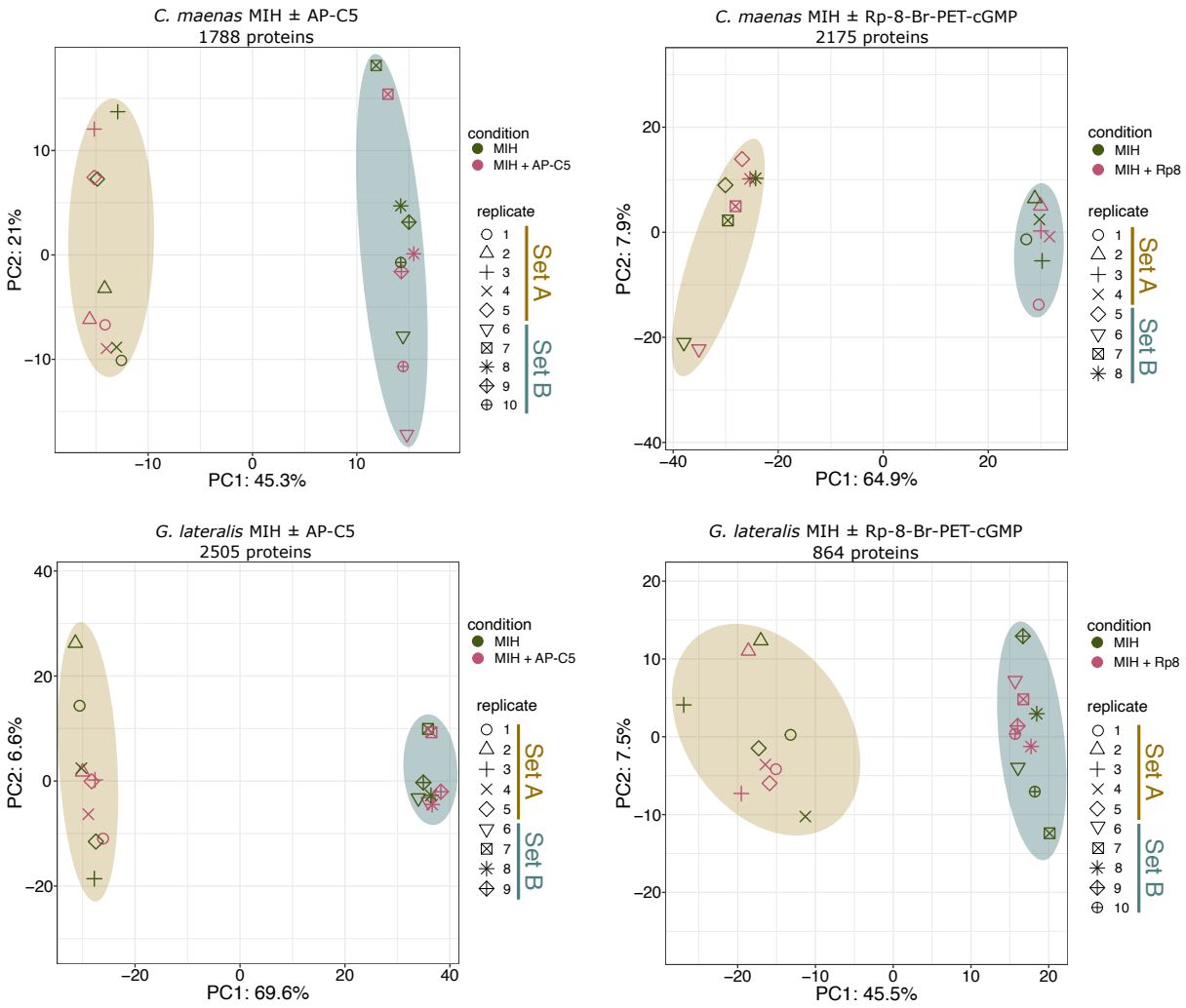

Figure 4.5. Principle component analysis of global proteome samples. Separation of all proteins identified for each experiment grouped within biological replicates by condition along principal component 1 (PC1, x-axis) and principal component 2 (PC2, y-axis). Treatment is indicated by color, for all experiments the MIH control is green and the experimental treatment, MIH + AP-C5 or MIH + Rp-8-Br-PET-cGMP, is pink. TMT sets are indicated with shaded ovals, strong batch effects are observed by separation of TMT sets along the x-axis for each experiment.

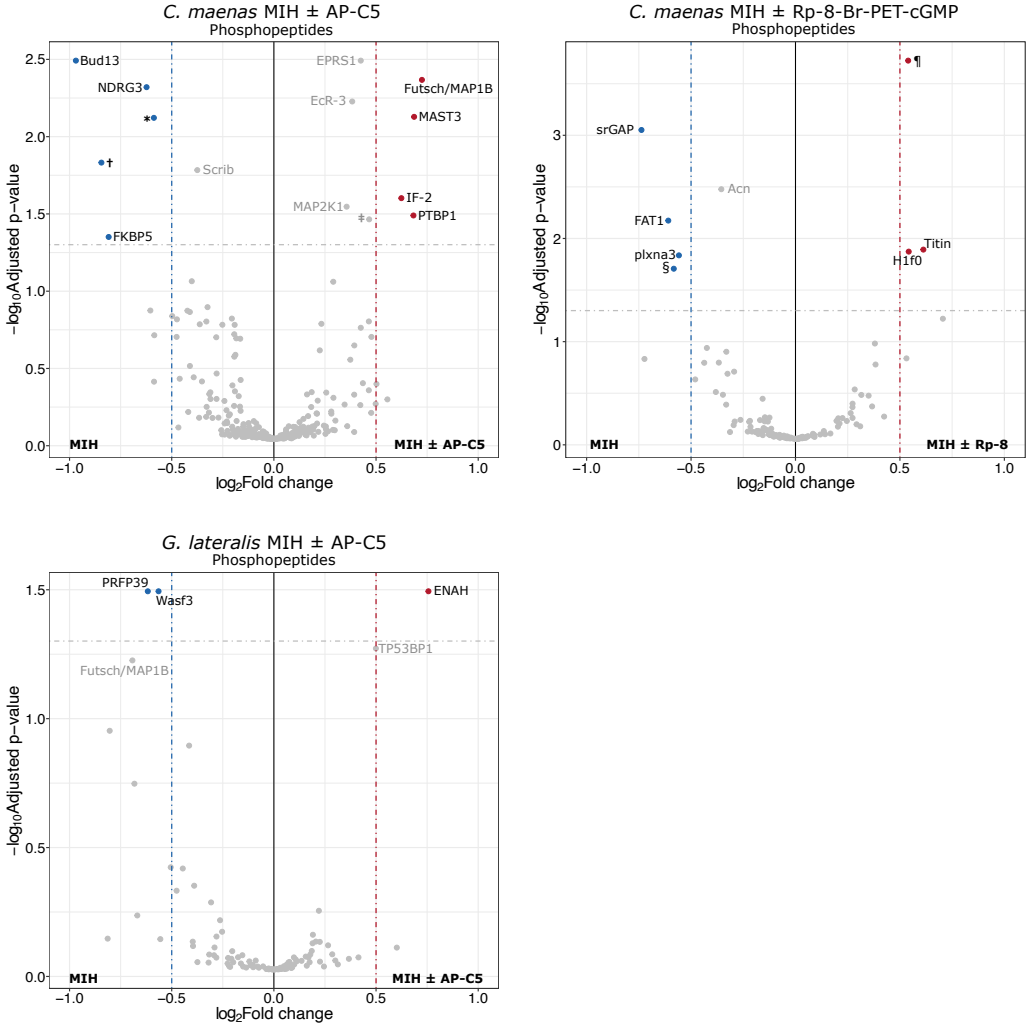

Figure 4.6. Volcano plots representing differential expression of YO phosphopeptides. Differential expression was determined by a threshold of a logFC cutoff of ± 0.5, and an adjusted p-value ≤ 0.05. Blue circles represent phosphopeptides that are upregulated in the MIH control samples and red circles represent phosphopeptides that are upregulated in the experimental treatment MIH + AP-C5 or MIH + Rp-8-Br-PET-cGMP. Phosphopeptide identification corresponds to the protein identified by the phosphopeptide(s). Proteins that are not considered differentially expressed but have either a significant FC or adjusted p-value are indicated in grey. Abbreviations: MAST3, microtubule associated serine/threonine kinase 3; IF-2, translation initiation factor 2; MAP1B, microtubule associated protein futsch-like; PTBP1, polypyrimidine tract-binding protein 1; MAP2K1, mitogen activated protein kinase kinase 1; EPRS1, bifunctional glutamate/proline tRNA ligase; EcR-3, ecdysteroid receptor 3; BUD13, Bud13 homolog; FKBP5, FK506-binding protein 5; NDRG3, N-myc downstream regulated gene; Scrib, Scribble homolog; H1f0, histone family member 0; srGAP, SLIT-ROBO Rho GTPase-activating protein; FAT1, protocadherin FAT1; plxna3, plexin A3; Enah, protein-enabled like; TP53BP1, P53 binding protein; Wasf3, Wiskott-Aldrich syndrome family member 3; PRPF39, pre-mRNA processing factor 39; LARK, RNA-binding protein LARK; B4GAT1, Beta-1,4,glucuronyltranserase 1; SLC7A8, solute carrier family 7 member 8.

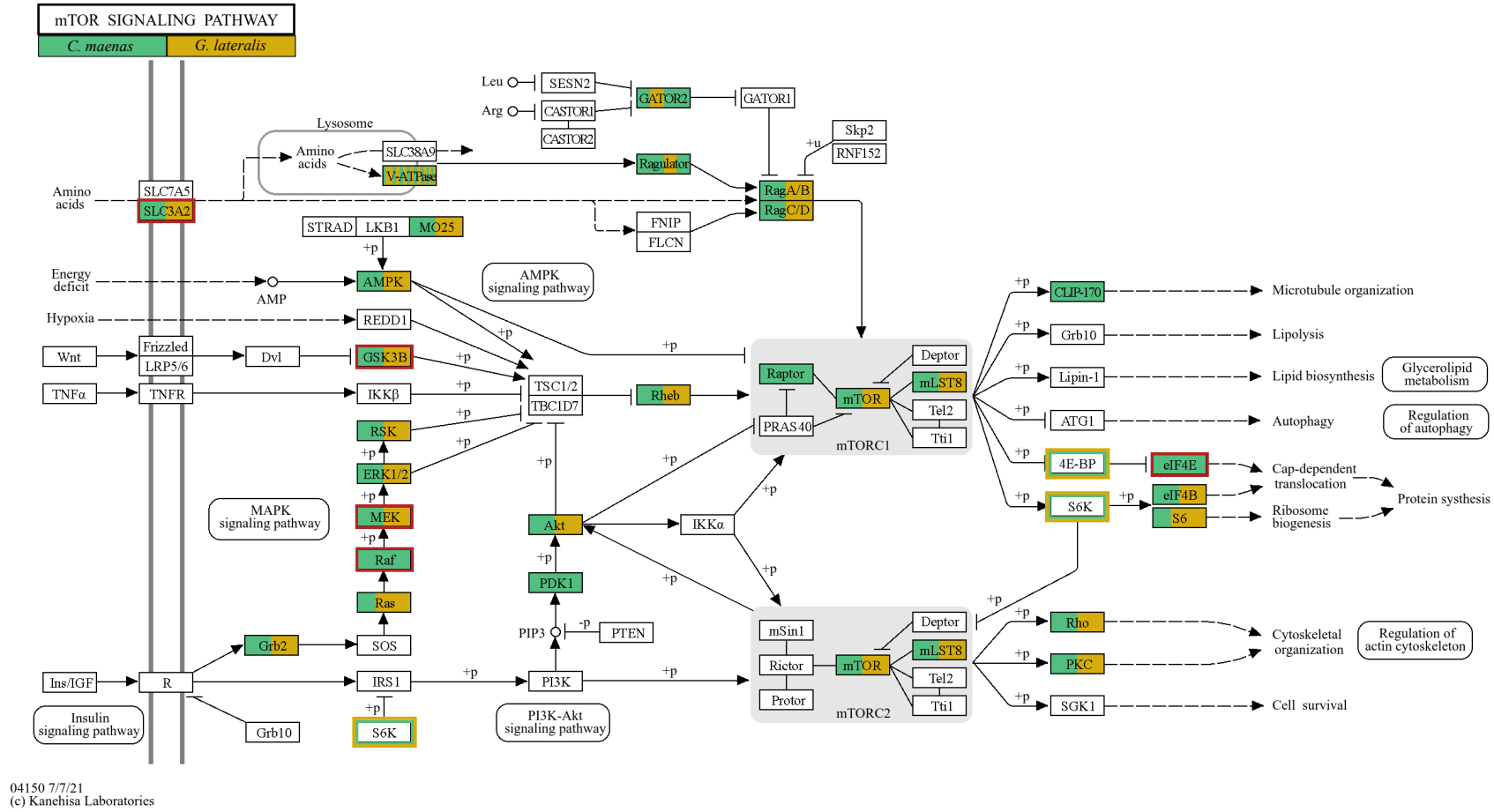

Figure 4.7. Identified components of the mTOR signaling pathway. Proteins were identified by KEGG enrichment. Green shading indicates identification of the protein in the global proteome of *C. maenas*, yellow shading indicates identification of the protein in the global proteome of *G. lateralis*. Proteins with phosphopeptides identified in any dataset are outlined in red. Proteins that were identified by manual annotation, but not KEGG mapping, are outlined in the corresponding colors for each species.

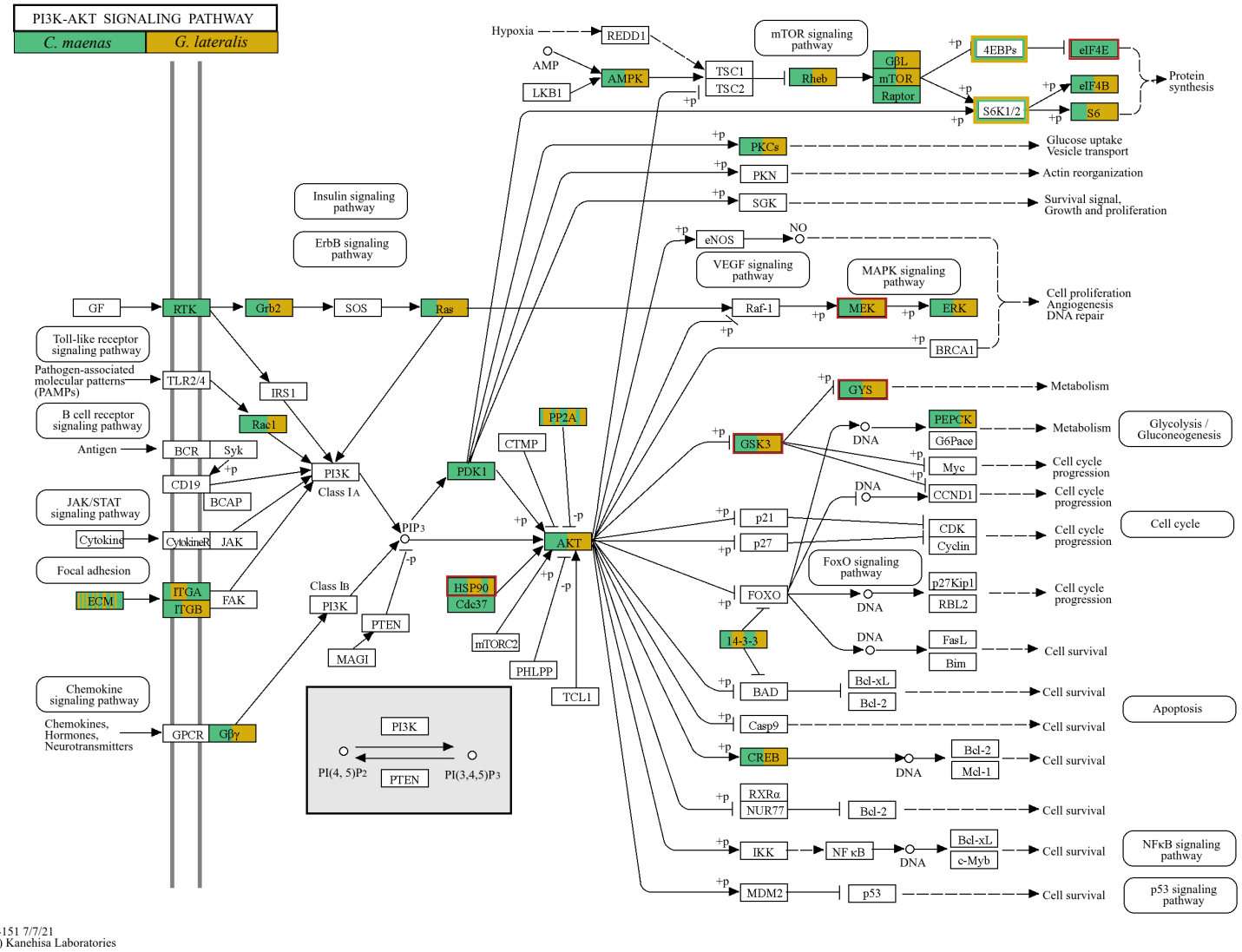

Figure 4.8. Proteins identified in the PI3K-AKT signaling pathway. Proteins were identified by KEGG enrichment. Green shading indicates identification of the protein in the global proteome of *C. maenas*, yellow shading indicates identification of the protein in the global proteome of *G. lateralis*. Proteins with phosphopeptides identified in any dataset are outlined in red. Proteins that were identified by manual annotation, but not KEGG mapping, are outlined in the corresponding colors for each species.

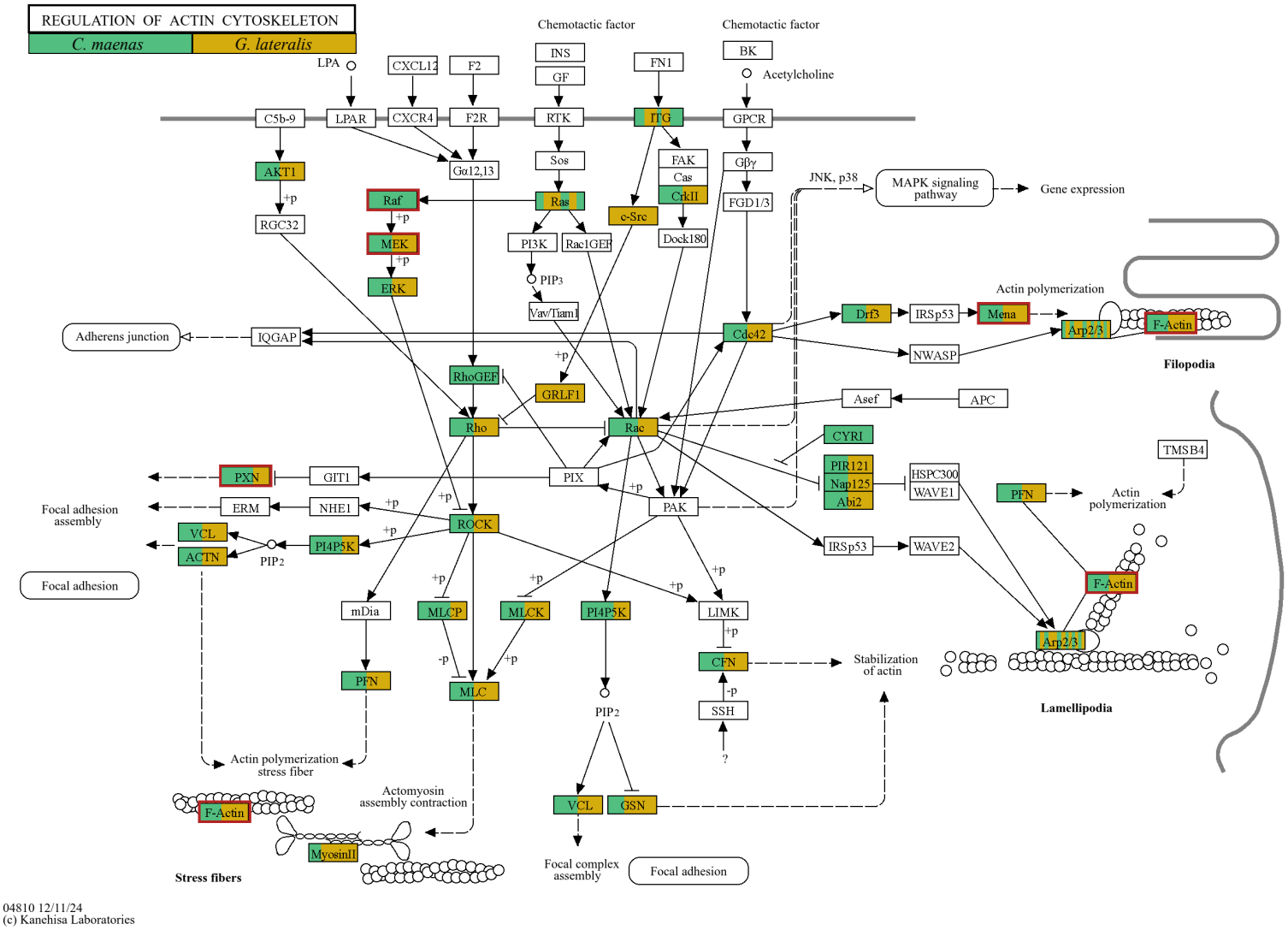

Figure 4.9. Proteins associated with cytoskeleton organization associated with actin. Proteins were identified by KEGG enrichment. Green shading indicates identification of the protein in the global proteome of *C. maenas*, yellow shading indicates identification of the protein in the global proteome of *G. lateralis*. Proteins with phosphopeptides identified in any dataset are outlined in red.

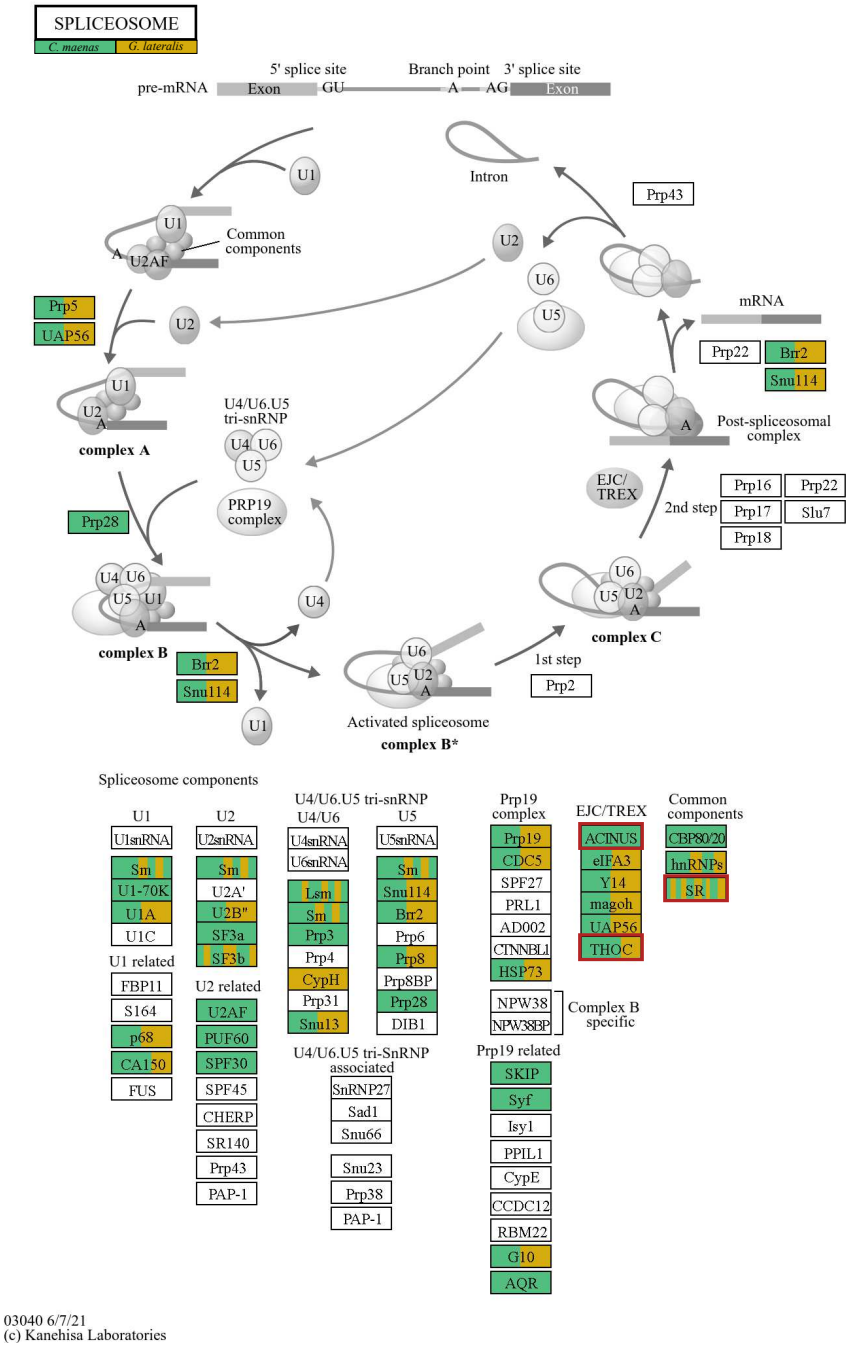

Figure 4.10. Components of the spliceosome identified in the global and phospho-proteome. Proteins were identified by KEGG enrichment. Green shading indicates identification of the protein in the global proteome of *C. maenas*, yellow shading indicates identification of the protein in the global proteome of *G. lateralis*. Proteins with phosphopeptides identified in any dataset are outlined in red.

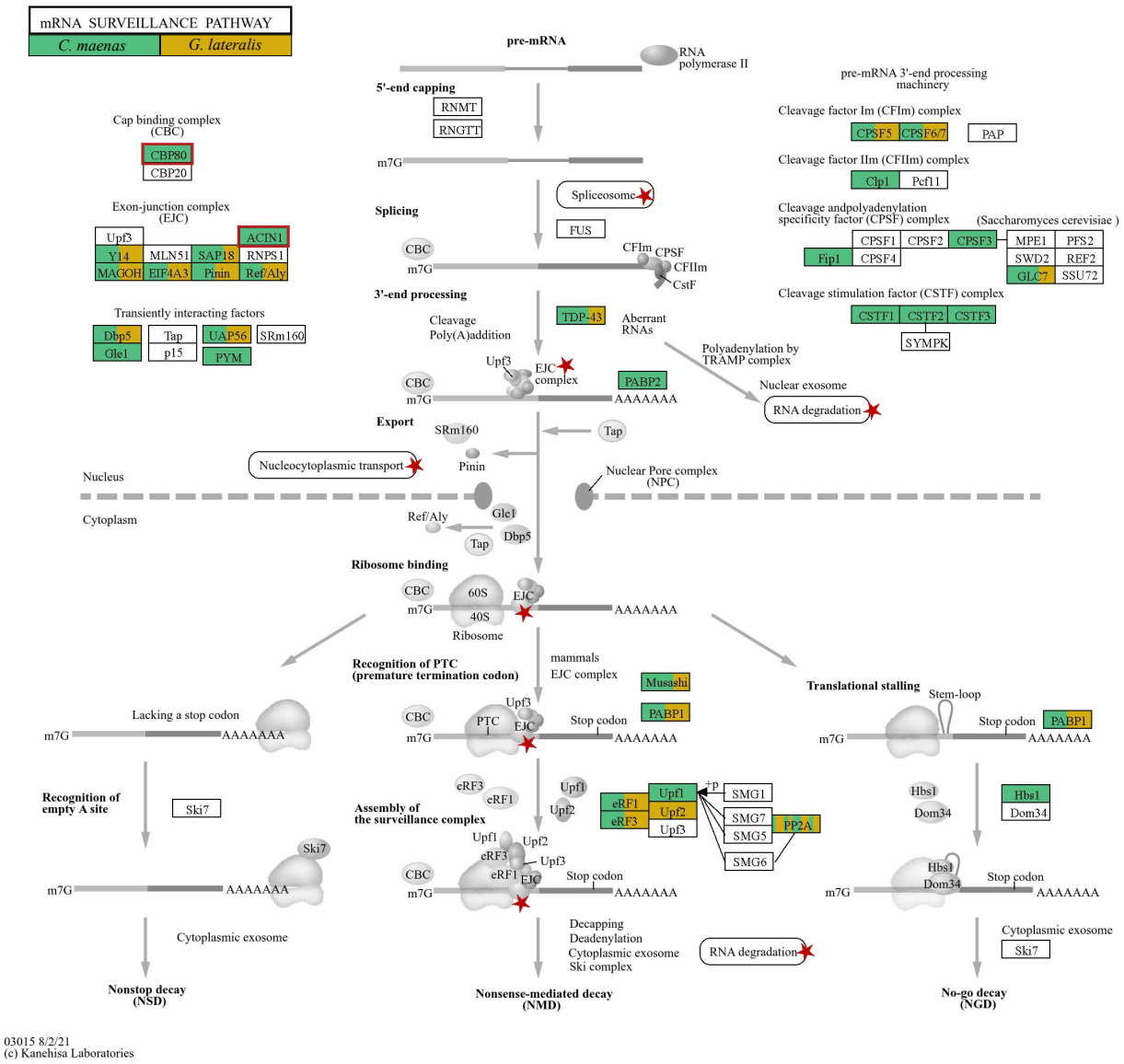

Figure 4.11. Components of the mRNA surveillance pathway in *G. lateralis* and *C. maenas* YOs. Proteins were identified by KEGG enrichment. Green shading indicates identification of the protein in the global proteome of *C. maenas*, yellow shading indicates identification of the protein in the global proteome of *G. lateralis*. Proteins with phosphopeptides identified in any dataset are outlined in red. Components of mRNA surveillance in which proteins identified by phosphopeptides are associated but not shown are indicated by red stars.

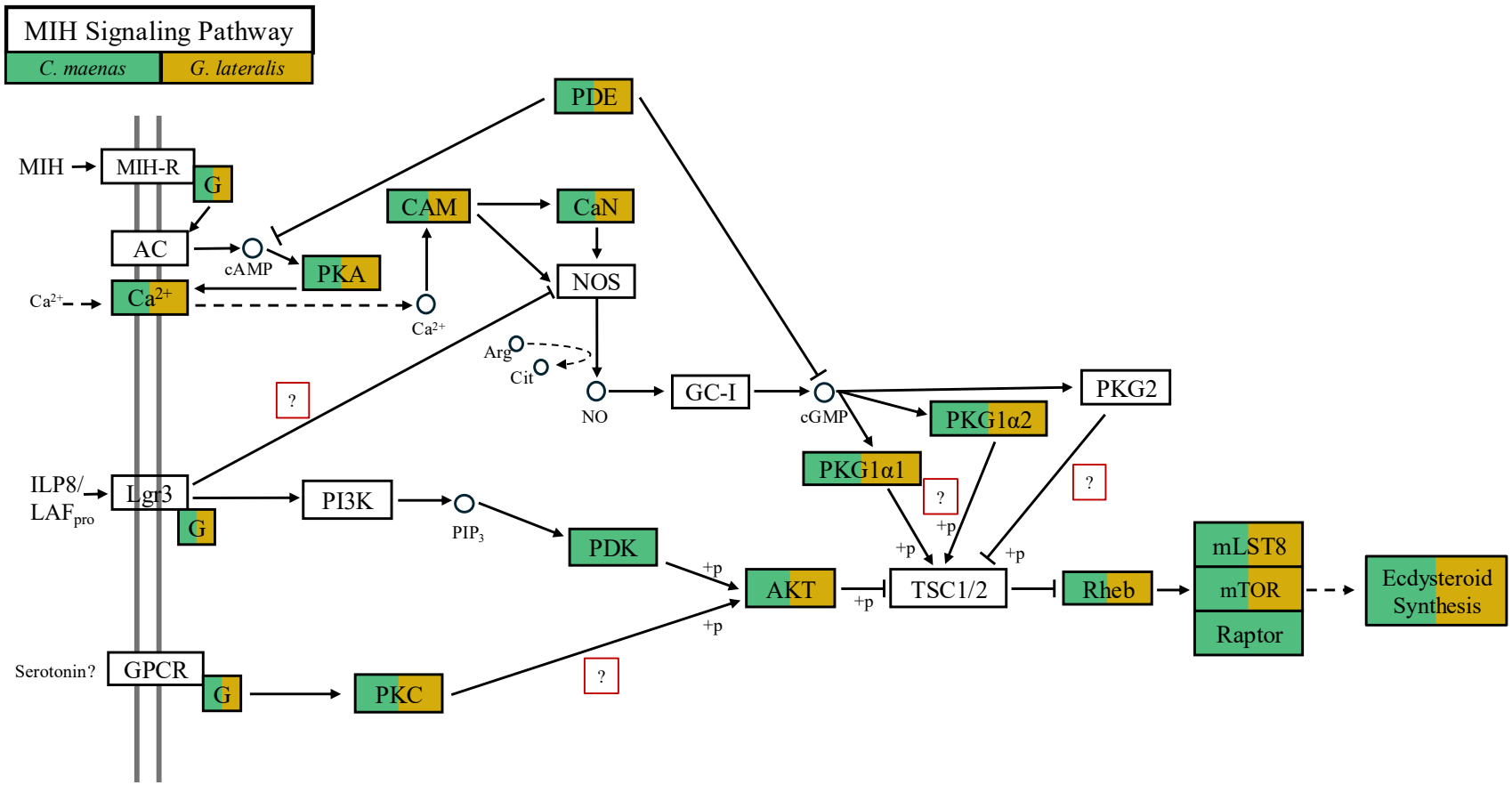

Figure 4.12. Proteins in the MIH signaling pathway identified in the global proteomes of *C. maenas* and *G. lateralis* YOs. Proteins were identified by functional annotation including BLAST, pfam, CDD, SMART, PANTHER, KEGG, InterProScan, and GO. PKG1 isoforms PKG1α1 and PKG1α2 were distinguished by unique peptides from the N-terminus of the proteins. A leucine-rich-repeat GPCR (Lgr4) was identified in the *G. lateralis* YO. Predicted protein interactions are indicated with a question mark. Multiple isoforms of G proteins were identified, a simplified diagram is shown here. Individual ecdysteroid synthetic enzymes are identified in Figure 4.13.

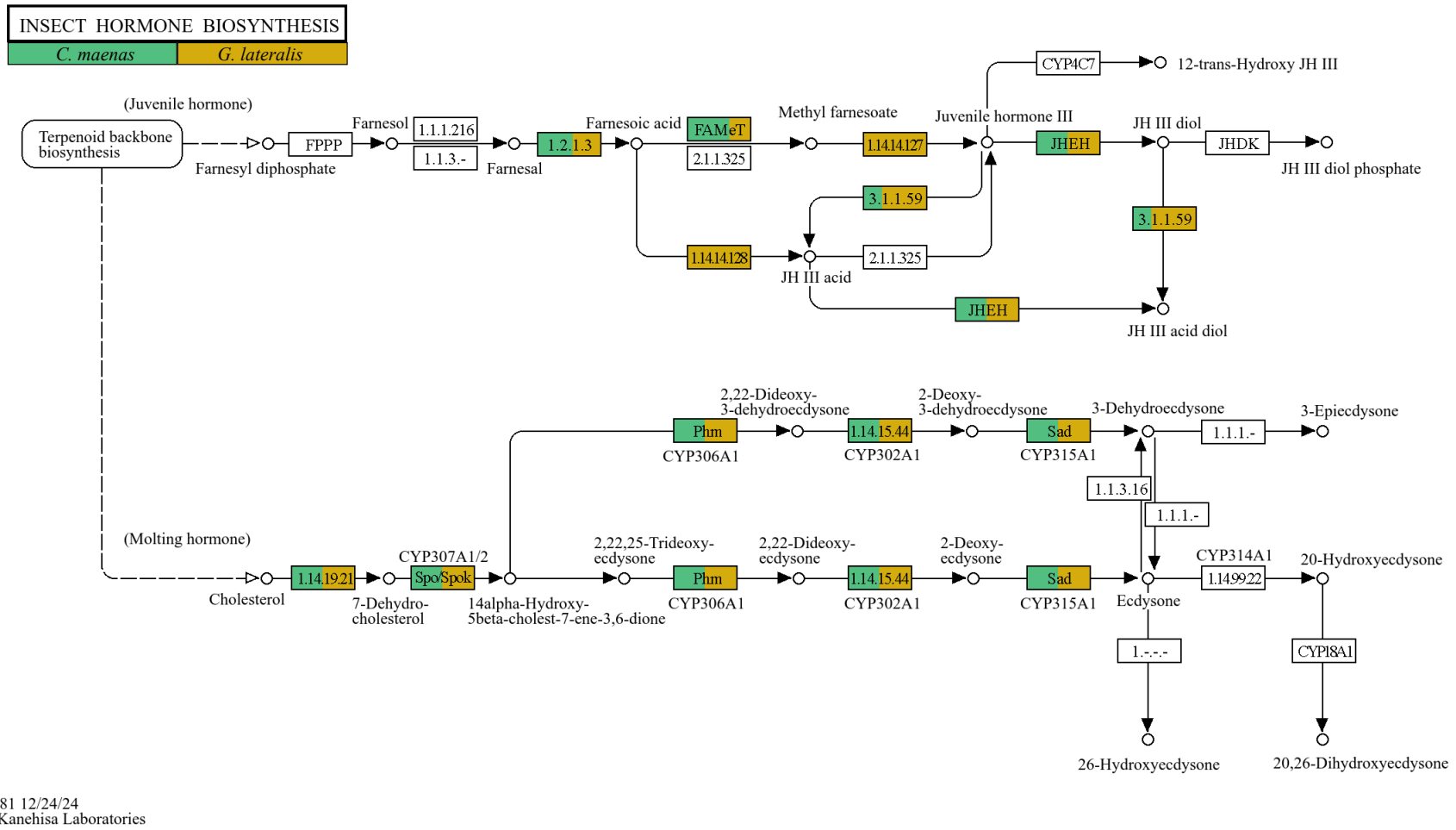

Figure 4.13. Biosynthetic enzymes of the juvenile hormone pathway and ecdysteroid pathway identified in *C. maenas* and *G. lateralis* YOs. Proteins were identified by KEGG enrichment. Green shading indicates identification of the protein in the global proteome of *C. maenas*, yellow shading indicates identification of the protein in the global proteome of *G. lateralis*. No identified phosphopeptides were associated with either pathway.

A.

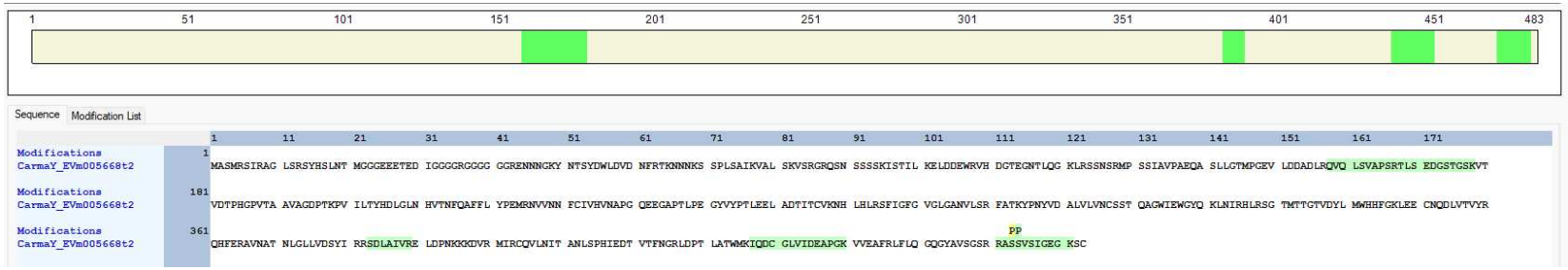

B.

ID	Position	Code	Kinase	Peptide
CarmaY_EVm005668t2| A0A0P4WAF9 Protein NDRG3 OS=Scylla olivacea	473	S	AGC/PKG/PKG1	VSGSRRASSVSIGEG
CarmaY_EVm005668t2| A0A0P4WAF9 Protein NDRG3 OS=Scylla olivacea	474	S	AGC/PKG/PKG1	SGSRRASSVSIGEGK
CarmaY_EVm005668t2| A0A0P4WAF9 Protein NDRG3 OS=Scylla olivacea	473	S	AGC/PKG/PKG2	VSGSRRASSVSIGEG

Figure 4.13. Peptides and phosphopeptides of N-myc downstream regulated gene 3 (NDRG3) in the *C. maenas* YO. (A) Four unique peptides, including one phosphopeptide, were used to identify NDRG3. Phosphorylation was observed at two neighboring serine residues S473 and S474. (B) Predicted phosphosites of PKG1 and PKG2 identified by GPS6.0 are identical to the observed phosphosites in the *C. maenas* YO.

REFERENCES

Abuhagr, A.M., MacLea, K.S., Chang, E.S. and Mykles, D.L. (2014b). Mechanistic target of rapamycin (mTOR) signaling genes in decapod crustaceans: Cloning and tissue expression of mTOR, Akt, Rheb, and p70 S6 kinase in the green crab, *Carcinus maenas*, and blackback land crab, *Gecarcinus lateralis*. *Comp. Biochem. Physiol.* **168A**, 25-39.

Abuhagr, A.M., MacLea, K.S., Mudron, M.R., Chang, S.A., Chang, E.S. and Mykles, D.L. (2016). Roles of mechanistic target of rapamycin and transforming growth factor-β signaling in the molting gland (Y-organ) of the blackback land crab, *Gecarcinus lateralis*. *Comp. Biochem. Physiol.* **198A**, 15-21.

Ahern-Djamali, S.M., Comer, A.R., Bachmann, C., Kastenmeier, A.S., Reddy, S.K., Beckerle, M.C., Walter, U. and Hoffmann, F.M. (1998). Mutations in Drosophila enabled and rescue by human vasodilator-stimulated phosphoprotein (VASP) indicate important functional roles for Ena/VASP homology domain 1 (EVH1) and EVH2 domains. *Molec. Biol. Cell.* **9**, 2157-2171.

Arif, A., Terenzi, F., Potdar, A.A., Jia, J., Sacks, J., China, A., Halawani, D., Vasu, K., Li, X., Brown, J.M., et al. (2017). EPRS is a critical mTORC1–S6K1 effector that influences adiposity in mice. *Nature.* **542**, 357-361.

Backe, S.J., Sager, R.A., Woodford, M.R., Makedon, A.M. and Mollapour, M. (2020). Post-translational modifications of Hsp90 and translating the chaperone code. *J. Biol. Chem.* **295**, 11099-11117.

Baghdassarian, D., deBesse, N., Saidi, B., Somme, G. and Lachaise, F. (1996). Neuropeptide-induced inhibition of steroidogenesis in crab molting glands: Involvement of cGMP-dependent protein kinase. *Gen. Comp. Endocrinol.* **104**, 41-51.

Ballou, L.M. and Lin, R.Z. (2008). Rapamycin and mTOR kinase inhibitors. *J. Biol. Chem.* **1**, 27-36.

Basnet, R., Basnet, B.B., Gupta, R., Basnet, T., Khadka, S. and Alam, M.S. (2023). Mammalian Target of Rapamycin (mTOR) signalling pathway-A potential target for cancer intervention: A short overview. *Curr. Molec. Pharmacol.* **17**, e310323215268.

Benrabaa, S.A.M., Chang, S.A., Chang, E.S. and Mykles, D.L. (2023). Effects of molting on the expression of ecdysteroid biosynthesis genes in the Y-organ of the blackback land crab, Gecarcinus lateralis. *Gen. Comp. Endocrinol.* **340**, 114304.

Benz, P.M., Frömel, T., Laban, H., Zink, J., Ulrich, L., Groneberg, D., Boon, R.A., Poley, P., Renne, T., de Wit, C., et al. (2023). Cardiovascular Functions of Ena/VASP Proteins: Past, Present and Beyond. *Cells.* **12**, 1740.

Bhosle, V.K., Tan, J.M., Li, T., Hua, R., Kwon, H., Li, Z., Patel, S., Tessier-Lavigne, M., Robinson, L.A., Kim, P.K., et al. (2023). SLIT2/ROBO1 signaling suppresses mTORC1 for organelle control and bacterial killing. *Life Sci. Alliance.* **6**, e202301964.

Bliss, D.E. and Welsh, J.H. (1952). The Neurosecretory System of Brachyuran Crustacea. *Biol. Bull.* **103**, 157-169.

Bliss, D.E., Durand, J.B. and Welsh, J.H. (1954). Neurosecretory systems in decapod Crustacea. *Z. Zellforch. Mik. Ana.* **39**, 520-536.

Bliss, D.E. and Boyer, J.R. (1964). Environmental regulation of growth in the decapod crustacean *Gecarcinus lateralis*. *Gen. Comp. Endocrinol.* **4**, 15-41.

Bordicchia, M., Liu, D., Amri, E.-Z., Ailhaud, G., Dessì-Fulgheri, P., Zhang, C., Takahashi, N., Sarzani, R. and Collins, S. (2012). Cardiac natriuretic peptides act via p38 MAPK to induce the brown fat thermogenic program in mouse and human adipocytes. *JCI.* **122**, 1022-1036.

Borst, D.W., Ogan, J., Tsukimura, B., Claerhout, T. and Holford, K.C. (2015). Regulation of the Crustacean Mandibular Organ. *Am. Zool.* **41**, 430-441.

Brandi, J., Noberini, R., Bonaldi, T. and Cecconi, D. (2022). Advances in enrichment methods for mass spectrometry-based proteomics analysis of post-translational modifications. *J. Chromatogr. A.* **1678**, 463352.

Brown, F.A. and Cunningham, O.N.A. (1939). Influence of the sinus gland of crustaceans on normal viability and ecdysis. *Biol. Bull.* **77**, 104-114.

Bubis, J.A., Gorshkov, V., Gorshkov, M.V. and Kjeldsen, F. (2020). PhosphoShield: Improving Trypsin Digestion of Phosphoproteins by Shielding the Negatively Charged Phosphate Moiety. *J. Am. Soc. Mass Spectrom.* **31**, 2053-2060.

Butt, E., Abel, K., Krieger, M., Palm, D., Hoppe, V., Hoppe, J. and Walter, U. (1994). cAMP- and cGMP-dependent protein kinase phosphorylation sites of the focal adhesion vasodilator-stimulated phosphoprotein (VASP) in vitro and in intact human platelets. *J. Biol. Chem.* **269**, 14509-17.

Carlisle, D.B. (1957). On the hormonal inhibition of moulting in decapod Crustacea II. The terminal anecdysis in crabs. *J. Mar. Biol. Assoc. U.K.* **36**, 291-307.

Chen, J. and Roberts, J.D., Jr. (2014). cGMP-dependent protein kinase I gamma encodes a nuclear localization signal that regulates nuclear compartmentation and function. *J. Cell Sig.* **26**, 2633-44.

Chen, M., Zhang, W., Gou, Y., Xu, D., Wei, Y., Liu, D., Han, C., Huang, X., Li, C., Ning, W., et al. (2023). GPS 6.0: an updated server for prediction of kinase-specific phosphorylation sites in proteins. *Nucleic Acids Res.* **51**, W243-W250.

Chung, J.S. and Webster, S.G. (2003). Moult cycle-related changes in biological activity of moult-inhibiting hormone (MIH) and crustacean hyperglycaemic hormone (CHH) in the crab, *Carcinus maenas*: From target to transcript. *Eur. J. Biochem.* **270**, 3280-3288.

Covi, J.A., Chang, E.S. and Mykles, D.L. (2012). Neuropeptide signaling mechanisms in crustacean and insect molting glands. *Invertebr. Reprod. Dev.* **56**, 33-49.

da Cruz, A.B., Schwärzel, M., Schulze, S., Niyyati, M., Heisenberg, M. and Kretzschmar, D. (2005). Disruption of the MAP1B-related Protein FUTSCH Leads to Changes in the Neuronal Cytoskeleton, Axonal Transport Defects, and Progressive Neurodegeneration in Drosophila. *Molec. Biol. Cell.* **16**, 2433-2442.

Daneri-Becerra, C., Zgajnar, N.R., Lotufo, C.M., Ramos Hryb, A.B., Piwien-Pilipuk, G. and Galigniana, M.D. (2019). Regulation of FKBP51 and FKBP52 functions by post-translational modifications. *Biochem. Soc. Trans.* **47**, 1815-1831.

Das, A., Xi, L. and Kukreja, R.C. (2008). Protein kinase G-dependent cardioprotective mechanism of phosphodiesterase-5 inhibition involves phosphorylation of ERK and GSK3beta. *J. Biol. Chem.* **283**, 29572-85.

Döppler, H. and Storz, P. (2013). Regulation of VASP by phosphorylation: consequences for cell migration. *Cell. Adh. Migr.* **7**, 482-6.

Doronzo, G., Viretto, M., Russo, I., Mattiello, L., Di Martino, L., Cavalot, F., Anfossi, G. and Trovati, M. (2011). Nitric oxide activates PI3-K and MAPK signalling pathways in human and rat vascular smooth muscle cells: Influence of insulin resistance and oxidative stress. *Atheroscler.* **216**, 44-53.

Echalier, G. (1954). Recherches expérimentales sur le rôle de “l'organe Y” dans la mue de *Carcinus moenas* (L.) Crustacé Décapode. *C. R. Acad. Sci. Paris.* **238**, 523-525.

Feng, Z., Fang, P., Zheng, H. and Zhang, X. (2023). DEP2: an upgraded comprehensive analysis toolkit for quantitative proteomics data. *Bioinformatics.* **39**, btad526.

Flores, K.A., Pérez-Moreno, J.L., Durica, D.S. and Mykles, D.L. (2024). Phylogenetic and transcriptomic characterization of insulin and growth factor receptor tyrosine kinases in crustaceans. *Front. Endocrinol.* **15**, 1379231.

Fukasawa, A. and Yasuda, C.I. (2024). Morphometric changes at terminal molt and reproductive capacity in the kelp crab *Pugettia ferox* Ohtsuchi & Kawamura, 2019 (Decapoda: Brachyura: Majoidea). *J. Crusacean Biol.* **44**, ruae032.

Gabe, M. (1953a). Sur l'existence, chez quelques crustacés Malacostraces, d'un organe comparable a la glande de la mue des Insects. *C. R. Acad. Sci. D.* **327**, 1111-1113.

Gabe, M. (1953b). Quelques acquisitions récentes sur les glandes endocrines des Arthropodes. *Experientia.* **9**, 352-356.

Gögel, S., Wakefield, S., Tear, G., Klämbt, C. and Gordon-Weeks, P.R. (2006). The Drosophila microtubule associated protein Futsch is phosphorylated by Shaggy/Zeste-white 3 at an homologous GSK3beta phosphorylation site in MAP1B. *Molec. Cell Neurosci.* **33**, 188-99.

Gray, B.C.T., Champion, C., Broadhurst, M.K., Coleman, M.A. and Benkendorff, K. (2025). Effects of contaminants and flooding on the physiology of harvested estuarine decapod crustaceans: A global review and meta-analysis. *Environ. Pollut.* **364**, 16.

Gupta, N. and Pevzner, P.A. (2009). False Discovery Rates of Protein Identifications: A Strike against the Two-Peptide Rule. *J. Proteome Res.* **8**, 4173-4181.

Guzmán-Palma, P., Contreras, E.G., Mora, N., Smith, M., González-Ramírez, M.C., Campusano, J.M., Sierralta, J., Hassan, B.A. and Oliva, C. (2021). Slit/Robo Signaling Regulates Multiple Stages of the Development of the Drosophila Motion Detection System. *Front. Cell. Dev. Biol.* **9**, 612645.

Halpain, S. and Dehmelt, L. (2006). The MAP1 family of microtubule-associated proteins. *Genome Biol.* **7**, 224.

Hamer, M. (2015). The proteomic response of the *Carcinus maenas* Y-organ over the course of the molt cycle. San Luis Obispo, CA, USA: California Polytechnic State University. M.S. Thesis. https://doi.org/10.15368/theses.2015.6.

Hanström, B. (1939). *Hormones in Invertebrates.* Great Britain, UK: Oxford University Press.

Harris, L., Fondrie, W.E., Oh, S. and Noble, W.S. (2023). Evaluating Proteomics Imputation Methods with Improved Criteria. *J. Proteome Res.* **22**, 3427-3438.

Haynes, W. (2013). Benjamini–Hochberg Method. *Encyclopedia of Systems Biology* (ed. W. Dubitzky, O. Wolkenhauer, K.-H. Cho and H. Yokota), pp. 78-78. New York, NY: Springer New York.

Head, T.B. (2017). Proteomic Analysis of the Crustacean Molting Gland (Y-organ) Over the Course of the Molt Cycle. San Luis Obispo, CA, USA: California Polytechnic State University. M.S. Thesis. https://doi.org/10.15368/theses.2018.85.

Head, T.B., Mykles, D.L. and Tomanek, L. (2019). Proteomic analysis of the crustacean molting gland (Y-organ) over the course of the molt cycle. *Comp. Biochem. Physiol.* **29D**, 193-210.

Head, T.B., Pérez-Moreno, J.L., Ventura, T., Durica, D.S. and Mykles, D.L. (2025). Two cGMP-dependent protein kinases have opposing effects on molt-inhibiting hormone regulation of Y-organ ecdysteroidogenesis. *J. Exp. Biol.* Pre-print DOI: 10.1242/jeb.249739.

Hoffmeister, L., Diekmann, M., Brand, K. and Huber, R. (2020). GSK3: A Kinase Balancing Promotion and Resolution of Inflammation. *Cells.* **9**, 820.

Hong, Y., Flinkman, D., Suomi, T., Pietilä, S., James, P., Coffey, E. and Elo, L.L. (2022). PhosPiR: an automated phosphoproteomic pipeline in R. *Brief. Bioinform.* **23**, bbab510.

Hou, X., Yang, H., Chen, X., Wang, J. and Wang, C. (2021). RNA interference of mTOR gene delays molting process in *Eriocheir sinensis*. *Comp. Biochem. Physiol.* **256B**, 7.

Huang, S.Y., Tsai, M.L., Chen, G.Y., Wu, C.J. and Chen, S.H. (2007). A systematic MS-based approach for identifying in vitro substrates of PKA and PKG in rat uteri. *J. Proteome Res*. **6**, 2674-84.

Huang, T., Choi, M., Tzouros, M., Golling, S., Pandya, N.J., Banfai, B., Dunkley, T. and Vitek, O. (2020). MSstatsTMT: Statistical Detection of Differentially Abundant Proteins in Experiments with Isobaric Labeling and Multiple Mixtures. *Molec. Cell Prot.* **19**, 1706-1723.

Inoki, K., Ouyang, H., Zhu, T., Lindvall, C., Wang, Y., Zhang, X., Yang, Q., Bennett, C., Harada, Y., Stankunas, K., et al. (2006). TSC2 Integrates Wnt and Energy Signals via a Coordinated Phosphorylation by AMPK and GSK3 to Regulate Cell Growth. *Cell.* **126**, 955-968.

Kanehisa, M. and Sato, Y. (2020). KEGG Mapper for inferring cellular functions from protein sequences. *J. Prot. Sci.* **29**, 28-35.

Karlson, P. and Skinner, D.M. (1960). Attempted extraction of crustacean moulting hormone from isolated Y-organs. *Nature.* **185**, 543-4.

Kim, K., Antcliffe, J., Daley, A.C. and Robinson-Rechavi, M. (2024). Moult cycle and setal development of the Atlantic ditch shrimp Palaemon varians Leach, 1814 (Decapoda: Caridea: Palaemonidae). *J. Crustacean Biol.* **44**, 8.

Kohler, D., Tsai, T.H., Verschueren, E., Huang, T., Hinkle, T., Phu, L., Choi, M. and Vitek, O. (2023). MSstatsPTM: Statistical Relative Quantification of Posttranslational Modifications in Bottom-Up Mass Spectrometry-Based Proteomics. *Molec. Cell Prot.* **22**, 100477.

Kohler, D., Staniak, M., Yu, F., Nesvizhskii, A.I. and Vitek, O. (2024). An MSstats workflow for detecting differentially abundant proteins in large-scale data-independent acquisition mass spectrometry experiments with FragPipe processing. *Nature Protoc.* **19**, 2915-2938.

Komalavilas, P., Shah, P.K., Jo, H. and Lincoln, T.M. (1999). Activation of Mitogen-activated Protein Kinase Pathways by Cyclic GMP and Cyclic GMP-dependent Protein Kinase in Contractile Vascular Smooth Muscle Cells. *J. Biol. Chem.* **274**, 34301-34309.

Lee, G.Y., Chun, Y.S., Shin, H.W. and Park, J.W. (2016). Potential role of the N-MYC downstream-regulated gene family in reprogramming cancer metabolism under hypoxia. *Oncotarget.* **7**, 57442-57451.

Lee, G.Y., Shin, S.-H., Shin, H.-W., Chun, Y.-S. and Park, J.W. (2018). NDRG3 lowers the metastatic potential in prostate cancer as a feedback controller of hypoxia-inducible factors. *Exp. Molec. Med.* **50**, 1-13.

Lee, H., Engel, U., Rusch, J., Scherrer, S., Sheard, K. and Van Vactor, D. (2004). The Microtubule Plus End Tracking Protein Orbit/MAST/CLASP Acts Downstream of the Tyrosine Kinase Abl in Mediating Axon Guidance. *Neuron.* **42**, 913-926.

Li, C., Zheng, Z., Wu, X., Xie, Q., Liu, P., Hu, Y., Chen, M., Liu, L., Zhao, W., Chen, L., et al. (2023). Stiff matrix induced srGAP2 tension gradients control migration direction in triple-negative breast cancer. *Theranostics.* **13**, 59-76.

Li, J., Ma, Y., Yang, Z., Wang, F., Li, J., Jiang, Y., Yang, D., Yi, Q. and Huang, S. (2023). FOXO-like Gene Is Involved in the Regulation of 20E Pathway through mTOR in Eriocheir sinensis. *J. Mar. Sci. Eng.* **11**, 1225.

Liu, D., Ceddia, R.P. and Collins, S. (2018). Cardiac natriuretic peptides promote adipose 'browning' through mTOR complex-1. *Molec. Metab.* **9**, 192-198.

Liu, G.Y. and Sabatini, D.M. (2020). mTOR at the nexus of nutrition, growth, ageing and disease. *Nature Rev. Molec. Cell Biol.* **21**, 183-203.

Liu, X., Guo, B., Li, Q. and Nie, J. (2024). mTOR in metabolic homeostasis and disease. *Exp. Cell Res.* **441**, 10.

Loureiro, J.J., Rubinson, D.A., Bear, J.E., Baltus, G.A., Kwiatkowski, A.V. and Gertler, F.B. (2002). Critical Roles of Phosphorylation and Actin Binding Motifs, but Not the Central Proline-rich Region, for Ena/Vasodilator-stimulated Phosphoprotein (VASP) Function during Cell Migration. *Molec. Biol. Cell.* **13**, 2533-2546.

Lu, L., Wang, T., Liu, A. and Ye, H.H. (2024). A Single-Cell Atlas of Crab Ovary Provides New Insights Into Oogenesis in Crustaceans. *Adv. Sci.* **12**. Preprint. DOI: 10.1002/advs.202409688.

Luo, L., Yang, L.S., Huang, J.H., Jiang, S.G., Zhou, F.L., Li, Y.D., Jiang, S. and Yang, Q.B. (2024). Effects of different salinity stress on the transcriptomic responses of freshwater crayfish (*Procambarus clarkii*, Girard, 1852). *Biology-Basel.* **13**, 19.

Martinez-Lopez, N., Mattar, P., Toledo, M., Bains, H., Kalyani, M., Aoun, M.L., Sharma, M., McIntire, L.B.J., Gunther-Cummins, L., Macaluso, F.P., et al. (2023). mTORC2–NDRG1–CDC42 axis couples fasting to mitochondrial fission. *Nature Cell Biol.* **25**, 989-1003.

Mehta, D., Rajput, K., Jain, D., Bajaj, A. and Dasgupta, U. (2024). Unveiling the Role of Mechanistic Target of Rapamycin Kinase (MTOR) Signaling in Cancer Progression and the Emergence of MTOR Inhibitors as Therapeutic Strategies. *ACS Pharmacol. Transl. Sci.* **22**. Preprint DOI: 10.1021/acsptsci.4c00530.

Melotte, V., Qu, X., Ongenaert, M., van Criekinge, W., de Bruïne, A.P., Baldwin, H.S. and van Engeland, M. (2010). The N-myc downstream regulated gene (NDRG) family: diverse functions, multiple applications. *FASEB J.* **24**, 4153-4166.

Muneer, G., Chen, C.-S. and Chen, Y.J. (2024). Advancements in Global Phosphoproteomics Profiling: Overcoming Challenges in Sensitivity and Quantification. *Proteomics.* **25**, e202400087.

Myers, S.A., Klaeger, S., Satpathy, S., Viner, R., Choi, J., Rogers, J., Clauser, K., Udeshi, N.D. and Carr, S.A. (2019). Evaluation of Advanced Precursor Determination for Tandem Mass Tag

(TMT)-Based Quantitative Proteomics across Instrument Platforms. *J. Proteome Res.* **18**, 542-547.

Mykles, D.L. and Chang, E.S. (2020). Hormonal control of the crustacean molting gland: Insights from transcriptomics and proteomics. *Gen. Comp. Endocrinol.* **294**, 113493.

Mykles, D.L. (2021). Signaling pathways that regulate the crustacean molting gland. *Front. Endocrinol.* **12**, 113658.

Mykles, D.L. (2024). Molting physiology. *Frontiers in Invertebrate Physiology* (ed. S. P. L. S. Saleuddin, R.D. Roer, I. Wilkie), pp. 229-274. Palm Bay, FL: Apple Academic Press.

Nagaraju, G.P.C. (2011). Reproductive regulators in decapod crustaceans: an overview. *J. Exp. Biol.* **214**, 3-16.

Nakatsuji, T., Sonobe, H. and Watson, R.D. (2006). Molt-inhibiting hormone-mediated regulation of ecdysteroid synthesis in Y-organs of the crayfish (*Procambarus clarkii*): involvement of cyclic GMP and cyclic nucleotide phosphodiesterase. *Molec. Cell Endocrinol.* **253**, 76-82.

Nakatsuji, T., Lee, C.-Y. and Watson, R.D. (2009). Crustacean molt-inhibiting hormone: Structure, function, and cellular mode of action. *Comp. Biochem. Physiol.* **152**, 139-148.

Noddings, C.M., Johnson, J.L. and Agard, D.A. (2023). Cryo-EM reveals how Hsp90 and FKBP immunophilins co-regulate the glucocorticoid receptor. *Nature Struct. Molec. Biol.* **30**, 1867-1877.

O'Leary, N.A., Wright, M.W., Brister, J.R., Ciufo, S., Haddad, D., McVeigh, R., Rajput, B., Robbertse, B., Smith-White, B., Ako-Adjei, D., et al. (2016). Reference sequence (RefSeq) database at NCBI: current status, taxonomic expansion, and functional annotation. *NAR.* **44**, D733-D745.

Oeing, C.U., Nakamura, T., Pan, S., Mishra, S., Dunkerly-Eyring, B.L., Kokkonen-Simon, K.M., Lin, B.L., Chen, A., Zhu, G., Bedja, D., et al. (2020). PKG1α cysteine-42 redox state controls mTORC1 activation in pathological cardiac hypertrophy. *Circulat. Res.* **127**, 522-533.

Panwar, V., Singh, A., Bhatt, M., Tonk, R.K., Azizov, S., Raza, A.S., Sengupta, S., Kumar, D. and Garg, M. (2023). Multifaceted role of mTOR (mammalian target of rapamycin) signaling pathway in human health and disease. *STTT.* **8**, 375.

Paysan-Lafosse, T., Blum, M., Chuguransky, S., Grego, T., Pinto, B.L., Salazar, G.A., Bileschi, M.L., Bork, P., Bridge, A., Colwell, L., et al. (2023). InterPro in 2022. *NAR.* **51**, D418-D427.

Pérez-Moreno, J.L., Kozma, M.T., DeLeo, D.M., Bracken-Grisson, H.D., Durica, D.S. and Mykles, D.L. (2023). CrusTome: a transcriptome database resource for large-scale analyses across Crustacea. *G3-Genes Genomes Genet.* **13**, jkad098.

Pitts, N.L., Schulz, H.M., Oatman, S.R. and Mykles, D.L. (2017). Elevated expression of neuropeptide signaling genes in the eyestalk ganglia and Y-organ of *Gecarcinus lateralis* individuals that are refractory to molt induction. *Comp. Biochem. Physiol.* **214A**, 66-78.

Ranek, M.J., Kokkonen-Simon, K.M., Chen, A., Dunkerly-Eyring, B.L., Pinilla Vera, M., Oeing, C.U., Patel, C.H., Nakamura, T., Zhu, G., Bedja, D., et al. (2019). PKG1-modified TSC2 regulated mTORC1 activity to counter adverse cardiac stress. *Nature.* **566**, 264-269.

Ritchie, M.E., Phipson, B., Wu, D., Hu, Y., Law, C.W., Shi, W. and Smyth, G.K. (2015). limma powers differential expression analyses for RNA-sequencing and microarray studies. *NAR.* **43**, e47.

Saidi, B., Debesse, N., Webster, S.G., Sedlmeier, D. and Lachaise, F. (1994). Involvement of cAMP and cGMP in the mode of action of molt-inhibiting hormone (MIH) a neuropeptide which inhibits steroidogenesis in a crab. *Molec. Cell Endocrinol.* **102**, 53-61.

Sanyal, A., Lochmatter, D., Preußner, A. and Pfeifer, A. (2013). Influence of PKG on insulin signalling and GSK3 phosphorylation in SH-SY5Y cells. *BMC Pharmacol. Toxicol.* **14**, P60.

Schonkeren, S.L., Massen, M., van der Horst, R., Koch, A., Vaes, N. and Melotte, V. (2019). Nervous NDRGs: the N-myc downstream–regulated gene family in the central and peripheral nervous system. *Neurogenet.* **20**, 173-186.

Schraink, T., Blumenberg, L., Hussey, G., George, S., Miller, B., Mathew, N., González-Robles, T.J., Sviderskiy, V., Papagiannakopoulos, T., Possemato, R., et al. (2023). PhosphoDisco: A Toolkit for Co-regulated Phosphorylation Module Discovery in Phosphoproteomic Data. *Molec. Cell Proteom.* **22**, 100596.

Shahbazian, D., Roux, P.P., Mieulet, V., Cohen, M.S., Raught, B., Taunton, J., Hershey, J.W., Blenis, J., Pende, M. and Sonenberg, N. (2006). The mTOR/PI3K and MAPK pathways converge on eIF4B to control its phosphorylation and activity. *EMBO J.* **25**, 2781-2791.

Shi, F. and Collins, S. (2023). Regulation of mTOR signaling: Emerging role of cyclic nucleotide-dependent protein kinases and implications for cardiometabolic disease. *Int. J. Molec. Sci.* **24**, 11497.

Shi, Q., Lin, Y.Q., Saliba, A., Xie, J., Neely, G.G. and Banerjee, S. (2019). Tubulin Polymerization Promoting Protein, Ringmaker, and MAP1B Homolog Futsch Coordinate Microtubule Organization and Synaptic Growth. *Front. Cell. Neurosci.* **13**, 00192.

Shyamal, S., Das, S., Guruacharya, A., Mykles, D.L. and Durica, D.S. (2018). Transcriptomic analysis of crustacean molting gland (Y-organ) regulation via the mTOR signaling pathway. *Sci. Reports.* **8**, 7307.

Stanciu, S.M., Jinga, M., Miricescu, D., Stefani, C., Nica, R.I., Stanescu-Spinu, II, Vacaroiu, I.A., Greabu, M. and Nica, S. (2024). mTOR dysregulation, insulin resistance, and hypertension. *Biomedicines.* **12**, 18.

Storey, A.J., Naceanceno, K.S., Lan, R.S., Washam, C.L., Orr, L.M., Mackintosh, S.G., Tackett, A.J., Edmondson, R.D., Wang, Z., Li, H.-y., et al. (2020). ProteoViz: a tool for the analysis and interactive visualization of phosphoproteomics data. *Molec. Omics.* **16**, 316-326.

Strimmer, K. (2008). A unified approach to false discovery rate estimation. *BMC Bioinform.* **9**, 303.

Subramoniam, T. (2000). Crustacean ecdysteriods in reproduction and embryogenesis. *Comp. Biochem. Physiol.* **125C**, 135-156.

Supriya, N.T., Sudha, K., Krishnakumar, V. and Anilkumar, G. (2017). Molt and reproduction enhancement together with hemolymph ecdysteroid elevation under eyestalk ablation in the female fiddler crab, Uca triangularis (Brachyura: Decapoda). *CJOL.* **35**, 645-657.

Szwed, A., Kim, E. and Jacinto, E. (2021). Regulation and metabolic functions of mTORC1 and mTORC2. *Physiol. Rev.* **101**, 1371-1426.

Teran Pumar, O.Y., Zanotelli, M.R., Lin, M.J., Schmitt, R.R., Green, K.S., Rojas, K.S., Hwang, I.Y., Cerione, R.A. and Wilson, K.F. (2024). A multiprotein signaling complex sustains AKT and mTOR/S6K activity necessary for the survival of cancer cells undergoing stress. *bioRxiv.* Preprint. DOI: 10.1101/2023.01.03.522657.

The Galaxy Community (2024). The Galaxy platform for accessible, reproducible, and collaborative data analyses: 2024 update. *NAR.* **52**, W83-W94.

The UniProt Consortium (2023). UniProt: the Universal Protein Knowledgebase in 2023. *NAR.* **51**, D523-D531.

Tong, M., Liu, Z., Li, J., Wei, X., Shi, W., Liang, C., Yu, C., Huang, R., Lin, Y., Wang, X., et al. (2024). PhosMap: An ensemble bioinformatic platform to empower interactive analysis of quantitative phosphoproteomics. *Comp. Biol. Med.* **174**, 108391.

Tran, N.M., Mykles, D.L., Elizur, A. and Ventura, T. (2019). Characterization of G-protein coupled receptors from the blackback land crab *Gecarcinus lateralis* Y organ transcriptome over the molt cycle. *BMC Genom.* **20**, 74.

Tukey, J.W. (1977). Exploratory data analysis. *Addison-Wesley*, Reading, MA. 192-197.

Välikangas, T., Suomi, T. and Elo, L.L. (2018). A systematic evaluation of normalization methods in quantitative label-free proteomics. *Brief. Bioinform.* **19**, 1-11.

Wang, J., Chitsaz, F., Derbyshire, M.K., Gonzales, N.R., Gwadz, M., Lu, S., Marchler, G.H., Song, J.S., Thanki, N., Yamashita, R.A., et al. (2023). The conserved domain database in 2023. *NAR.* **51**, D384-D388.

Wang, L. (2011). FKBP51 regulation of AKT/protein kinase B phosphorylation. *Curr. Opin. Pharmacol.* **11**, 360-364.

Wang, Y.M., Vandewalle, N., De Veirman, K., Vanderkerken, K., Menu, E. and De Bruyne, E. (2024). Targeting mTOR signaling pathways in multiple myeloma: Biology and implication for therapy. *Cell Commun. Signal.* **22**, 320.

Webster, S.G. (1986). Neurohormonal control of ecdysteroid biosynthesis by *Carcinus maenas* Y-organs *in vitro*, and preliminary characterization of the putative molt-inhibiting hormone (MIH). *Gen. Comp. Endocrinol.* **61**, 237-247.

Webster, S.G. and Keller, R. (1986). Purification, characterization and amino-acid composition of the putative molt-inhibiting hormone (MIH) of *Carcinus maenas* (Crustacea, Decapoda). *J. Comp. Physiol.* **156B**, 617-624.

Welsh, J.H. (1961). Neurohumors and Neurosecretion. *The Physiology of Crustacea, Vol. 2* (ed. T. H. Waterman), pp. 281-311. New York City, New York, USA: Academic Press.

Yang, X., An, L. and Li, X. (2013). NDRG3 and NDRG4, two novel tumor-related genes. *Biomed. Pharmacol.* **67**, 681-684.

Zhang, H., Steele, J.R., Kahrood, H.V., Lucas, D.D., Shah, A.D. and Schittenhelm, R.B. (2023). Phospho-Analyst: An Interactive, Easy-to-Use Web Platform To Analyze Quantitative Phosphoproteomics Data. *J. Proteome Res.* **22**, 2890-2899.

Zhao, R., Davey, M., Hsu, Y.C., Kaplanek, P., Tong, A., Parsons, A.B., Krogan, N., Cagney, G., Mai, D., Greenblatt, J., et al. (2005). Navigating the chaperone network: an integrative map of physical and genetic interactions mediated by the hsp90 chaperone. *Cell.* **120**, 715-727.

Zhao, X., Zhuang, S., Chen, Y., Boss, G.R. and Pilz, R.B. (2005). Cyclic GMP-dependent protein kinase regulates CCAAT enhancer-binding protein beta functions through inhibition of glycogen synthase kinase-3. *J. Biol. Chem.* **280**, 32683-92.

CHAPTER FIVE

SUMMARY AND FUTURE DIRECTIONS

The regulation of ecdysteroid synthesis, and thus molting, in decapod crustaceans involves the integration of many biological and environmental signals. The neuropeptide molt-inhibiting hormone (MIH) is the predominant inhibitory factor that acts on the molting gland (Y-organ, YO) to inhibit ecdysteroid synthesis. MIH signaling involves a transient increase in cAMP levels followed by a sustain increase in cGMP, characteristic of G protein coupled receptor (GPCR) signaling pathways. Ecdysteroid synthesis is dependent upon activation of the mechanistic target of rapamycin complex 1 (mTORC1), which is hypothesized to stimulate ecdysteroid synthesis through increased translation of ecdysteroid biosynthetic enzymes. This dissertation examines the role of cGMP-depdendent protein kinase (PKG) as a link between MIH signaling and subsequent mTORC1 inhibition using bioinformatics, physiological experiments, and phosphoproteomic analysis.

In chapter two, it was established that Pancrustacea expresses PKG transcripts homologous to mammalian genes *pkg1* and *pkg2.* Alternative splicing at the N-terminal region of PKG1 results in isoforms that can be attributed to PKG1α and PKG1β, as in mammals. To determine whether the splice sites themselves are conserved across metazoans, future phylogenetic analysis should separately analyze the alternatively spliced regions from the rest of the conserved gene to separate the evolutionary history of the isoforms and reduce the influence of the un-spliced gene region. Novel isoforms of PKG1α were identified as a result of alternative splicing, and a novel insertion within the kinase domain of PKG1α and PKG1β

isoforms unique to decapods indicates that alternative splicing may occur outside of the N-terminus.

In vitro assays of YOs from *G. lateralis* and *C. maenas* examined the effects of PKG inhibition in YOs incubated with MIH. When both PKG1 and PKG2 were inhibited by the cGMP analog Rp-8-Br-PET-cGMP in the presence of MIH, ecdysteroid secretion increased relative to paired YOs treated only with MIH. When only PKG2 was inhibited by the small molecule AP-C5 in the presence of MIH, ecdysteroid secretion was reduced to 10% of the control and 24% of the control in *C. maenas* and *G. lateralis* respectively. These findings indicate that PKG1 and PKG2 have opposing roles in regulating ecdysteroid synthesis. It has been broadly accepted, though not explained, that MIH inhibition in the YO cannot completely inhibit ecdysteroid synthesis even at high concentrations. The opposing roles of PKG1 and PKG2 finally resolves a long-standing paradox of how MIH signaling suppresses, but does not completely diminish, ecdysteroid synthesis during intermolt.

In chapter three, transcript expression of all PKG isoforms across the molt cycle in YOs of *G. lateralis* and *C. maenas* were assessed. *PKG1α2* is the major isoform expressed at all molt stages in both species. In response to eyestalk ablation (ESA) transcript expression of *Gl-PKG1α2* was 35 times higher than other *PKG* isoforms. In both species, *PKG2* expression was at least two orders of magnitude lower than *PKG1* isoforms. The trends in *Gl-PKG* transcript expression in the YOs reported here do not entirely correspond to previously reported changes in expression over the molt cycle in *G. lateralis*. Three factors are likely to contribute to this discrepancy: 1) Previously reported expression only assessed one PKG isoform, as others had not been characterized, whereas the isoform-specific expression reported here can unmask patterns that were previously concatenated. 2) The transcriptome assembled for this analysis consists of a

much larger sample size than what was available for the transcripts assembled in 2016 and 2018. 3) Different pipelines were used to assemble and quantify the different transcriptomic databases. The next step in addressing these discrepancies is to re-assemble each of the transcriptomes using the same pipeline to standardize the methods used for quality control, quantification, and distinguishing isoforms. Looking forward, re-assembly of RNAseq data from 2016 and 2018 alongside the larger dataset presented here will aid in comparisons and cross-validation between the studies.

Liquid chromatography/tandem mass spectrometry (LC-MS/MS) analysis of phosphopeptides enriched from PKG-inhibited YOs from *C. maenas* and *G. lateralis* revealed several novel potential substrates of PKG. Strong batch effects at the global and phospho-enriched levels were identified between TMT sets within the same experiments. The results presented within this dissertation should be considered as preliminary and interpreted as such until the normalized dataset is available.

Phosphopeptides from slit-robo Rho-GTPase activating protein (srGAP), enabled-protein homolog (Enah), and Futsch among several other cytoskeleton-associated proteins were identified in YOs from both species and all combinations of MIH ± PKG-inhibition. This suggests that cytoskeletal organization and stability may be a component of ecdysteroid regulation by directing the subcellular location of signaling proteins. Additionally, phosphopeptides from signaling pathways, including glycogen synthase kinase 3β (GSK3B), mitogen-activated protein kinase kinase (MAP2K1/MEK), and FK506-binding protein 5 (FKBP5) appear to be the most likely PKG substrate candidates in the YO. Specifically, GSK3B is a characterized substrate of PKG in several mammalian tissues and can regulate both Akt and TSC in the mTORC1 pathway. MAP2K is one component of the Ras/Raf/MEK/ERK signaling

cascade that is typical of growth factor signaling. Given the numerous signaling pathways integrated in the YO, including growth factors, it is reasonable that cross talk and/or convergence between signaling pathways occurs. Particularly, PI3K-AKT signaling and mTORC1 signaling pathways both include GSK3B and MEK. Identifying phosphorylated FKBP5 and Hsp90 proteins also presents an interesting mechanism through which cytoskeletal and signaling pathways could be integrated, particularly as the FKBP5/Hsp90 complex inhibits AKT by using a microtubule scaffold. Finally, specific phosphosites identified within the N-myc downstream regulated gene 3 (NDRG3) align with those predicted to be phosphosites of both PKG1 and PKG2.

Looking forward, normalization of the proteomic datasets to correct for batch effects will likely unmask differential expression of additional phosphopeptides. This will require a custom workflow that can be combined with current analysis programs, as well as custom processing scripts. By normalizing for batch effects and quantifying phosphopeptides at the peptide level, we may identify whether specific phosphopeptides or phosphosites are associated with PKG1 or PKG2 activity. This will be particularly interesting within GSK3B, where multiple phosphopeptides were identified.

Additionally, two experiments were not presented in this dataset but should still be acknowledged, as they provide a basis for future work. First, RNA interference (RNAi) in *C. maenas,* using double stranded RNA for PKG1 isoforms, was completed over the course of two weeks to measure the effects of PKG knockdown. Unfortunately, during the timing of the experiment all collected specimens were in or entering premolt. The predicted effect of PKG1 knockdown would be premature entry into premolt. Animals in the control group, which received injections of double stranded green fluorescent protein, showed entry into premolt and

increased ecdysteroidogenesis over the course of the experiment along with those that received dsPKG RNA.

The RNAseq data from *G. lateralis* animals induced to molt by MLA will also include paired proteomic data. One YO from each animal was used for RNA sequencing, and the other for proteomic analysis. The proteomic samples have been isobarically labeled and prepared but await LC-MS/MS analysis. Together, this dataset will allow for comparisons between transcript and protein expression levels across the molt cycle. Preliminary evidence suggests that differences in expression between PKG1 and PKG2 allow MIH to maintain basal ecdysteroid synthesis during intermolt.

In summary, this dissertation examined the role of PKG in the YO as a key enzyme linking MIH signaling to the suppression of ecdysteroid synthesis. PKG1 and PKG2 have opposing roles in regulating ecdysteroid synthesis in the YO, answering a long-standing question about incomplete ecdysteroidogenic inhibition by MIH. Differences in protein expression of the two PKGs may be the mechanism through which ecdysteroid synthesis is repressed but not completely stopped. The YO integrates numerous signaling pathways to regulate ecdysteroid synthesis, and these pathways primarily converge on mTORC1. PKG signaling stimulated by MIH likely interacts with other signaling pathways to inhibit (PKG1) or stimulate (PKG2) ecdysteroid synthesis, including GSK3B, MAP2K1, FKBP5, and proteins that regulate cytoskeletal organization and stability (Fig. 5.1).

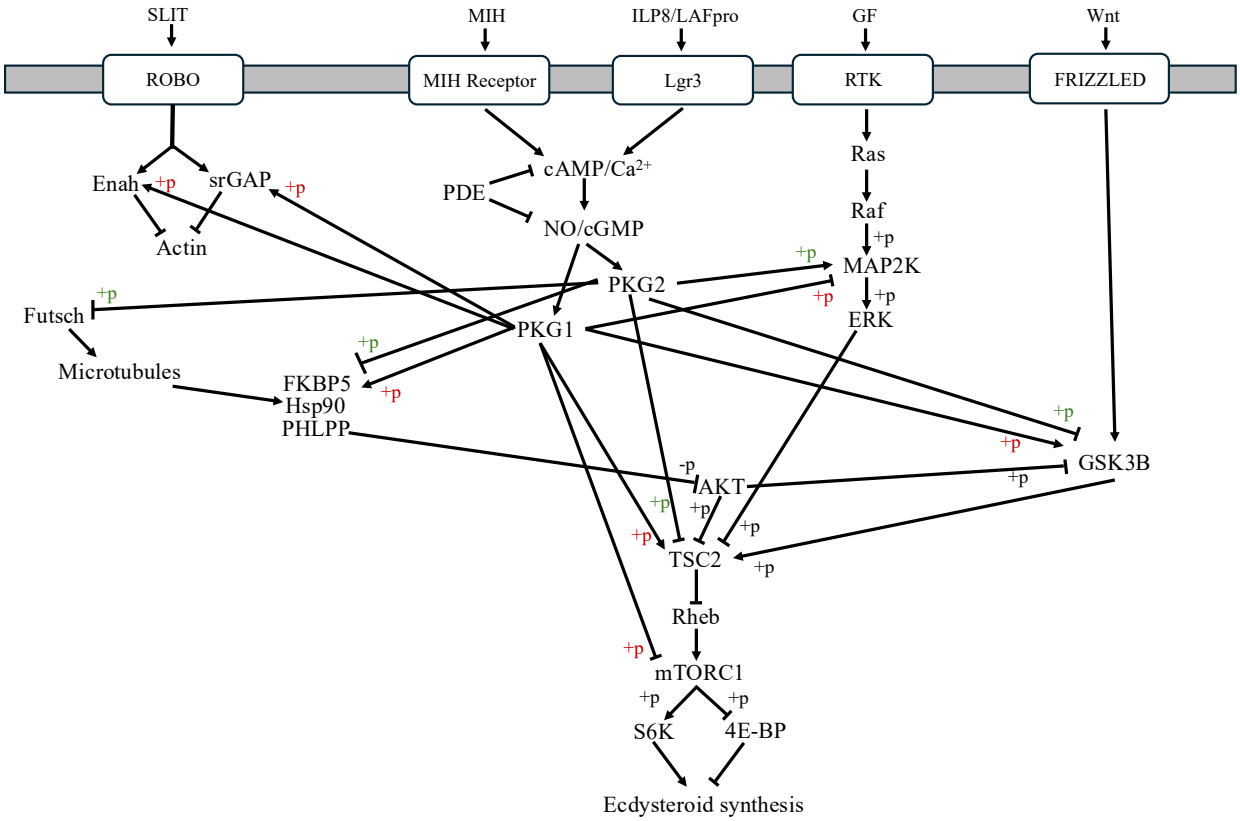

Figure 5.1. Putative signaling pathways through which PKG1 and PKG2 regulate ecdysteroid synthesis in the decapod Y-organ. Binding of MIH to its receptor activates a transient increase in cAMP followed by a sustained NO-dependent increase in cGMP. Both PKG1 and PKG2 are activated by MIH. Phosphorylation by PKG1 is inhibitory to ecdysteroid synthesis and indicated in red, phosphorylation by PKG2 is stimulatory to ecdysteroid synthesis and indicated in green. PKG1 and PKG2 may both phosphorylate TSC2, resulting in inhibition or activation of mTORC1 respectively. PKG1 may directly inhibit mTORC1 activation by phosphorylation of Raptor, a component of mTORC1. Activation of the Ras/Raf/MEK/ERK pathway is initiated by binding of GF to RTKs. Inhibitory (PKG1) or stimulatory (PKG2) phosphorylation of MEK alters its ability to stimulate inhibitory phosphorylate of TSC2 by ERK. GSK3B is stimulated by Wnt signaling, and stimulatory phosphorylation of GSK3B by PKG1 induces stimulatory phosphorylation of TSC2. Conversely, inhibitory phosphorylation of GSK3B by PKG2 prevents TSC2 activation. Both PKG1 and PKG2 may regulate ecdysteroid synthesis by altering cytoskeletal organization and stability. PKG1 phosphorylation of Enah and srGAP results in actin depolymerization. Not shown, srGAP inhibits cdc42 which is an activator of mTORC1. PKG2 phosphorylates Futsch, thereby depolymerizing microtubules through which FKBP5/Hsp90/PHLPP are transported to AKT, where dephosphorylation by PHLPP deactivates AKT. Both PKG1 and PKG2 may also directly phosphorylate FKBP5, changing its ability to bind Hsp90. Abbreviations: 4E-Bp, Eukaryotic initiation factor 4E-binding protein; AKT, protein kinase B; Enah, protein enabled homolog; ERK, extracellular signal-regulated kinase; FKBP5, FK506-binding protein 5; GF, growth factor; GSK3B, glycogen synthase kinase 3β;

Hsp90, heat shock protein 90; ILP8, insulin-like peptide 8; LAFpro, limb autotomy factor proecdysis; Lgr3, leucine-rich repeat G protein coupled receptor 3; MEK, mitogen-activated protein kinase kinase /MAP2K; MIH, molt-inhibiting hormone; mTORC1, mechanistic target of rapamycin complex 1; NO, nitric oxide; PDE, phosphodiesterase; PHLPP, PH domain and leucine rich repeat protein phosphatase; PKG, cGMP-dependent protein kinase; Rheb, Ras homolog enriched in brain; RTK, receptor tyrosine kinase; S6K, ribosomal protein S6 kinase; srGAP, slit-robo GTPase activating protein.

APPENDICES

APPENDIX A

Table A1. Primer sequences used for amplification and sequence validation for all *G. lateralis* and *C. maenas PKG* transcripts.

Gene	Contig	Sequence (5' - 3')	Annealing Temperature	Amplicon Size (bp)
Gl-PKG1α1	*GeclaM_EVm002389t2*	F: TAGAGATGCTGGAGATCCTCAC	55.4	313
		R: AAGTCATTCTCCAGGATCG	51.4	
Gl-PKG1α2	*GeclatEVm002420t2*	F: CCGCAGCTAATGACAGAT	52.1	371
		R: AAGTCATTCTCCAGGATCG	51.4	
Gl-PKG1α3	*GeclatEVm002420t3*	F: GGACAATGAGATAATGGAGC	50.6	249
		R: AAGTCATTCTCCAGGATCG	51.4	
Gl-PKG1β	*GeclatEVm002420t1*	F: CTACACAACCGCCTCTC	52.4	299
		R: AAGTCATTCTCCAGGATCG	51.4	
Gl-PKG2	*GeclatEVm001732t1*	F: GTGTGATAGCCTGAGAACTGG	55.1	505
		R: GCACGTAGTTACAAAGCAAGG	54.2	
Cm-PKG1α1	*CarmaY_EVm003118t2*	F: TGCTGGAGATTCTCACCAAGAAG	56.7	305
		R: GTCATTCTCCAGGATCGC	52.8	
Cm-PKG1α2	*CarmaY_EVm003118t1*	F: CAGATGCCAACGAGTGC	54	359
		R: GTCATTCTCCAGGATCGC	52.8	
Cm-PKG1α3	*CarmaC_EVm005181t4*	F: CAGTTGGAGGCTGTAGTGAAAG	55.5	273
		R: GTCATTCTCCAGGATCGC	52.8	
Cm-PKG1β	*Cmae_CNS_GFXF0106319*	F: CCTTCGCACTCACAATAACC	53.7	280
		R: GTCATTCTCCAGGATCGC	52.8	
Cm-PKG2	*Cmae_GFYV01329795*	F: AGGACTTCAGGTCCAAGC	54.3	377
		R: GTCTTCCATACGCTTCAGTCC	55.3	

Table A2. Contig IDs for PKG1ins sequences containing kinase domain insertion, and corresponding contig IDs for the paired sequences without the insertion. Full sequences and MSAs are available on Dryad: https://doi.org/10.5061/dryad.1g1jwsv7b.

Isoform	Contig ID	ins Contig ID	Taxon	Species
PKG1β	Clitri_EVm000637t2	Clitri_EVm000637t1	Anomura	*Clibanarius tricolor*
PKG1α3	Clitri_EVm000637t4	Clitri_EVm000637t3		
PKG1α2	Clivit_EVm000851t2	Clivit_EVm000851t1	Anomura	*Clibanarius vittatus*
PKG1β	Homarus_americanus_XP_042243236	Homarus_americanus_XP_042243235	Astacidea	*Homarus americanus*
PKG1β	Procl1_EVm001493t2	Procl1_EVm001493t1	Astacidea	*Procambarus clarkii*
PKG1α2	Erisi1_EVm002590t3	Erisi1_EVm002590t1	Brachyura	*Eriocheir sinensis*
PKG1α3	Erisi1_EVm002590t4	Erisi1_EVm002590t2		
PKG1β	-	Minpug_EVm002714t1	Brachyura	*Leptuca pugilator*
PKG1α4	Cuaame_EVm001332t2	Cuaame_EVm001332t1	Caridea	*Cuapetes americanus*
PKG1α4	-	Lysamb_EVm000932t1	Caridea	*Lysmata amboinensis*
PKG1α4	ParausEVm002971t3	ParausEVm002971t1	Caridea	*Paratya australiensis*
PKG1α-	ParausEVm002971t4	ParausEVm002971t2		
PKG1α-	SysdeE_EVm001204t3	SysdeE_EVm001204t2	Caridea	*Systellaspisis debilis*
PKG1α	OraoraEVm000810t3	OraoraEVm000810t2	Stomatopoda	*Oratosquilla oratoria*

Table A3. Artist credits from PhyloPic for icons used in phylogenetic trees.

Taxa	Species	Artist
Achelata	*Panulirus interruptus*	Joanna Wolfe
Amphipoda	*Hyalella sp.*	Christoph Schomburg
Anomopoda	*Daphnia magna*	Mathilde Cordellier
Anomura	*Eumunida picta*	T. Michael Keesy
Astacidea	*Procambarus clarkii*	Mattia Menchetti
Brachyura	*Gecarcinus quadratus*	Margot Michaud
Caridea	*Typhlocaris salentina*	Steven Traver
Chordata	*Branchiostoma lanceolatum*	Yan Wong
Copepoda	*Acartia fossae*	Polina Drozdova
Euphausiacea	*Euphausia pacifica*	Steven Haddock
Eutardigrada	*Eutardigrada sp.*	Levi Simmons
Insecta	*Anoplophora glabripennis*	Kristina Gagalova
Isopoda	*Proasellus sp.*	Stefano Mammola
Limulidae	*Limulus polyphemus*	Andy Wilson
Penaeidae	*Penaeus sp.*	Christoph Schomburg
Pycnogonida	*Pycnogonidae*	T. Michael Keesey
Remipedia	*Speleonectes tanumekes*	Gemma Martínez-Redondo
Sessilia	*Balanus sp.*	James Bernot
Stomatopoda	*Squilla mantis*	T. Michael Keesey
Trombidiformes	*Tetranychus urticae*	Christoph Schomburg
Vertebrata	*Vulpes vulpes*	Anthony Caravaggi

APPENDIX B

Table B1. Program and workflow settings used in Proteome Discoverer.

Proteome Discoverer version: 3.1.0.638				
Protein identification and quantification parameters used in the Proteome Discoverer workflow.				
Processing step	Spectrum Files	Search Settings	File Name(s)	.raw
			Protein Database	UniProt_Brachyura_taxID6752.fasta; Database_2.fasta
			Enzyme Name	Trypsin/LysC
			Precursor Mass Tolerance	20 ppm
	Reporter Ions Quantifier	Peak Integration	Integration Tolerance	20 ppm
			Integration Method	Most Confident Centroid
		Scan Event Filters	Mass Analyzer	FTMS
			MS Order	MS2
			Activation Type	HCD
			Min. Collision Energy	0
			Max. Collision Energy	1000
	Spectrum Selector	General Settings	Precursor Selection	Use MS1 Precursor
			Use Isotope Pattern in Precursor Reevaluation	True
			Provide Profile Spectra	Automatic
			Spectra to Store	All
		Spectrum Properties Filter	Lower RT Limit	0
			Upper RT Limit	0
			First Scan	0
			Last Scan	0
			Ignore Specified Scans	None
			Lowest Charge State	0
			Highest Charge State	0
			Min. Precursor Mass	350 Da
			Max. Precursor Mass	6,000 Da
			Total Intensity Threshold	0
			Minimum Peak Count	1
		Scan Event Filters	Mass Analyzer	Is FTMS
			MS Order	In MS2
			Activation Type	Is HCD
			Acquisition Type	Is DDA
			Min. Collision Energy	0
			Max. Collision Energy	1,000
			Scan Type	Is Full
			Polarity Mode	Positive
		Peak Filters	S/N Threshold (FT-only)	1.5
		Replacements for Unrecognized Properties	Unrecognized Charge Replacements	Automatic
			Unrecognized Mass Analyzer Replacements	Ion Trap (ITMS)
			Unrecognized MS Order Replacements	MS2
			Unrecognized Activation Type Replacements	CID (Collision Induced Dissociation)
			Unrecognized Polarity Replacements	Positive
			Unrecognized MS Resolution@200 Replacements	60,000
			Unrecognized MSn Resolution@200 Replacements	30,000
		Precursor Pattern Extraction	Precursor Clipping Range Before	2.5 Da
			Precursor Clipping Range After	5.5 Da
	CHIMERYS	General	Processing Mode	One Job Per File
			Failed Job Case	Continue Workflow
			Feature Traces to Store	All
		Input Data	Protein Database	UniProt_Brachyura_taxID6752.fasta, Database_2.fasta
			Prediction Model	inferys_3.3.3_fragmentation
			CHIMERYS Inlusion File	NONE

Processing step	**CHIMERYS**	**Input Data**	**Enzyme Name**	Trypsin
			Max. Missed Cleavage Sites	2
			Min. Peptide Length	7
			Max. Peptide Length	30
			Min. Peptide Charge	1
			Max. Peptide Charge	6
		Tolerances	**Fragment Mass Tolerance**	40 ppm
		Dynamic Modifications	**Dynamic Modification**	Phospho (S)
			Dynamic Modification	Phospho (Y)
			Max. Dynamic Modifications Per Peptide	3
		Static Modifications	**Peptide N-Terminus**	TMT6/10/11 Tandem Mass Tag (N-terminus)
			Static Modification	Carbamidomethyl (C)
			Static Modification	TMT6/10/11 Tandem Mass Tag (N-terminus)
		Validation	**Target FDR (Strict)**	0.01
			Target FDR (Relaxed)	0.05
			Generate Extra Validation Columns	FALSE
	Sequest HT	**Input Data**	**Protein Database**	UniProt_Brachyura_taxID6752.fasta; Database_2.fasta
			Enzyme Name	Trypsin (Full)
			Max. Missed Cleavage Sites	2
			Min. Peptide Length	7
			Max. Peptide Length	55
			Max. Number of Peptides Reported	10
		Tolerances	**Precursor Mass Tolerance**	20 ppm
			Fragment Mass Tolerance	1.0005 Da
			Use Average Precursor Mass	False
			Use Average Fragment Mass	False
		Spectrum Matching	**Use Neutral Loss a Ions**	True
			Use Neutral Loss b Ions	True
			Use Neutral Loss y Ions	True
			Use Flanking Ions	True
			Weight of a Ions	0
			Weight of b Ions	1
			Weight of c Ions	0
			Weight of x Ions	0
			Weight of y Ions	1
			Weight of z Ions	0
		Dynamic Modifications	**Max. Equal Modifications Per Peptide**	3
			Max. Dynamic Modifications Per Peptide	4
			Dynamic Modification	Phospho / +79.966 Da (S, T, Y)
			Dynamic Modification	Oxidation / +15.995 Da (M)
		Dynamic Modification (Peptide Terminus)	**N-Terminal Modification**	None
			C-Terminal Modification	None
		Dynamic Modification (Protein Terminus)	**N-Terminal Modification**	None
			C-Terminal Modification	None
		Static Modifications	**Static Modification**	TMT6plex / +229.163 Da (K)
			Static Modification	Carbamidomethyl / +57.021 Da (C)
			Peptide N-Terminus	TMT6plex / +229.163 Da (Any N-Terminus)
			Peptide C-Terminus	None
	Comet	**Selection Parameters**	**Protein Database**	UniProt_Brachyura_taxID6752.fasta; Database_2.fasta
		Variable Modifications	**Variable Modification 1**	Phospho / +79.966 Da (S, T, Y)
			Variable Modification 2	Oxidation / +15.995 Da (M)
		Static Modifications	**Peptide N-Terminus**	TMT6plex / +229.163 Da (Any N-Terminus)
			Static Modification	TMT6plex / +229.163 Da (K)
			Static Modification	Carbamidomethyl / +57.021 Da (C)
	Percolator	**Target/Decoy Strategy**	**Target/Decoy Selection**	Concatenated
			Validation based on	q-Value
		Input Data	**Maximum Delta Cn**	0.05
			Maximum Rank	0

Processing step	Percolator	FDR Targets	Target FDR (Strict)	0.01
			Target FDR (Relaxed)	0.05
	IMP-ptmRS	Scoring	PhosphoRS Mode	TRUE
			Report Only PTMs	TRUE
			Use Diagnostic Ions	TRUE
			Use Fragment Mass Tolerance of Search Node	TRUE (1.0005 Da)
			Consider neutral loss peaks for CID, HCD	Automatic
			Maximum Peak Depth	8
			Use a mass accuracy correction	FALSE
		Performance	Macimum Number of Position Isoforms	500
			Maximum PTMs per peptide	10
Consensus Step	MSF Files	Storage Settings	Spectra to Store	Identified or quantified
			Feature Traces to Store	All
		Merging of Identified Peptide and Proteins	Merge Mode	Globally by Search Engine Type
		FASTA Title Line Display	Reported FASTA Title Lines	Best match
			Title Line Rule	Standard
			Preferred Accession	
			Preferred Taxonomy	
			Avoid Expressions	
		PSM Filters	Maximum Delta Cn	0.05
			Maximum Rank	0
			Maximum Delta Mass	0 ppm
			Score	
			Threshold	0
	PSM Grouper	Peptide Group Modifications	Site Probability Threshold	75
	Peptide Validator	General Validation Settings	Validation Mode	Automatic (Control Peptide-Level Error Rate if Possible)
			Target FDR (Strict) for PSMs	0.01
			Target FDR (Relaxed) for PSMs	0.05
			Target FDR (Strict) for Peptides	0.01
			Target FDR (Relaxed) for Peptides	0.05
		Specific Validation Settings	Validation Based On	q-Value
			Target/Decoy Selection for PSM Level FDR	Automatic
			Reset Confidence for Nodes without Decoy	False
	Peptide and Protein Filter	Peptide Filters	Peptide Confidence at Least	Medium
			Keep Lower Confident PSMs	False
			Minimum Peptide Length	7
			Remove Peptides Without Protein Reference	False
		Protein Filter	Minimum Number of Peptide Sequences	1
			Count Only Rank 1 Peptides	False
			Count Peptides Only for Top Scored Protein	False
	Protein Scorer	Contaminant Database	Protein Database	UniProt_Homosapiens_taxID9606.fasta
		Annotate Species	As species map	FALSE
			As Species Names	FALSE
		Mark Additional Entities	Annotation Groups	FALSE
			Pathway Groups	FALSE
			Moditifcation Sites	TRUE
			Peptide Isoform Groups	TRUE
	Protein FDR Validator	Confidence Threshold	Target FDR (Strict)	0.01
			Target FDR (Relaxed)	0.05
	Protein Grouping	Protein Grouping	Apply Strict Parsimony Principle	TRUE
	Modification Sites	General	Report Only PTMs	TRUE
			Only Master Proteins	FALSE
			Motif Radius	6

Consensus Step	**Peptide in Protein Annotation**	**Flanking Residues**	**Annotate Flanking Residues of the Peptide**	TRUE
			Number Flanking Residues in Connection Tables	1
		Modifications in Peptide	**Protein Modifications Reported**	For All Proteins
		Modifications in Protein	**Modifications Sites Reported**	All and Specific
			Minimum PSM Confidence	Medium
			Report Only PTMs	TRUE
			N-Terminal Modification	TMT6plex / +229.163 Da (Any N-Terminus)
			C-Terminal Modification	None
			Modification	Phospho / +79.966 Da (S, T, Y)
			Modification	TMT6plex / +229.163 Da (Any N-Terminus)
			Modification	Oxidation / +15.995 Da (M)
		Position in Protein	**Protein Positions for Peptides**	Only for Master Proteins
	Protein Annotations	**Annotation Aspects**	**Aspect**	Biological Process
			Aspect	Cellular Component
			Aspect	Molecular Function
			Aspect	Gene Ontology
			Aspect	Pfam
			Aspect	WikiPathways
		Annotation/Pathway Groups	**Protein Database**	UniProt_Brachyura_taxID6752.fasta; Database_2.fasta
	Reporter Ions Quantifier	**General Quantification Settings**	**Peptides to Use**	Unique + Razor
			Consider Protein Groups for Peptide Uniqueness	True
			Use Shared Quan Results	True
			Reject Quan Results with Missing Channels	False
		Reporter Quantification	**Reporter Abundance Based On**	Intensity
			Apply Quan. Value Correction	TRUE
			Co-Isolation Threshold	50
			Normalized CHIMERYS Coefficient Threshold	0.8
			Min. Average Reporter S/N Threshold	5
			Max. Average Reporter S/N Threshold	0
			SPS Mass Matches [%]	0
			Minimum Channel Occupancy [%] Threshold	0
		Normalization and Scaling	**Normalization Mode**	Total Peptide Amount
			Proteins For Normalization	
			Scaling Mode	None
		Exclude Peptides from Protein Quantification	**For Normalization**	Use All Peptides
			For Protein Roll-Up	Use All Peptides
			For Pairwise Ratios	Use All Peptides
			Considered Peptide Modification	Phospho / +79.966 Da (S, T, Y)
			Considered Peptide Modification	TMT6plex / +229.163 Da (Any N-Terminus)
			N-Terminal Considered Peptide Modification	TMT6plex / +229.163 Da (Any N-Terminus)
		Quan Rollup and Hypothesis Testing	**Protein Ratio Calculation**	Pairwise Ratio based
			Maximum Allowed Fold Change	100
			Imputation Mode	None
			Hypothesis Test	t-test (Background Based)
			Calculate Hypothesis Test for Peptides	TRUE
		Quan Ratio Distributions	**1st Fold Change Threshold**	2
			2nd Fold Change Threshold	4
			3rd Fold Change Threshold	6
			4th Fold Change Threshold	8
			5th Fold Change Threshold	10

Appendix C

RNAinterference Methods

RNA was purified and cDNA was synthesized as previously described (Chapter 3) from *C. maenas* gill, heart, and thoracic ganglion. PCR reactions were assembled with 2 µl cDNA, 6.5 µl nuclease-free water, 12.5 µl GoTaq Green Master Mix (Promega, Madison, WI, USA), and 2 µl each of 20 µM forward and 20 µM reverse primers (Table C1). Primers were designed for *Cm-PKG1α2* and *Cm-PKG1β*, as other isoforms of PKG1α had not yet been identified. Conditions of the PCR reaction were: 2 mins at 95ºC; 35 cycles of 30 sec at 95ºC, 30 sec at 58ºC, and 45 sec at 72ºC; and final extension for 10 mins at 72ºC. Successful amplification was verified by visualization of 4 µl of each sample on a 1% agarose gel stained with ethidium bromide.

A second set of primers was synthesized with the T7 RNA polymerase promoter sequence (5'- TAATACGACTCACTATAGGG – 3') appended (Table C1). PCR reactions were used as template for a second round of amplification to append the T7 promoter sequence, using an annealing temperature of 64ºC and the same conditions listed above. T7-PCR products were cleaned the Monarch PCR + DNA Cleanup Kit (New England BioLabs, Ipswich, MA, USA).

Double stranded RNA (dsRNA) was synthesized using the HiScribe T7 High Yield RNA Synthesis Kit (New England BioLabs, Ipswich, MA, USA). Briefly, 20 µl reactions were assembled with 0.7 µg of T7-PCR product as template. Reactions were incubated at 37ºC for 10 hours, followed by the addition of 1 µl DNase and incubation at 37ºC for 1 hour. RNA was cleaned up by adding an equal volume of acidic phenol: chloroform: isoamyl alcohol to each reaction and vortexing for 30 sec. RNA samples were centrifuged for 15 minutes at 16,000 x g at 4ºC. The upper aqueous layer was transferred to a new tube, and 1/10 sample volume of 5 mM sodium acetate and 2.5 sample volumed of ice-cold pure ethanol was added to each sample. Samples were vortexed for 30 sec, then incubated at -20ºC for 4 hours. RNA pellet was then collected by centrifugation and the supernatant was discarded. The RNA pellet was washed with 500 µl of ice-cold 70% EtOH. The pellet was then resuspended in 50 µl of 0.1 mM EDTA.

A mixture of dsRNA was pooled based on the final volumes synthesized for *Cm-PKG1α2* and *Cm-PKG1β*. The final dsPKG mixture consisted of 44% *Cm-PKG1α2* dsRNA and 56% *Cm-PKG1β* dsRNA. A sample of green fluorescent protein (GFP) dsRNA was provided by collaborator Dr. Tomer Venture (University of the Sunshine Coast) and used as a negative control (dsGFP).

The effects of dsRNA injections were measured at 7 days after injection, and 14 days after a second injection at 7 days (Figure C1). At day 0, all animals were measured and weighed, and a small volume of hemolymph was drawn, weighed, and mixed with an equal volume of anti-coagulant solution. Then, each animal received an injection of 2µg dsRNA per gram of body weight of either dsPKG or dsGFP into the left arthroidial membrane. The injection site was held with pressure from a KimWipe for ~1 minute after injection to prevent bleeding and immediate loss of the injected dsRNA. At day 7, a hemolymph sample was draw from all animals as described. Half of the animals from each group were scarified and tissues (YO, hepatopancreas, brain, eyestalk ganglia, heart, gill, claw muscle, testis, thoracic ganglia, midgut, and hindgut) were stored in RNAlater (Invitrogen, Waltham, MA, USA). The other half of animals from each group received a second dsRNA injection at day 7 as previously described. At day 14, a hemolymph sample was taken and tissues were collected in RNAlater. Hemolymph ecdysteroid titers were measured using a competitive ELISA as described in Chapter 2, Figure C2).

Table C1. Primers used for amplification of *Cm-PKG1α2* and *Cm-PKG1β*, and primers with the T7 RNA polymerase promoter appended for RNA synthesis.

Gene	Sequence (5' - 3')	Annealing Temp.	Amplicon Size (bp)
Cm-PKG1α2	F: AGATGCCAACGAGTGC	59.1	357
	R: TCATTCTCCAGGATCGC	58.0	
Cm-PKG1β	F: CTTCGCACTCACAATAACC	58.4	278
	R: TCATTCTCCAGGATCGC	58.0	
Cm-PKG1α2 ***- T7***	F: TAATACGACTCACTATAGGGCAGATGCCAACGAGTGC	65.0	399
	R: TAATACGACTCACTATAGGCGTCATTCTCCAGGATCGC	64.0	
Cm-PKG1β ***- T7***	F: TAATACGACTCACTATAGGGCCTTCGCACTCACAATAACC	64.2	320
	R: TAATACGACTCACTATAGGGCTCATTCTCCAGGATCGC	64.0	

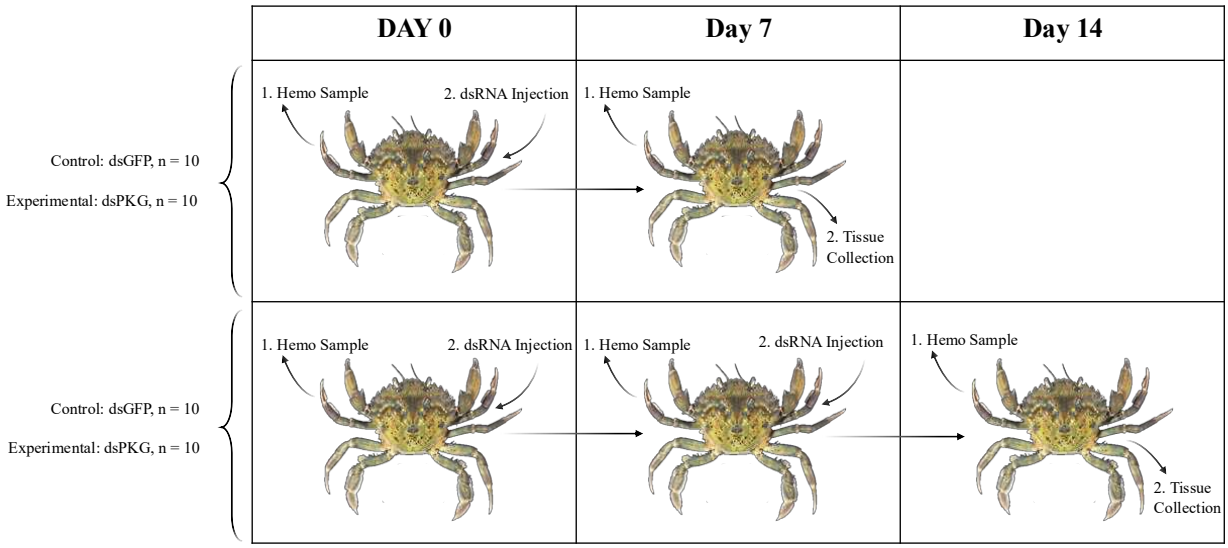

Figure C1. Hemolymph sample and dsRNA injection workflow. At Day 0, a small hemolymph sample was taken for all animals prior to injection of dsRNA. Injection of dsRNA was 2 µg per gram of body weight, control animals received dsGFP, and experimental animals received dsPKG. At Day 7, a hemolymph sample was taken for all animals. For a subset (n = 10) from each the control and the experimental groups, the animal was sacrificed, and tissue was collected. The remainder (n = 10) for each the control and experimental group, received a second injection of dsRNA at 2 µg per gram of body weight. At Day 14, a small hemolymph sample was taken for all animals, then animals were sacrificed, and tissues were collected.

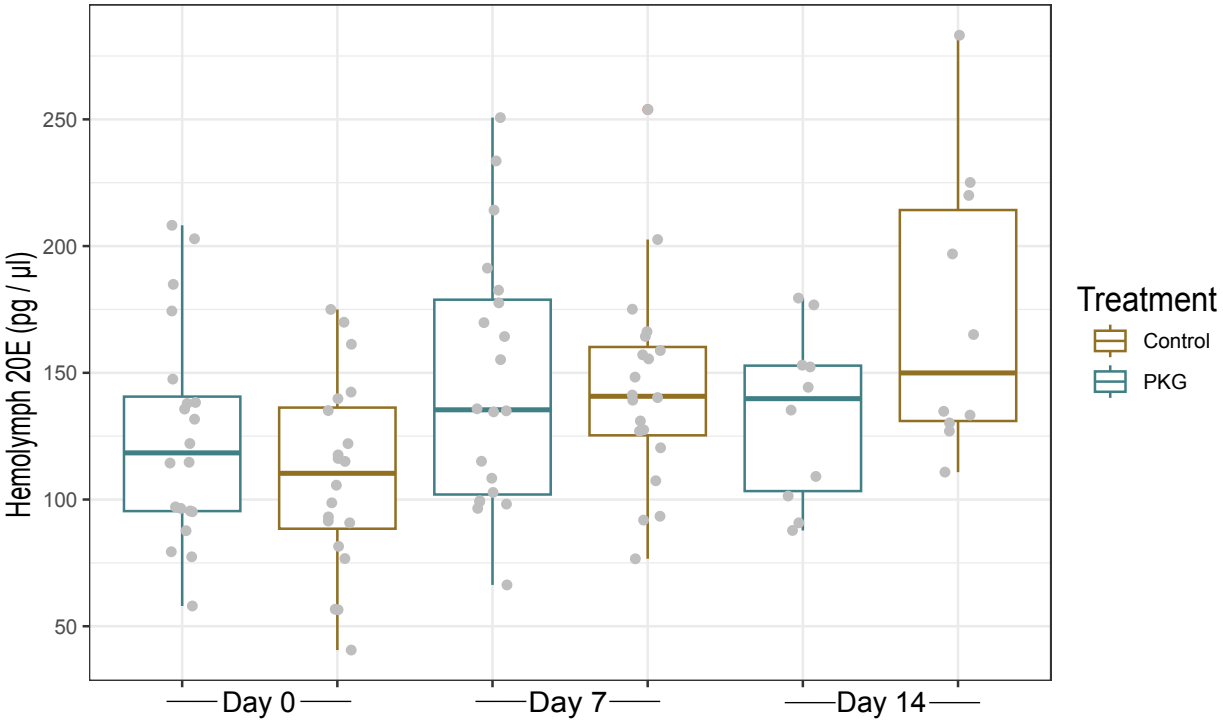

Figure C2. *C. maenas* hemolymph ecdysteroids at days 0, 7, and 14 after double stranded RNA injections. A competitive 20E ELISA was used to quantify circulating hemolymph ecdysteroid (20E) concentrations. Hemolymph concentrations increased at Day 7 and Day 14 relative to Day 0 for both the experimental (dsPKG) and control (dsGFP) groups. For the majority of animals in each group, hemolymph samples at Day 0 were above 100 pg/µl, indicating the animals were in early premolt.

LIST OF ABBREVIATIONS

Abbreviation	Term
20E	20-hydroxyecdysteroid
AC	Adenylyl cyclase
ACN	Acetonitrile
AI	Autoinhibitory
AKT	Protein kinase B
AP-C5	PKG2 small molecule inhibitor
BL	Blocked
BLAST	Basic Local Alignment Search Tool
CaM	Calmodulin
CaN	Calcineurin
cDNA	complimentary DNA
CDS	Conserved domain search
CNB	Cyclic nucleotide binding
CNS	Central nervous system
DMSO	Dimethyl sulfoxide
dsRNA	Double-stranded RNA
EF2	Translation elongation factor 2
ELISA	Enzyme-linked immunosorbent assay
Enah	Protein enabled homolog
EP	Early premolt
ESA	Eyestalk ablation
ESG	Eyestalk ganglia
FA	Formic acid
FDR	False discovery rate
FKBP5	FK506-binding protein 5
GC	Guanylyl cyclase
GKAP	G-kinase anchoring protein
GPCR	G-protein coupled receptor
GSK3B	Glycogen synthase kinase 3β
Hsp90	Heat shock protein 90
IM	Intermolt
IPS	InterPro Scan
LC-MS/MS	Liquid chromatography with tandem mass spectrometry
logFC	log2 Fold Change
LP	Late premolt
LZ	Leucine zipper
MAP2K	Mitogen activated protein kinase kinase (aka MEK)

MIH	Molt inhibiting hormone
MLA	Multiple leg autotomy
MP	Mid premolt
MSA	Multiple sequence alignment
mTOR	mechanistic Target of Rapamycin
NDRG	N-my downstream regulated gene
NO	Nitric oxide
NOS	Nitric oxide synthase
ORF	Open reading frame
PCR	Polymerase chain reaction
PG	Prothoracic gland
PKA	Protein kinase A
PKC	Protein kinase C
PKG	Protein kinase G
PM	Postmolt
PTTH	Prothoracicotropic hormone
Rheb	Ras-homolog enriched in brain
ROS	Reactive oxygen species
Rp-8-Br-PET-cGMP	cGMP analog, general PKG inhibitor
SG	Sinus gland
srGAP	Slit-Robo Rho GTPase activating protein
TFA	Trifluoroacetic acid
TMT	Tandem mass tag
TPM	Transcripts per million reads
TSC	Tuberous sclerosis complex (made of TSC1/TSC2)
TSC1	Hamartin
TSC2	Tuberin
UTR	Untranslated region
XO	X-organ
YO	Y-organ